

Summer 5-2014

# EFFECTS OF THE ENDOCANNABINOID ANANDAMIDE ON EXCITABILITY AND CALCIUM SIGNALING IN RAT VENTRICULAR MYOCYTES

Lina Tareq Al-Kury

Follow this and additional works at: [https://scholarworks.uaeu.ac.ae/all\\_dissertations](https://scholarworks.uaeu.ac.ae/all_dissertations)

Part of the [Medicine and Health Sciences Commons](#)

---

## Recommended Citation

Al-Kury, Lina Tareq, "EFFECTS OF THE ENDOCANNABINOID ANANDAMIDE ON EXCITABILITY AND CALCIUM SIGNALING IN RAT VENTRICULAR MYOCYTES" (2014). *Dissertations*. 34.  
[https://scholarworks.uaeu.ac.ae/all\\_dissertations/34](https://scholarworks.uaeu.ac.ae/all_dissertations/34)

This Dissertation is brought to you for free and open access by the Electronic Theses and Dissertations at Scholarworks@UAEU. It has been accepted for inclusion in Dissertations by an authorized administrator of Scholarworks@UAEU. For more information, please contact [fadl.musa@uaeu.ac.ae](mailto:fadl.musa@uaeu.ac.ae).

United Arab Emirates University  
College of Medicine and Health Sciences

EFFECTS OF THE ENDOCANNABINOID ANANDAMIDE ON  
EXCITABILITY AND CALCIUM SIGNALING IN RAT  
VENTRICULAR MYOCYTES

Lina Tareq Al-Kury

This dissertation is submitted in partial fulfillment of the requirements  
for the degree of Doctor of Philosophy

Under the direction of Dr. Murat Oz

May 2014

## **DECLARATION OF ORIGINAL WORK**

I, Lina Tareq Al-Kury, the undersigned, a graduate student at the United Arab Emirates University (UAEU) and the author of this dissertation entitled “Effects of the endocannabinoid anandamide on excitability and calcium signaling in rat ventricular myocytes”, hereby solemnly declare that this dissertation is an original work done and prepared by me under the guidance of Dr. Murat Oz, in the Collage of Medicine and Health Sciences at UAEU. This work has not previously formed the basis for the award of any degree, diploma or similar title at this or any other university. The materials borrowed from other sources and included in my dissertation have been properly acknowledged.

Student’s Signature.....

Date.....

Copyright © 2014 by Lina Tareq Al-Kury  
All Rights Reserved

**SIGNATURE PAGE**

Accepted by

Dean of the College: Professor Tar-Ching Aw

Signature..... Date.....

Dean of the College of Graduate Studies: Professor Nagi Wakim

Signature..... Date.....

## ABSTRACT

Endogenous cannabinoids (endocannabinoids) exert a wide range of biological effects. In addition to having their well-known neurobehavioral effects, a role for the major endocannabinoid anandamide (N-arachidonoyl ethanolamide; AEA), in the cardiovascular system in various pathological conditions has been reported. The aim of this thesis is to explore the effects of AEA on contractility,  $\text{Ca}^{2+}$  signaling, and action potential (AP) characteristics in rat ventricular myocytes. A video edge detection system was used to measure myocyte shortening. Intracellular  $\text{Ca}^{2+}$  was measured in cells loaded with the fluorescent indicator fura-2 AM. AEA (1  $\mu\text{M}$ ) caused a significant decrease in the amplitude of electrically-evoked myocyte shortening. The effect of AEA was not altered in the presence of pertussis toxin (PTX), AM251 and SR141716 ( $\text{CB}_1$  antagonists) or AM630 and SR 144528 ( $\text{CB}_2$  antagonists). AEA also caused a significant decrease in the amplitudes of electrically-evoked  $\text{Ca}^{2+}$  transients. However, the amplitudes of caffeine-evoked  $\text{Ca}^{2+}$  transients and the rate of recovery of electrically-evoked  $\text{Ca}^{2+}$  transients following caffeine application were not altered. In the whole-cell mode of patch-clamp technique, AEA (1  $\mu\text{M}$ ) significantly decreased the duration of APs. The inhibition was not altered in the presence of PTX, AM251 and AM630. Furthermore, AEA inhibited voltage-activated inward  $\text{Na}^+$  ( $I_{\text{Na}}$ ) and  $\text{Ca}^{2+}$  ( $I_{\text{L,Ca}}$ ) currents; major ionic currents shaping the APs in ventricular myocytes, in a voltage and PTX-independent manner. Cardiac  $\text{Na}^+/\text{Ca}^{2+}$  exchanger (NCX1)-mediated currents were also suppressed by AEA. The effect of AEA was not influenced by the inhibition of fatty acid amide hydrolase (FAAH) or in the presence of PTX, AM251 and AM630 or following the inclusion of GDP- $\beta$ -S in pipette solution. The results of this study indicate for the first time that impaired

Ca<sup>2+</sup> signaling underlies the negative inotropic actions of AEA in rat ventricular myocytes, and that the direct interaction of AEA with ion channel(s) shaping APs, mediates, at least in part, the effects of AEA on myocyte contractility. In addition, the results indicate for the first time that, under normal conditions, AEA can directly inhibit the activity of NCX1 in ventricular myocytes. In view of the massive release of various N-acylethanolamines (NAEs), including AEA, during cardiac ischemia and hypoxic conditions, further understanding of their mechanism(s) of action and target proteins is essential in the development of better treatment modalities under pathological conditions.

**Keywords:** Endocannabinoids, anandamide, myocyte shortening, voltage-activated inward Na<sup>+</sup> current, voltage-activated inward Ca<sup>2+</sup> current.



## ACKNOWLEDGMENTS

First and foremost, I would like to express my special appreciation and gratitude to my supervisor Dr. Murat Oz. He has been a tremendous mentor for me. He taught and guided me with remarkable patience, enthusiasm and understanding. I would like to thank him for encouraging my research and for allowing me to grow as a research scientist. His guidance and advice on my research have been priceless.

I sincerely thank the members of my thesis advisory committee, Prof. Chris Howarth, Prof. Sehamuddin Galadari and Dr. Rajesh Mohanraj for their brilliant comments, invaluable suggestions and encouragement throughout my graduate studies. I would also like to thank them for giving me the chance to work in their laboratories and for making me so welcome. In addition, I will always be thankful to Dr. Dymtro Isaev from Bogomoletz Institute of Physiology, Kiev, for his support and unfailing guidance.

Everyone in the laboratory has been helpful and made the past four years highly enjoyable. Special thanks go to Mr. Anwar Qureshi for his generous help in cardiac cell isolation and contractility studies. I would like to thank Dr. Nurulain for always being there to give help and for his useful suggestions and for helping me with statistical analysis. I would also like to express my deep thanks to Dr. Faisal Thayyullathil for his generous guidance in conducting the biochemical studies and for always being such a helpful person. Many thanks go to my friends and colleagues who always supported me, specially, Abrar Ashoor, Khawla Salim, Kholoud Arafat, Elham Al Kubaisy, Mohammad Mahgoub and Ramez Ali.

Words cannot express how grateful I am to my mother and father for all of the sacrifices that they have made on my behalf. I would not have got to this point without you. Special thanks go to my brothers Ahmad, Amjad and Ameer for their continuous encouragement. My mother-in-law, your prayers for me were what has sustained me thus far. My deep appreciation goes to my husband Mohammad for his continuous help during the course of my study. He was always my support in the moments when there was no one to answer my queries.

## **DEDICATION**

DEDICATED TO MY HUSBAND AND MY BELOVED CHILDREN

AYA AND FARIS

## TABLE OF CONTENTS

DECLARATION OF ORIGINAL WORK.....	II
SIGNATURE PAGE .....	IV
ABSTRACT .....	VI
ACKNOWLEDGMENTS.....	VIII
DEDICATION .....	X
TABLE OF CONTENTS.....	XI
LIST OF TABLES.....	XV
LIST OF FIGURES .....	XVI
LIST OF ABBREVIATIONS .....	XVIII
1. INTRODUCTION .....	1
1.1. Cardiac cell electrophysiology .....	1
1.1.1 Cardiac action potential .....	1
1.1.2 Cardiac inward ion currents .....	5
1.1.2.1 Voltage-gated Na <sup>+</sup> channels .....	5
1.1.2.2 Voltage-gated Ca <sup>2+</sup> channel.....	9
1.1.3 Myocardial Ca <sup>2+</sup> handling.....	13
1.1.4 Role of the Na <sup>+</sup> /Ca <sup>2+</sup> exchanger in calcium homeostasis .....	17
1.2. The endocannabinoid system .....	20
1.2.1 Introduction.....	20
1.2.2 Endocannabinoids.....	21
1.2.3 Endocannabinoid receptors.....	25
1.2.4 Synthesis and metabolism of anandamide .....	26
1.2.5 Cellular and molecular mechanisms of endocannabinoid actions....	30
1.2.5.1 Signal transduction mechanisms.....	30
1.2.5.2 Receptor-dependent and independent effects of endocannabinoids on voltage-gated ion channels.....	36
1.2.5.2.1 Effects on Na <sup>+</sup> channels.....	36
1.2.5.2.2 Effects on Ca <sup>2+</sup> channels.....	37
1.2.6 Role of endocannabinoids in the cardiovascular system .....	42
1.2.6.1 Cardiovascular effects of endocannabinoids <i>in vivo</i> .....	43
1.2.6.2 Cardiovascular effects of endocannabinoids <i>in vitro</i> .....	47
1.2.6.3 Endocannabinoid system in cardiovascular disease .....	51

2. MATERIALS AND METHODS .....	57
2.1 Experimental animals .....	57
2.2 Ventricular myocyte isolation .....	57
2.3 Measurement of ventricular myocyte shortening .....	59
2.4 Western immunoblot assay .....	64
2.5 Measurement of intracellular Ca <sup>2+</sup> concentration .....	65
2.6 Measurement of sarcoplasmic reticulum Ca <sup>2+</sup> content .....	67
2.7 Assessment of myofilament sensitivity to Ca <sup>2+</sup> .....	67
2.8 Electrophysiological recording of whole-cell currents (Patch clamp technique) .....	68
2.8.1 Pipettes .....	68
2.8.2 Seal Penetration .....	68
2.8.3 Measurement of action potentials .....	72
2.8.3.1 Protocol for measuring action potentials .....	72
2.8.3.2 Solutions .....	73
2.8.4 Measurement of Na <sup>+</sup> currents .....	73
2.8.4.1 Protocol for measuring Na <sup>+</sup> currents .....	73
2.8.4.2. Solutions .....	75
2.8.5 Measurement of L-type Ca <sup>2+</sup> currents .....	75
2.8.5.1 Protocol for measuring L-type Ca <sup>2+</sup> currents .....	75
2.8.5.2 Solutions .....	76
2.8.6 Measurement of Na <sup>+</sup> /Ca <sup>2+</sup> exchanger currents in cardiomyocytes ...	76
2.8.6.1 Protocol for measuring Na <sup>+</sup> /Ca <sup>2+</sup> exchanger currents .....	76
2.8.6.2 Solutions .....	77
2.9 Biochemical assessment of cell viability and membrane integrity of ventricular cardiomyocytes .....	77
2.9.1 MTT cell viability assay .....	77
2.9.2 Homogenous membrane integrity assay .....	78
2.10 Preparation of drugs and stock solutions .....	80
2.10.1 Anandamide and methanandamide .....	80
2.10.2 Cannabinoid receptor antagonists .....	80
2.10.3 Pertussis toxin .....	81
2.10.4 Indomethacin .....	81
2.10.5 URB597 .....	82

2.10.6 <i>N</i> -ethylmaleimide .....	82
2.10.7 Clenbuterol.....	82
2.10.8 BRL-37344.....	82
2.11 Data analysis .....	83
3. RESULTS.....	84
3.1 Anandamide inhibits ventricular myocyte shortening.....	84
3.2 Ventricular myocytes express cannabinoid receptors .....	88
3.3 Cannabinoid receptors are not involved in the effect of anandamide on myocyte shortening .....	88
3.4 Anandamide inhibits intracellular Ca <sup>2+</sup> transients.....	92
3.5 Anandamide has no effect on sarcoplasmic reticulum (SR) Ca <sup>2+</sup> transport	95
3.6 Anandamide has no effect on myofilament sensitivity to Ca <sup>2+</sup> .....	95
3.7 Anandamide suppresses the action potentials in ventricular myocytes.....	98
3.8 Cannabinoid receptors are not involved in the effect of anandamide on the action potentials in ventricular myocytes .....	105
3.9 Anandamide inhibits voltage-dependent Na <sup>+</sup> channels in ventricular myocytes .....	105
3.10 Anandamide inhibits voltage-dependent Ca <sup>2+</sup> channels in ventricular myocytes .....	113
3.11 Anandamide inhibits Na <sup>+</sup> /Ca <sup>2+</sup> exchanger in ventricular myocytes.....	126
3.12 Anandamide has no effect on cell viability in ventricular myocytes .....	135
3.13 Anandamide has no effect on membrane integrity in ventricular myocytes .....	135
4. DISCUSSION.....	138
4.1 Myocyte shortening and intracellular Ca <sup>2+</sup> measurements experiments ...	139
4.2 Involvement of cannabinoid receptors in the negative inotropic effect ....	142
4.3 Action potential measurements .....	144
4.4 Experiments with voltage-dependent Na <sup>+</sup> channels .....	145
4.5 Experiments with voltage-dependent Ca <sup>2+</sup> channels.....	147
4.6 Experiments with cardiac Na <sup>+</sup> /Ca <sup>2+</sup> exchanger.....	150
4.7 Mechanism of action of AEA .....	152
5. CONCLUSION.....	159
6. LIMITATIONS AND FUTURE WORK.....	160
7. BIBLIOGRAPHY .....	162

APPENDIX ..... 190

## LIST OF TABLES

Table 1.1 Subunit composition and function of Ca <sup>2+</sup> channel types .....	12
--	----



## LIST OF FIGURES

Figure 1.1 Cardiac action potential and cardiac ion currents .....	3
Figure 1.2 Structure of voltage-gated Na <sup>+</sup> channel .....	6
Figure 1.3 Structure of voltage gated Ca <sup>2+</sup> channel.....	10
Figure 1.4 Ca <sup>2+</sup> -induced Ca <sup>2+</sup> release and Ca <sup>2+</sup> cycling in a cardiac cell .....	15
Figure 1.5 Hypothetical functional organization of Na <sup>+</sup> /Ca <sup>2+</sup> exchanger .....	19
Figure 1.6 Chemical structures of the proposed endocannabinoids .....	23
Figure 1.7 Chemical structures of anandamide and related N-acylethanolamines	24
Figure 1.8 Mechanisms of anandamide formation and deactivation.....	27
Figure 1.9 Typical traces showing the influence of AEA on cardiovascular parameters in anaesthetized rat.....	44
Figure 2.1 Langendorff apparatus .....	58
Figure 2.2 Micrographs of ventricular cells .....	60
Figure 2.3 The recording system used for video edge detection and Ca <sup>2+</sup> imaging experiments .....	61
Figure 2.4 Video edge motion detection.....	63
Figure 2.5 Patch clamp experimental setup: .....	69
Figure 2.6 Schematic presentation of whole cell configuration of patch clamp technique. ....	71
Figure 2.7 Release of LDH from damaged cells: .....	79
Figure 3.1 Effects of AEA and metAEA on ventricular myocyte shortening: .....	85
Figure 3.2 Effects of preincubation with URB597 or indomethacin on AEA- induced inhibition of ventricular myocyte shortening .....	87
Figure 3.3 Expression of CB <sub>1</sub> and CB <sub>2</sub> receptors in rat heart .....	89
Figure 3.4 Effects of cannabinoid receptor antagonists on AEA-induced inhibition of cardiomyocyte shortening:.....	90
Figure 3.5 Effects of pertussis toxin and <i>N</i> -ethylmaleimide on AEA-induced inhibition of cardiomyocyte shortening .....	91
Figure 3.6 Effect of pretreatment with PTX or NEM on G-protein mediated inhibition of cardiomyocyte shortening by clenbuterol.....	93
Figure 3.7 Effects of AEA on amplitude and time-course of intracellular Ca <sup>2+</sup> in ventricular myocytes.....	94
Figure 3.8 Effect of AEA on sarcoplasmic reticulum Ca <sup>2+</sup> transport.....	96
Figure 3.9 Effect of AEA on myofilament sensitivity to Ca <sup>2+</sup> .....	97
Figure 3.10 Effect of AEA on the excitability of ventricular myocytes.....	100
Figure 3.11 Summary of the effect of AEA on the amplitude and the shape of APs in cardiomyocytes.....	101
Figure 3.12 Effects of high concentration of AEA on the excitability of ventricular myocytes .....	103
Figure 3.13 Summary of the effect of high concentration of AEA on the amplitude and the shape of APs in cardiomyocytes .....	104

3.14 Effect of cannabinoid receptor antagonists and PTX pretreatment on AEA-induced changes in myocyte excitability .....	107
Figure 3.15 Effect of AEA on $I_{Na}$ in rat ventricular myocytes.....	108
Figure 3.16 Effect of increasing AEA and vehicle concentrations on $I_{Na}$ recorded in rat ventricular myocytes .....	110
Figure 3.17 Effect of AEA on steady state activation and inactivation of $I_{Na}$ in rat ventricular myocytes .....	112
Figure 3.18 Effect of PTX pretreatment on AEA inhibition of the maximal $I_{Na}$ amplitudes. ....	114
Figure 3.19 Effect of AEA on $I_{L,Ca}$ in rat ventricular myocytes .....	115
Figure 3.20 Effects of increasing AEA and vehicle concentrations on $I_{L,Ca}$ recorded in rat ventricular myocytes .....	117
Figure 3.21 Effect of AEA on steady state activation and inactivation of $I_{L,Ca}$ in rat ventricular myocytes.....	119
Figure 3.22 Effect of sidedness of AEA application on $I_{L,Ca}$ in rat ventricular myocytes .....	120
Figure 3.23 Effect of AEA on $Ba^{2+}$ currents mediated by L-type VGCCs.....	122
Figure 3.24 Effects of cannabinoid receptor antagonists on AEA inhibition of L-type VGCCs .....	123
Figure 3.25 Effects of PTX pretreatment on AEA inhibition of L-type VGCCs	124
Figure 3.26 Effect of PTX pretreatment on BRL-37344 inhibition of $I_{L,Ca}$ recorded in rat ventricular myocytes .....	125
Figure 3.27 Effect of AEA on $I_{NCX1}$ in rat ventricular myocytes .....	128
Figure 3.28 Effect of increasing AEA concentration on $I_{NCX1}$ in rat ventricular myocytes .....	130
Figure 3.29 Effects of metAEA and URB597 on $I_{NCX1}$ in rat ventricular myocytes .....	131
Figure 3.30 Effects of cannabinoid receptor antagonists on AEA inhibition of $I_{NCX1}$ recorded in ventricular cardiomyocytes .....	133
Figure 3.31 Effects of PTX pretreatment and intracellular application of GDP- $\beta$ -S on AEA inhibition of $I_{NCX1}$ in ventricular cardiomyocytes.....	134
Figure 3.32 Effect of AEA on morphological characteristics and cell viability of ventricular cardiomyocytes .....	136
Figure 3.33 Cytotoxicity of AEA as assessed by LDH assay .....	137
Figure 4.1 Proposed model for the actions of AEA on cellular excitability.....	155

## LIST OF ABBREVIATIONS

- [<sup>3</sup>H]BTX-B: [<sup>3</sup>H] Batrachotoxinin A20- $\alpha$ -benzoate
- 2-AG: 2-arachidonylglycerol
- AA: Arachidonic acid
- AC: Adenylyl cyclase
- ACEA: Arachidonoyl-2 Chloroethylamide
- ACPA: Arachidonoyl cyclopropylamide
- AEA: N-arachidonylethanolamine (anandamide)
- AMT: Anandamide membrane transporter
- AP: Action potential
- APD<sub>60</sub>: Action potential duration at 60% level of repolarization
- BK<sub>Ca</sub> Channels: Large conductance Ca<sup>2+</sup>-activated K<sup>+</sup> channels
- CB<sub>1</sub>: Cannabinoid receptor 1
- CB<sub>2</sub>: Cannabinoid receptor 2
- CGRP: Calcitonin gene-related peptide
- CHO: Chinese hamster ovary
- DA: Dopamine
- DHP: Dihydropyridine
- DMSO: Dimethyl sulphoxide
- DOX: Doxorubicin
- ECS: Endocannabinoid system
- FAAH: Fatty acid amide hydrolase
- G<sub>i/o</sub>: Inhibitory G protein
- GPCRs: G-protein coupled receptors
- HRP: Horseradish peroxidase
- I<sub>L,Ca</sub>: L-type Ca<sup>2+</sup> current

$I_{Na}$ :  $Na^+$  current  
 $I_{NCX1}$ :  $Na^+/Ca^{2+}$  exchanger current  
 $I_{to}$ : Transient outward current  
 $I-V$ : Current-voltage relationship  
 $K_{IR}$ : Inwardly rectifying  $K^+$  channels  
LDH: Lactate dehydrogenase  
MAGL: Monoacylglycerol lipase  
MAPK: Mitogen-activated protein kinase  
MetAEA: Methanandamide  
MTT: 3-(4,5-dimethylthiazol-2-yl)-2,5-diphenyl tetrazolium  
NADA: N-arachidonoyl-dopamine  
NAEs: N-acylethanolamines  
NAPE: N-arachidonoyl phosphatidyl ethanolamine  
NAPE-PLD: NAPE-selective phospholipase D  
NCX: Sodium-calcium exchanger  
NEM: N-ethylmaleimide  
NO: Nitric oxide  
NOS: Nitric oxide synthase  
NT: Normal Tyrode  
OEA: Oleoylethanolamide  
PBS: Phosphate buffer solution  
PEA: Palmitoylethanolamide  
PIP<sub>2</sub>: Phosphatidylinositol-4,5-biphosphate  
PKA: Protein kinase A  
PKC: Protein kinase C  
PLB: Phospholamban  
PLC: Phospholipase C

PPARs: Peroxisome proliferator-activated receptors

PTX: Pertussis toxin

RCL: Resting cell length

ROS: Reactive oxygen species

RyR2: Ryanodine receptor 2

SERCA: SR Ca<sup>2+</sup>-ATPase

SR: Sarcoplasmic reticulum

SSA: Steady state activation

SSI: Steady state inactivation

TEA: Tetraethylammonium

T<sub>HALF</sub> relaxation: Time from peak to half relaxation

THC: Δ<sup>9</sup>-tetrahydrocannabinol

TnC: Troponin C

TnI: Troponin I

TnT: Troponin

TPK: Time to peak

TRP channel: Transient receptor potential channel

TRPV1 receptor: Transient receptor potential vanilloid receptor 1

TTX: Tetrodotoxin

V<sub>1/2</sub>: Voltage of half-maximal activation

VGCCs: Voltage-gated calcium channels

VGICs: Voltage-gated ion channels

VGSCs: Voltage-gated sodium channels

V<sub>rev</sub>: Reversal potential

τ<sub>i</sub>: Inactivation time constants.

# 1. INTRODUCTION

## 1.1. Cardiac cell electrophysiology

### 1.1.1 Cardiac action potential

Physiological function of the heart results from the periodic execution of a series of coordinated and interdependent mechanical, chemical, and electrical processes within the cardiac tissue. An important event central to these processes is the cardiac action potential (AP) and the mechanism by which this electrical excitation initiates cardiac muscle contraction is called excitation-contraction coupling.

The AP of a cardiac cell arises from the coordinated opening and closing (gating) of ion channels; membrane proteins that control ion passage across cell membranes and constitute the molecular foundation for the generation of APs. Depending on the cell type, the transmembrane voltage in resting cardiac tissue cells ranges from -60 mV to -90 mV, where the intracellular space is negatively charged with respect to the extracellular space due to the differences in ion concentration that exist between the intracellular and the extracellular milieu (Grant, 2009). This concentration difference not only gives rise to diffusion of ions across the membrane, but also generates a potential difference that counteracts the diffusion and determines the electrochemical equilibrium according to the Nernst Equation (Kettenmann, et al., 1983). It is also important to note that due to involvement of multiple ions, the sum of conductances of different ion channels determines the final value of the resting membrane potential.

The electrophysiological characteristics of excitable cells are shaped in large part by the regulation of voltage-gated ion channels (VGICs). These channels are deemed voltage-gated since changes in membrane potential lead to alterations in their conformation or gating characteristics. Voltage-gated ion channels comprise three main families:  $\text{Na}^+$ ,  $\text{Ca}^{2+}$  and  $\text{K}^+$  channels (Bezanilla, 2005). In general, at any given moment, VGICs can be found in one of three gating states; closed, open, or inactive (Karmazinova and Lacinova, 2010). Channels in their closed state can be opened by an appropriate change in membrane potential. Channels in their open state allow the generation of ionic conductance for a particular permeable ion. However, in the inactive state, channels at depolarized potentials enter a transient non-conducting refractory period in which no changes in membrane potential can re-open them. After this refractory period, inactive channels can return to their closed state and become available for the generation of the next AP (Bähring and Covarrubias, 2011).

The AP in a ventricular muscle cell lasts for 200-300 ms and is divided into five sequential phases: resting (phase 4), upstroke (phase 0), early repolarization (phase 1), plateau (phase 2), and final repolarization (phase 3) (figure 1.1) (Amin, et al., 2010). At the resting membrane potential,  $\text{Na}^+$  and  $\text{Ca}^{2+}$  channels are mainly in the closed state and the activity of  $\text{K}^+$  channels, especially the inwardly rectifying  $\text{K}^+$  ( $\text{K}_{\text{IR}}$ ) channels, determine the resting membrane potential. Because the resting state has higher permeability to  $\text{K}^+$ , resting membrane potential of most ventricular cardiomyocytes stabilizes near the voltage required to oppose the  $\text{K}^+$  concentration gradient, i.e., the  $\text{K}^+$  equilibrium potential (Chung and Kuyucak, 2002). Upon the arrival of a brief, suprathreshold depolarizing stimulus, voltage-gated  $\text{Na}^+$  channels (VGSCs) in the resting state

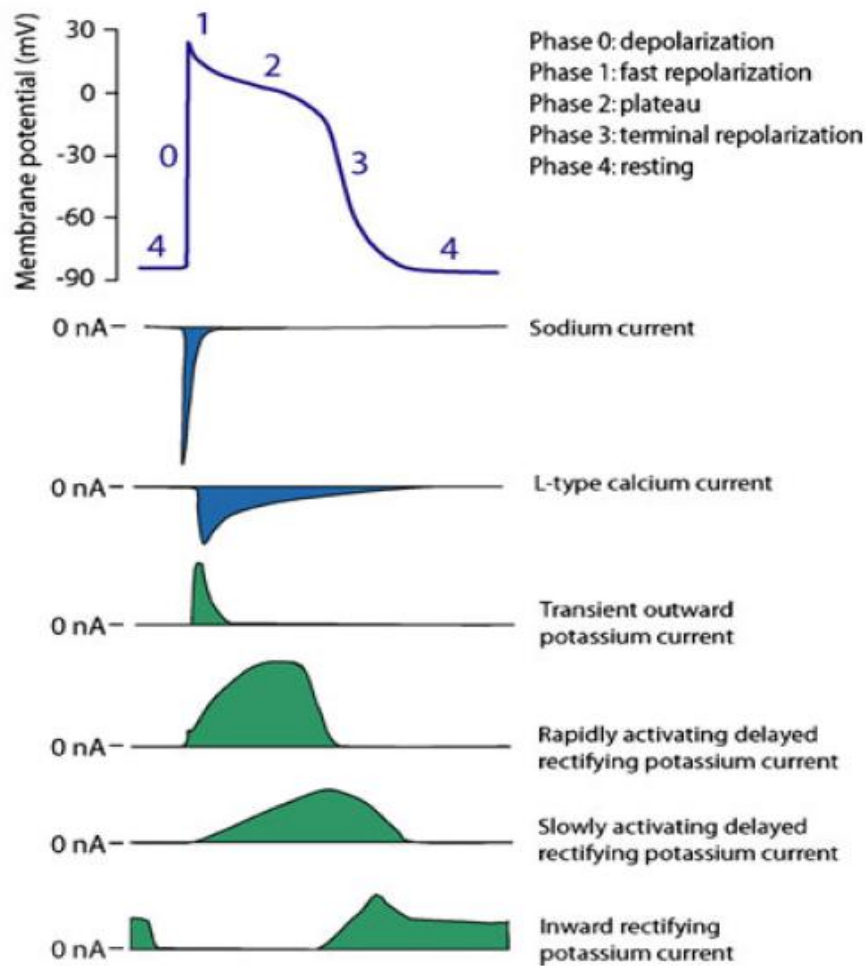


**Figure 1.1 Cardiac action potential and cardiac ion currents:** The cardiac action potential is generated by transmembrane inwardly and outwardly directed ion currents. The inward (depolarizing)  $\text{Na}^+$  and  $\text{Ca}^{2+}$  currents point downwards. The outward (repolarizing)  $\text{K}^+$  currents are pointed upwards. Adapted from Amin, *et al.*, 2010.



begin to open allowing for the rapid influx of  $\text{Na}^+$  ions into the cell down their electrochemical gradient. The influx of positively charged  $\text{Na}^+$  ions further depolarizes the membrane resulting in the opening of more  $\text{Na}^+$  channels and progressively increasing  $\text{Na}^+$  influx (phase 0). This fast feed forward mechanism will bring the membrane potential towards  $\text{Na}^+$  equilibrium value which is about 20 mV. It is important to note that this initial depolarizing phase is central to fast impulse propagation within the cardiac muscle. During depolarization,  $\text{Na}^+$  channels rapidly enter their inactive state in which no amount of stimulus will re-open them and  $\text{Na}^+$  current decays within a few milliseconds (Grant, 2009; Moreno, et al., 2012). Following this initial upstroke, a first repolarization phase, coined phase 1, is initiated by the opening of a particular  $\text{K}^+$  channel that generates a transient outward current ( $I_{to}$ ) and causes a repolarizing notch in the AP (Dong, et al., 2006). Meanwhile, the  $\text{Ca}^{2+}$  channels, which exhibit slower kinetics than  $\text{Na}^+$  channels, also open in response to depolarization leading to a period of prolonged (100-200 ms) depolarization of the membrane potential called the plateau phase of the AP (phase 2). This plateau phase results from a delicate balance between depolarizing (inward) and repolarizing (outward) currents (Qu and Chung, 2012). During the prolonged depolarization, VGCCs begin to inactivate, while delayed rectifier  $\text{K}^+$  channels begin to activate. Eventually, the prevailing repolarizing current carried by  $\text{K}^+$  channels brings the membrane back towards the resting membrane potential (phase 3) (Moreno, et al., 2012; Grant, 2009). As mentioned earlier, the resting state of the AP (phase 4) is maintained by the  $\text{K}_{IR}$ . This channel is the primary conductance controlling the resting potential, and permitting a significant repolarizing current during the terminal stage of the AP (Wu, et al., 2012).

The characteristic shape of the AP changes significantly across the myocardial wall from the endocardium, midmyocardium, to epicardium. For example, epicardial cells have a prominent phase 1 and a shorter duration of AP (Voitychuk, et al., 2012). On the other hand, AP duration is the longest in the midmyocardial region of ventricular muscle (Antzelevitch, et al., 1991; Grant, 2009).

## **1.1.2 Cardiac inward ion currents**

### **1.1.2.1 Voltage-gated Na<sup>+</sup> channels**

Voltage-gated Na<sup>+</sup> channels (VGSCs) play an essential role in the initiation and propagation of APs in neurons and other excitable cells such as cardiac myocytes (Catterall, et al., 2005a). The voltage-gated Na<sup>+</sup> channel is a large multimeric complex, consisting of an  $\alpha$  subunit associated with auxiliary  $\beta$  subunits (Figure 1.2) (Catterall, 2012). The pore forming  $\alpha$  subunit is large (molecular weight is about 227 kDa) and is sufficient for functional expression, but the kinetics and the voltage dependence of channel gating are modified significantly in the presence of the  $\beta$  subunits. In the heart, the Na<sup>+</sup> channels contain  $\beta_1$  through  $\beta_4$  subunits. These auxiliary subunits are involved in channel localization and interaction with cell adhesion molecules, extracellular matrix and intracellular cytoskeleton (Catterall, et al., 2005a).

Analysis of the primary sequence predicts that the  $\alpha$  subunit folds into four main domains (I-IV), that are similar to one another and contain six transmembrane  $\alpha$  helices (S1-S6). In each of the domains, the voltage sensor is located in the S4 segments which contain positively charged amino acid residues at every third position. These residues move across the membrane to initiate

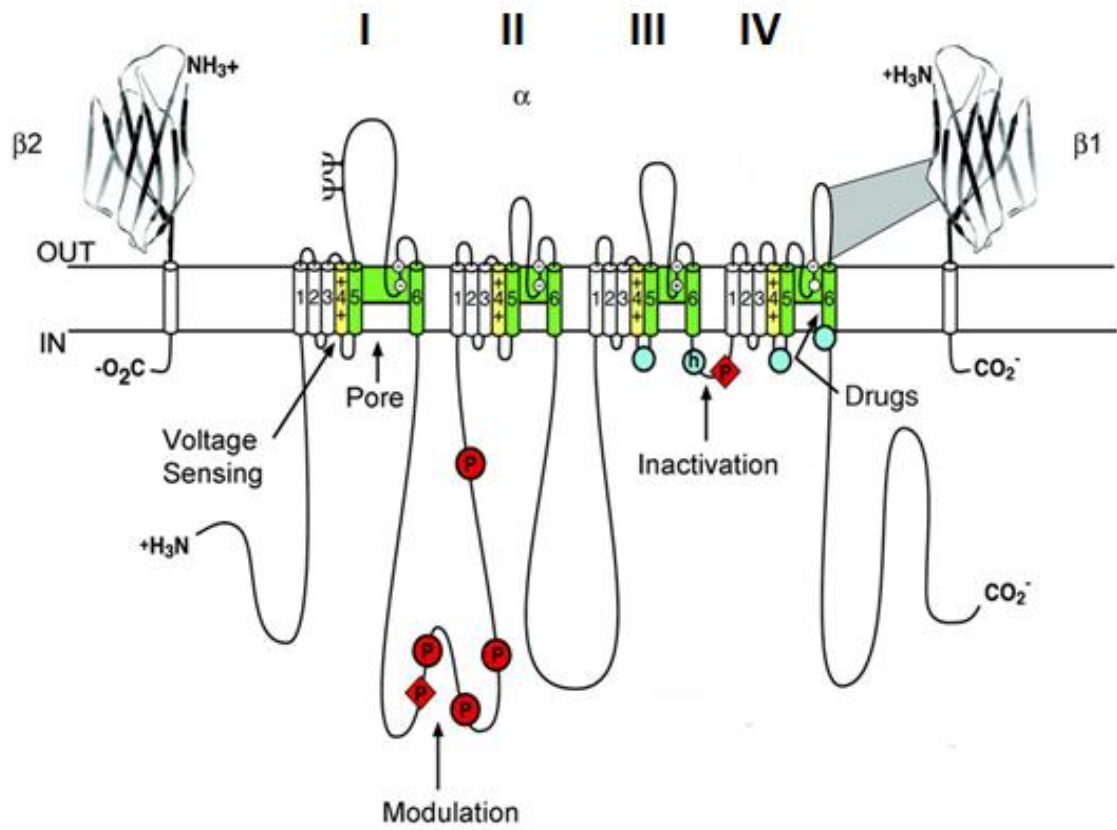


**Figure 1.2 Structure of voltage-gated Na<sup>+</sup> channel:** The  $\alpha$  subunit of Na<sup>+</sup> channel is illustrated together with the  $\beta 1$  and  $\beta 2$  subunits. Roman numerals indicate the  $\alpha$  subunit domains; segments 5 and 6 are the pore-lining segments and the S4 helices make up the voltage sensors. Modified from Catterall, 2012.

channel activation in response to membrane depolarization. The short intracellular loop connecting the homologous domains III and IV serves as the inactivation gate, folding into the channel structure and blocking the pore from the inside during sustained depolarization of the membrane. A re-entrant loop between helices S5 and S6 is embedded into the transmembrane region of the channel in order to form the narrow ion-selective filter at the extracellular end of the pore. The wider intracellular end of the pore is formed by the four S6 segments. Small extracellular loops connect the transmembrane segments, with the largest ones connecting the S5 or S6 segments to the membrane re-entrant loop (Yu and Catterall, 2003; Catterall, et al., 2005a).

According to the primary sequence of the  $\alpha$  subunit, nine subtypes of  $\text{Na}^+$  channels ( $\text{Na}_v1.1$ - $\text{Na}_v1.9$ ) have been functionally characterized (Dib-Hajj, et al., 2009; Yu and Catterall, 2003; Catterall, et al., 2005a). The nine  $\text{Na}^+$  channel isoforms are greater than 50% identical in amino acid sequence in the transmembrane and extracellular domains (Catterall, et al., 2005a). Generally,  $\text{Na}_v1.1$  and  $\text{Na}_v1.3$  are localized in the soma of the neuron, while  $\text{Na}_v1.2$  subtype is expressed mainly in unmyelinated axons. Moreover,  $\text{Na}_v1.1$  and  $\text{Na}_v1.6$  subtypes are highly expressed in peripheral nervous system, and  $\text{Na}_v1.4$  and  $\text{Na}_v1.5$  subtypes are found in skeletal and cardiac myocytes, respectively (Rogart, et al., 1989). Cardiac  $\text{Na}^+$  channels ( $\text{Na}_v1.5$ ) have a conductance of 19-22 pS (Catterall, et al., 2005a). The fraction of channels available for opening varies from about 100 % at -90 mV to zero at around -40 mV (Yu and Catterall, 2003; Grant, 2009).

The cardiac  $\text{Na}_v1.5$  channel has consensus sites for phosphorylation by protein kinase A (PKA), protein kinase C (PKC) and  $\text{Ca}^{2+}$ -calmodulin kinase

(Catterall, et al., 2005a). Moreover, biochemical studies have shown that purified  $\text{Na}^+$  channels are phosphorylated by the cAMP-dependent PKA and PKC at multiple sites in the intracellular loop between domains I and II (Cantrell and Catterall, 2001). Although, in earlier studies,  $\text{Na}^+$  currents have been shown to be modulated by the cAMP pathway, the results of these experiments are not conclusive; some studies reporting a decrease, whereas others reporting an increase in the  $\text{Na}^+$  current (Ono, et al., 1989; Kirstein, et al., 1996; Frohnwieser, et al., 1997). However, functional studies have consistently found that phosphorylation of the channel by PKC results in a decrease in  $I_{\text{Na}}$  (Murray, et al., 1997; Hallaq, et al., 2012). In a recent study, it was reported that a mutation in glycerol-3 phosphate dehydrogenase like 1 kinase was associated with Brugada syndrome, and resulted in differential modulation of  $\text{Na}^+$  channel activity. In this study, *in vitro* expression of the channel showed that mutated enzyme action is associated with a decrease in  $I_{\text{Na}}$  (London, et al., 2007).

Modulation of  $\text{Na}^+$  channel currents is undoubtedly important *in vivo*, although specific deficits that directly affect the function of  $\text{Na}^+$  channel are not yet known. In the heart, point mutations and deletions in  $\text{Na}_v1.5$  cause long QT syndrome and idiopathic ventricular fibrillation due to a slow and an incomplete inactivation of the cardiac  $\text{Na}^+$  current resulting in prolongation of the AP (Keating and Sanguinetti, 2001). It has also been shown that mutations that subtly alter  $\text{Na}^+$  channel function, can lead to human diseases of hyperexcitability (Yu and Catterall, 2003).

Besides genetic modification, various pharmacological agents also modify the function of  $\text{Na}^+$  channels. For example,  $\text{Na}^+$  channels are activated by a number of compounds such as veratridine, batrachotoxin and aconitine, and

blocked by tetrodotoxin (TTX), saxitoxin, local anesthetics and antiarrhythmic drugs (Yu and Catterall, 2003). In this context, it is important to note that although neuronal Na<sup>+</sup> channels have high sensitivity to TTX (in nanomolar concentration), cardiac Na<sup>+</sup> channels are only affected at micromolar concentration and therefore, are called TTX-resistant Na<sup>+</sup> channels (Zimmer, 2010).

### **1.1.2.2 Voltage-gated Ca<sup>2+</sup> channel**

Voltage-gated Ca<sup>2+</sup> channels (VGCCs) are key transducers of membrane potential changes into intracellular Ca<sup>2+</sup> transients that initiate various physiological events, ranging from neurotransmitter release to muscle contraction (Catterall, et al., 2005b). Voltage-gated Ca<sup>2+</sup> channels consist of five subunits called  $\alpha_1$ ,  $\alpha_2$ ,  $\gamma$ ,  $\beta$ , and  $\delta$  of which  $\alpha_1$  constitutes the pore forming subunit (Figure 1.3). The associated subunits have several functions including regulation of channel trafficking and modulation of current kinetics (Bodi, et al., 2005). The channel protein forming the  $\alpha_1$  subunit consists of more than 2000 amino acids (molecular weight ~170 kDa) and contains four homologous domains (I-IV). Each domain contains six transmembrane segments (S1-S6) and a membrane associated loop between S5 and S6 segments. The S4 segment of each homologous domain serves as the voltage sensor for activation; moving outward and rotating under the influence of the electric field and initiating a conformational change that leads to the opening of the pore. The S5 and S6 segments and the membrane-associated pore loop between them form the pore lining of the VGCC (Catterall, 2011; Grant, 2009). Each of the four pore-lining loops (P-I through P-IV) of each domain contributes a glutamate residue (E) to the pore structure. These conserved residues (EEEE) in the pore have been shown to be critical for Ca<sup>2+</sup> selectivity of the channel (Sather and McCleskey, 2003). Expression of the  $\alpha_1$  subunit is sufficient

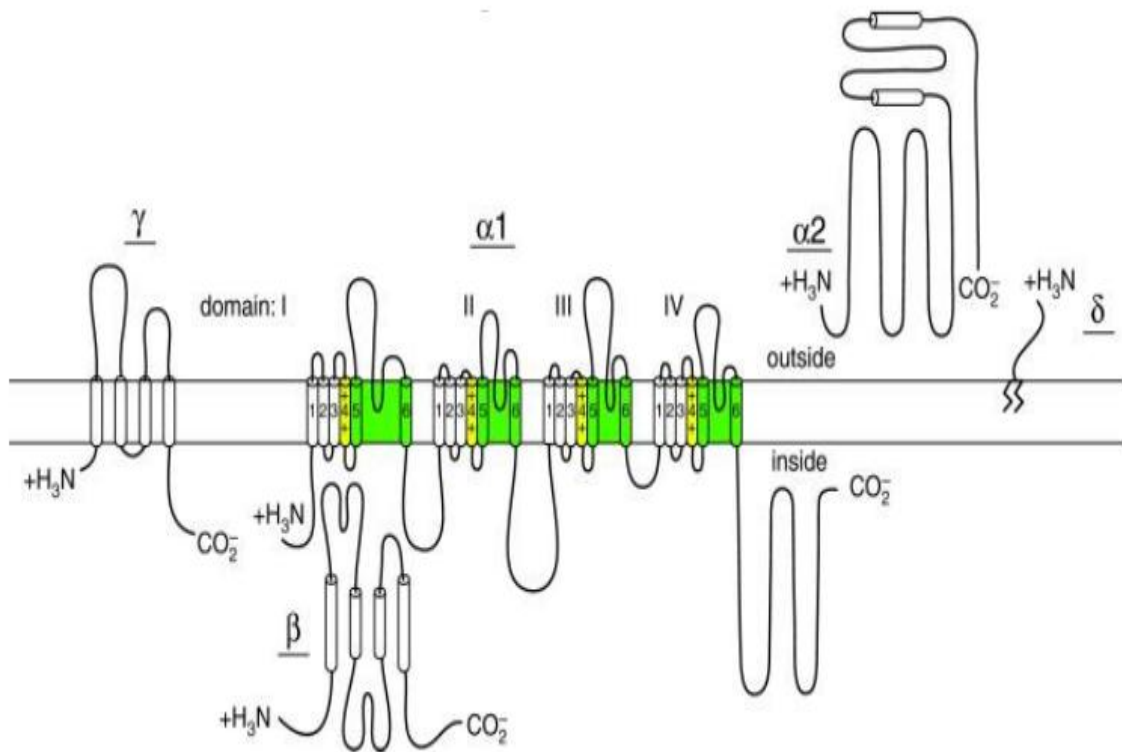


**Figure 1.3 Structure of voltage gated  $\text{Ca}^{2+}$  channel:** The  $\alpha$  subunit of  $\text{Ca}^{2+}$  channel is illustrated together with the  $\beta$ ,  $\gamma$  and  $\alpha_2\delta$  subunits. Roman numerals indicate the domains of  $\alpha$  subunit; segments 5 and 6 are the pore-lining segments and the S4 helices make up the voltage sensors. Adapted from Catterall, 2011.

to produce a functional  $\text{Ca}^{2+}$  channel, but it displays low expression level, abnormal kinetics, and voltage dependence (Perez-Reyes, et al., 1989). Studies have shown that co-expression of  $\alpha_2\delta$  subunit and  $\beta$  subunit enhances the level of expression and confers more physiological gating properties (Lacerda, et al., 1991; Singer, et al., 1991).

To date, ten subtypes of VGCCs have been described in mammals (Table 1). These subtypes serve distinct roles in signal transduction and other cellular functions (Catterall, 2011). The L-type subfamily (or  $\text{Ca}_v1$ ) of VGCCs initiate contraction, secretion, regulation of gene expression and integration of synaptic input in neurons (Minor, Jr. and Findeisen, 2010). The neuronal  $\text{Ca}_v2$  subfamily which includes the N-type ( $\text{Ca}_v2.1$ ), P/Q-type ( $\text{Ca}_v2.2$ ), and R-type ( $\text{Ca}_v2.3$ ) channels is responsible for initiation of synaptic transmission at fast synapses (Catterall, et al., 2005b). The T-type channels (or  $\text{Ca}_v3$ ) are important for repetitive firing of action potentials in rhythmically firing cells such as cardiac cells (Minor, Jr. and Findeisen, 2010; Catterall, 2011).

In cardiac muscle, the two types of VGCCs, the L-type (long lasting)  $\text{Ca}^{2+}$  channels and the T-type (transient)  $\text{Ca}^{2+}$  channels play an important role in muscle contraction and automaticity, respectively (Grant, 2009). There are four  $\alpha_1$  subunit variants of the L-type  $\text{Ca}^{2+}$  channels:  $\text{Cav}1.1$  ( $\alpha_{1S}$ ),  $1.2$  ( $\alpha_{1C}$ ),  $1.3$  ( $\alpha_{1D}$ ) and  $1.4$  ( $\alpha_{1F}$ ) of which  $\text{Cav}1.2$  ( $\alpha_{1C}$ ) subunit is the cardiac specific L-type  $\text{Ca}^{2+}$  channel subunit (Table 1.1) (Minor, Jr. and Findeisen, 2010).

In the presence of  $\text{Ca}^{2+}$ , the currents are rapidly inactivated via a  $\text{Ca}^{2+}$ /calmodulin-dependent mechanism (Ferreira, et al., 1997). This process is crucial for limiting  $\text{Ca}^{2+}$  entry during long cardiac APs. Moreover, reuptake of  $\text{Ca}^{2+}$  by the sarcoplasmic reticulum (SR) during prolonged depolarization can



<b>Ca<sup>2+</sup> current type</b>	<b>α1 subunits</b>	<b>Conductance, pS</b>	<b>Activation threshold</b>	<b>Inactivation rate</b>	<b>Location and Functions</b>	<b>References</b>
<b>L</b>	Cav1.1 Cav1.2 Cav1.3 Cav1.4	25	High	Slow	Excitation contraction coupling in muscle, cardiac pacemaking, endocrine secretion and neuronal Ca <sup>2+</sup> transients	Bodi, et al., 2005; Catterall, et al., 2005b; Cens, et al., 2006.
<b>N</b>	Cav2.1	20	High	Moderate	Neurons only; neurotransmitter release	Catterall, et al., 2005b; Minor, Jr. and Findeisen, 2010.
<b>P/Q</b>	Cav2.2	10-20	High	Fast	Neurons only; neurotransmitter release	Catterall, et al., 2005b; Minor, Jr. and Findeisen, 2010.
<b>R</b>	Cav2.3	-	High	-	Neurons only; neurotransmitter release	Catterall, et al., 2005b; Minor, Jr. and Findeisen, 2010.
<b>T</b>	Cav3.1 Cav3.2 Cav3.3	5-10	Low	Fast	Cardiac sinoatrial node, neurons; repetitive spiking and spike activity	Catterall, et al., 2005b; Minor, Jr. and Findeisen, 2010; Catterall, 2011.

**Table 1.1 Subunit composition and function of Ca<sup>2+</sup> channel types**

result in the recovery from  $\text{Ca}^{2+}$ -dependent inactivation, and enable secondary depolarization (Grant, 2009). The carboxyl termini of L-type  $\text{Ca}^{2+}$  channels have multiple  $\text{Ca}^{2+}$  binding sites and  $\text{Ca}^{2+}$ /calmodulin-dependent kinase activity. Binding of calmodulin to these domains has been shown to cause  $\text{Ca}^{2+}$ -dependent inactivation of L-type  $\text{Ca}^{2+}$  channels (Bodi, et al., 2005; Cens, et al., 2006). Importantly, using  $\text{Ba}^{2+}$  as a charge carrier removes the  $\text{Ca}^{2+}$ -induced inactivation. In other words, activation of L-type  $\text{Ca}^{2+}$  channels in the presence of  $\text{Ba}^{2+}$  results in inward  $\text{Ba}^{2+}$  currents that activate rapidly, but inactivate slowly (Ferreira, et al., 1997).

In comparison to L-type  $\text{Ca}^{2+}$  channels, there are three  $\alpha_1$  subunit variants of T-type  $\text{Ca}^{2+}$  channels: Cav3.1 ( $\alpha_{1G}$ ), 3.2 ( $\alpha_{1H}$ ) and 3.3 ( $\alpha_{1I}$ ) (Zhang, et al., 2013). These channels are activated at much more negative membrane potentials (activation starts at -60 mV), inactivated rapidly, have a small single channel conductance (<10 pS), and are insensitive to the conventional L-type  $\text{Ca}^{2+}$  channel antagonists dihydropyridines, phenylalkylamines and benzothiazepines (Bodi, et al., 2005; Zhang, et al., 2013). While L-type  $\text{Ca}^{2+}$  channels are important in maintaining the plateau phase of AP in ventricular cells, both L-type and T-type  $\text{Ca}^{2+}$  channels play a role in generating the AP in cells that are involved in rhythmic electrical behavior; sinoatrial node and atrioventricular node (Catterall, et al., 2005b; Bodi, et al., 2005; Zhang, et al., 2013).

### **1.1.3 Myocardial $\text{Ca}^{2+}$ handling**

The importance of  $\text{Ca}^{2+}$  signaling in the heart has been appreciated for decades. With each heartbeat,  $\text{Ca}^{2+}$  concentration in the cytosol of cardiac myocytes is elevated approximately 10-fold from a resting level of about 100 nM to  $\sim 1 \mu\text{M}$  (Bodi, et al., 2005). The levels of cytosolic  $\text{Ca}^{2+}$  control the activation of

contractile proteins. In other words, the onset, the duration and the intensity of myocardial contraction are strictly controlled by intracellular  $[Ca^{2+}]_i$ . The electrical activation with the spreading of the AP throughout the heart initiates contraction by causing a transient increase in cytosolic  $Ca^{2+}$  concentration, leading to a brief (~400 ms)  $Ca^{2+}$  transient (Bers, 2002).

The AP generates the cytosolic  $Ca^{2+}$  transient via a process called  $Ca^{2+}$ -induced  $Ca^{2+}$  release (Fabiato, 1983; Eisner, et al., 2013) (Figure 1.4). During this process, the influx of a small amount of  $Ca^{2+}$  via voltage-gated L-type  $Ca^{2+}$  channels located in the T-tubules, induces  $Ca^{2+}$  release from the SR by activating ryanodine receptor 2 (RyR2). This leads to a considerable amplification of the initial  $Ca^{2+}$  influx to a level required for the optimal binding of  $Ca^{2+}$  to the myofilament protein troponin C in the troponin complex on the thin filament, which in turn switches on the contractile machinery (Bodi, et al., 2005). The troponin complex is composed of troponin C (TnC or the  $Ca^{2+}$  binding subunit), troponin I (TnI, involved in inhibition of actin-myosin interaction in the absence of  $Ca^{2+}$ ), and troponin T (TnT which binds the troponin complex to tropomyosin, another filament protein) in a stoichiometric ratio of 1:1:1 (Gomes, et al., 2002). The thin (actin) and thick (myosin) filaments slide along each other driven by ATP hydrolysis resulting in muscle shortening and force production. Relaxation occurs after 100-200 ms when  $Ca^{2+}$  gradually decays back to diastolic levels. In this case, tropomyosin is positioned such that actin and myosin cannot interact leading to the relaxation of cardiac muscle cell (Huke and Knollmann, 2010).

Calcium homeostasis is particularly important in cardiac muscle cells. The decline in cytosolic  $Ca^{2+}$  concentration is due to termination of  $Ca^{2+}$  release from the SR (inactivation of RyR2) and rapid removal of  $Ca^{2+}$  from the cytosol. Two

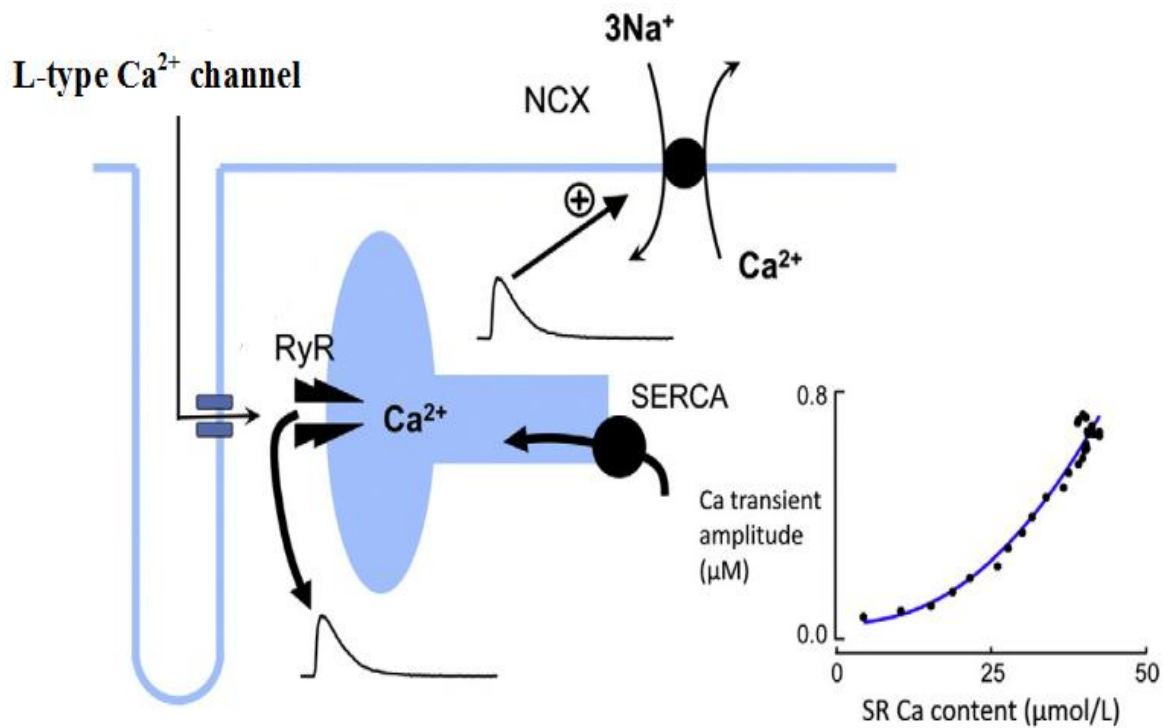


**Figure 1.4  $\text{Ca}^{2+}$ -induced  $\text{Ca}^{2+}$  release and  $\text{Ca}^{2+}$  cycling in a cardiac cell:**  $\text{Ca}^{2+}$  entry via the L-type  $\text{Ca}^{2+}$  channel causes the release of  $\text{Ca}^{2+}$  from the SR via RyR resulting in  $\text{Ca}^{2+}$  transient and muscle contraction. Relaxation occurs by the  $\text{Ca}^{2+}$  being taken back into the SR by SERCA and pumped out of the cell by NCX. The inset shows the amplitude of the  $\text{Ca}^{2+}$  transient as a function of SR  $\text{Ca}^{2+}$  content. Modified from Eisner, *et al.*, 2013.

major routes are responsible for  $\text{Ca}^{2+}$  removal from the cytosol: the SR  $\text{Ca}^{2+}$ -ATPase (SERCA2a) that uses ATP to pump  $\text{Ca}^{2+}$  back into the SR and the sodium-calcium exchanger (NCX) (Ottolia, et al., 2013) (Figure 1.4). Under physiologic conditions, NCX removes approximately the same amount of  $\text{Ca}^{2+}$  that entered the cell through L-type  $\text{Ca}^{2+}$  channel in order to maintain the cellular  $\text{Ca}^{2+}$  balance (Bridge, et al., 1990). Sarcolemmal  $\text{Ca}^{2+}$ -ATPase and the mitochondrial  $\text{Ca}^{2+}$  uniport are considered minor players in  $\text{Ca}^{2+}$  homeostasis, although there is accumulating evidence that they can also influence the levels of  $\text{Ca}^{2+}$  in cellular  $\text{Ca}^{2+}$  stores and modify excitation-contraction coupling (Dedkova and Blatter, 2013; Ottolia, et al., 2013).

As mentioned earlier, the amplitude of the  $\text{Ca}^{2+}$  transient determines the level of myofilament activation, and therefore the magnitude of contraction. The two main factors that determine the amount of  $\text{Ca}^{2+}$  released from the SR and the amplitude of the  $\text{Ca}^{2+}$  transient are: the amplitude of the L-type  $\text{Ca}^{2+}$  current (Trafford, et al., 2001), and the  $\text{Ca}^{2+}$  concentration in the SR (Shannon, et al., 2000). The SR  $\text{Ca}^{2+}$  concentration can be increased by the stimulation of SERCA2a activity and prolongation of the duration of the AP, and decreased by the stimulation of NCX working in the forward mode (Ottolia, et al., 2013).

In general, any alternation in  $\text{Ca}^{2+}$  flux results in an overall change in contractility (Ottolia, et al., 2013). For example, a persistent reduction in cellular  $\text{Ca}^{2+}$  efflux, not matched by a decrease in  $\text{Ca}^{2+}$  influx, results in an increased cellular  $\text{Ca}^{2+}$  which will accumulate in the SR rather than the cytoplasm. The increased amount of  $\text{Ca}^{2+}$  in SR typically results in larger  $\text{Ca}^{2+}$  transients and therefore contractility (Bassani, et al., 1995; Shannon, et al., 2000). Conversely, an increase in  $\text{Ca}^{2+}$  efflux will deplete SR stores and depress contractility.

Under *in vivo* conditions, the main modulator of  $\text{Ca}^{2+}$  transient amplitude is  $\beta$ -adrenergic stimulation that is mediated by cAMP/PKA which has three main actions on  $\text{Ca}^{2+}$  signaling (Catterall, 2011). First, it stimulates the L-type VGCCs to increase the amount of  $\text{Ca}^{2+}$  that enters during each AP. Second, it phosphorylates the protein phospholamban (PLB) to reduce its inhibitory effect on SERCA2a pump, which is then able to increase the luminal  $\text{Ca}^{2+}$  concentration so that more  $\text{Ca}^{2+}$  is released from the SR. Third, cAMP/PKA phosphorylates the RyR2, thereby enhancing its ability to release  $\text{Ca}^{2+}$  (Frank, et al., 2003). Therefore, the activation of both L-type  $\text{Ca}^{2+}$  channel and SERCA2a leads to a substantial increase in the amplitude of  $\text{Ca}^{2+}$  transients.

#### **1.1.4 Role of the $\text{Na}^+/\text{Ca}^{2+}$ exchanger in calcium homeostasis**

The NCX is a plasma membrane transport protein and is considered as the main extrusion pathway for  $\text{Ca}^{2+}$  from ventricular myocytes. It is directly involved in the regulation of excitation-contraction coupling by means of modulating  $\text{Ca}^{2+}$  efflux, SR  $\text{Ca}^{2+}$  load (Bers, et al., 1989; Bers and Weber, 2002), SR  $\text{Ca}^{2+}$  release (Litwin, et al., 1998) and  $\text{Ca}^{2+}$  spark frequency (Goldhaber, et al., 1999). This is likely to contribute, alongside other proteins such as SR  $\text{Ca}^{2+}$ -ATPase and calmodulin, as an effective buffering mechanism to maintain steady-state  $\text{Ca}^{2+}$  flux during short term  $\text{Ca}^{2+}$  transients.

The NCX can extrude intracellular  $\text{Ca}^{2+}$  across the cell membrane against its chemical gradient by using the downhill gradient of  $\text{Na}^+$ . It is widely accepted that the stoichiometry of this ion exchange occurs such that while one positive charge ( $\text{Ca}^{2+}$ ) go out, three positive charges ( $3 \text{Na}^+$ ) are taken up by the cell (Bers, 2002; Bers and Weber, 2002). Therefore, NCX activity is electrogenic. Under

resting conditions, NCX functions in forward mode. However, NCX is bidirectional and can also mediate  $\text{Ca}^{2+}$  entry and outward movement of  $\text{Na}^+$ . This is referred to as the reverse mode. The direction and amplitude of the NCX current is governed by  $\text{Na}^+$  and  $\text{Ca}^{2+}$  gradients across the cell membrane, as well as, the membrane potential. The most recognized action of NCX is its  $\text{Ca}^{2+}$  removal in the forward mode at membrane voltages less than the equilibrium potential, which under physiological conditions, is about -50 mV to -60 mV (Reuter, et al., 2005; Ottolia, et al., 2013).

Recently, the molecular structure of NCX protein has been elucidated (Figure 1.5) (Morad, et al., 2011). It has been shown that mammalian NCX forms a multigene family of homologous proteins comprising three isoforms. Sodium-calcium exchanger 1 (NCX1) was the first NCX cloned and is highly expressed in cardiac muscle and brain and to a lesser extent in many other tissues (Hilgemann, et al., 2013; Lytton, 2007). Sodium-calcium exchanger 2 (NCX2) is expressed primarily in the brain (Canitano, et al., 2002), while sodium-calcium exchanger 3 (NCX3) is expressed in the brain, as well as, skeletal tissue (Canitano, et al., 2002; Lytton, 2007).

The cardiac NCX1 consists of 970 amino acids with a molecular weight of about 110 kDa. Although recent crystal structure of NCX1 strongly supports the presence of 10 transmembrane segments (Ren and Philipson, 2013), biochemical analysis has indicated the presence of nine transmembrane segments, and a large hydrophilic group with conserved regions between transmembrane segments five and six. The N- and C-termini are located on the external and internal sides, respectively (Shigekawa and Iwamoto, 2001; Ren and Philipson, 2013).

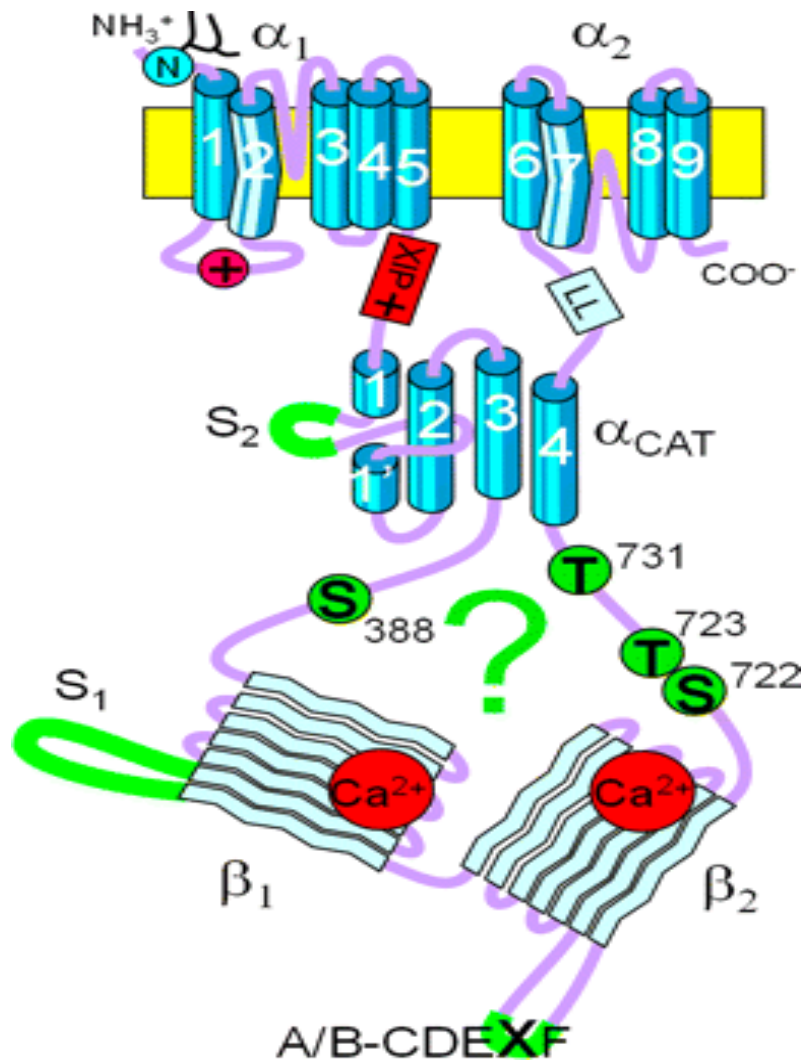


**Figure 1.5 Hypothetical functional organization of  $\text{Na}^+/\text{Ca}^{2+}$  exchanger:** The critical residues T731, T723, and S722 are important for cAMP-dependent regulation. Detailed structures have only been determined for the  $\text{Ca}^{2+}$ -binding domains  $\beta_1$  and  $\beta_2$ . The detailed arrangement and function of all other components, including the  $\alpha$ -helices of the transmembrane-spanning (top) and  $\alpha$ -catenin-like ( $\alpha\text{Cat}$ ) domains and the unstructured linker sequences (S1, S2, A/B-CDEXF) remain to be ascertained. Adapted from Morad, *et al.*, 2011.



Similar to  $\text{Ca}^{2+}$  channels, NCX is also regulated allosterically by  $[\text{Ca}^{2+}]_i$  (Ottolia, et al., 2013). In addition, the activity of NCX is regulated by the signaling lipid phosphatidylinositol-4,5-bisphosphate ( $\text{PIP}_2$ ) (Hilgemann and Ball, 1996), free radicals, pH and temperature, as well as, PKA (Schulze, et al., 2003; Wei, et al., 2003) and PKC (Blaustein and Lederer, 1999; Iwamoto, et al., 1996). However, the physiological significance of these factors as *in vivo* regulators of NCX remains to be established.

## **1.2. The endocannabinoid system**

### **1.2.1 Introduction**

The psychoactive properties of the plant *Cannabis sativa* have been known to man for thousands of years. The popularity of marijuana, one of the most commonly used drugs of abuse, reflects its powerful effects on sensory perception, learning and anxiety. Non-psychoactive uses of marijuana include pain relief, muscle relaxation, attenuation of nausea and vomiting and treatment of multiple sclerosis (Pertwee, 2001; Howlett, 2002; Smith, 2004). Despite its use for centuries, it is only during the last few decades that the biological basis of the effects of marijuana and its bioactive ingredients, collectively called cannabinoids, has begun to unfold (Kunos, et al., 2000). In the 1960s,  $\Delta^9$ -tetrahydrocannabinol (THC) was discovered as the primary psychoactive component of *Cannabis sativa* (Mechoulam and Gaoni, 1965; Mechoulam, et al., 1995). However, it is important to note that *Cannabis* contains over 60 chemicals with closely related structures. Among them, THC, cannabinol and cannabidiol are the most commonly studied cannabinoids (Di Marzo, V, 2006).

The isolation of THC paved the way for the development of THC-based ligands and led to the discovery of cannabinoid receptors. The first cannabinoid

binding site in rat brain was identified in 1988 (Devane, et al., 1988), and the receptor was cloned later in 1990 (Matsuda, et al., 1990). This receptor was named cannabinoid receptor 1 (CB<sub>1</sub>). The second receptor, cannabinoid receptor 2 (CB<sub>2</sub>), was discovered shortly after (Munro, et al., 1993).

In earlier studies, the presence of opiate receptors in the mammalian brain (Pert and Snyder, 1973) has led to the discovery of endogenous opioid peptides. Therefore, several groups have searched for endogenous ligands that mimic the action of *Cannabis*. Only in the early nineties, similar to the opioid system, cannabinoid receptors were found to have endogenously produced ligands (Devane, et al., 1992). These are now called the endocannabinoids.

The endocannabinoid system (ECS) is a complex and ubiquitously expressed signaling system which includes several neuromodulatory lipids (endocannabinoids), their receptors and a set of enzymes that synthesize and degrade endocannabinoids. The ECS has been identified in most human organs and tissues, and has important regulatory roles in a wide range of normal and pathological processes, such as pain, energy homeostasis, fertility, immune response and behavior (Rodriguez de, et al., 2005; De and Di, V, 2009a).

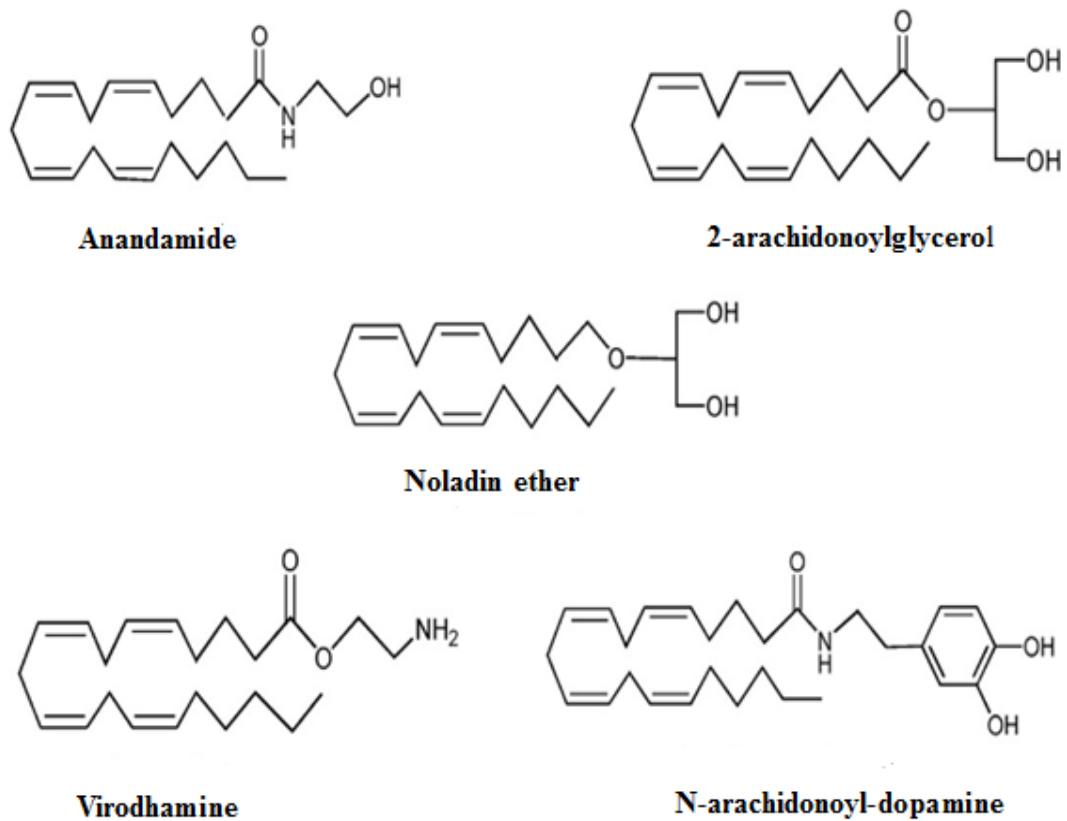
### **1.2.2 Endocannabinoids**

Endocannabinoids belong to a family of polyunsaturated fatty acid-based compounds synthesized from the lipid precursors in the plasma membranes of virtually all types of cells ranging from neurons and endocrine cells to skeletal muscle fibers and cardiomyocytes (Pacher, et al., 2006). They are implicated in a wide variety of physiological processes including memory, immunity, sleep, pain sensation, perception, reproduction (Martin, et al., 1999) and cardiovascular functions (Clapper, et al., 2006; Sterin-Borda, et al., 2005; Randall and Kendall,

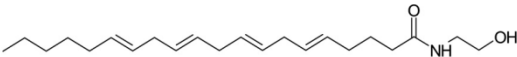
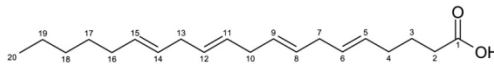
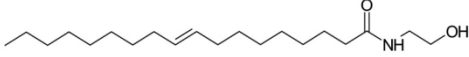
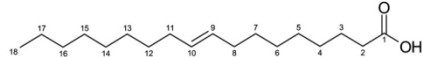
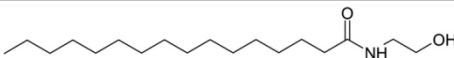
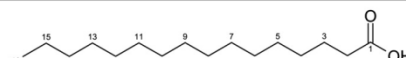
1997). To date, the two most extensively studied endocannabinoids are N-arachidonylethanolamine (AEA), also known as anandamide (from the Sanskrit ‘ananda’ for happiness, joy or enjoyment), and its glycerol ester analogue 2-arachidonoylglycerol (2-AG). Anandamide was first described in 1992 (Devane, et al., 1992). However, 2-AG was discovered as the second endocannabinoid a few years later (Mechoulam, et al., 1995; Sugiura, et al., 1995) (Figure 1.6).

In addition to AEA and 2-AG, other endocannabinoids with similar fatty acid-based chemical structures were also identified during the last decade, including, 2-arachidonylglycerol ether (noladin ether) (Hanus, et al., 2001), N-arachidonoyl-dopamine (NADA) (Bisogno, et al., 2000), and virodhamine (Porter, et al., 2002) (Figure 1.6). Virodhamine has a very similar structure to AEA, but opposite orientation around the arachidonic acid (AA)-ethanolamine bond (Porter, et al., 2002). Likewise, noladin ether and 2-AG are structurally similar (Figure 1.6). However, pharmacological characterization of these chemicals has not been well established.

Anandamide belongs to a group of chemicals termed N-acylethanolamines (NAEs). Other NAEs are not usually considered as endocannabinoids but are produced by the same enzymes that synthesize AEA. In recent years, several studies have shown that these chemicals play a role in vascular control (Ho, et al., 2008), food intake, energy balance (Borrelli and Izzo, 2009) and neuroprotection (Hansen, et al., 2000; Hansen, 2010). Two of these NAEs, oleoylethanolamide (OEA) and palmitoylethanolamide (PEA) have been extensively investigated as they are present at higher concentration than the endocannabinoids in many mammalian tissues (Alexander and Kendall, 2007; Lambert and Muccioli, 2007) (Figure 1.7).



**Figure 1.6** Chemical structures of the proposed endocannabinoids. Adapted from Di Marzo, 2009

Compound	Fatty acid
<i>N</i> -Arachidonylethanolamine (anandamide)	Arachidonic acid (20:4 n-6)
	
<i>N</i> -Oleoylethanolamine	Oleic acid (18:1 n-9)
	
<i>N</i> -Palmitoylethanolamine	Palmitic acid (16:0)
	

**Figure 1.7** Chemical structures of anandamide and related *N*-acylethanolamines.

### 1.2.3 Endocannabinoid receptors

As mentioned earlier, to date, at least two endocannabinoid receptors have been identified and cloned based on their pharmacological properties and gene structure. The CB<sub>1</sub> receptors are principally located in the central nervous system, where they are highly abundant and appear to participate in negative retrograde signaling (Matsuda, et al., 1990; Mackie, 2008). In addition, they are found in several peripheral tissues including the heart and the vasculature (Ishac, et al., 1996; Bonz, et al., 2003; Liu, et al., 2000). The CB<sub>2</sub> receptors, on the other hand, are expressed primarily in the immune system (Munro, et al., 1993) and hematopoietic cells (Valk and Delwel, 1998), but recently their presence in the brain (Van, et al., 2005), liver (Mallat and Lotersztajn, 2008; Mackie, 2008), myocardium (Montecucco, et al., 2009; Defer, et al., 2009), vascular endothelial and smooth muscle cells (Rajesh, et al., 2007), have also been demonstrated. Both receptors are G protein-coupled receptors (GPCRs) with seven transmembrane spanning domains (Howlett, et al., 1990). Most of the G proteins linked to the cannabinoid receptors are inhibitory proteins (G<sub>i/o</sub>). They are sensitive to pertussis toxin (PTX) and inhibit adenylyl cyclase (AC) activity and thus, inhibit the formation of cAMP (Pertwee, 2006). However, coupling of cannabinoid receptors to PTX-insensitive G<sub>q</sub> protein has also been reported in recent studies (Straiker, et al., 2002; McIntosh, et al., 2007).

The CB<sub>1</sub> receptor can be activated by both AEA and 2-AG, although 2-AG is more potent, and AEA is often considered to be a partial agonist (Hillard, 2000). Similarly, both endocannabinoids are agonists of CB<sub>2</sub> receptor, although again 2-AG is more potent. Both AEA (K<sub>D</sub> values for CB<sub>1</sub> and CB<sub>2</sub> receptors are 61-543 nM and 279-1940 nM, respectively) and 2-AG (K<sub>D</sub> values for CB<sub>1</sub> and

CB<sub>2</sub> receptors are 58-472 nM and 145-1400 nM, respectively) have greater affinities for CB<sub>1</sub> receptor than CB<sub>2</sub> receptor (Munro, et al., 1993; Pertwee, 2006; Pertwee, et al., 2010). It appears that the selectivity of endocannabinoids varies significantly. For example, the endocannabinoid noladin ether is a selective CB<sub>1</sub> receptor agonist, while virodhamine is a partial CB<sub>2</sub> agonist and a CB<sub>1</sub> receptor antagonist. On the other hand, NADA appears to be a selective agonist for CB<sub>1</sub> receptor (Pertwee, et al., 2010; Pertwee and Ross, 2002).

#### **1.2.4 Synthesis and metabolism of anandamide**

Endocannabinoids are synthesized predominantly via the cleavage of membrane phosphoglyceride precursors (Bisogno, 2008). As the endocannabinoid precursors are physiological chemical constituents of cell membranes, it is the anatomical location of endocannabinoid synthesizing enzymes and receptors that dictate their activity and therefore, their physiological roles in cellular environments (Di, Marzo, et al., 2007). Endocannabinoids are often referred to as signaling molecules which are synthesized “on demand” and in neurons, at least, endocannabinoids are synthesized and released very rapidly (within tens of milliseconds) upon stimulation (Alger and Kim, 2011).

As mentioned earlier, the biosynthetic pathway for AEA is thought to involve the breakdown of pre-formed arachidonoyl phospholipids in the cell membrane (Figure 1.8). It was shown that the primary route for AEA biosynthesis is the formation of N-arachidonoyl phosphatidylethanolamine (NAPE) (Hiley, 2009) which is produced by the transfer of AA from phospholipids to the nitrogen atom of phosphatidylethanolamine. Subsequently, it is transformed into AEA via multiple pathways, the most direct of which is catalyzed by Ca<sup>2+</sup>-sensitive NAPE-

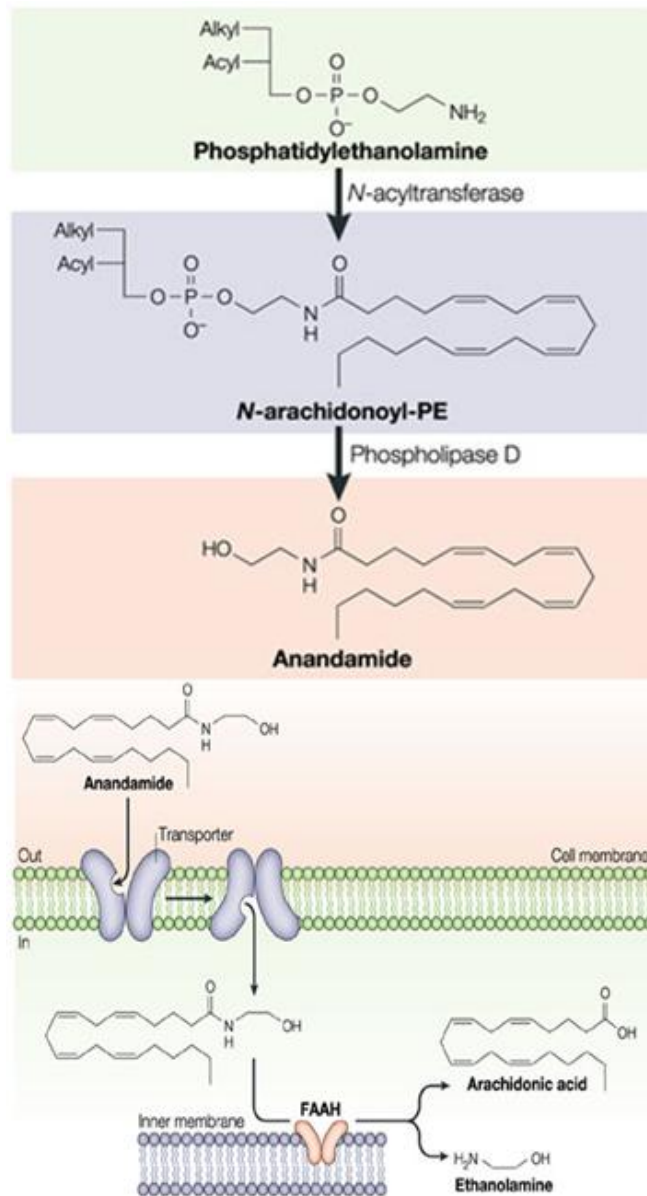


**Figure 1.8 Mechanisms of anandamide formation and deactivation:** The formation of AEA is thought to include the synthesis of the AEA precursor N-arachidonoyl phosphatidylethanolamine (NAPE) catalyzed by the enzyme N-acyltransferase and then the cleavage of NAPE to yield AEA, catalyzed by phospholipase D (upper panel). AEA can be internalized by cells through a high affinity transport mechanism; the endocannabinoid transporter. Once inside the cell, it can be hydrolyzed by FAAH to yield arachidonic acid and ethanolamine (lower panel). Modified from Piomelli, 2003.



selective phospholipase D (NAPE-PLD) (De Petrocellis and Di Marzo, 2009a). This enzyme catalyzes the hydrolysis of the bond between phosphate and ethanolamine resulting in the formation of AEA and phosphatidic acid.

Endocannabinoid signaling is terminated by a rapid clearance from the extracellular milieu (half-life is seconds to minutes) (De Petrocells, et al., 2004). Studies suggest that following cannabinoid receptor activation, AEA is taken up by cells via a facilitated transport mechanism mediated by a putative anandamide membrane transporter (AMT) (Bari, et al., 2006; Piomelli, 2003) followed by intracellular degradation. Although data from several biochemical and pharmacological studies support the existence of an AMT, this is a controversial topic, and the structure of AMT protein remains to be identified at the molecular level (De Petrocellis, et al., 2004). Currently, it is well established that AEA is predominantly degraded in the cytosol under the action of FAAH to ethanolamine and AA (Hiley, 2009; Deutsch and Chin, 1993; Cravatt, et al., 1996). On the other hand, 2-AG is predominantly broken down by a specific monoacylglycerol lipase (MAGL) (Vandevoorde and Lambert, 2005). *In vitro* experiments indicate that endocannabinoids are also substrates for oxidative metabolism via cyclooxygenase (Fowler, 2007) and lipoxygenase (Kozak, et al., 2002) pathways.

Fatty acid amide hydrolase was identified in 1996 (Cravatt, et al., 1996). It has multiple substrates, but exhibits specificity for the long-chain amides of ethanolamine (Schmid, et al., 1985). There are two isoforms of FAAH, FAAH-1 and FAAH-2, which share approximately 20 % DNA sequence homology, although, the catalytic site is relatively well conserved (Wei, et al., 2006a). The two isoforms are differentially expressed across tissues. In human kidney, liver, lung and prostate both isoforms are expressed. However, only FAAH-1 levels are

high in human brain, small intestine and testis. FAAH-2 is predominantly expressed in the heart (Wei, et al., 2006a). It is important to note that the two isoforms have different substrate specificity, with FAAH-1 having significantly greater hydrolytic activity on AEA than FAAH-2 (rates of hydrolysis in nmol/min.mg are  $17\pm 1$  and  $0.46\pm 0.04$ , respectively) (Wei, et al., 2006a). Due to the pharmacological implication of modulating endocannabinoid levels, in recent years, several inhibitors have been synthesized (Fowler, et al., 2001). For example, URB597, JP104, OL-92 and OL-135 are potent inhibitors of FAAH (Michaux, et al., 2006; Min, et al., 2011). However, these inhibitors differ in their selectivity. While JP104 is a potent inhibitor of both FAAH-1 and FAAH-2 (Wei, et al., 2006b), URB597 is more potent at FAAH-2 (Piomelli, et al., 2006).

FAAH is a membrane bound enzyme (McKinney and Cravatt, 2005) and is thought to form homodimers (Bracey, et al., 2002). The location and structure of FAAH may allow the hydrolysis of AEA within the close vicinity of plasma membrane (McKinney and Cravatt, 2005). Indeed, the rate of AEA hydrolysis in tissues from FAAH knockout mice is 50-100 fold reduced, and AEA concentrations in the brain (Cravatt, et al., 2001; Lichtman, et al., 2002) and liver (Tourino, et al., 2010) are elevated significantly.

In recent years, FAAH has emerged as a target for modulating endocannabinoid signaling (Ahn, et al., 2008) with a therapeutic potential in anxiety, pain and various inflammatory disorders (Cravatt, et al., 2001; Cravatt, et al., 2004). In the heart, FAAH plays a key role in controlling endocannabinoid-induced myocardial tissue injury in pathological conditions associated with acute oxidative stress (Mukhopadhyay, et al., 2011). It was found that AEA induced enhanced cell death in human cardiomyocytes that were pretreated with FAAH

inhibitor, and enhanced sensitivity to reactive oxygen species (ROS) generation in inflammatory cells of FAAH knockouts, all of which suggest a role for FAAH in controlling tissue injury (Mukhopadhyay, et al., 2011).

## **1.2.5 Cellular and molecular mechanisms of endocannabinoid actions**

### **1.2.5.1 Signal transduction mechanisms**

Signal transduction through CB<sub>1</sub> and CB<sub>2</sub> receptors is mediated by G-protein (G<sub>i/o</sub>) which couples negatively to AC and thus, inhibits cAMP generation. Modulation of intracellular cAMP concentration regulates PKA phosphorylation, and thereby results in major changes in cAMP-dependent signal transduction pathway (Demuth and Molleman, 2006). In fact, the first characterized CB<sub>1</sub> receptor signal transduction response was the inhibition of AC by micromolar concentration of THC in neuroblastoma cells (Howlett and Fleming, 1984). Subsequent studies demonstrating the blockade of this response by PTX treatment suggested that G<sub>i/o</sub> type G-proteins are involved (Howlett, et al., 1986). Typical G<sub>i/o</sub>-mediated intracellular events coupled to CB<sub>1</sub> activation are the inhibition of VGCCs of most types, including P/Q (Twitchell, et al., 1997), N (Wilson, et al., 2001) and L-type (Gebremedhin, et al., 1999; Straiker, et al., 1999) channels and the stimulation of potassium channels such as K<sub>IR</sub> channels (McAllister, et al., 1999) and mitogen-activated protein kinase (MAPK) (Derkinderen, et al., 2001).

In the central nervous system, the role of endocannabinoids in retrograde signaling has been well established. It has been shown that the activation of presynaptic CB<sub>1</sub> receptors controls the release of several neurotransmitters, such as glutamate and GABA (Lovinger, 2008; Foldy, et al., 2006). Synthesis of endocannabinoids occurs following the release of excitatory neurotransmitters and their diffusion outside the synaptic region. The action of glutamate on its receptor

in the postsynaptic membrane leads to the release of intracellular  $\text{Ca}^{2+}$  and the opening of VGCCs. An elevated level of  $\text{Ca}^{2+}$  activates the enzymes responsible for endocannabinoid synthesis from lipid precursors. Anandamide and/ or 2-AG are released and following retrograde diffusion in the synaptic cleft, presynaptic  $\text{CB}_1$  receptors are activated. This activation results in the inhibition of VGCCs or activation of  $\text{K}^+$  channels resulting in decreased intracellular  $\text{Ca}^{2+}$  concentration, preventing further neurotransmitter release from the presynaptic terminal (Vaughan and Christie, 2005).

Recent studies indicate that the interaction of cannabinoids with G proteins is not limited to  $\text{G}_{i/o}$  subtype. Evidence suggests that  $\text{CB}_1$  receptors can also interact with  $\text{G}_s$  protein under conditions of PTX treatment that prevents the receptor's interaction with  $\text{G}_{i/o}$  protein (Howlett, et al., 1986).  $\text{CB}_2$  receptors, in contrast, do not seem to couple to  $\text{G}_s$  subtype, suggesting further differences between  $\text{CB}_1$  and  $\text{CB}_2$  receptor signaling (Glass and Felder, 1997). For example, stimulation of cAMP accumulation by HU-210 (the synthetic analogue of THC) and CP 55,940 (a highly potent cannabinoid agonist) was observed after PTX treatment of Chinese hamster ovary (CHO) cells expressing the human  $\text{CB}_1$  but not  $\text{CB}_2$  receptors (Calandra, et al., 1999; Glass and Felder, 1997). In addition to the dual coupling of cannabinoid receptors to  $\text{G}_s$  and  $\text{G}_{i/o}$  proteins, the presence of distinct isoforms of AC in different cellular preparations has also been shown to contribute to the diversity of cannabinoid actions. To date, nine isoforms of AC have been identified (AC-I, AC- II, AC-III, AC-IV, AC-V, AC-VI, AC-VII, AC-VIII and AC-IX) (Demuth and Molleman, 2006). The isoform AC-I is found mainly in the brain while the isoforms AC-V and AC-VI are highly expressed in brain and heart. When monkey kidney (COS-7) cells expressing exogenous  $\text{CB}_1$

receptors were transfected with each AC isoform in turn and stimulated with the cannabinoid agonists HU-210 and WIN 55,212-2, the isoforms AC-I, AC-V, AC-VI and AC-VIII were shown to be inhibited, whereas, AC-II, AC-IV and AC-VII were stimulated by CB<sub>1</sub> receptor activation (Rhee, et al., 1998). Collectively, all these results suggest that CB<sub>1</sub> receptors may be dually coupled to both G<sub>s</sub> and G<sub>i/o</sub> proteins in some systems. It is likely that the contrasting effects of cannabinoids on AC activity could be attributed to the specific isoform present in different cellular preparations. However, physiological significance of these diverse coupling mechanisms of cannabinoid receptors to various G-proteins needs further investigation.

Another effect described for both CB<sub>1</sub> and CB<sub>2</sub> receptors is the modulation of intracellular Ca<sup>2+</sup> concentration. CB<sub>1</sub> receptor agonists, including AEA and 2-AG, were shown to directly stimulate the hydrolysis of PIP<sub>2</sub> by phospholipase C (PLC-β) with subsequent release of IP<sub>3</sub> followed by Ca<sup>2+</sup> mobilization from the endoplasmic reticulum via either G<sub>q</sub>-mediated or G<sub>i/o</sub>-mediated mechanisms (Sugiura, et al., 1996; Ho, et al., 1999; Lauckner, et al., 2005). In NG108-15 cells (Sugiura, et al., 1996) and in cultured cerebellar granule cells (Netzeband, et al., 1999), cannabinoid receptor agonists have been shown to increase intracellular Ca<sup>2+</sup> concentration by releasing Ca<sup>2+</sup> from IP<sub>3</sub>-sensitive stores. It appears that these effects of cannabinoids are sensitive to CB<sub>1</sub> antagonism and PTX treatment (Sugiura, et al., 1996; Netzeband, et al., 1999).

Activation of CB<sub>2</sub> receptors has also been shown to increase intracellular Ca<sup>2+</sup> levels, although, CB<sub>2</sub> receptor-mediated Ca<sup>2+</sup> responses are less pronounced than the potent CB<sub>1</sub> receptor-mediated effects (Felder, et al., 1995; Zoratti, et al., 2003). In calf pulmonary endothelial cells, Zoratti *et al.*, observed CB<sub>2</sub>-dependent

increase in cytosolic  $\text{Ca}^{2+}$  via activation of PLC and a subsequent release of  $\text{Ca}^{2+}$  from  $\text{IP}_3$ -sensitive stores (Zoratti, et al., 2003).

However, in some other experiments, cannabinoid-induced  $\text{Ca}^{2+}$  release has been shown to be associated with the release of nitric oxide (NO). For example, in cultured human arterial endothelial cells, AEA evoked an increase in intracellular  $\text{Ca}^{2+}$  concentration in an SR141716A-sensitive manner. This increase was shown to be coupled to NO release (Fimiani, et al., 1999). In human umbilical endothelial cells, intracellular  $\text{Ca}^{2+}$  increase was insensitive to PTX and only marginally blocked by SR141716A. Anandamide also significantly increased NO synthase activity (Mombouli, et al., 1999). Collectively, these results suggest that  $\text{CB}_1$  receptor-dependent and independent increase in intracellular  $\text{Ca}^{2+}$  and subsequent NO production may account for some of the vasodilator actions of AEA. However, the increase in intracellular  $\text{Ca}^{2+}$  concentration seems at odds particularly with cannabinoid inhibition of neuronal excitability which is thought to be caused by VGCCs inhibition. In addition to NO synthase activation mechanism, it is possible that subcellular localization of signaling pathways could explain this paradox. For example, it may be envisaged that  $\text{Ca}^{2+}$  release from intracellular stores in excitable cells can be inhibitory through activation of  $\text{Ca}^{2+}$ -dependent  $\text{K}^+$  channels, leading to hyperpolarization. This would then prevent the activation of VGCCs and large  $\text{Ca}^{2+}$  influx (Demuth and Molleman, 2006).

In addition to the second-messenger pathways described above, functional modulation of various ion channels and receptors by endocannabinoids has also been demonstrated. One of these ion channels is the transient receptor potential (TRP) channel which constitutes a large and a functionally versatile family of cation-permeable transmembrane proteins. To date, vanilloid receptors (TRPV1)

are the best characterized TRP channels. They are primarily heat receptors expressed in sensory neurons and their activation leads to  $\text{Ca}^{2+}$  entry and neurotransmitter release (Demuth and Molleman, 2006).

The realization that AEA is chemically similar to capsaicin, an agonist of TRPV1 channel (Di Marzo, et al., 1998) lead to the discovery that AEA can serve as an agonist not only on cannabinoid receptors but also on TRPV1 channels. For example, the TRPV1 receptor-mediated vasodilatory effect of AEA in rat and guinea pig arteries has been shown to be blocked by the TRPV1 antagonist capsazepine (Zygmunt, et al., 1999). Similarly, application of AEA (10  $\mu\text{M}$ ) causes activation of TRPV1 receptors in cultured cells transfected with rat or human TRPV1 receptors or in neurons of neonatal rat dorsal root ganglia (Zygmunt, et al., 1999; Smart, et al., 2000; Ross, et al., 2001). Furthermore, the ability of AEA to stimulate TRPV1 receptors appears to be regulated by the state of activation of protein kinase A and protein kinase C (Premkumar and Ahern, 2000; Di Marzo, et al., 2002). In this context, it is important to note that co-localization of cannabinoid receptors and TRPV1 channels have made the interpretation of some experiments difficult (Hermann, et al., 2003; Di Marzo and Cristino, 2008).

In recent years, it has been shown that endocannabinoids are ligands for peroxisome proliferator-activated receptors (PPARs) (O'Sullivan, et al., 2005; Lenman and Fowler, 2007). PPARs are nuclear transcription factors that are highly expressed in metabolically active tissues such as liver, adipose, skeletal muscle and heart (Stienstra, et al., 2007). These receptors play key roles in regulating cellular differentiation, lipid metabolism and inflammation (Glass and Ogawa, 2006). In the heart, these receptors can modulate myocardial lipid

metabolism, as well as, glucose and energy homeostasis (Lee, et al., 2011). Cannabinoid-related agonists identified to date for PPARs include AEA, 2-AG, OEA, THC, NADA and cannabidiol (Fu, et al., 2005; O'Sullivan, et al., 2009a; O'Sullivan, et al., 2009b; O'Sullivan, et al., 2005; Rockwell, et al., 2006). In some studies, it has been shown that the anti-inflammatory effects of AEA and 2-AG are sensitive to PPARs antagonism (Rockwell and Kaminski, 2004; Rockwell, et al., 2006). In addition, a study carried by O'Sullivan *et al.*, has shown that the endocannabinoid AEA, activates PPARs in rat aorta, leading to NO-dependent relaxation (O'Sullivan, et al., 2009a). Activation of PPARs in the heart by some endocannabinoids may represent a novel mechanism for endocannabinoid regulation of the cardiovascular system (O'Sullivan, et al., 2009a).

Further to these well-recognized endocannabinoid targets, emerging evidence demonstrates that, beyond their receptor-mediated effects, AEA and other cannabinoid-receptor ligands are able to alter the functional properties of ligand-gated ion channels in a cannabinoid receptor-independent manner (Oz, 2006). Direct effects of endocannabinoids include modulation of the function of serotonin type 3 (5-HT-3) receptors (Oz, et al., 2002), nicotinic acetylcholine receptors (Jackson, et al., 2008; Oz, et al., 2004a; Butt, et al., 2008), muscarinic acetylcholine receptors (Christopoulos and Wilson, 2001) and glycine receptors (Hejazi, et al., 2006; Xiong, et al., 2012).

In addition to ligand-gated ion channels, endocannabinoids have been shown to interact with several classes of voltage-gated ion channels in a cannabinoid receptor-dependent and independent manner (Oz, 2006). Evidences for both mechanisms are discussed in the following section.



## **1.2.5.2 Receptor-dependent and independent effects of endocannabinoids on voltage-gated ion channels**

### **1.2.5.2.1 Effects on Na<sup>+</sup> channels**

Endocannabinoids have been shown to inhibit directly the functions of voltage-gated Na<sup>+</sup> channels (VGSCs) in neuronal structures. In an earlier study, Nicholson *et al.*, have demonstrated the ability of AEA and WIN 55, 212-2 to inhibit VGSCs (activated by veratridine) in mouse synaptosomes (Nicholson, et al., 2003). The cannabinoids also blocked the veratridine-induced release of neurotransmitters from synaptosomes including GABA and glutamate. The CB<sub>1</sub> antagonist AM251 did not attenuate Na<sup>+</sup> channel inhibition (Nicholson, et al., 2003). In addition, AEA and WIN 55, 212-2 were able to displace the binding of [<sup>3</sup>H]batrachotoxinin A 20- $\alpha$ -benzoate ([<sup>3</sup>H]BTX-B) to VGSCs (Nicholson, et al., 2003). Together, the data suggest that cannabinoids can directly modulate the activity of VGSCs, depressing synaptic transmission in the brain, and in turn, reduce both excitatory and inhibitory neurotransmitter release.

In rat dorsal root ganglion neurons, AEA inhibited both tetrodotoxin (TTX)-sensitive and TTX-resistant Na<sup>+</sup> currents in a concentration-dependent manner. This inhibition was not reversed by the CB<sub>1</sub> antagonist AM251, the CB<sub>2</sub> antagonist AM630 and the vanilloid receptor antagonist capsazepine, suggesting a direct action of AEA on Na<sup>+</sup> channels (Kim, et al., 2005). In a study carried out by Duan *et al.*, 2-AG and NADA were found to modify the binding of [<sup>3</sup>H]BTX-B to VGSCs of mouse brain and inhibit their function *in vitro* (Duan, et al., 2008). These effects were not influenced by the application of the CB<sub>1</sub> receptor antagonist AM251. It was concluded that 2-AG and NADA directly inhibit Na<sup>+</sup> channel function, which contributes to the suppression of neuronal excitation and inhibition of neurotransmitter release in the presynaptic membranes (Duan, et al.,

2008). A recent study has shown that AEA blocks sensory neuronal Na<sup>+</sup> channel isoform Nav1.7 in stably transfected human embryonic kidney (HEK) 293 cells (Theile and Cummins, 2011). However, inhibition of VGSCs is not limited to endocannabinoids. Other members of NAEs family have also been shown to act on Na<sup>+</sup> channels. In mouse brain synaptosomes, OEA inhibited the binding of [<sup>3</sup>H]BTX-B. In addition, OEA at a concentration of 10 μM, decreased peak Na<sup>+</sup> currents in cultured N1E-115 neuroblastoma cells in a voltage-dependent manner, and caused a hyperpolarizing shift in the inactivation curve of the channel. In this respect, the effect of OEA reflects the actions of local anesthetic drugs used as antiarrhythmic agents. Therefore, OEA is likely to regulate cardiac cell excitability (Nicholson, et al., 2001). Indeed, a recent study in neonatal cardiomyocytes showed that the two NAEs, SEA and OEA, influenced the voltage-dependence of activation, inactivation, and the kinetics of Na<sup>+</sup> currents (Voitychuk, et al., 2012). These effects may in part be responsible for the decrease in cardiomyocytes' excitability by these lipids under normal as well as pathological conditions. Interestingly, the effects of endocannabinoids such as AEA and 2-AG on cardiac Na<sup>+</sup> channels have not been reported.

#### **1.2.5.2.2 Effects on Ca<sup>2+</sup> channels**

In earlier studies it has been shown that AEA, WIN 55, 213-2, and CP 55, 940 act via CB<sub>1</sub> receptors to decrease Ca<sup>2+</sup> influx in NG 108-15 cells (Mackie and Hille, 1992; Mackie, et al., 1993). This effect was blocked by pretreatment with PTX, demonstrating its mediation by G<sub>i/o</sub> protein, and was independent of cAMP pathway, as the response was not reversed by the addition of 8-Bromo-cAMP (Mackie and Hille, 1992; Mackie, et al., 1993). Similarly, in rat superior cervical ganglion neurons transfected with CB<sub>1</sub> receptors, WIN55,212-2 and CP55,940

inhibited N-type  $\text{Ca}^{2+}$  currents in a PTX-sensitive manner (Pan, et al., 1996). Another study in rat striatal neurons indicated that WIN55,212-2 inhibited corticostriatal glutamatergic synaptic transmission in an SR141716A- and a PTX-sensitive manner. The inhibition of N-type  $\text{Ca}^{2+}$  channels was thought to mediate this effect as  $\omega$ -conotoxin abolished the WIN55,212-2-mediated synaptic inhibition (Huang, et al., 2001). On the other hand, another study has reported the direct effect of AEA (1-10  $\mu\text{M}$ ) on N-type VGCCs in superior cervical ganglion neurons that do not express endogenous cannabinoid receptors. The effect persisted in the presence of either SR141716A or PTX. However, 2-AG (10  $\mu\text{M}$ ) did not have similar effects (Guo and Ikeda, 2004).

In cultured rat hippocampal neurons, AEA, WIN55,212-2 and CP55,940 inhibited N- and P/Q type  $\text{Ca}^{2+}$  currents in an SR 141716A- and PTX-sensitive manner (Twitchell, et al., 1997; Shen and Thayer, 1998). In the presence of SR141716, Win55,212-2 (nanomolar concentrations) inhibited N-Type VGCCs by only 2 % (Shen and Thayer, 1998). Interestingly, at concentrations higher than 1 $\mu\text{M}$ , Win55,212-2 inhibited N-Type VGCCs in a manner independent of SR141716A. In addition, the inactive stereoisomer WIN55,212-3 (micromolar concentrations) also inhibited  $\text{Ca}^{2+}$  currents in an SR141716A-insensitive manner. Collectively, these findings indicate that at micromolar concentrations, the effects of WIN55,212-2 are not mediated by  $\text{CB}_1$  receptors, suggesting a direct effect of cannabinoids on N-type VGCCs.

In addition to neuronal  $\text{Ca}^{2+}$  channels, modulation of T-type  $\text{Ca}^{2+}$  channels by endocannabinoids has also been demonstrated in several studies. Previously, direct inhibitory effect of AEA on T-type VGCCs has been reported (Chemin, et al., 2001). T-type VGCCs are known to contribute to pacemaker activity in the

central nervous system and in the heart. All three cloned T-type VGCCs ( $\alpha_{1H}$ ,  $\alpha_{1I}$  and  $\alpha_{1G}$ ) which were transfected in HEK 293 and CHO cells and endogenously expressed in NG 108-15 cells, were inhibited by AEA in the concentration range of 0.01-10  $\mu$ M (Chemin, et al., 2001). This inhibitory effect was not mimicked by synthetic cannabinoids including WIN55,212-2, CP55,940 and HU-210, and was not blocked by SR141716A (Chemin, et al., 2001). Notably, AEA continued to inhibit T-type VGCCs in excised inside-out patches of HEK-293 cells (Chemin, et al., 2001) suggesting that the effect of AEA is membrane delimited, and is not mediated by second messenger pathway. Furthermore, the effect of AEA was mimicked by methanandamide (metAEA), the metabolically stable analogue of AEA (Abadji, et al., 1994), indicating that the metabolic products of AEA hydrolysis, such as AA and ethanolamine, are not involved in the inhibition of T-type  $Ca^{2+}$  currents (Chemin, et al., 2001). From these observations it was suggested that AEA directly inhibits T-type VGCCs by acting on the cell membrane. A more recent study supporting these finding was carried out by Ross *et al.* (Ross, et al., 2009). Human recombinant T-type VGCCs expressed in HEK 293 cells and native mouse T-type VGCCs were used to test the effect of the endocannabinoid NADA. The results of this study have shown that NADA robustly inhibits both human recombinant and native mouse T-type VGCCs (The rank order of potency was ( $pEC_{50}$ ) of  $CaV3.3$  (6.45)  $\geq$   $CaV3.1$  (6.29)  $>$   $CaV3.2$  (5.95)) (Ross, et al., 2009). These results were broadly similar to those previously reported for AEA (Chemin, et al., 2001; Chemin, et al., 2007).

Besides N-type and T-type  $Ca^{2+}$  channels, L-type  $Ca^{2+}$  channels have also been shown as target proteins for endocannabinoids. In cat cerebral arterial smooth muscle cells, it was found that activation of  $CB_1$  receptors inhibits L-type

VGCCs, resulting in cerebral vasodilation (Gebremedhin, et al., 1999). WIN55,212-2 and AEA induced concentration-dependent inhibition of peak L-type  $\text{Ca}^{2+}$  current. The inhibitory effects of both ligands were abolished by PTX pretreatment and by the  $\text{CB}_1$  antagonist SR141716A. In addition, both WIN55,212-2 and AEA produced concentration-dependent relaxation of pre-constricted cerebral arterial segments that was abolished by SR141716A (Gebremedhin, et al., 1999). These findings suggest that  $\text{CB}_1$  receptor and its endogenous ligand may play an important role in the regulation of cerebral arterial tone by modulating the influx of  $\text{Ca}^{2+}$  through L-type VGCCs (Gebremedhin, et al., 1999). Furthermore, in isolated rat ventricular myocytes, AEA (1, 10 and 100 nM) caused a concentration-dependent inhibition of L-type  $\text{Ca}^{2+}$  current and shifted the current-voltage relationship curve of the  $\text{Ca}^{2+}$  current. Anandamide (100 nM) shifted the steady-state inactivation curve to the left and the recovery curve to the right (Li, et al., 2009). Blockade of  $\text{CB}_1$  receptors with AM251, but not  $\text{CB}_2$  receptors with AM630, eliminated the effect of AEA on L-type VGCCs. These data suggest that AEA suppresses L-type VGCCs in cardiac myocytes through the activation of  $\text{CB}_1$  receptors (Li, et al., 2009).

The above mentioned studies have indicated that cannabinoids inhibit L-type  $\text{Ca}^{2+}$  channels by the activation of  $\text{CB}_1$  receptors. However, the  $\text{CB}_1$  receptor-independent modulation of L-type  $\text{Ca}^{2+}$  channels by cannabinoids has also been reported. In 1988, Janis *et al.*, isolated a lipid fraction from bovine brain and showed that AEA inhibits the specific [ $^3\text{H}$ ] nitrendipine binding to L-type  $\text{Ca}^{2+}$  channels in rat cardiac membranes, and it blocks  $\text{Ca}^{2+}$  currents in GH3 pituitary cells (Janis, et al., 1988). Further studies in cortical membranes have also

identified AEA as an endogenous modulator of L-type  $\text{Ca}^{2+}$  channels (Johnson, et al., 1993).

T-tubules of the skeletal muscles are known to be the richest source of L-type VGCCs. In T-tubule membrane vesicles from rabbit skeletal muscle fibers, AEA inhibited the binding of dihydropyridine (DHP) ( $[^3\text{H}]\text{PN200-110}$ ), phenylalkylamine ( $[^3\text{H}]\text{D888}$ ), and 1,5-benzothiazapine ( $[^3\text{H}]\text{diltiazem}$ ) class of  $\text{Ca}^{2+}$  channel antagonists with  $\text{IC}_{50}$  values of 4  $\mu\text{M}$ , 8  $\mu\text{M}$  and 29  $\mu\text{M}$ , respectively (Shimasue, et al., 1996). In addition, functional studies in T-tubule membranes indicated that AEA (1-10  $\mu\text{M}$ ) and metAEA can inhibit the depolarization-induced  $^{45}\text{Ca}^{2+}$  fluxes mediated by the activation of L-type  $\text{Ca}^{2+}$  channels in a manner that was insensitive to SR141716A or PTX (Oz, et al., 2000). Further studies on T-tubule membranes showed that not only AEA, but also 2-AG (1-10  $\mu\text{M}$ ), inhibited  $^{45}\text{Ca}^{2+}$  fluxes and displaced the specific binding of DHP (Oz, et al., 2004a). However, direct effects of these endocannabinoids on L-type  $\text{Ca}^{2+}$  channels were not mimicked by the major psychoactive cannabinoid compound of marijuana, THC, and synthetic  $\text{CB}_1$  receptor agonists CP55,940 and WIN55,212-2.

In adult rat ventricular myocytes, the effect of AA, the metabolic product of AEA hydrolysis, on L-type  $\text{Ca}^{2+}$  channels was also studied (Liu, 2007). It was found that the exposure to AA directly alters the voltage dependence of gating properties of L-type  $\text{Ca}^{2+}$  channels, and thereby, reduces L-type  $\text{Ca}^{2+}$  current, which accounts for AA inhibition of contraction and  $\text{Ca}^{2+}$  transient in rat ventricular myocytes (Liu, 2007). In a more recent study, it was found that the synthetic cannabinoid A-955840 inhibits the function of L-type  $\text{Ca}^{2+}$  channels in

rabbit heart in a manner that is not sensitive to CB<sub>1</sub> and CB<sub>2</sub> antagonists (Su, et al., 2011).

### **1.2.6 Role of endocannabinoids in the cardiovascular system**

The cardiovascular effects of cannabinoid compounds have been recognized for several decades (Randall, et al., 2002; Pacher, et al., 2005a). In humans, the acute effect of smoking *Cannabis* usually manifests as an increase in heart rate with no significant change in blood pressure (Kanakis, et al., 1976). However, chronic use of marijuana in man, as well as, both acute and prolonged administration of THC to experimental animals, have been shown to cause long lasting decrease in blood pressure and heart rate (Benowitz and Jones, 1975). Because of the well-known effects of cannabinoids on the central nervous system, early research on their cardiovascular effects concentrated on the ability of these compounds to inhibit sympathetic tone as their mechanism of action (Vollmer, et al., 1974).

Since the discovery of the endocannabinoid system, regulation of various cardiovascular functions by these molecules has been studied extensively (Pacher, et al., 2005a; Pacher and Kunos, 2013). In both *in vitro* and *in vivo* studies, endocannabinoids have been shown to exert complex cardiovascular effects, both mediated by receptor-dependent and independent mechanisms. In experimental animals and humans (depending on the route of administration, duration and dose), the cardiovascular effects of endocannabinoids may include CB<sub>1</sub>-mediated bradycardia/tachycardia, hypotension, and depressed cardiac contractility (Malinowska, et al., 2012). Mechanisms of these effects involve modulation of autonomic outflow through sites of action at presynaptic autonomic nerve terminals and in the central nervous system, as well as direct effects on

myocardium and the vasculature (Pacher, et al., 2005a). Despite evidences on the presence of CB<sub>2</sub> receptors in the myocardium (Mukhopadhyay, et al., 2007; Bouchard, et al., 2003; Montecucco, et al., 2009) and a few recent studies implicating this receptor in myocardial protection (Bouchard, et al., 2003; Montecucco, et al., 2009), its role in cardiomyocytes remains elusive. Although the endocannabinoid system appears to play a limited role in cardiovascular regulation under normal physiological conditions, it may become overactivated and play important protective and/or detrimental roles in various disease conditions (Mukhopadhyay, et al., 2008). The various cardiovascular effects of the endocannabinoid system are described in the following sections.

#### **1.2.6.1 Cardiovascular effects of endocannabinoids *in vivo***

Systemic administration of cannabinoids in anesthetized rats and mice causes hypotension and bradycardia by peripheral inhibition of sympathetic outflow and increased vagal activity, respectively (Pacher, et al., 2005a). Anandamide was found to elicit a triphasic blood pressure response with bradycardia (Figure 1.9) (Varga, et al., 1995; Varga, et al., 1996; Lake, et al., 1997a; Malinowska, et al., 2012) similar to that reported earlier for THC (Siqueira, et al., 1979). The initial phase of the response consisted of bradycardia (with brief secondary hypotension) that lasted for a few seconds only, and was believed to be vagally mediated, as it was abolished by atropine treatment and vagotomy. This vagal component was followed by a brief pressor response which persisted in the presence of  $\alpha$ -adrenergic blockade, and also in rats in which sympathetic tone was abolished by pithing, and was thus not sympathetically mediated (Varga, et al., 1995).



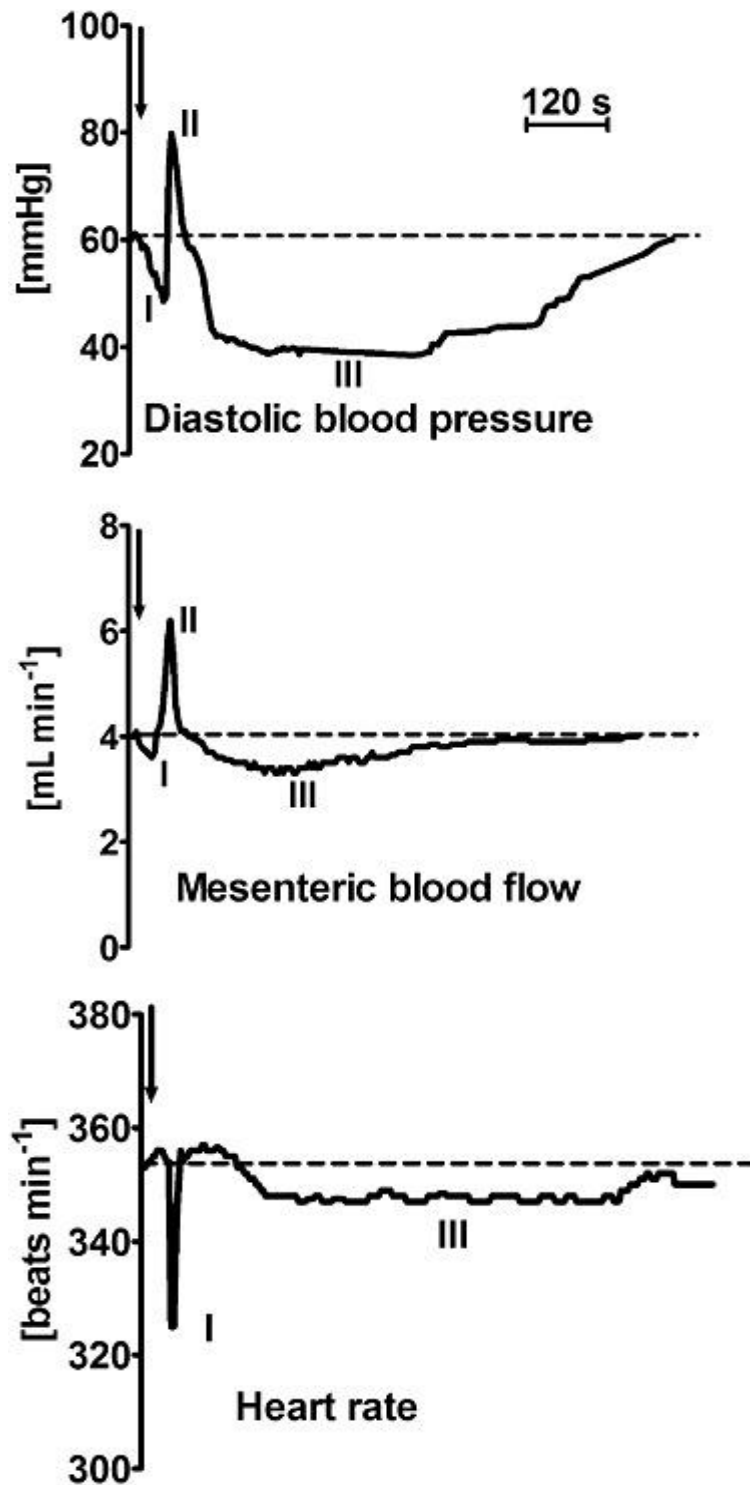


Figure 1.9 Typical traces showing the influence of AEA on cardiovascular parameters in anaesthetized rat. Adapted from Malinowska *et al.*, 2012.

The pressor component, which constitutes the second phase, was also unaffected by CB<sub>1</sub> receptor antagonists and it persisted in CB<sub>1</sub> knockout mice (Jarai, et al., 1999; Pacher, et al., 2004), indicating the lack of involvement of CB<sub>1</sub> receptors. The exact mechanism of this vasoconstrictive response is not well understood, however, direct action on the vascular smooth muscle has been proposed (Jarai, et al., 1999). Although the central involvement in the pressor response was ruled out, centrally administered cannabinoids can increase the activity of sympathoexcitatory neurons in the cardiovascular regulatory centers (Niederhoffer and Szabo, 1999). Therefore, the potential exists that cannabinoids may increase blood pressure via actions on the central nervous system. Currently known mechanisms of cannabinoid receptor signaling would suggest that they principally act via inhibition of neurotransmitter release, suggesting that the central sympathoexcitatory effects of cannabinoids may be mediated by disinhibition of inhibitory neurons.

The third phase of AEA effect was hypotension associated with moderate bradycardia that lasted for 2-10 minutes (Varga, et al., 1995; Varga, et al., 1996; Lake, et al., 1997a). Interestingly, the third phase was absent in conscious normotensive rats (Stein, et al., 1996; Lake, et al., 1997a) but present and more prolonged in conscious, spontaneously hypertensive rats (Lake, et al., 1997b; Batkai, et al., 2004b). Since sympathetic tone is known to be low in conscious undisturbed normotensive rats (Carruba, et al., 1987), these observations appear to be compatible with a sympatho-inhibitory mechanism, underlying AEA-induced hypotension and bradycardia. The reduction of the sympathetic tone by AEA is also compatible with early findings with THC, where experimental manipulations to decrease sympathetic tone resulted in a parallel decrease in the depressor

response to THC (Vollmer, et al., 1974). Likewise, AEA was unable to reduce blood pressure in anesthetized rats after cervical transection of the spinal cord or after blockade of  $\alpha$ -adrenoreceptor (Varga, et al., 1995). The finding that metAEA causes similar but more prolonged hypotension and bradycardia, eliminates the possibility that the effects of AEA are mediated indirectly by a metabolite (Kunos, et al., 2000).

Several lines of evidence implicate CB<sub>1</sub> receptors in AEA-induced hypotension and bradycardia. For example, these effects are effectively inhibited by the selective CB<sub>1</sub> receptor antagonist SR141716A (Lake, et al., 1997a; Varga, et al., 1995). This finding was supported by the total absence of cannabinoid-induced hypotension and bradycardia in CB<sub>1</sub> receptor-knockout mice (Ledent, et al., 1999). Interestingly, in a study carried out by Jerai *et al.*, it was found that AEA-induced mesenteric vasodilation persisted in mice deficient in CB<sub>1</sub> receptors or in both CB<sub>1</sub> and CB<sub>2</sub> receptors, suggesting a vasodilatory effect through a site distinct from CB<sub>1</sub> or CB<sub>2</sub> receptors (Jarai, et al., 1999). Further evidence for the involvement of CB<sub>1</sub> receptors is that the rank order of the hypotensive and bradycardiac potency of a series of cannabinoid analogs, including AEA, is identical to the rank order of potency of the same substances for binding to the CB<sub>1</sub> receptors in rat brain (Lake, et al., 1997a).

Studies have shown that stimulation of presynaptic CB<sub>1</sub> receptors inhibits norepinephrine release on peripheral sympathetic nerves, both *in vitro* (Ishac, et al., 1996; Vizi, et al., 2001) and *in vivo* (Varga, et al., 1996; Malinowska, et al., 1997), which has a major impact on blood pressure regulation. A recent study showed that the use of AM3506 (a FAAH inhibitor) in rodents revealed that the antihypertensive effects of endogenously elevated AEA levels are mediated via

activation of CB<sub>1</sub> receptors in the central nervous system, and a reduction in sympathetic tone (Godlewski, et al., 2010). Wagner *et al.*, showed that cannabinoids are potent coronary and cerebral vasodilator agents in the rats *in vivo* (Wagner, et al., 2001b). In the same study, the synthetic cannabinoid HU-210 (as a full agonist for CB<sub>1</sub> receptors ) and AEA (as a partial agonist for CB<sub>1</sub> receptors), differed in their effects on cardiac output and systemic vascular resistance (Wagner, et al., 2001b). Previous studies have also demonstrated that AEA caused SR141716A-sensitive coronary vasorelaxation in isolated perfused rat hearts (Randall and Kendall, 1997; Fulton and Quilley, 1998), implicating the involvement of cannabinoid receptors.

An *in vivo* study by Ellis *et al.* demonstrated that AEA causes cerebrovascular relaxation in the rat that was sensitive to indomethacin application, indicating that the effect was likely mediated by stimulating the release and metabolism of endogenous AA (Ellis, et al., 1995).

#### **1.2.6.2 Cardiovascular effects of endocannabinoids *in vitro***

The vasorelaxant effects of AEA are complex and appear to involve multiple cellular and molecular mechanisms. Anandamide has been shown to act via the release of endothelium-derived NO in a range of human blood vessels and the right atrium (Bilfinger, et al., 1998). Vasorelaxant effects were also seen in the rat isolated mesenteric (Randall, et al., 1996; Randall, et al., 1997; Plane, et al., 1997) and coronary vasculature (Randall and Kendall, 1997). However, in both preparations, AEA-induced relaxation was insensitive to cyclooxygenase inhibitors, endothelial denudation and inhibition of NO synthesis.

Further studies on the mechanism of AEA-induced vasorelaxant effect suggest that K<sup>+</sup> channels are also involved in their actions. For example, the

endothelium-independent relaxations by AEA in the mesentery (Randall, et al., 1996; White and Hiley, 1997) were blocked by raising extracellular  $K^+$ , suggesting that AEA-induced responses are mediated by the activation of  $K^+$  channels (Randall, et al., 1996; Plane, et al., 1997; White and Hiley, 1997; White and Hiley, 1998). Furthermore, relaxation to AEA was also sensitive to  $K^+$  channel blockade with tetraethylammonium (TEA) (Randall, et al., 1997). In line with these findings, AEA was found to inhibit delayed rectifier  $K^+$  channels in rat aortic and hepatic arterial myocytes (Zygmunt, et al., 1997; Van, I and Vanheel, 2000). The effect of endocannabinoids on  $Ca^{2+}$ -activated  $K^+$  channels has been equivocal. Whereas several studies in rat mesenteric arteries suggested a role for the large conductance  $Ca^{2+}$ -activated  $K^+$  (BKCa) channels (Plane, et al., 1997; Ishioka and Bukoski, 1999), others did not (White and Hiley, 1997; Ishioka and Bukoski, 1999; Fulton and Quilley, 1998). In addition to  $K^+$  channels,  $Ca^{2+}$  channels have also been shown to be modulated by endocannabinoids. For example, AEA-induced relaxation has been attributed to the inhibition of L-type VGCCs in cat cerebral arterioles (Gebremedhin, et al., 1999). However, another study has suggested that inhibition of  $Ca^{2+}$  mobilization mediates AEA effect in rat hepatic arteries (Zygmunt, et al., 1997).

Interestingly, the relaxant effect of AEA shows a significant tissue selectivity as it does not relax certain blood vessels such as rat carotid arteries (Holland, et al., 1999) and the rat aorta (Herradon, et al., 2007). However, AEA does relax rat hepatic and guinea pig basilar arteries (Zygmunt, et al., 1999) and the bovine coronary artery. Therefore, it is possible that there are regional and species differences in the actions of endocannabinoids.

In several studies in rat coronary, mesenteric, renal and rabbit mesenteric arteries, the vasorelaxant effects of AEA were antagonized by SR141716A, suggesting the involvement of CB<sub>1</sub> receptors (Randall, et al., 1996; Deutsch, et al., 1997; White, et al., 2001; Fulton and Quilley, 1998; Chaytor, et al., 1999). In contrast, the relaxant effect of AEA in other studies in rat mesenteric and bovine coronary arteries was insensitive to SR141716A (Plane, et al., 1997; Pratt, et al., 1998; Zygmunt, et al., 1999). In a study done in rat mesenteric and hepatic arteries, and in guinea pig basilar artery, it was reported that AEA-induced relaxation was unrelated to either endothelium or cannabinoid receptor, but attributable to activation of TRPV1 receptors located on the perivascular sensory nerves causing the release of the vasodilatory peptide calcitonin gene-related peptide (CGRP) (Zygmunt, et al., 1999). Similarly, involvement of TRPV1 receptors in the mesenteric vasodilator action of metAEA has also been suggested (Ralevic, et al., 2000). In this study, CGRP receptor antagonist and capsazepine inhibited the response to metAEA supporting the involvement of TRPV1 channels in the vasorelaxant action of AEA (Ralevic, et al., 2000).

In contrast to the increasing knowledge on the vascular effects of endocannabinoids, little is known about the effects of endocannabinoids on cardiac muscle. In earlier studies, the cardiodepressant effects of HU-210 and AEA, have been shown in isolated electrically stimulated human atrial appendages (Bonz, et al., 2003) and in isolated Langendorff rat hearts (Ford, et al., 2002). These *in vitro* studies are in agreement with earlier *in vivo* studies, indicating that AEA reduces both cardiac contractility and total peripheral resistance (Batkai, et al., 2004b). In isolated section of human right atrium (atrial appendage), AEA, metAEA and HU-210 dose-dependently decreased the

contractile performance. The negative inotropic effect was blocked by AM251 but not AM630. Indomethacin did not prevent the depression of contractility by AEA, and metAEA displayed the same effects as AEA (Bonz, et al., 2003). Furthermore, AEA continued to decrease the contractile performance in the presence of L-NAME, an inhibitor of nitric oxide synthase (NOS) (Bonz, et al., 2003). These findings suggest that the effects of AEA on contractile function are not mediated by CB<sub>2</sub> receptor activation, NO, or prostanoid release. Consistent with these findings, HU-210 decreased left ventricular pressure in isolated perfused rat heart (Maslov, et al., 2004; Krylatov, et al., 2005), and decreased myocardial contractility without a major effect on the total peripheral resistance (Pacher, et al., 2005a).

In an electrophysiological study in rat cardiac papillary muscle, AEA, at low concentrations (0.1-1µM), decreased the AP duration in a concentration-dependent manner and suppressed the amplitudes of cardiac APs (Li, et al., 2009). Furthermore, AEA inhibited L-type Ca<sup>2+</sup> currents in ventricular myocytes. Blockade of CB<sub>1</sub> receptors with AM251, but not CB<sub>2</sub> receptors with AM630, eliminated the effect of AEA suggesting that the effects of AEA are mediated through CB<sub>1</sub> receptors (Li, et al., 2009). In another study in rat heart, Ford *et al.*, showed that AEA induces negative inotropic responses in isolated Langendorff heart (Ford, et al., 2002). Interestingly, the cannabinoid antagonists SR141716A, AM281 and SR144528 significantly blocked the negative inotropic responses to AEA that were not significantly affected by AM251, AM630 and capsazepine, which led the authors to propose a novel site distinct from the classic CB<sub>1</sub> and CB<sub>2</sub> receptors (Ford, et al., 2002).

In addition to cannabinoid receptor-dependent effects in the heart, endocannabinoids can also interact directly with several classes of cardiac voltage-gated ion channels in a cannabinoid receptor-independent manner. For example, AEA is a potent blocker of potassium channel Kv1.5 which is highly expressed in human atria, and contributes to AP repolarization of human atrial myocytes (Barana, et al., 2010; Amoros, et al., 2010; Moreno-Galindo, et al., 2010). Concurrent with these results, AEA has been also shown to block cardiac Kv4.3 potassium channel in a receptor-independent manner (Amoros et al., 2010). Overall, these earlier studies suggest that cannabinoids have negative inotropic action on cardiac muscle. However, the role of cannabinoid receptors in mediating this effect is currently not clear.

### **1.2.6.3 Endocannabinoid system in cardiovascular disease**

Despite the presence of cannabinoid receptors, endocannabinoids and their metabolizing enzymes, the molecular mechanisms and physiological significance of the endocannabinoid system in the cardiovascular system under normal and pathological conditions are not fully understood. It has been widely accepted that the endocannabinoid system plays a limited role in cardiovascular regulation under normal physiological conditions, which is supported by the normal blood pressure, myocardial contractility and baroreflex sensitivity of cannabinoid receptor, or FAAH knockout mice (Pacher, et al., 2005b; Pacher, et al., 2006). Baseline cardiovascular parameters, systolic and diastolic functions, and baroreflex sensitivity were found to be similar in FAAH<sup>-/-</sup> and FAAH<sup>+/+</sup> mice. This suggests that, under normal physiological conditions, the absence of FAAH does not lead to the appearance of an endocannabinergic tone on the cardiovascular system (Pacher, et al., 2005b). In addition, in normotensive mice, it



was found that baseline blood pressure is similar in CB<sub>1</sub>-knockout mice and their wild-type littermates (Ledent, et al., 1999). However, in many pathological conditions such as heart failure, the endocannabinoid system may become overactivated and may contribute to hypotension/cardiodepression through cardiovascular cannabinoid receptors (Manitiu, 2013).

The levels of AEA, but not 2-AG, are elevated in the hearts of FAAH<sup>-/-</sup> mice (Pacher, et al., 2005b). Interestingly, these mice also show decreased deterioration of cardiac function with age relative to their FAAH<sup>+/+</sup> littermates (Batkai, et al., 2007), which may be due to the enhancement of the effects of endogenous AEA. The finding of measurable levels of AEA in mouse heart contrasts with an earlier report that AEA was undetectable in lipid extracts of normal rat heart, although 2-AG was present (Schmid, et al., 2000). Nevertheless, it seems that both synthetic and metabolic pathways for endocannabinoids are present in the mammalian heart. However, the capacity for producing NAPE precursor appears to be low in several species, including humans (Moesgaard, et al., 2002), and with the exception of mice, the evidence for AEA synthesis and activity is generally circumstantial. On the other hand, alterations in endocannabinoid system tone has been suggested to be associated with various pathological states as a result of the altered expression of cannabinoid receptors, endocannabinoid metabolizing enzymes and synthetic pathways, in a tissue specific and time-dependent manner (Pacher and Kunos, 2013).

Earlier studies in cardiac muscle have shown that a considerable elevation in NAEs content can occur under hypoxic conditions when extensive membrane degradation occurs during myocardial infarction (Schmid, et al., 1996; Epps, et al., 1979; Epps, et al., 1982). In fact, accumulation of NAEs during pathological

conditions was first observed in experimental myocardial infarction induced by ligation of coronary arteries in canine heart (Epps, et al., 1982; Epps, et al., 1979).

In cultured human coronary artery endothelial cells (Rajesh, et al., 2010) and cardiomyocytes (Mukhopadhyay, et al., 2010), CB<sub>1</sub> activation has been shown to promote stress signaling, cell death, and decreased contractility (Pacher, et al., 2008; Montecucco and Di Marzo, 2012). Furthermore, in several pathological conditions (e.g. shock, heart failure, cardiomyopathies and advanced liver cirrhosis), the endocannabinoid system may become activated to promote hypotension and cardiodepression through cardiovascular CB<sub>1</sub> receptors (Pacher, et al., 2006; Pacher, et al., 2008). In rat models of acute and chronic myocardial infarction, studies with CB<sub>1</sub> agonists/antagonists yielded conflicting results. For example, the findings by Wagner *et al.* indicated that the activation of CB<sub>1</sub> receptors contributes to severe hypotension after experimental myocardial infarction in rats. In this study, the selective CB<sub>1</sub> antagonist SR141716A prevented post-myocardial infarction hypotension, but aggravated early endothelial dysfunction and worsened mortality (Wagner, et al., 2001a). In a subsequent study, the authors reported a deleterious effect of CB<sub>1</sub> antagonism with AM251 on cardiac function in a chronic myocardial infarction model. On the other hand, treatment with the synthetic agonist HU-210 prevented hypotension and endothelial dysfunction in aortic rings isolated from treated rats (Wagner, et al., 2003). A possible explanation of the conflicting results in these two studies might be the involvement of non-CB<sub>1</sub> receptor mediated effects.

More recent evidence suggested a cardioprotective role of CB<sub>1</sub> antagonism. The role of the endocannabinoid system was explored in a model of doxorubicin (DOX)-induced heart failure (Mukhopadhyay, et al., 2010).

Following DOX administration, the tissue AEA content, but not CB<sub>1</sub>/CB<sub>2</sub> receptor expression, was elevated in the myocardium and also in cardiomyocytes exposed to DOX *in vitro*, suggesting activation of the endocannabinoid system. Pretreatment of mice with CB<sub>1</sub> antagonists, SR141716A and AM281, not only improved DOX-induced cardiac dysfunction, but also attenuated the DOX-induced cell death *in vivo* and *in vitro*. These observations suggest that the cytoprotective role of CB<sub>1</sub> antagonists in cardiac pathologies may extend beyond the hemodynamic effects.

Other studies have also supported the role of the endocannabinoid system in cellular metabolism and viability. For example, AEA was shown to limit the damage induced by ischemia-reperfusion in rat isolated hearts (Underdown, et al., 2005; Lepicier, et al., 2007). Similarly, AEA has been shown to protect the heart from adrenaline-induced arrhythmias (Ugdyzhekova, et al., 2001) and arrhythmias induced by ischemia-reperfusion through the stimulation of CB<sub>2</sub> receptors (Krylatov, et al., 2002). Furthermore, using potent CB<sub>2</sub> receptor agonists and knockout mice, it has been demonstrated that CB<sub>2</sub> receptor activation has a protective effect against myocardial ischemic-reperfusion injury (Hajrasouliha, et al., 2008). Another study in isolated rat heart provided direct evidence of the potential cardioprotective role of endocannabinoids and AEA-related mediator signaling in ischemia-reperfusion injury was investigated (Lepicier, et al., 2003). Interestingly, it was shown that perfusion with PEA and 2-AG, but not AEA, decreased myocardial damage in isolated rat hearts. In addition, infarct size was limited by either a selective CB<sub>1</sub> agonist (arachidonoyl-2-chloroethylamide; ACEA) or a selective CB<sub>2</sub> agonist (JWH015). However, PEA is supposedly inactive at CB<sub>1</sub> and CB<sub>2</sub> receptors, a fact supported by the finding that PEA was

devoid of activity when administered to rat isolated heart (Ford, et al., 2002). In contrast, AEA causes negative inotropy and coronary vasodilatation in rat isolated hearts (Ford, et al., 2002). It is therefore interesting that AEA failed to reduce myocardial infarction injury while PEA and 2-AG were effective. In a subsequent study in isolated rat heart, however, AEA perfusion reduced the infarct size, which was blocked by either CB<sub>1</sub> or CB<sub>2</sub> antagonism, using SR141716A or SR144528, respectively. However, using Arachidonoyl cyclopropylamide (ACPA; CB<sub>1</sub> agonist) and JWH-133 (CB<sub>2</sub> agonist) could not mimic the effect of AEA, suggesting the involvement of a novel cannabinoid site of action (Underdown, et al., 2005).

Activation of CB<sub>2</sub> receptors in inflammatory cells and endothelium has been suggested to attenuate TNF- $\alpha$ -induced endothelial inflammatory response, chemotaxis, and adhesion of inflammatory cells to the activated endothelium. Subsequent release of various proinflammatory mediators (key processes involved in the initiation and progression of atherosclerosis, restenosis and reperfusion injury) (Mach, et al., 2008; Pacher and Hasko, 2008), and smooth muscle proliferation have also been proposed to be decreased after the activation of CB<sub>2</sub> receptors (Rajesh, et al., 2007). However, the role of myocardial CB<sub>2</sub> receptors during ischemia-reperfusion and other cardiovascular pathologies is currently not well established.

The main objectives of the current study are:

1. To test the effects of AEA on contractility and  $\text{Ca}^{2+}$  signaling in rat ventricular myocytes.
2. To test the effects of AEA on the characteristics of cardiac action potential.
3. To study the effects of AEA on cardiac voltage-activated inward  $\text{Na}^+$  ( $I_{\text{Na}}$ ) and  $\text{Ca}^{2+}$  ( $I_{\text{L,Ca}}$ ) currents, which are the major inward currents shaping the action potential in ventricular myocyte.
4. To study the effects of AEA on cardiac sodium-calcium exchanger (NCX).

## 2. MATERIALS AND METHODS

### 2.1 Experimental animals

The work was performed with approval of the Animal Research Ethics Committee of the College of Medicine and Health Sciences (Al Ain, UAE). The original stock of Wistar rats were purchased from Harlan Laboratories (Oxon, England). Animals were bred at our own Animal Facility from the original stock. The animals were housed in polypropylene cages (43 x 22.5 x 20.5 cm; six rats/cage) in climate and access controlled rooms (22-24 °C; 50 % humidity). The day/night cycle was 12 h/12h. Food and water were provided *ad libitum*. The food was standard maintenance diet for rats purchased from Emirates Feed Factory (Abu Dhabi, UAE).

### 2.2 Ventricular myocyte isolation

Ventricular myocytes were isolated from adult male Wistar rats ( $264 \pm 19$  g) according to previously described technique (Howarth, et al., 2002). The animals were euthanized using a guillotine and hearts were removed rapidly and immersed in cold perfusate to limit any ischemic injury during the period between excision and the restoration of vascular perfusion. Having cleared extraneous tissue, the aorta was carefully eased over the tip of the cannula and mounted for retrograde perfusion according to Langendorff method. The Langendorff apparatus (Figure 2.1) employed a roller (peristaltic) pump (Minipuls3, Gilson, France) which was set to deliver isolation solution at a constant flow rate (8 ml/minute/g weight of tissue) and at 36-37 °C with a solution containing (mM):

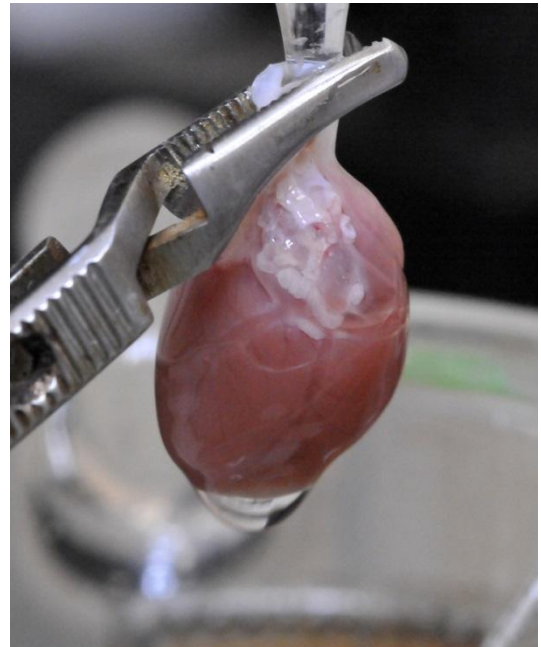
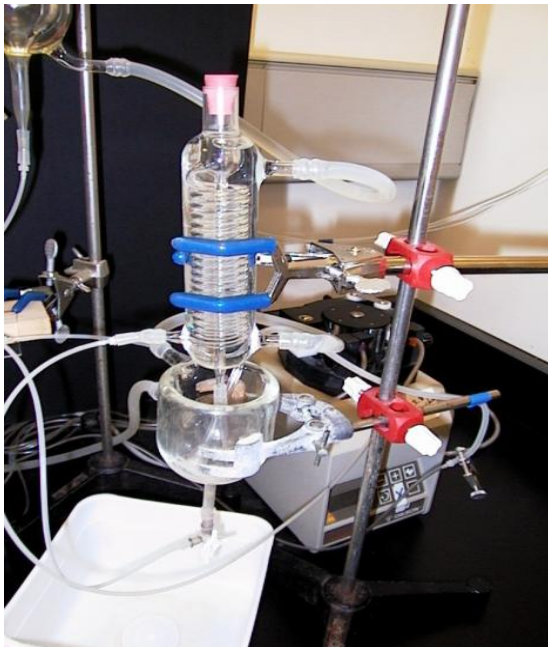
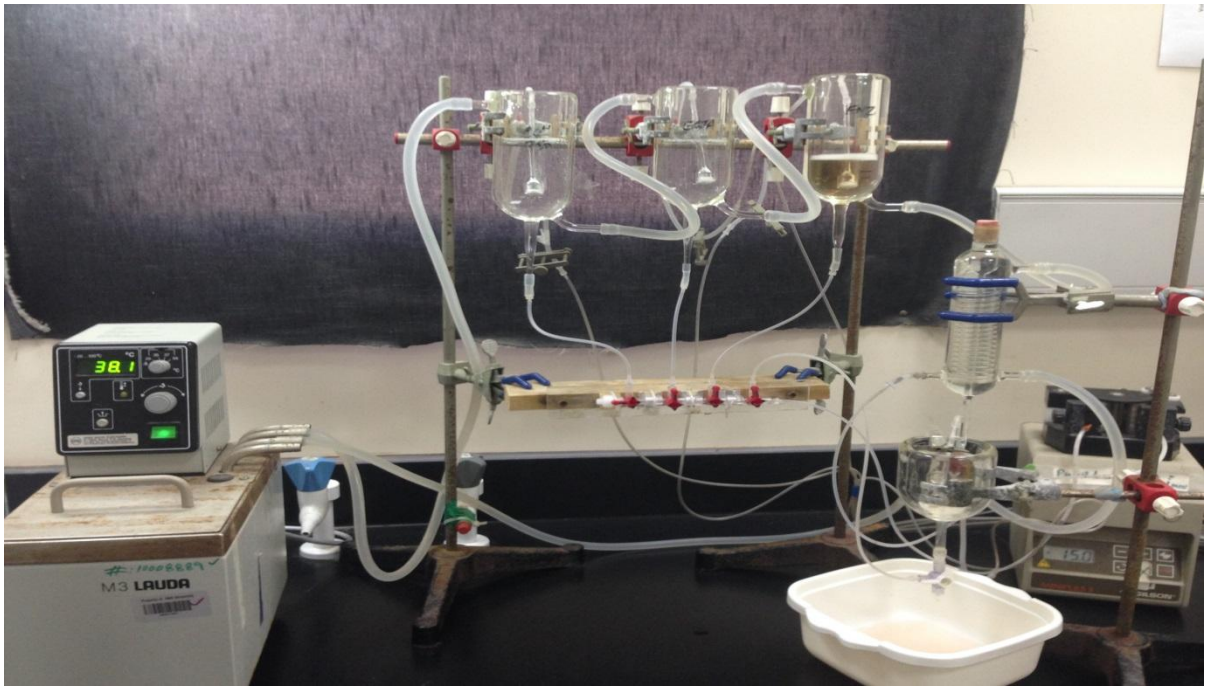


**Figure 2.1 Langendorff apparatus:** Arrangement of the system (upper panel), heat exchanger and heart warming jacket (lower left panel) and cannulated heart (lower right panel).

130 NaCl, 5.4 KCl, 1.4 MgCl<sub>2</sub>, 0.75 CaCl<sub>2</sub>, 0.4 NaH<sub>2</sub>PO<sub>4</sub>, 5 HEPES, 10 glucose, 20 taurine, and 10 creatine set to pH 7.3 with NaOH.

Once the heart contraction had stabilized, perfusion was continued for 4 minutes with Ca<sup>2+</sup>-free isolation solution containing 0.1 mM EGTA, and then for 6 minutes with cell isolation solution containing 0.05 mM Ca<sup>2+</sup>, 0.75 mg/ml collagenase (type 1; Worthington Biochemical Corp, USA) and 0.075 mg/ml protease (type X1 V; Sigma, Germany). Ventricles were then excised from the heart, minced and gently shaken in a collagenase-containing isolation solution supplemented with 1 % BSA for 4 minutes at 36-37 °C. The suspension was then filtered through a nylon mesh (pores of 300 µm). Tissue remaining in the nylon mesh was re-suspended in collagenase-containing isolation solution supplemented with 1 % BSA and shaken for 4 minutes at 36-37 °C. The filtrate suspension of cells was centrifuged at 400 rpm for 1 minute. Subsequently, the supernatant was removed and the cell pellet was re-suspended in isolation solution containing 0.75 mM Ca<sup>2+</sup>. This process was repeated four times. Ventricular myocytes were collected from second, third and fourth shakes and stored at 4 °C. Experiments were performed in ventricular myocytes that displayed rod-shaped morphology and regular striations (Figure 2.2).

### **2.3 Measurement of ventricular myocyte shortening**

Shortening of myocytes was recorded using a video edge detection system (VED-114, Crystal Biotech, USA) (Figure 2.3; for the arrangement of the recording system used for video edge detection experiments). This system is used for measuring the length or width of cells or small tissues in real-time. The video edge detection system was composed of a high-speed video camera (Myotrac,



Crystal Biotech, UT, USA), an analog dual-edge detector (VED-114, Crystal Biotech, USA), a data logging device (CED-1401+, Cambridge Electronic Design, Cambridge, Cambridge, UK), a PC and a monitor. The system is able to record up to 240 length measurements per second.

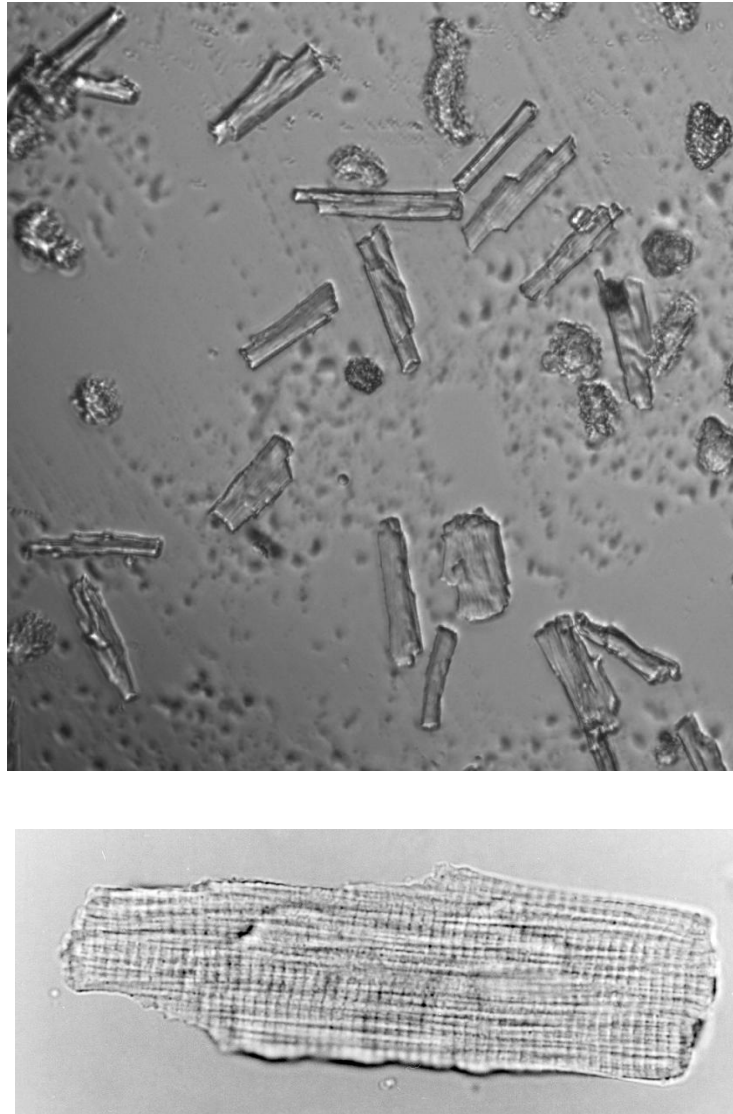


**Figure 2.2 Micrographs of ventricular cells:** The upper panel shows a collection of viable (rod-shaped) and nonviable (round-shaped) ventricular myocytes. The lower panel shows a single freshly isolated ventricular myocyte. Myocytes were typically 80-120  $\mu\text{m}$  in length.



**Figure 2.3** The recording system used for video edge detection and  $\text{Ca}^{2+}$  imaging experiments: The system includes an anti-vibration table (A), a Faraday cage (B), an inverted microscope (C), a cell superfusion system (D) with a temperature control system (E), a video edge motion detector (F), a microfluorescence photometry system (G) and an electrical stimulator (H).

Ventricular myocytes were first allowed to settle on the glass bottom of a Perspex chamber mounted on the stage of an inverted microscope (Axiovert 35, Zeiss, Germany). Cells were then electrically stimulated at 1 Hz to produce contraction by means of two platinum electrodes positioned around the circumference of the chamber and connected to an electrical stimulator (SD-5, Grass Instruments, USA). Using a microscope equipped with a high-speed camera, the cell is positioned so that the axis of contraction runs from left to right on the video screen. The cursors were positioned over the edges of the cell (Figure 2.4). The raster line was adjusted to move the cursors upwards or downwards. The edge detector triggers on the first large white/black or black/white transition within the left cursor and the last white/black or black/white transition within the right cursor. Switches set the desired transition type (black/white or white/black) and the threshold for each cursor. Under these conditions, slightly defocusing the cell image can enhance the edge contrast. A white dot within each cursor shows the edge as detected by the system. An analog voltage output proportional to the distance between the two edges is conveyed to the data logging device (CED1401+, Cambridge Electronic Design, Cambridge, UK), and to the computer. Data were acquired and analyzed with Signal Averager software v 6.37 (Cambridge Electronic Design, UK).

Myocytes were superfused (3–5 ml/min) with normal Tyrode (NT) containing (in mM): 140 NaCl, 5 KCl, 1 MgCl<sub>2</sub>, 10 glucose, 5 HEPES and 1.8 CaCl<sub>2</sub> (pH 7.4). Inflow of superfusate to the chamber was controlled by two micropumps (P07002-39/P07002-33, Cole-Parmer, USA). Outflow and the level of fluid in the chamber was controlled by a glass tube dipping into the chamber and connected to a waste bottle which in turn was connected to a service vacuum

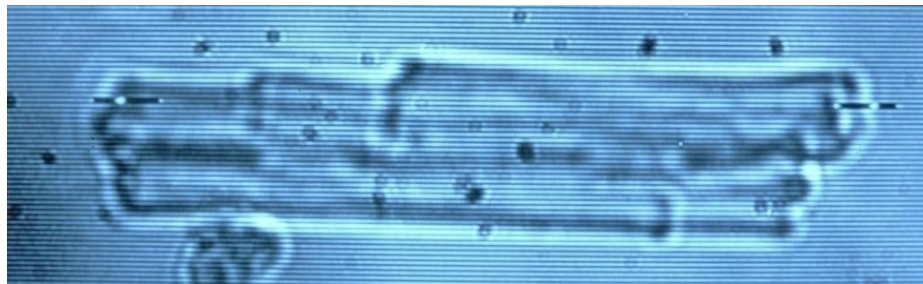


**Figure 2.4 Video edge motion detection:** The upper panel shows the video edge motion detector. The lower panel shows a ventricular myocyte with video edge cursors positioned across the edges of the cell.

line. The temperature of the chamber solution was regulated by a temperature controller (TC-20, NPI, Germany), which comprised a heating coil wound around the inflow line, a thermistor located in the chamber and the control system. Resting cell length (RCL), time to peak (TPK) shortening, time from peak to half relaxation ( $T_{\text{HALF}}$ ) and amplitude of shortening (expressed as a % of resting cell length) were measured under these conditions.

#### **2.4 Western immunoblot assay**

Ventricles were obtained from normal Wistar rats as described earlier in section 2.2. In the first step, tissue samples were flash-frozen in liquid nitrogen and stored at -80 °C for later use. After thawing, tissue extracts were prepared by homogenization on ice with RIPA buffer (Pierce Biotechnology, IL, USA) supplemented with protease inhibitors (Roche, GmbH, IN, USA). Later, the extracts were clarified to remove the cellular debris by centrifugation at 13000 r.p.m. for 15 minutes at 4 °C. Protein content in the extracts was determined using the Lowry assay (BioRad). A measure of 50 µg protein was resolved in 12 % SDS-PAGE and was transferred onto nitrocellulose membranes (GE Healthcare, UK). Blocking was performed for 2 hours at room temperature with 5 % non-fat skimmed milk powder prepared in phosphate buffer solution (PBS) containing 0.1 % Tween 20 (Sigma, CA, USA). After washing with phosphate-buffered saline 0.1 % Tween 20 (PBST), the membranes were probed with either rabbit polyclonal CB<sub>1</sub> (Cayman Chemicals, 1: 1000 dilution) or with an antibody raised against the last 15 residues of rat CB<sub>1</sub> or CB<sub>2</sub> antibody (Cayman Chemicals, 1: 1000 dilution) overnight at 4 °C. After subsequent washing with PBST, the secondary antibody (goat anti- rabbit) coupled with HRP (horseradish peroxidase) (GE Biosciences, UK) was added and the blots were incubated at room

temperature for 1 hour. Later, the membranes were developed using a chemiluminescence detection kit (Super Signal-West Pico Substrate, Pierce). To confirm uniform loading, the membranes were stripped and re-probed with  $\beta$ -actin (Chemicon, CA, USA).

## **2.5 Measurement of intracellular $\text{Ca}^{2+}$ concentration**

In order to measure intracellular  $\text{Ca}^{2+}$  concentration, ventricular myocytes were loaded with the fluorescent indicator fura-2 AM (F-1221, Oregon, Molecular Probes, USA) (Howarth, et al., 2002). Fura-2, a polyamino carboxylic acid, is an ultra violet light-excitable ratiometric  $\text{Ca}^{2+}$  indicator. In its salt form, fura-2 can be introduced into the cell by microinjection. As an acetoxymethyl (AM) ester, it can passively diffuse across cell membranes. Once inside the cell, the esters are cleaved by intracellular esterases to yield cell-impermeable fluorescent indicators. Upon binding to  $\text{Ca}^{2+}$ , fura-2 AM exhibits an absorption shift that can be observed by scanning the excitation spectrum at wavelengths between 300 nm and 400 nm, while monitoring the fluorescence emission at wavelength  $\sim$  510 nm.

The fluorescence photometry system was used to generate excitation light and collect emissions (Cairn Research, Kent, UK). A monochromator, comprising the light source (75 W Xenon arc lamp), rapid galvanometer diffraction grating and automated exit slit generated excitation light of required wavelength, bandwidth and intensity. In the case of fura-2 AM, the excitation light alternated rapidly between 340 and 380 nm. The light was transmitted from the source via a liquid light guide and various mirrors and a FLUAR 40x/1.30 (ultraviolet transmitting) oil-immersed objective to the fura-2 AM loaded cell. A 400 nm long pass dichroic filter reflected light  $<$  400 nm to the cell. Light emitted from the cell

was directed through the objective and through a 600 nm long pass dichroic filter which transmitted red bright field light  $> 600$  nm to a high-speed video camera (Myotrac, Crystal Biotech, UT, USA) so that the cell could be visualized on a monitor. Finally, fluorescence light  $< 600$  nm was directed via a 480 nm long-pass emission filter to a bi-alkali photomultiplier tube (C151, Cairn Research, Kent, UK) and thence, as a high voltage signal, to the control system (C208, Cairn Research, Kent, UK). The control system collected 340 and 380 nm signals and generated a ratio (340/380 nm) signal. These signals were conveyed via a data logging device (CED-1401+, Cambridge Electronic Design, Cambridge, UK) to the computer for processing and for display on the computer monitor. The 340/380 fura-2 AM ratio provided the index of intracellular  $\text{Ca}^{2+}$ .

In our experiments, 6.25  $\mu\text{l}$  of a 1 mM stock solution of fura-2 AM (dissolved in DMSO) was added to 2.5 ml of cells to give a final fura-2 AM concentration of 2.5  $\mu\text{M}$ . Myocytes were shaken gently for 10 minutes at room temperature. After loading, myocytes were centrifuged, washed with normal Tyrode to remove extracellular fura-2 AM and then left for 30 minutes to ensure complete hydrolysis of the intracellular ester. In order to measure intracellular  $\text{Ca}^{2+}$  concentration, myocytes were alternately illuminated by 340 nm and 380 nm light using a monochromator (as mentioned earlier) which changed the excitation light every 2 milliseconds. The resulting fluorescence emitted at 510 nm was recorded by the photomultiplier tube and the ratio of the emitted fluorescence at the two excitation wavelengths (340/380 ratio) was calculated to provide an index of intracellular  $\text{Ca}^{2+}$  concentration.

Data were acquired and analyzed with Signal Averager software v 6.37 (Cambridge Electronic Design, UK). Resting fura-2 ratio, TPK  $\text{Ca}^{2+}$  transient,

$T_{\text{HALF}}$  decay of the  $\text{Ca}^{2+}$  transient, and the amplitude of the  $\text{Ca}^{2+}$  transient were measured in electrically stimulated (1 Hz) myocytes.

## **2.6 Measurement of sarcoplasmic reticulum $\text{Ca}^{2+}$ content**

Sarcoplasmic reticulum (SR)  $\text{Ca}^{2+}$  release was assessed using previously described technique (Howarth, et al., 2002; Bassani, et al., 1995). After establishing steady state  $\text{Ca}^{2+}$  transients in electrically stimulated (1 Hz) myocytes maintained at 35–36 °C and loaded with fura-2, stimulation was paused for a period of 5 seconds. Caffeine (20 mM) was then applied for 10 seconds using a solution switching device customized for rapid solution exchange. Electrical stimulation was resumed and the  $\text{Ca}^{2+}$  transients were allowed to recover to steady state levels. SR-releasable  $\text{Ca}^{2+}$  was assessed by measuring the area under the curve of the caffeine-evoked  $\text{Ca}^{2+}$  transient. Fractional release of SR  $\text{Ca}^{2+}$  was assessed by comparing the amplitude of the electrically evoked steady state  $\text{Ca}^{2+}$  transients with that of the caffeine-evoked  $\text{Ca}^{2+}$  transient and refilling of SR was assessed by measuring the rate of recovery of electrically evoked  $\text{Ca}^{2+}$  transients following application of caffeine.

## **2.7 Assessment of myofilament sensitivity to $\text{Ca}^{2+}$**

In some cells shortening and fura-2 ratio were recorded simultaneously. Myofilament sensitivity to  $\text{Ca}^{2+}$  was assessed from phase-plane diagrams of fura-2 ratio vs. cell length by measuring the gradient of the fura-2-cell length trajectory during late relaxation of the twitch contraction (Spurgeon, et al., 1992). The position of the trajectory reflects the relative myofilament response to  $\text{Ca}^{2+}$  and hence, can be used as a measure of myofilament sensitivity to  $\text{Ca}^{2+}$ .



## **2.8 Electrophysiological recording of whole-cell currents (Patch clamp technique)**

### **2.8.1 Pipettes**

The pipettes for recording in ventricular myocytes were fabricated from filamented BF 150-86-10 borosilicate glass (OD= 1.5 mm, ID= 0.86 mm, Sutter Instruments Co., CA, USA) using a horizontal puller (Sutter Instruments Co., CA, USA). In order to get a good contact between the electrode and the cell membrane without damaging the cell membrane, the electrode tips were fire-polished using a microforge (Zeiss ID03, Germany). Electrode resistance ranged between 2.0 and 4.0 M $\Omega$  as assessed in our standard pipette and extracellular solutions using the pClamp 10 software.

### **2.8.2 Seal Penetration**

Whole-cell version of the patch clamp technique was used to measure ion currents (see Figure 2.5; for the arrangement of the patch clamp setup). Cells were mounted on the stage of an inverted phase-contrast microscope (Nikon diaphot, Tokyo, Japan). The output signals were filtered at 5 KHz with an 8 pole filter, and stored on the hard disk of a computer for off-line analysis. The pipette, which had a small positive internal pressure in order to keep the tip clean, was pushed gently onto the cell surface by using a three-axis micromanipulator (ACCi UI, Scientifica, UK). A tight seal (gigaseal) between the membrane and the tip of the pipette (1-10 G $\Omega$ ) was obtained by the application of suction through the pipette. Further suction disrupted the membrane under the tip of the pipette allowing the pipette solution to dialyze the cell (Figure 2.6). The experiments were carried out at room temperature (22–24 °C) in order to ensure a longer survival time of patched cells and a better time resolution of the membrane currents.

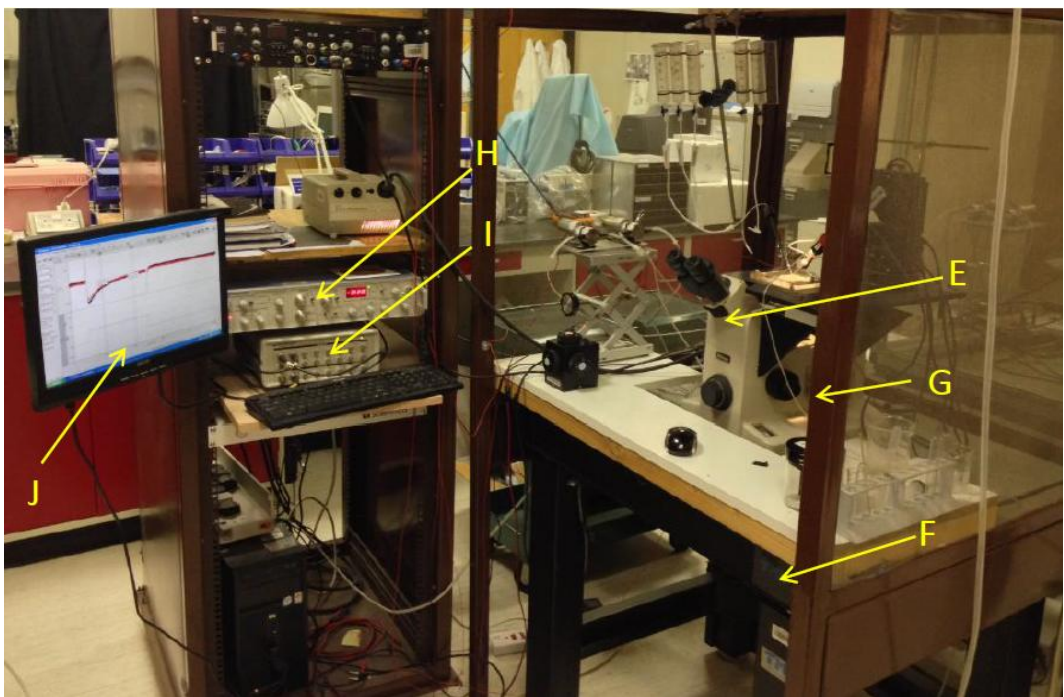
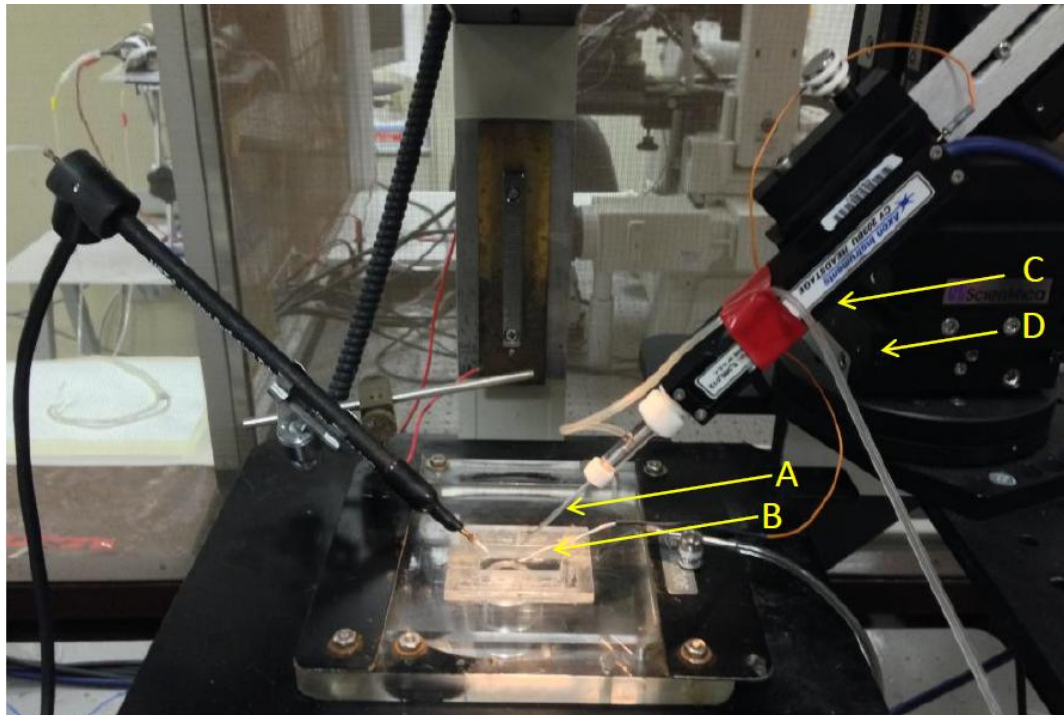


**Figure 2.5 Patch clamp experimental setup:** The patch pipette with internal recording electrode (A) and reference electrode (B) are connected to the headstage (C) which is mounted on a micromanipulator (D). Isolated cells are visualized with an inverted light microscope (E). The microscope, the micromanipulator, and

headstage are placed on an anti-vibration table (F) to isolate these components from vibrations that may interfere with gigaseal formation and placed in a Faraday cage (G) to shield the setup from ambient electrical noise. The flow of the currents into the pipette can be recorded using a highly sensitive amplifier (H) which is connected to an analog to digital converter (digitizer) (I), where the signal is digitized and sent to a computer for data analysis. A computer screen (J) is used for monitoring experiments and for data display.

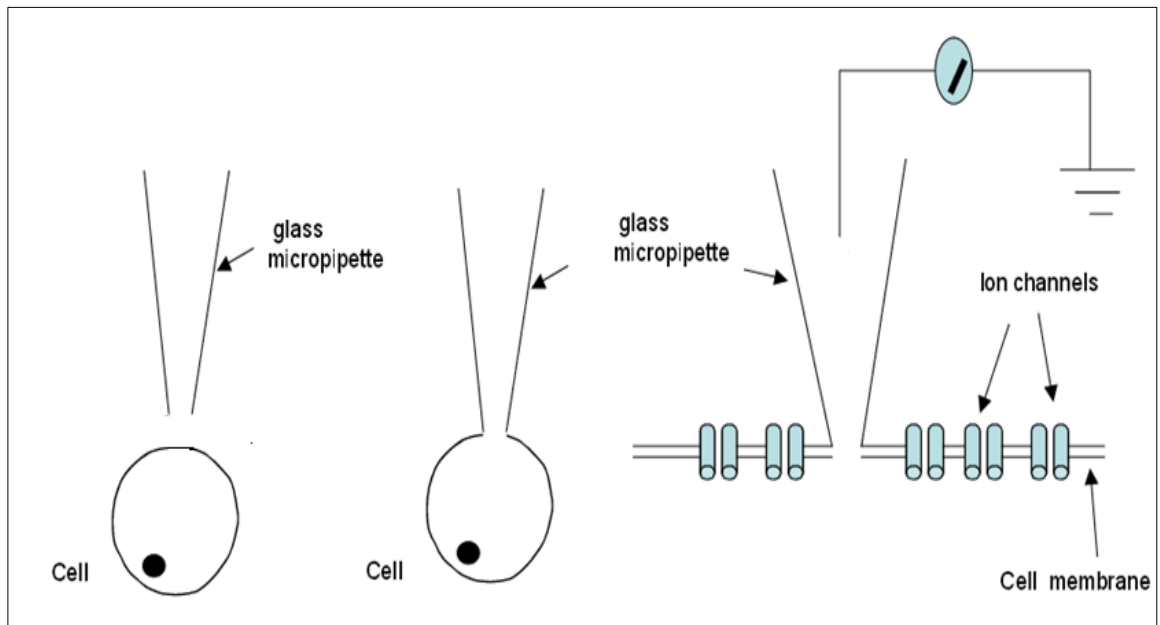


**Figure 2.6 Schematic presentation of whole cell configuration of patch clamp technique.**

The membrane currents of cardiac ventricular myocytes were recorded using an Axopatch 200B amplifier (Molecular Devices, Downingtown, PA, USA) linked to an A/D interface (Digidata 1322; Molecular Devices) connected to an IBM computer.

Cells that had stable currents from the third to fifth minutes after penetration of the membrane were used in the majority of our experiments. Drugs were tested once the whole-cell currents had reached a stable level (usually 10 minutes after obtaining the whole-cell configuration). A series of voltage steps were applied to determine the current-voltage relationship. Different drugs were then added directly to the bath solution and the change in the magnitude of current was monitored continuously. In some cells the bath solution was changed to assess the recovery after washout of tested compound.

The rate of solution flow to the recording chamber was controlled by two micropumps (Micropump Inc., WA, USA). Changes of external solutions and application of drugs were performed using a multi-line perfusion system with a common outflow connected to recording chamber. Electrophysiological data were analyzed using pClamp 10.2 (Molecular Devices, Union City, CA) and Origin 7.0 (OriginLab Corp., Northampton, MA) software. The amplitudes of the currents were normalized to cell membrane capacitance (nA/pF).

### **2.8.3 Measurement of action potentials**

#### **2.8.3.1 Protocol for measuring action potentials**

APs were measured using the current clamp mode of the whole-cell patch clamp technique. After giga seal formation, the membrane was ruptured with gentle suction to obtain whole cell configuration. The generation of APs was

evoked by 0.9-1 nA depolarizing current pulses of 4 ms duration applied at a frequency of 0.2 Hz. During a typical experiment, the following protocol was employed: first, whole-cell configuration was established and 4 to 5 minutes dialysis of the myocytes with pipette solution was allowed to ensure the equilibrium conditions between the pipette solution and intracellular milieu. Subsequent to achieving stable recordings of baseline electrical activity ( $V_{rest}$  and AP parameters), myocytes were exposed to the tested drug for 10 to 15 minutes and subsequently it was washed out.

### **2.8.3.2 Solutions**

Basic extracellular solutions used for electrophysiological recordings contained (in mM): 144 NaCl, 5.4 KCl, 1.8 CaCl<sub>2</sub>, 1.2 MgCl<sub>2</sub>, 1 NaH<sub>2</sub>PO<sub>4</sub>, 10 HEPES, 10 glucose, and pH 7.4 (adjusted with NaOH). Recording patch pipettes were filled with intracellular solution containing (in mM): 10 KCl, 10 KOH, 105 K-aspartate, 15 NaCl, 1 MgCl<sub>2</sub>, 10 HEPES, 4 Mg-ATP, 5 Sucrose, and pH 7.2 (adjusted with HCl).

### **2.8.4 Measurement of Na<sup>+</sup> currents**

#### **2.8.4.1 Protocol for measuring Na<sup>+</sup> currents**

For recording of sodium currents ( $I_{Na}$ ), data were elicited from a holding potential of -80 mV and depolarized with 50 ms pulses to +60 mV in 10 mV increments every 10 seconds. Steady-state activation (SSA) curves of  $I_{Na}$  before and after AEA application were derived by fitting the respective current-voltage relationship ( $I-V$ ) with the product of Boltzmann equation which describes voltage-dependence of SSA. This allowed us to determine if the drug influences

the parameters of  $I_{Na}$  SSA, the voltage of half-maximal activation ( $V_{1/2}$ ) and the slope factor ( $k$ ).

The conductance was calculated using the following equation,  $G = I/(V_m - V_{rev})$ , where  $I$  is the current amplitude,  $V_m$  is the test potential and  $V_{rev}$  is the reversal potential. The corresponding steady-state activation curves were obtained by normalizing the conductance to the peak conductance. The normalized conductances ( $G/G_{max}$ ) were then plotted against the test potentials and fitted with the Boltzmann equation:

$$G / G_{max} = 1 / (1 + \exp[-(V_m - V_{1/2}) / k])$$

where  $V_{1/2}$  is the voltage at half-maximal conductance and  $k$  is the slope factor.

In order to determine if the drug influences the properties of VGSCs inactivation, we compared steady-state inactivation (SSI) dependencies of  $I_{Na}$  in the absence and presence of tested drug. SSI curves were acquired using a standard voltage protocol consisting of a prolonged (400 ms) preconditioning pulse to various  $V_m$  in the range of -100 mV to +70 mV which was immediately followed by the constant  $I_{Na}$  activating test pulse to  $V_m = -20$  mV. SSI-dependency was plotted as normalized amplitude of  $I_{Na}$  at  $V_m = -20$  mV against the value of conditioning  $V_m$ . Current amplitude was normalized to the peak current ( $I/I_{max}$ ), and plotted against each conditioning potential. The steady-state inactivation curves were fitted with the Boltzmann function,

$$I / I_{max} = 1 / (1 + \exp[(V_m - V_{1/2}) / k])$$

where  $V_{1/2}$  is the voltage at which half the channels are available for opening, and  $k$  is the slope factor.

#### 2.8.4.2. Solutions

Extracellular solution for recordings of  $I_{Na}$  consisted of (in mM): 100 TEACl, 40 NaCl, 10 Glucose, 1 MgCl<sub>2</sub>, 5 CsCl, 0.1 CaCl<sub>2</sub>, 1 NiCl<sub>2</sub>, and 10 HEPES (adjusted to pH 7.3 with CsOH). Intracellular solution contained (in mM) 135 CsCl, 5 NaCl, 10 EGTA, 10 HEPES and 1 MgATP (adjusted to pH 7.25 with CsOH).

#### 2.8.5 Measurement of L-type Ca<sup>2+</sup> currents

##### 2.8.5.1 Protocol for measuring L-type Ca<sup>2+</sup> currents

For recording of Ca<sup>2+</sup> currents ( $I_{L,Ca}$ ), data were elicited from a holding potential of -50 mV to membrane potentials ranging from -70 mV to +70 mV in 10 mV increments for 300 ms. Elimination of contaminating  $I_{Na}$  during recording of  $I_{Ca}$  was achieved by applying voltage step-pulses from relatively depolarized  $V_h$  of -50 mV, which produced steady-state  $I_{Na}$  inactivation.

The conductance was calculated using the following equation,  $G = I/(V_m - V_{rev})$ , where  $I$  is the current amplitude,  $V_m$  is the test potential and  $V_{rev}$  is the reversal potential. The corresponding steady-state activation curves were obtained by normalizing the conductance to the peak conductance. The normalized conductances ( $G/G_{max}$ ) were then plotted against the test potentials and fitted with the Boltzmann equation:

$$G / G_{max} = 1 / (1 + \exp[-(V_m - V_{1/2}) / k])$$

where  $V_{1/2}$  is the voltage at half-maximal conductance and  $k$  is the slope factor.

The steady-state inactivation curves were obtained using a standard voltage protocol, in which 1 second preconditioning pulses from a holding



potential of -50 mV were elicited in the voltage range of -70 mV to +70 mV in 10 mV increments which was immediately followed by the constant  $I_{L,Ca}$  activating test pulse to  $V_m = +10$  mV. SSI-dependency was plotted as normalized amplitude of  $I_{L,Ca}$  at  $V_m = +10$  mV against the value of conditioning  $V_m$ . Current amplitude was normalized to the peak current ( $I/I_{max}$ ), and plotted against each conditioning potential. The steady-state inactivation curves were also fitted with the Boltzmann function,

$$I/I_{max} = 1 / (1 + \exp[(V_m - V_{1/2}) / k])$$

where  $V_{1/2}$  is the voltage at which half the channels are available for opening, and  $k$  is the slope factor.

### **2.8.5.2 Solutions**

In order to prevent the cells from contracting during patching, they were first patched in a  $Ca^{2+}$  free solution which consisted of (in mM): 120 NaCl, 1 EGTA, 10  $MgCl_2$ , 10 Glucose, 10 HEPES, 1  $NaH_2PO_4$  and 5 KCl. Once the whole cell configuration was obtained, the recording solution was applied. The whole-cell bath solution contained (in mM): 95 NaCl, 50 TEACl, 2  $MgCl_2$ , 2  $CaCl_2$ , 10 HEPES and 10 Glucose (adjusted to pH 7.35 with NaOH). The pipette solution contained (in mM): 140 CsCl, 10 TEACl, 2  $MgCl_2$ , 2 HEPES 1 MgATP and 10 EGTA (adjusted to pH 7.25 with CsOH).

### **2.8.6 Measurement of $Na^+/Ca^{2+}$ exchanger currents in cardiomyocytes**

#### **2.8.6.1 Protocol for measuring $Na^+/Ca^{2+}$ exchanger currents**

$I_{NCX}$  was recorded using a descending voltage ramp from +100 mV to -100 mV from a holding potential of -40 mV for 2 seconds duration. As described previously (Hinde, et al., 1999),  $I_{NCX}$  was measured as current sensitive to nickel

(Ni<sup>2+</sup>). Therefore, Ni<sup>2+</sup>-insensitive components were subtracted from total currents to isolate  $I_{NCX}$ .

### 2.8.6.2 Solutions

The cells were first patched in a Ca<sup>2+</sup>-free solution as described previously (section 2.7.5.2). External solution contained (in mM): 150 NaCl, 5 CsCl, 2 CaCl<sub>2</sub>, 2 MgCl<sub>2</sub>, 10 HEPES, 10 Glucose (pH=7.4). Nifedipine (10 μM), Oubain (100 μM), and Niflumic acid (30 μM) were used to block Ca<sup>2+</sup>, Na<sup>+</sup>-K<sup>+</sup> ATPase, and Cl<sup>-</sup> currents, respectively. 10 mM nickel chloride solution was used to block  $I_{NCX}$ . K<sup>+</sup> currents were minimized by Cs<sup>+</sup> substitution for K<sup>+</sup> in both pipette and external solutions. The pipette solution contained (in mM): 120 CsCl, 20 NaCl, 10 TEACl, 2 MgCl<sub>2</sub>, 1 CaCl<sub>2</sub>, 10 HEPES, 1 MgATP and 10 BAPTA (pH= 7.2 with CsOH). The combination of 10 mM BAPTA and 1 mM Ca<sup>2+</sup> in the pipette solution gave a free [Ca<sup>2+</sup>]<sub>i</sub> of 20 nM (calculated with the “Maxchelator program”; WEBMAX v 2.10, Stanford, CA, USA, which was supplied by Dr. D. Bers).

## 2.9 Biochemical assessment of cell viability and membrane integrity of ventricular cardiomyocytes

### 2.9.1 MTT cell viability assay

The effect of AEA on cell viability was measured using MTT assay which is based on the reduction of 3-(4,5-dimethylthiazol-2-yl)-2,5-diphenyl tetrazolium (MTT) bromide into formazan crystals by the mitochondrial succinate dehydrogenase of viable cells. Cells were plated in 96-well plates at a density 10,000 cells/well in a Ca<sup>2+</sup>-free solution (See section 2.6.4.2 for solution composition). Cell count was estimated by mixing 20 μl of cells with 180 μl of trypan blue and counting the number of viable cells using a hemocytometer. Cells were incubated for 40 minutes with or without tested drug at 37 °C in a 5 % CO<sub>2</sub>

humidified atmosphere. 2  $\mu$ l of Triton X-100 (9 % in water solution) per 100  $\mu$ l original volume was used as a positive control to produce cell lysis. After incubation, 25  $\mu$ l of MTT (5 mg/ml) were added to each well and the plates were incubated for a further 3 h at 37 °C. Then the plates were centrifuged at 1500 rpm for 5 minutes and the solutions were carefully decanted from all the wells. The formazan crystals that formed were then solubilized in a 200  $\mu$ l of DMSO. The colored solution was quantified at 570 nm using Perkin Elmer Victor-3 Spectrophotometer. The cytotoxicity was expressed as percentage over control.

### **2.9.2 Homogenous membrane integrity assay**

Membrane integrity was assessed using the CytoTox-ONE Assay (Promega, Madison, USA). This is a rapid, fluorescent measure of the release of lactate dehydrogenase (LDH) from cells with a damaged cell membrane. The test is based on the conversion of resazurin into resorufin as shown in figure 2.7. Generation of the fluorescent resorufin product is proportional to the amount of LDH, and therefore the number of lysed cells. Cells were plated in 96-well plates at a density 10,000 cells/well in a  $\text{Ca}^{2+}$ -free solution (See section 2.6.4.2 for solution composition). Cell count was estimated using a hemocytometer (as mentioned in the previous section). Cells were incubated for 40 minutes with or without tested drug. A volume of CytoTox-ONE Reagent equal to the volume of the solution containing the cells was then added and incubated for 10 minutes after which a stop solution was added to each well and the fluorescent signal was measured. 2  $\mu$ l of Triton X-100 (9 % in water solution) per 100  $\mu$ l original volume was used as a positive control to produce maximum LDH release (cell lysis). All average fluorescence values were subtracted from background fluorescence. The fluorescence was recorded with an excitation wavelength of 560 nm and an

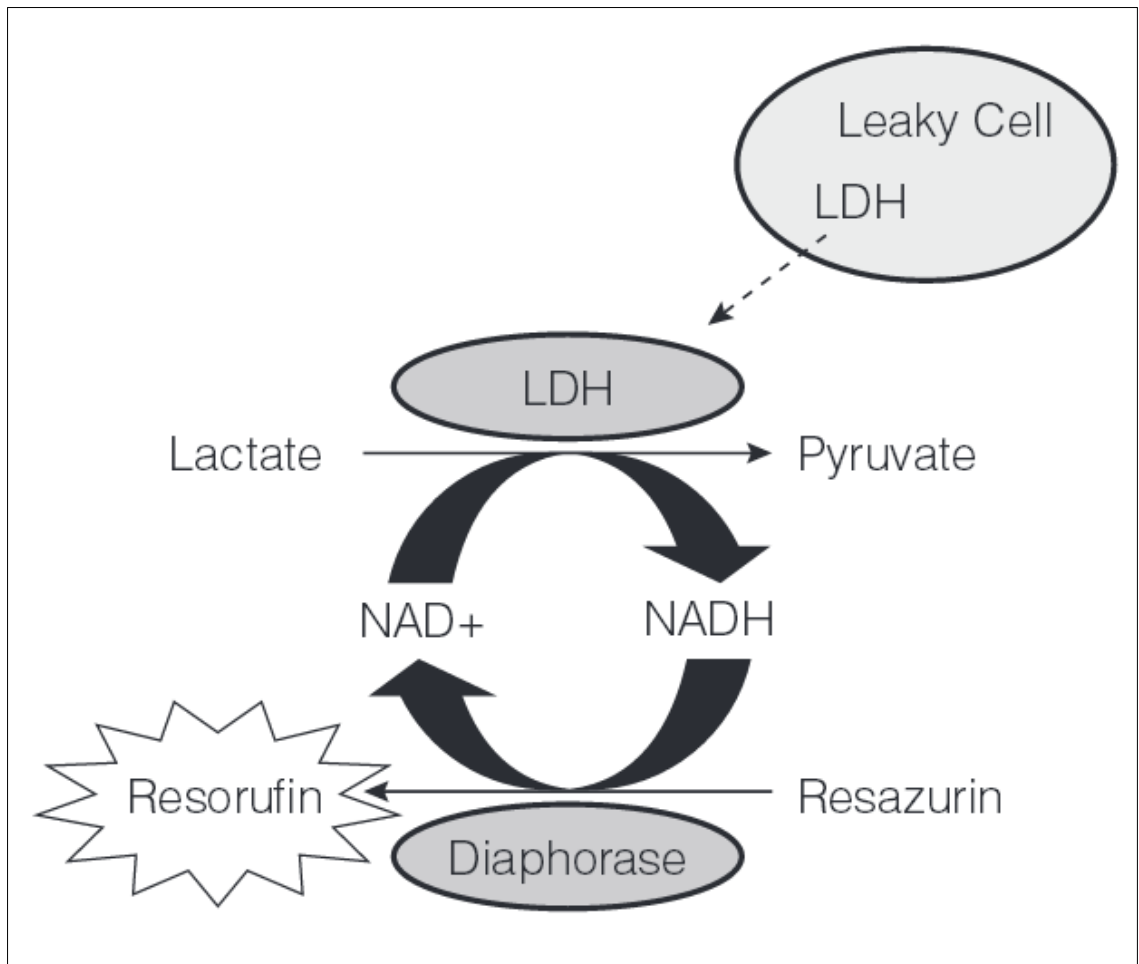


**Figure 2.7 Release of LDH from damaged cells:** LDH release is measured by supplying lactate,  $\text{NAD}^+$ , and resazurin as substrates in the presence of diaphorase. Generation of the fluorescent resorufin product is proportional to the amount of LDH.

emission wavelength of 590 nm and the percent toxicity of experimental drug was calculated as follows:

$$\text{Percent toxicity} = 100 \times (\text{experimental-background}) / (\text{maximum LDH release-background})$$

## **2.10 Preparation of drugs and stock solutions**

Experimental solutions were prepared from stocks immediately prior to each experiment. Therefore, the cells were perfused with the freshly made bath solutions containing the desired concentrations of the drugs.

### **2.10.1 Anandamide and methanandamide**

AEA (MW 347.5) and metAEA (MW 361.56) were purchased from Ascent Scientific, Cambridge, UK). AEA was already dissolved in ethanol (5 mg/ml). The concentration of AEA was 14.4 mM. From this stock solution, 7  $\mu\text{L}$  of AEA were taken to obtain a final test concentration of 1  $\mu\text{M}$ . Similarly, 70  $\mu\text{L}$  of AEA were taken to achieve a final test concentration of 10  $\mu\text{M}$ . Therefore, the ethanol concentrations in the control and in presence of AEA were in the range of 0.007-0.07 % (v/v). MetAEA was also dissolved in ethanol (5 mg/ml) and metAEA solution was prepared in the same way as AEA solution. Stock solutions were kept at -20 °C until their use.

### **2.10.2 Cannabinoid receptor antagonists**

AM251 (MW 555.24) and AM630 (MW 504.37) were purchased from Ascent Scientific, Cambridge, UK). AM251 was dissolved in ethanol (8 mg/ml ethanol) to make a final stock concentration of 14.4 mM. From this stock solution, 7  $\mu\text{L}$  were taken to get a final test concentration of 1  $\mu\text{M}$ . However, AM630 did not dissolve easily in ethanol and larger volumes of ethanol were required to

completely dissolve it (the highest concentration of stock solution of AM630 that could be obtained was 2 mM). In this case, the final concentration of ethanol would be 0.05 %. Therefore, AM630 was dissolved in dimethyl sulphoxide (DMSO) (7 mg/ml) to get a final stock concentration of 14.4 mM. From this stock solution, 7  $\mu$ L were taken to get a final test concentration of 1  $\mu$ M. Stock solutions of AM251 and AM630 were kept at -20 °C until their use.

SR141716 (MW 500.25) was purchased from Sigma-Aldrich (St. Louis, MO, USA). SR144528 (MW 475.2) was obtained through NIDA drug supply system (Baltimore, USA). Both drugs were dissolved in DMSO. The final concentration of DMSO used in the experiments did not exceed 0.007 % (v/v) (Bonz, et al., 2003).

### **2.10.3 Pertussis toxin**

PTX was purchased from Sigma-Aldrich (St. Louis, MO, USA). PTX was dissolved in distilled water and stock solution of 250  $\mu$ g/500 ml was kept in the refrigerator. Cells were incubated with PTX (2  $\mu$ g/ml) for 3 hours at 37 °C (control cells to this group were incubated in the same conditions with distilled water only).

### **2.10.4 Indomethacin**

Indomethacin (MW 357.8) was purchased from Tocris (Ballwin, MO, USA) and a stock solution of indomethacin was prepared in ethanol. Cells were incubated with 30  $\mu$ M indomethacin for 30 minutes (control cells to this group were incubated in the same conditions with ethanol only).

### **2.10.5 URB597**

The FAAH inhibitor URB597 (MW 338.4) was purchased from Tocris (Ellisville, MO, USA). URB597 was dissolved in ethanol to make a 20 mM stock solution. Cells were incubated with 1  $\mu$ M URB597 for 45 minutes at 37 °C (control cells to this group were incubated in the same conditions with ethanol only).

### **2.10.6 *N*-ethylmaleimide**

*N*-ethylmaleimide (NEM) (MW 125.3) was purchased from Sigma-Aldrich (St. Louis, MO, USA). Stock solution of NEM (40 mM) was prepared in ethanol. Cells were incubated with 50  $\mu$ M NEM for 30 minutes at 37 °C (control cells to this group were incubated in the same conditions with ethanol only).

### **2.10.7 Clenbuterol**

Clenbuterol (MW 313.65) was purchased from Sigma-Aldrich (St. Louis, MO, USA) and was dissolved in distilled water. Cells were perfused with clenbuterol at a concentration of 30  $\mu$ M.

### **2.10.8 BRL-37344**

BRL-37344 (MW 385.82) was obtained from Tocris (Ballwin, MO, USA) and was dissolved in distilled water. Cells were perfused with BRL37,344 at a concentration of 1  $\mu$ M.

All materials mentioned elsewhere were purchased from Sigma-Aldrich (St. Louis, MO, USA).

## 2.11 Data analysis

Each experiment was performed on several myocytes from different hearts. The results of the experiments were expressed as mean  $\pm$  standard error of the mean (S.E.M.). Statistical significance was evaluated using paired *t*-test (within the same cell analysis) or independent sample *t*-test and one way ANOVA followed by Bonferroni Post-hoc analysis (for analysis of data from different groups). Statistical analysis of the data was performed using Origin 7.0 software (OriginLab Corp., Northampton, MA) and IBM SPSS statistics version 20. On all graphs (\*) denotes statistical significance with  $P < 0.05$ , between specified values, or if not specified to the respective control.



### 3. RESULTS

#### 3.1 Anandamide inhibits ventricular myocyte shortening

In initial control experiments and in line with earlier studies conducted under similar conditions (Danziger, et al., 1991; Delbridge, et al., 2000; Bebarova, et al., 2010), bath application of control solution (NT) containing ethanol at the highest concentration used in contractility studies (0.07 % v/v; used as vehicle for 10  $\mu$ M AEA) caused 18-20 % inhibition of the shortening (n=7-10;  $P<0.05$  compared to 0 time point) in experiments lasting up to 20-25 minutes in response to electrical stimulation (1Hz; 60 pulses delivered every 1 minute). No further run down of the shortening amplitudes was observed. However, unless it was stated otherwise, ethanol was included routinely in control solutions during shortening and  $\text{Ca}^{2+}$  transient experiments.

In the first set of experiments, the effect of AEA on the contractility of acutely isolated rat ventricular myocytes was tested. Figure 3.1A shows typical records of shortening in an electrically stimulated (1 Hz) myocyte superfused with either NT (containing 0.007 % ethanol in all experiments) or NT + 1  $\mu$ M AEA. The amplitude of shortening was significantly reduced up to  $47.3 \pm 2.6$  % of control (n=12-14;  $P<0.05$ ) (Figure 3.1B), when the concentration of AEA was increased in the range of 10 nM to 10  $\mu$ M compared to NT.

The negative inotropic effect (decrease of shortening amplitudes) by AEA could be due to degradation products of AEA such as AA. For this reason, we investigated the effects of metAEA, a non hydrolyzable analog of AEA (Abadji, et al., 1994) and URB597, an inhibitor of FAAH enzyme (Kathuria, et al., 2003).

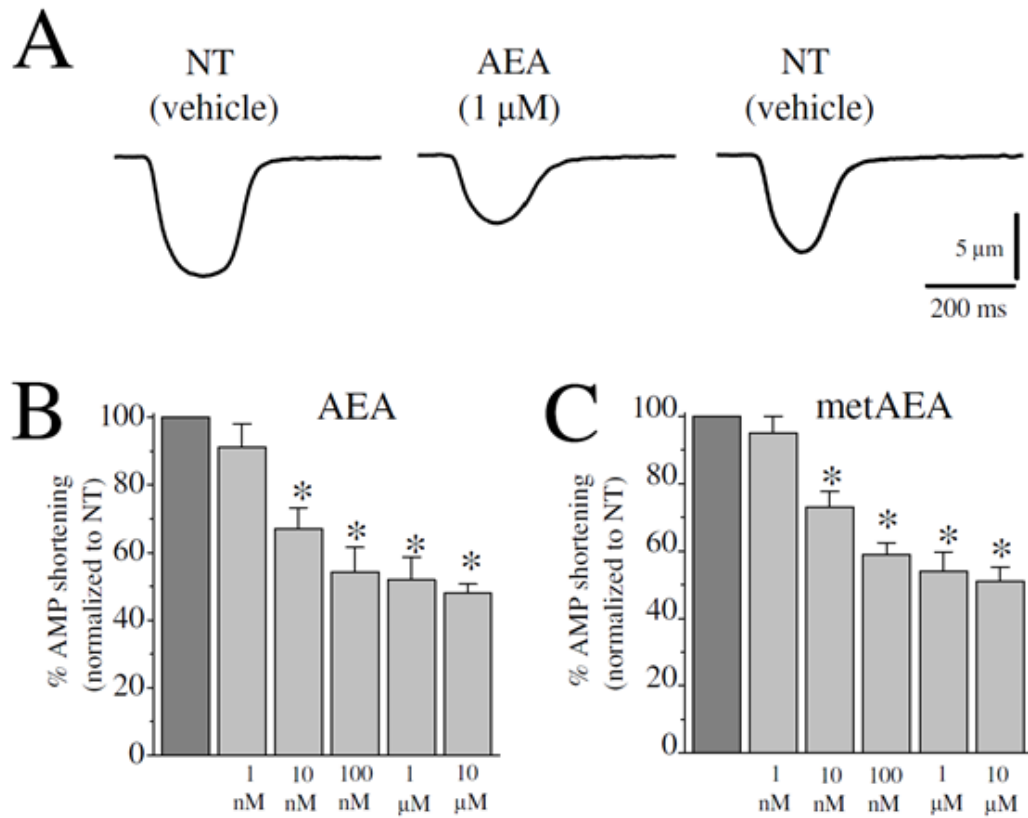


**Figure 3.1 Effects of AEA and metAEA on ventricular myocyte shortening:**

(A) Typical records of shortening in an electrically stimulated (1 Hz) ventricular myocyte superfused with either NT or NT + 1  $\mu$ M AEA and during washout with NT. (B) Bar graph showing the mean amplitudes (AMP) of shortening expressed as a percentage of control values, and in presence of AEA (1 nM to 10  $\mu$ M). Data are analyzed using ANOVA and are expressed as means  $\pm$  S.E.M.,  $n = 12-14$  cells. \* indicates statistically significant difference at the level of  $P < 0.05$ . (C) Bar graph showing the mean amplitudes (AMP) of shortening expressed as a percentage of control values, and in presence of metAEA (1 nM to 10  $\mu$ M). Data are analyzed using ANOVA and are expressed as means  $\pm$  S.E.M.,  $n = 7-8$  cells. \* indicates statistically significant difference at the level of  $P < 0.05$ .

In cardiomyocytes treated for 10 minutes with 0.1-10  $\mu\text{M}$  metAEA (Figure 3.1C), the extent of inhibition was not significantly different from that of AEA ( $n=7-8$ ;  $P>0.05$ ). Similarly, pretreatment with 1  $\mu\text{M}$  URB597 for 45 minutes at 37  $^{\circ}\text{C}$  (Kathuria, et al., 2003; Amoros, et al., 2010) did not alter the extent of AEA inhibition (Figure 3.2A). In the absence and presence of URB597 treatment, AEA (1  $\mu\text{M}$ ) inhibited myocyte shortening by  $62.7 \pm 8.4$  % of controls and  $68.2 \pm 4.8$  % of controls, respectively. There were no statistically significant differences in the inhibitory effect of AEA between control (NT+ 0.007 % ethanol after 45 minutes pretreatment) and URB597 pretreated cells ( $n=9-11$ ;  $P>0.05$ ). We have also tested whether cyclooxygenase products of AEA metabolites would mediate the observed actions of this compound. The results indicated that the extent of myocyte shortening was not significantly different after incubating the cells with 30  $\mu\text{M}$  indomethacin, a cyclooxygenase inhibitor, for 30 minutes ( $n=8-11$ ;  $P>0.05$ ) (Figure 3.2B).

Furthermore, the effect of synthetic cannabinoid WIN55,212-2 on myocytes shortening was also tested. When compared to AEA, application of 1  $\mu\text{M}$  WIN55,212-2 did not cause a significant alteration in the amplitudes of myocyte shortening ( $n=7$ ;  $P>0.05$ ).

Among other contraction parameters measured, resting cell length (RCL) was not significantly altered ( $n=12-14$ ;  $P>0.05$ ) by 10 minutes superfusion with AEA (1 nM to 1  $\mu\text{M}$ ). However, increasing the concentration of AEA to 10  $\mu\text{M}$  caused a small but statistically significant reduction of RCL in about 60 % of cells tested ( $n=12-14$ ;  $P<0.05$ ). Similarly, time to peak (TPK) shortening was significantly reduced ( $n=12-14$ ;  $P<0.05$ ) to  $90.2 \pm 4.2$  ms by 10  $\mu\text{M}$  AEA compared to  $104.7 \pm 1.7$  ms in NT.

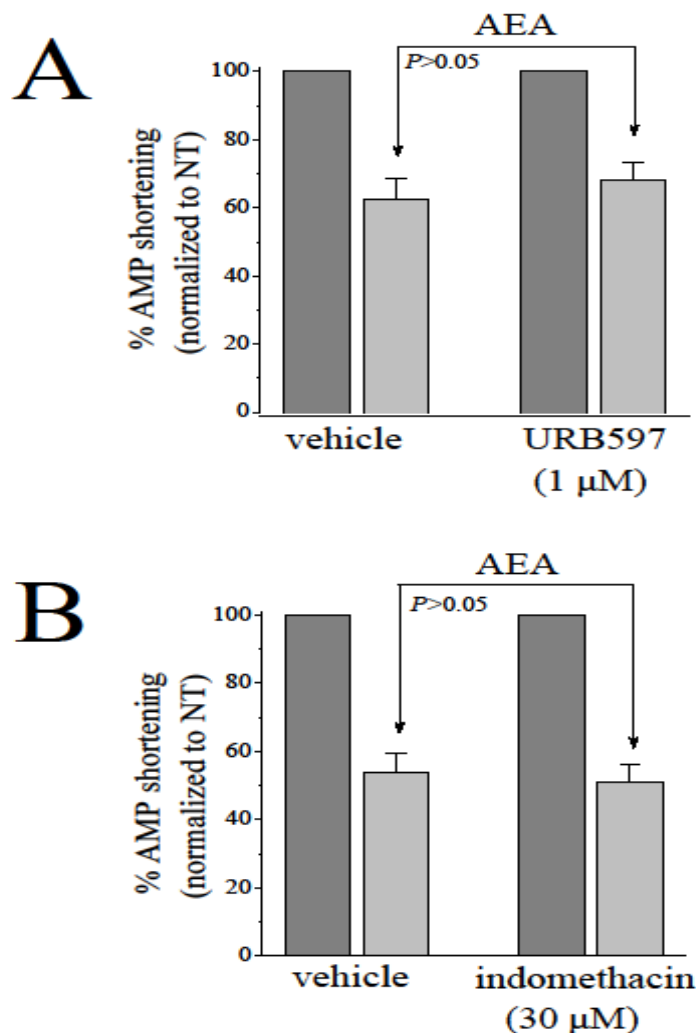


**Figure 3.2 Effects of preincubation with URB597 or indomethacin on AEA-induced inhibition of ventricular myocyte shortening:** (A) Bar graph showing the effect of AEA on the mean amplitude (AMP) of shortening expressed as percentage of control values in NT containing 0.007 % ethanol or after 45 minutes incubation with 1 μM URB597 at 37 °C. Data are analyzed using ANOVA and are expressed as means ± S.E.M., n=9-11 cells. (B) Bar graph showing the effect of AEA on the mean amplitudes (AMP) of shortening expressed as percentage of control values in NT containing 0.007 % ethanol or after 30 minutes incubation with 30 μM indomethacin at 37 °C. Data are analyzed using independent sample *t*-test and are expressed as means ± S.E.M., n=8-11 cells.

### **3.2 Ventricular myocytes express cannabinoid receptors**

In order to test for the involvement of cannabinoid receptors in the effect of AEA on myocyte shortening, the expression of these receptors in the ventricular tissue was confirmed by Western blot analysis. Figure 3.3 shows that both CB<sub>1</sub> and CB<sub>2</sub> receptors (MW about 63 kDa and 40 kDa, respectively) are expressed in the ventricular tissue of Wistar rats.

### **3.3 Cannabinoid receptors are not involved in the effect of anandamide on myocyte shortening**

To test whether the inhibitory effect of AEA on myocyte shortening is mediated by the activation of cannabinoid receptors, the effects of established antagonists of CB<sub>1</sub> and CB<sub>2</sub> receptors on AEA inhibition of shortening amplitudes were studied. Two structurally different CB<sub>1</sub> receptor antagonists (AM251 with a K<sub>i</sub> of 7.5 nM; Figure 3.4A and SR141716 with a K<sub>i</sub> of 1.8 nM; Figure 3.4B) (Pertwee, 2006; Shire, et al., 1999) and two CB<sub>2</sub> receptor antagonists (AM630 with a K<sub>i</sub> of 32.1 nM; Figure 3.4C and SR144528 with K<sub>i</sub> of 0.6 nM; Figure 3.4D) (Pertwee, 2006; Shire, et al., 1999) were tested. At 300 nM concentration, these antagonists were not able to reverse the inhibitory effect of AEA on the shortening amplitudes of cardiomyocytes (n=8-12;  $P>0.05$ ).

Since the activation of both CB<sub>1</sub> and CB<sub>2</sub> receptors are mediated by G<sub>i/o</sub> subtypes of G-proteins (Pertwee, 2006), the effect of inhibitors of G<sub>i/o</sub> proteins such as PTX and *N*-ethylmaleimide (NEM) on AEA-induced inhibition of cardiomyocyte shortening were examined (Figures 3.5A and 3.5B). Preincubation of cardiomyocytes in either PTX (2 µg/ml, 3 hours at 37 °C) or NEM (50 µM for 30 minutes at 37 °C; (Oz, et al., 2007b)) did not alter the extent of AEA inhibition of cardiomyocyte shortening (n=9-12;  $P>0.05$ ).

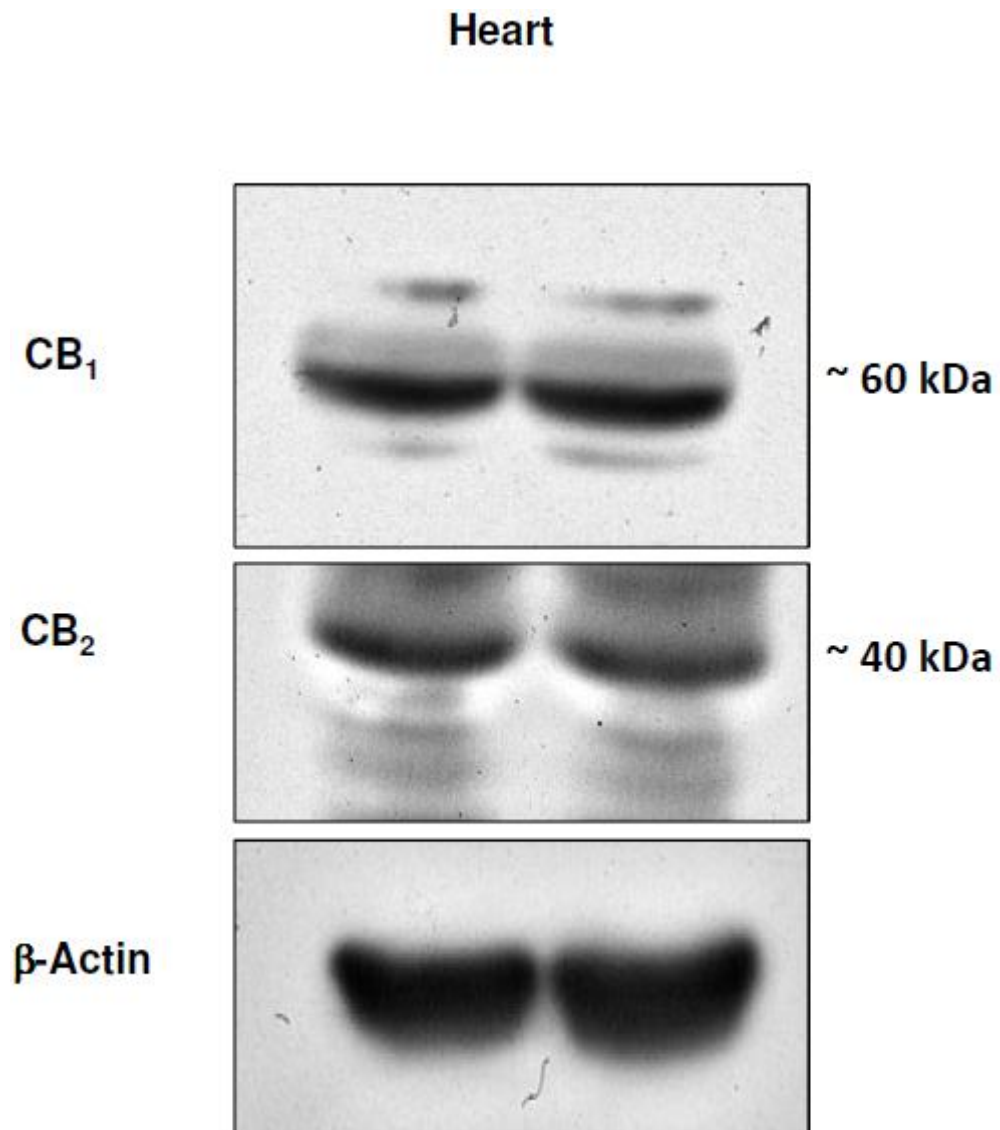


**Figure 3.3 Expression of CB<sub>1</sub> and CB<sub>2</sub> receptors in rat heart:** Expression of CB<sub>1</sub> and CB<sub>2</sub> receptors in the heart of control Wistar rats (n= 3) were analyzed by Western blotting.

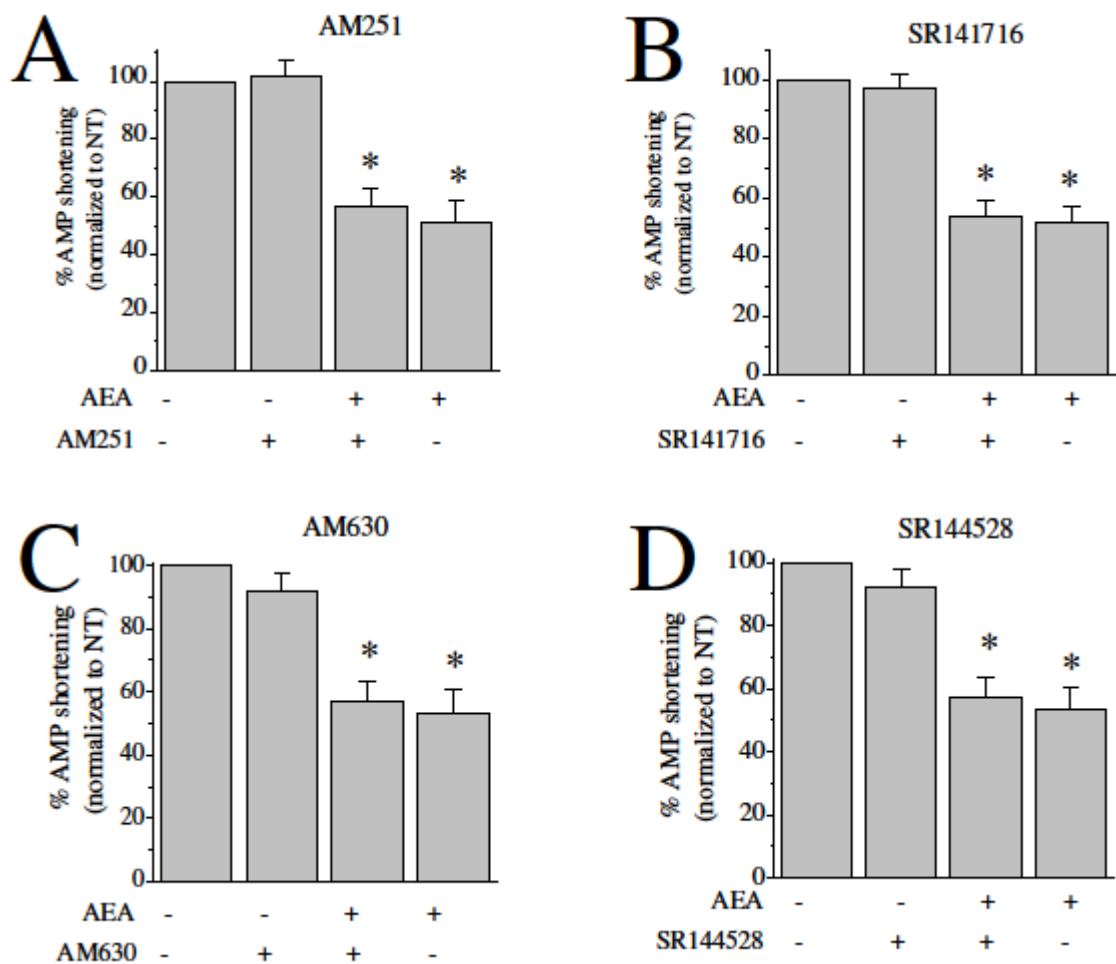


**Figure 3.4 Effects of cannabinoid receptor antagonists on AEA-induced inhibition of cardiomyocyte shortening:** Bar graphs showing the mean amplitudes (AMP) of shortening expressed as a percentage of control values in presence of CB<sub>1</sub> receptor antagonist AM251 (A), CB<sub>1</sub> receptor antagonist SR141716 (B), CB<sub>2</sub> receptor antagonist AM630 (C), and CB<sub>2</sub> receptor antagonist SR144528 (D). Data are analyzed using ANOVA and are expressed as means  $\pm$  S.E.M., n= 8-12 cells for each group. \* indicates statistically significant difference at the level of  $P < 0.05$ .

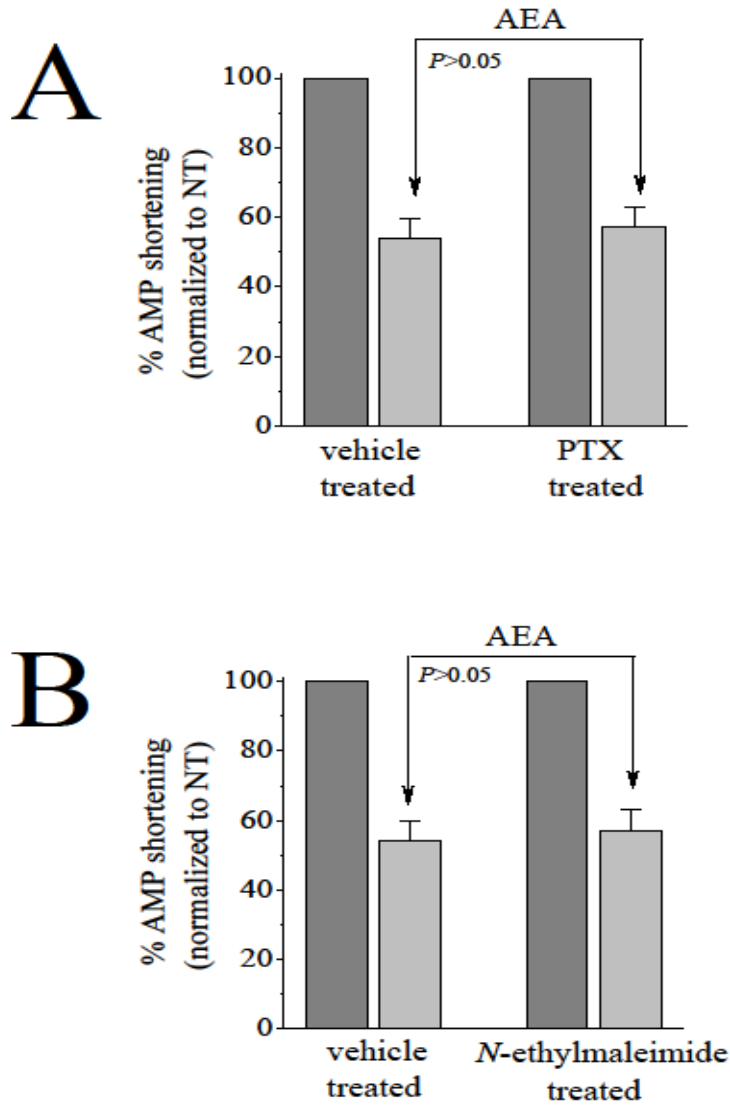


**Figure 3.5 Effects of pertussis toxin and *N*-ethylmaleimide on AEA-induced inhibition of cardiomyocyte shortening:** (A) Bar graph showing the effect of AEA on the mean amplitudes (AMP) of shortening expressed as a percentage of control values and pertussis toxin pretreatment. (B) Bar graph showing the effect of AEA on the mean amplitudes (AMP) of shortening expressed as a percentage of control values and *N*-ethylmaleimide (NEM) pretreatment. Data are analyzed using independent sample *t*-test and are expressed as means  $\pm$  S.E.M.,  $n = 9-12$  cells.



In order to test the effectiveness of the experimental protocols used to investigate the role of G-proteins, the efficacy of PTX or NEM pretreatments on clenbuterol ( $\beta_2$  adrenergic receptor agonist)-induced inhibition of cardiomyocyte shortening was tested. In agreement with earlier studies (Siedlecka, et al., 2008), 3 hours pretreatment with 2  $\mu\text{g/ml}$  PTX (Figure 3.6A) or 30 minutes pretreatment with 50  $\mu\text{M}$  NEM (Figure 3.6B) effectively blocked the inhibitory effect of the  $\beta_2$  adrenoceptor agonist clenbuterol (30  $\mu\text{M}$ ) on cardiomyocyte shortening (n=10-12;  $P<0.05$ ).

### **3.4 Anandamide inhibits intracellular $\text{Ca}^{2+}$ transients**

In these experiments, the effect of 10 minutes bath application of 1  $\mu\text{M}$  AEA on the resting intracellular  $\text{Ca}^{2+}$  levels and on the amplitudes and kinetics of  $\text{Ca}^{2+}$  transients elicited by electrical-field stimulation were investigated. Typical records of  $\text{Ca}^{2+}$  transients in a myocyte superfused with either NT or NT + 1  $\mu\text{M}$  AEA and during washout with NT are shown in Figure 3.7A. The effects of 1  $\mu\text{M}$  AEA on resting fura-2 ratio, TPK  $\text{Ca}^{2+}$  transient,  $T_{\text{HALF}}$  decay of  $\text{Ca}^{2+}$  transient, and AMP of  $\text{Ca}^{2+}$  transients are shown in Figure 3.7B-E, respectively. Although, AEA has been shown to alter intracellular  $\text{Ca}^{2+}$  levels in various types of cells [for review, (Goodfellow and Glass, 2009)], application of 1  $\mu\text{M}$  AEA for 10 minutes did not cause a significant alteration in resting fura-2 ratio and TPK  $\text{Ca}^{2+}$  transient (n=21-24 cells;  $P>0.05$ ) (Figure 3.7B and C). However,  $T_{\text{HALF}}$  decay of the  $\text{Ca}^{2+}$  transients and AMP of the  $\text{Ca}^{2+}$  transients were significantly reduced by 1  $\mu\text{M}$  AEA to  $118.9 \pm 5.5$  ms and  $0.243 \pm 0.032$  fura-2 ratio units compared to  $129.3 \pm 5.2$  ms (n=24 cells;  $P<0.05$ ) and  $0.326 \pm 0.024$  fura-2 ratio units (n =24 cells;  $P<0.05$ ) in controls, respectively (Figure 3.7D and E).

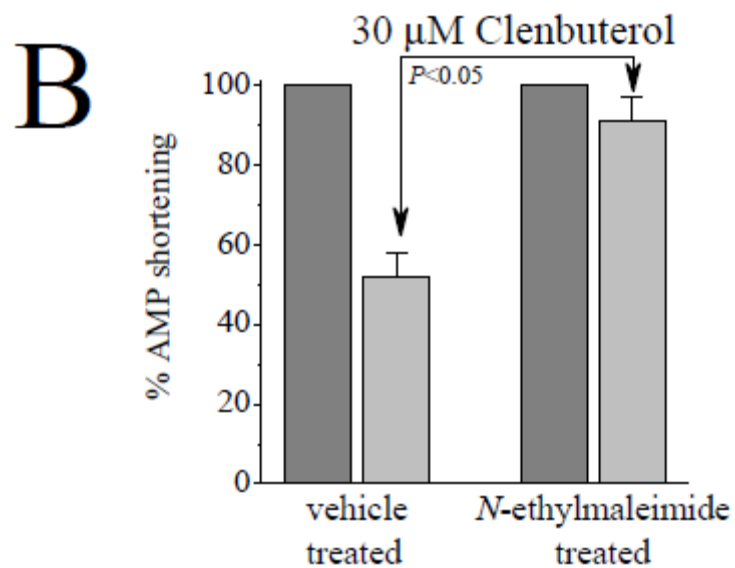
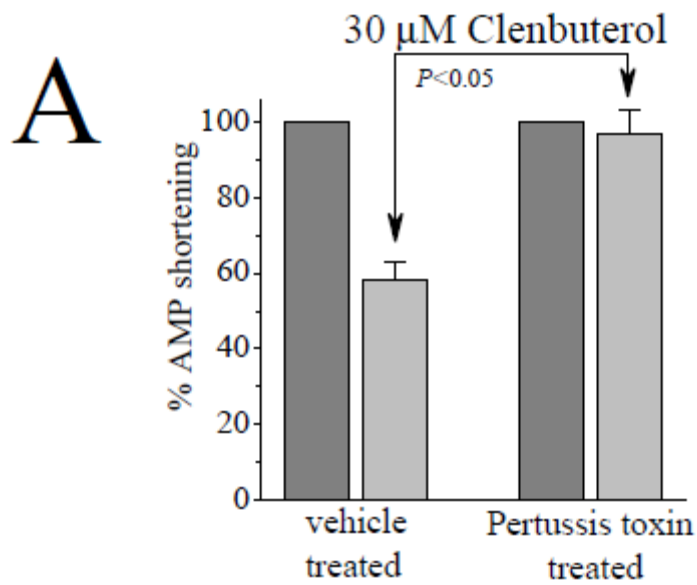


**Figure 3.6 Effect of pretreatment with PTX or NEM on G-protein mediated inhibition of cardiomyocyte shortening by clenbuterol:** Data are analyzed using independent sample *t*-test and are expressed as means  $\pm$  S.E.M., n = 10-12 cells.

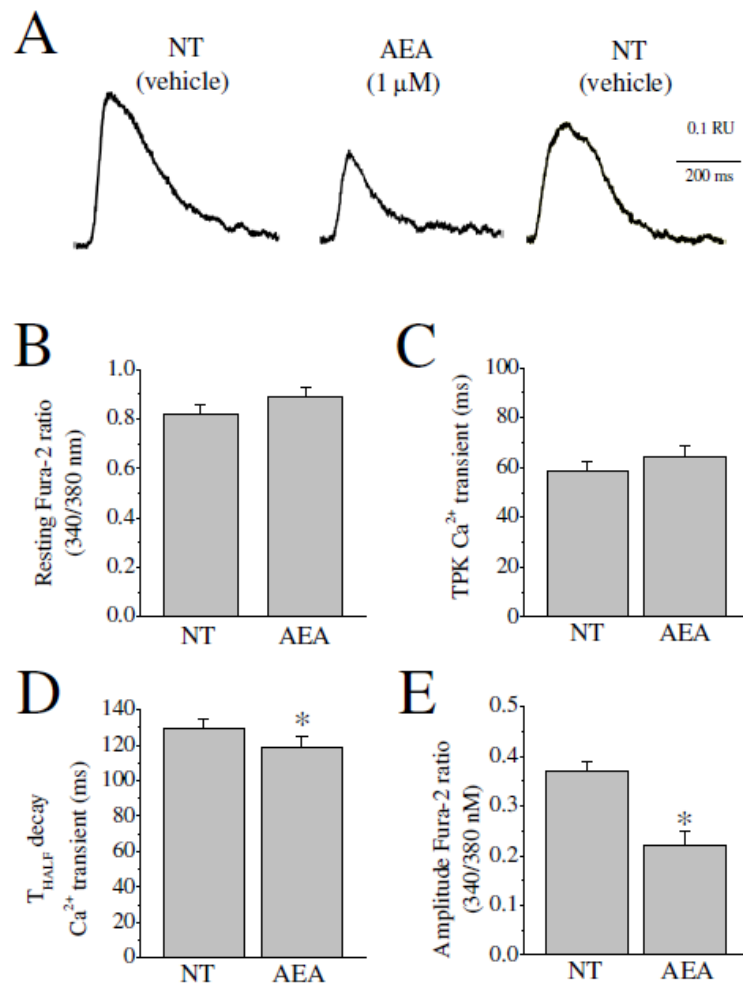


**Figure 3.7 Effects of AEA on amplitude and time-course of intracellular Ca<sup>2+</sup> in ventricular myocytes:** (A) Typical records of Ca<sup>2+</sup> transients in an electrically stimulated (1 Hz) ventricular myocyte superfused with either NT or NT + 1 μM AEA and during washout with NT; scale bar indicates 0.1 fura-2 ratio unit (RU). Also shown resting fura-2 ratio (340/380 nm) (B), time to peak (TPK) Ca<sup>2+</sup> transient (C), time to half (T<sub>HALF</sub>) decay of the Ca<sup>2+</sup> transient (D) and amplitude (AMP) of the Ca<sup>2+</sup> transient (E). Myocytes were maintained at 35-36 °C and superfused with AEA for 10 minutes. Data are analyzed using paired *t*-test and are expressed as means ± S.E.M., n=21-24 cells. \* indicates statistically significant difference at the level of P < 0.05.

### **3.5 Anandamide has no effect on sarcoplasmic reticulum (SR) Ca<sup>2+</sup> transport**

The effect of 1  $\mu$ M AEA on Ca<sup>2+</sup> transport was investigated in myocytes exposed to 20 mM caffeine. Figure 3.8A shows a typical recording illustrating the protocol used in these experiments. Initially, the myocyte was electrically stimulated at 1 Hz. Electrical stimulation was then turned off for 5 seconds and caffeine was applied for 10 seconds using a rapid solution exchanger device. Electrical stimulation was then restarted and the recovery of intracellular Ca<sup>2+</sup> was recorded during a period of 60 seconds. Sarcoplasmic reticulum Ca<sup>2+</sup> content was assessed by measuring caffeine-evoked Ca<sup>2+</sup> release (area under the caffeine-evoked Ca<sup>2+</sup> transient), and fractional release of Ca<sup>2+</sup>, by comparing the amplitude of the electrically evoked steady-state Ca<sup>2+</sup> transients with that after caffeine application in the presence of either NT or NT + 1  $\mu$ M AEA. Fractional release of SR Ca<sup>2+</sup> was not significantly altered in the presence of 1  $\mu$ M AEA compared to NT ( $0.749 \pm 0.024$  in AEA versus  $0.753 \pm 0.028$  in controls;  $n = 23$  cells;  $P > 0.05$ ; Figure 3.8B). The area of caffeine-evoked Ca<sup>2+</sup> transient (Figure 3.8C) and recovery of the Ca<sup>2+</sup> transient during electrical stimulation following application of caffeine (Figure 3.8D) were also not significantly altered in myocytes exposed to 1  $\mu$ M AEA compared to control cells ( $n = 21-23$  cells;  $P > 0.05$ ).

### **3.6 Anandamide has no effect on myofilament sensitivity to Ca<sup>2+</sup>**

The effects of AEA on myofilament sensitivity to Ca<sup>2+</sup> were also investigated. These experiments investigated whether AEA decreases the mechanical responses by altering the affinity of the contractile machinery of the ventricular myocytes to intracellular Ca<sup>2+</sup> (Spurgeon, et al., 1992). A typical record of myocyte shortening and fura-2 ratio and phase-plane diagrams of fura-2 ratio *versus* cell length in myocytes exposed to NT are shown in Figure 3.9A.

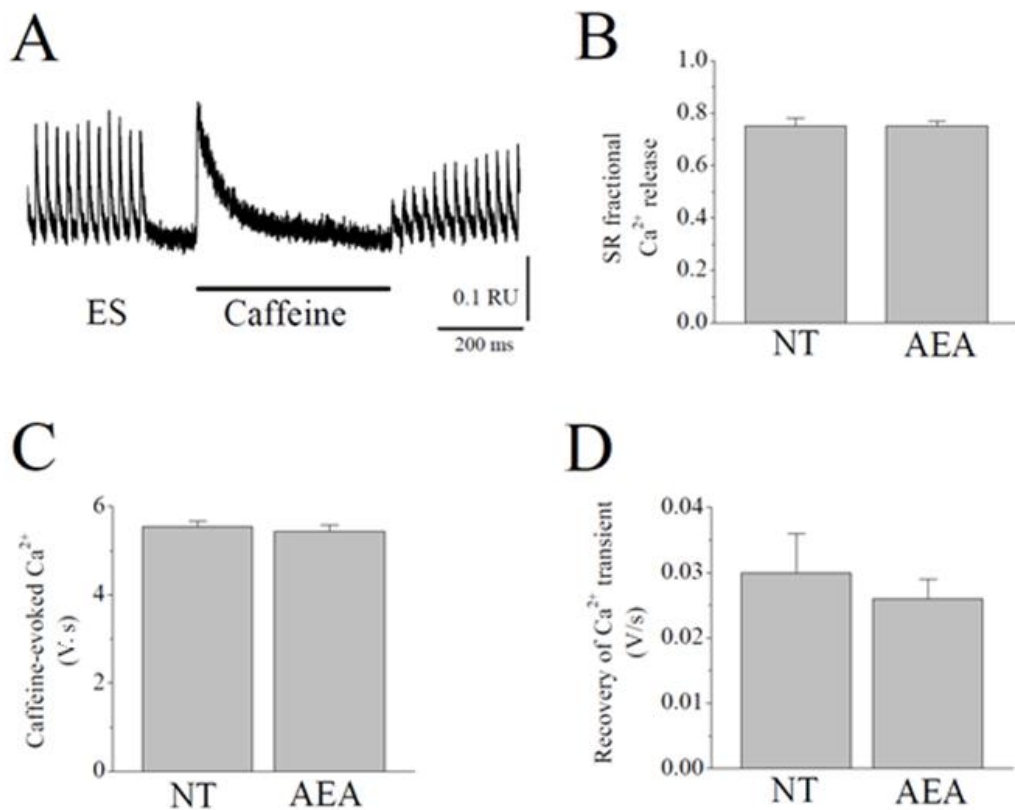


**Figure 3.8 Effect of AEA on sarcoplasmic reticulum  $\text{Ca}^{2+}$  transport:** (A) Typical record illustrating the effects of electrical stimulation (ES) and rapid application of caffeine on fura-2 ratio in a rat ventricular myocyte. Also shown are mean amplitude of SR fractional release of  $\text{Ca}^{2+}$  (B), area under the caffeine-evoked  $\text{Ca}^{2+}$  transient (C) and recovery of electrically evoked intracellular  $\text{Ca}^{2+}$  after application of caffeine (D). Data are analyzed using paired *t*-test and are expressed as means  $\pm$  S.E.M., *n* = 21-23 cells.

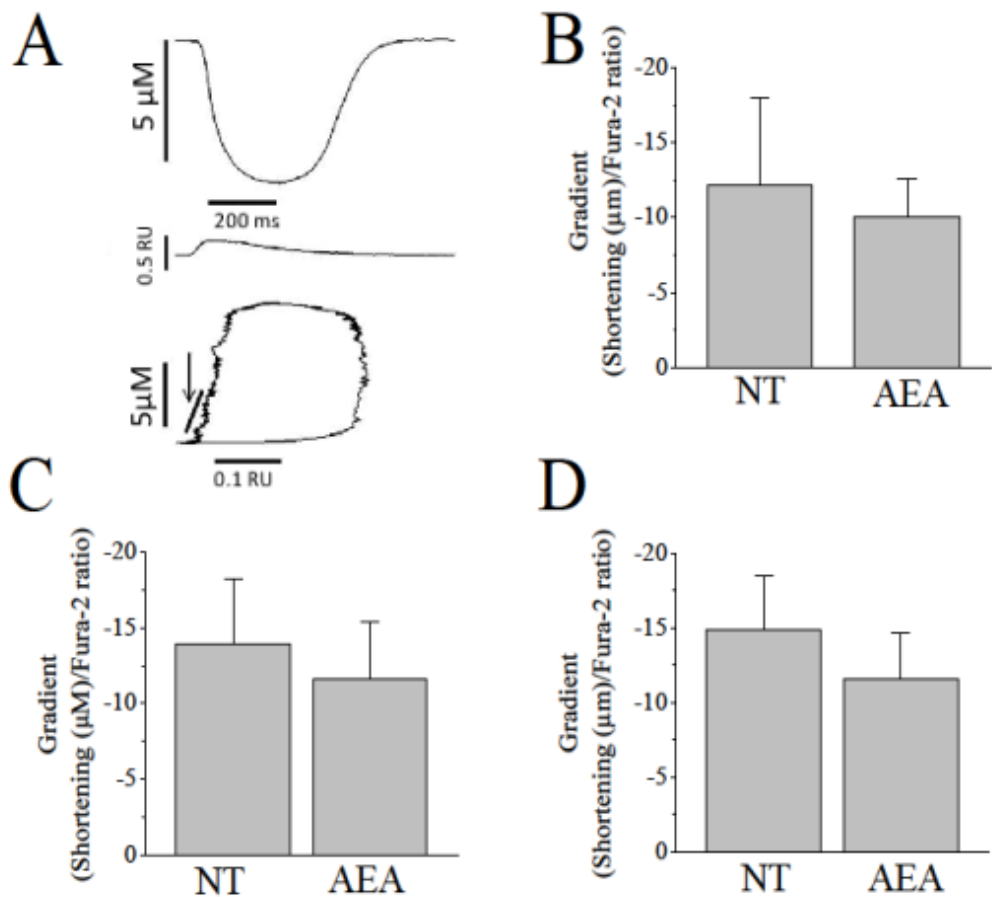


**Figure 3.9 Effect of AEA on myofilament sensitivity to  $\text{Ca}^{2+}$ :** (A) Typical records of myocyte shortening, fura-2 ratio and phase-plane diagrams of fura-2 ratio vs. cell length in a myocyte exposed to NT. The arrow indicates the region where the gradient was measured. **B-D** show the effect of 1  $\mu\text{M}$  AEA on the mean gradient of the fura-2–cell length trajectory during late relaxation of the twitch contraction during the periods 500-600 (B), 500-700 (C) and 500-800 ms (D) Data are analyzed using paired *t*-test and are expressed as means  $\pm$  S.E.M.,  $n = 23$ -30 cells.

The gradient of the trajectory reflects the relative myofilament response to  $\text{Ca}^{2+}$  and hence, has been used as a measure of myofilament sensitivity to  $\text{Ca}^{2+}$  (Spurgeon, et al., 1992). The gradients of the fura-2-cell length trajectory during late relaxation of the twitch contraction, measured during the periods 500-600 ms (Figure 3.9B), 500-700 ms (Figure 3.9C), and 500–800 ms (Figure 3.9D), were not significantly altered in the presence of 1  $\mu\text{M}$  AEA, suggesting that myofilament sensitivity to  $\text{Ca}^{2+}$  is not reduced by AEA ( $n = 23\text{-}30$  cells;  $P > 0.05$ ).

### **3.7 Anandamide suppresses the action potentials in ventricular myocytes**

Generation of the cardiac AP requires a specific temporal activation pattern of several ion channels. Anandamide has been shown to influence the functional properties of these channels either directly or indirectly [for reviews, (Oz, 2006; Goodfellow and Glass, 2009)]. Therefore, in this set of experiments, the effect of AEA on cardiac APs was investigated. In agreement with earlier studies in rat cardiomyocytes (Danziger, et al., 1991; Delbridge, et al., 2000; Bebarova, et al., 2010), AP waveforms remained unchanged in the presence of ethanol concentrations up to 0.07 % (v/v).

Patch-clamped cardiomyocytes were exposed to AEA while continuously monitoring their  $V_{\text{rest}}$  and APs in the current clamp mode. The generation of APs was evoked by 0.9-1 nA depolarizing current pulses of 4 ms duration applied at a frequency of 0.2 Hz. A typical experimental protocol included: 1) the establishment of the whole-cell configuration, 2) 4 to 5 minute dialysis of the myocytes with pipette solution to ensure equilibrium conditions between the pipette solution and intracellular milieu, 3) recording of the myocytes baseline

electrical activity following stabilization of  $V_{rest}$  and AP parameters, 4) exposure of the myocytes to AEA for 10 to 15 minutes, and 5) washout of AEA.

In initial experiments, effects of AEA were tested on the passive membrane properties of cardiomyocytes. The passive properties of the ventricular cells from controls were not significantly different from those of the AEA-treated cells. Resting membrane potentials (mean  $\pm$  SEM) were  $-76.3 \pm 1.7$ , and  $-74.2 \pm 1.6$  mV in control (n=11) and AEA treated (n=14) myocytes, respectively. The mean cell capacitance in the control group of cells was  $109.6 \pm 12.8$  pF, whereas in the AEA treated cells was  $104.7 \pm 11.6$  pF. The input resistance was  $82.3 \pm 13.4$  M $\Omega$  in control cells and  $85.6 \pm 11.8$  M $\Omega$  in AEA treated cells. In control cells, these passive membrane properties were not altered significantly in experiments lasting up to 25 to 30 minutes.

In agreement with earlier studies in rat ventricular myocytes [for a review, (Antzelevitch, et al., 1991)], two main types of waveforms were observed according to the duration of their APs; endocardial (with long AP durations; Figure 3.10A;  $44.6 \pm 2.9$  ms; n=23 cells) and epicardial (with short AP durations; Figure 3.10B;  $14.9 \pm 1.6$  ms; n=26 cells) myocytes. Resting membrane potentials were  $-77.6 \pm 1.3$  mV in endocardial cells, and  $-78.5 \pm 1.4$  mV in epicardial cells (Figure 3.11A). Similar to earlier findings (Antzelevitch, et al., 1991), the amplitudes of APs ( $122.6 \pm 8.9$  mV *versus*  $110.7 \pm 7.1$  mV) (Figure 3.11B) and maximal rate of rise ( $dV/dt_{max}$ ) values ( $177.3 \pm 8.4$  V/s *versus*  $141.6 \pm 7.2$  V/s) (Figure 3.11C) in endocardial cells were higher than those of epicardial cells



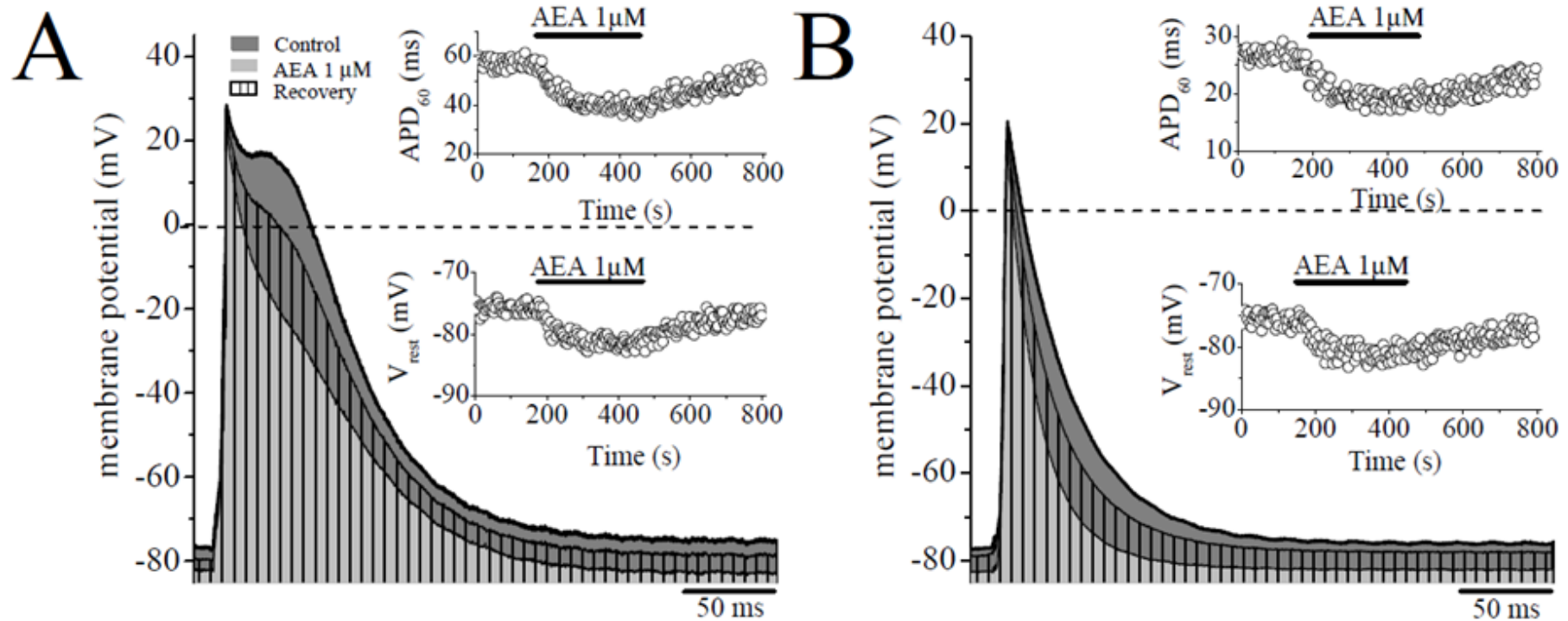


**Figure 3.10 Effect of AEA on the excitability of ventricular myocytes:** Representative recordings of APs in controls (dark grey area), in the presence of 1 μM AEA (light grey area) and after washout (striped area) in ventricular endocardial (A) and epicardial (B) myocytes; the *insets* on panels A and B show the time course of the action potential duration (APD<sub>60</sub>) and resting potential (V<sub>rest</sub>) changes in response to AEA application (indicated by horizontal bars).

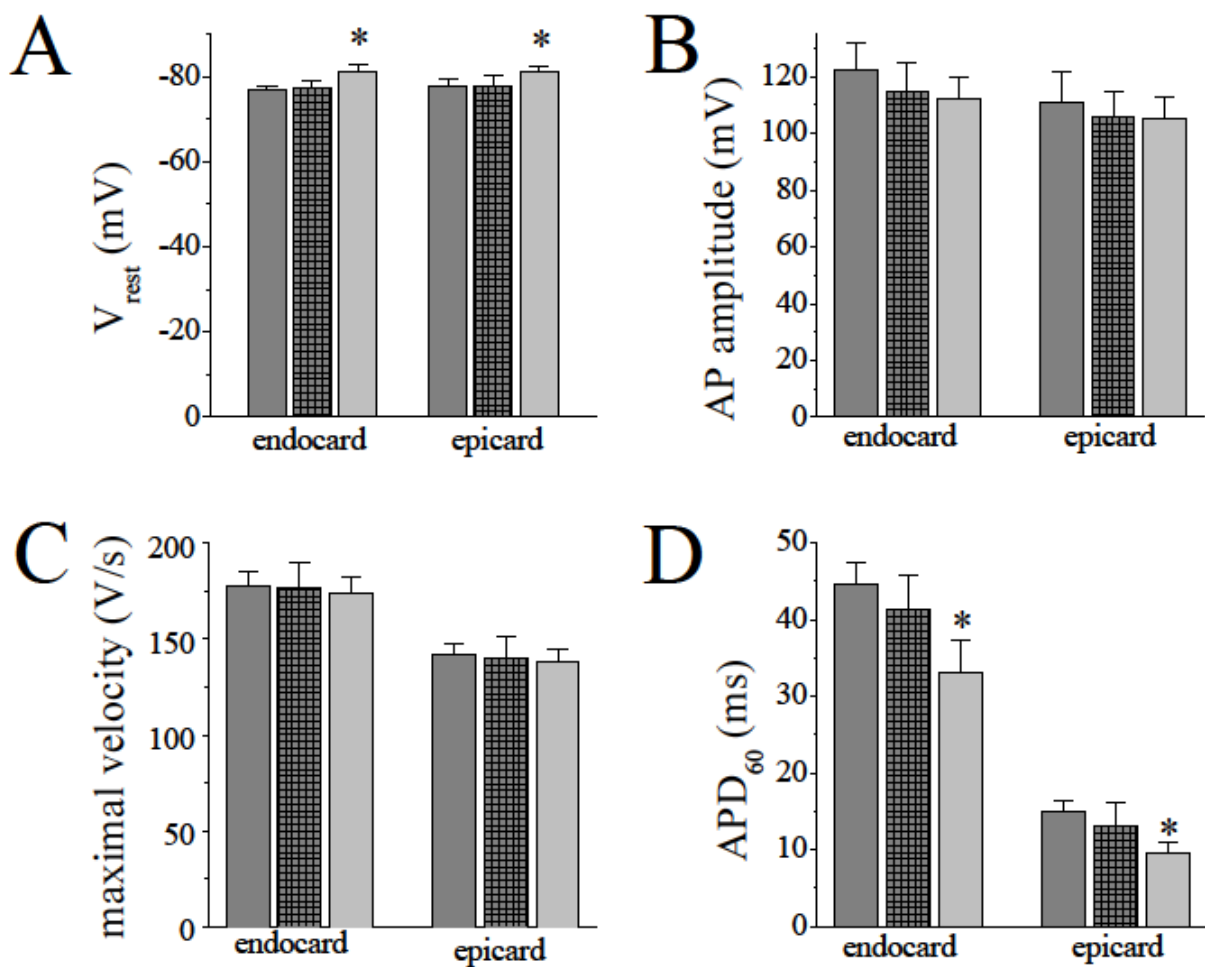


**Figure 3.11 Summary of the effect of AEA on the amplitude and the shape of APs in cardiomyocytes:** Quantification of the changes in  $V_{rest}$  (A), AP amplitude (B), AP maximal rate of rise (C) and AP duration (D), characterized by  $APD_{60}$  in controls (dark grey bars) and in response to 0.1  $\mu$ M (cross hatched bars) or 1  $\mu$ M AEA (light grey bars). Data are analyzed using ANOVA and are expressed as means  $\pm$  S.E.M. from 8 to 12 myocytes for each group. \* indicates statistically significant difference at the level of  $P < 0.05$ .

At concentrations of 0.1  $\mu\text{M}$  and 1  $\mu\text{M}$ , AEA consistently shortened the duration of AP in both cell types (measured at 60 % of repolarization,  $\text{APD}_{60}$ ; Figure 3.11D), with a hyperpolarizing shift in  $V_{\text{rest}}$  (Figure 3.11A). Changes in AP shortening in response to AEA (1  $\mu\text{M}$ ) application were noticeable within 1-2 minutes (*insets* to Figures 3.10A and 3.10B). Recoveries were usually partial and required longer time. Similar effect of AEA was observed in 5 cells recorded at physiological temperatures (35-36  $^{\circ}\text{C}$ ).  $\text{APD}_{60}$  decreased from  $33.8 \pm 4.6$  ms in controls to  $21.4 \pm 3.2$  ms in the presence of AEA ( $n=5$ ;  $P<0.05$ ).

Effects of AEA on  $V_{\text{rest}}$  (Figure 3.11A), and  $\text{APD}_{60}$  (Figure 3.11D) reached a statistically significant level at 1  $\mu\text{M}$  AEA ( $n=8-12$  cells for each group;  $P<0.05$ ). However, AP amplitude (Figure 3.11B) and  $dV/dt_{\text{max}}$  of AP (Figure 3.11C) were not altered significantly in both types of cells at 0.1  $\mu\text{M}$  and 1  $\mu\text{M}$  AEA ( $n=10-12$  cells for each group;  $P>0.05$ ).

At higher concentration (10  $\mu\text{M}$ ), AEA caused 5-10 mV depolarization (Figures 3.12A, 3.12B and 3.13A) in endocardial ( $n=18$  cells;  $P<0.05$ ) and epicardial cells ( $n=24$  cells;  $P<0.05$ ) and decreased significantly the AP amplitudes and  $dV/dt_{\text{max}}$  in both types of myocytes (Figures 3.13B and 3.13C;  $n=18-24$  cells;  $P<0.05$ ). AEA (10  $\mu\text{M}$ ) also caused a significant decrease in  $\text{APD}_{60}$  (Figure 3.13D). However, in a subgroup of endocardial (5 out of 18) and epicardial (4 out of 24) cells, AEA, although caused a significant depolarization and a significant decrease in AP amplitude and maximum rate of rise of AP, it did not alter  $\text{APD}_{60}$  values significantly.

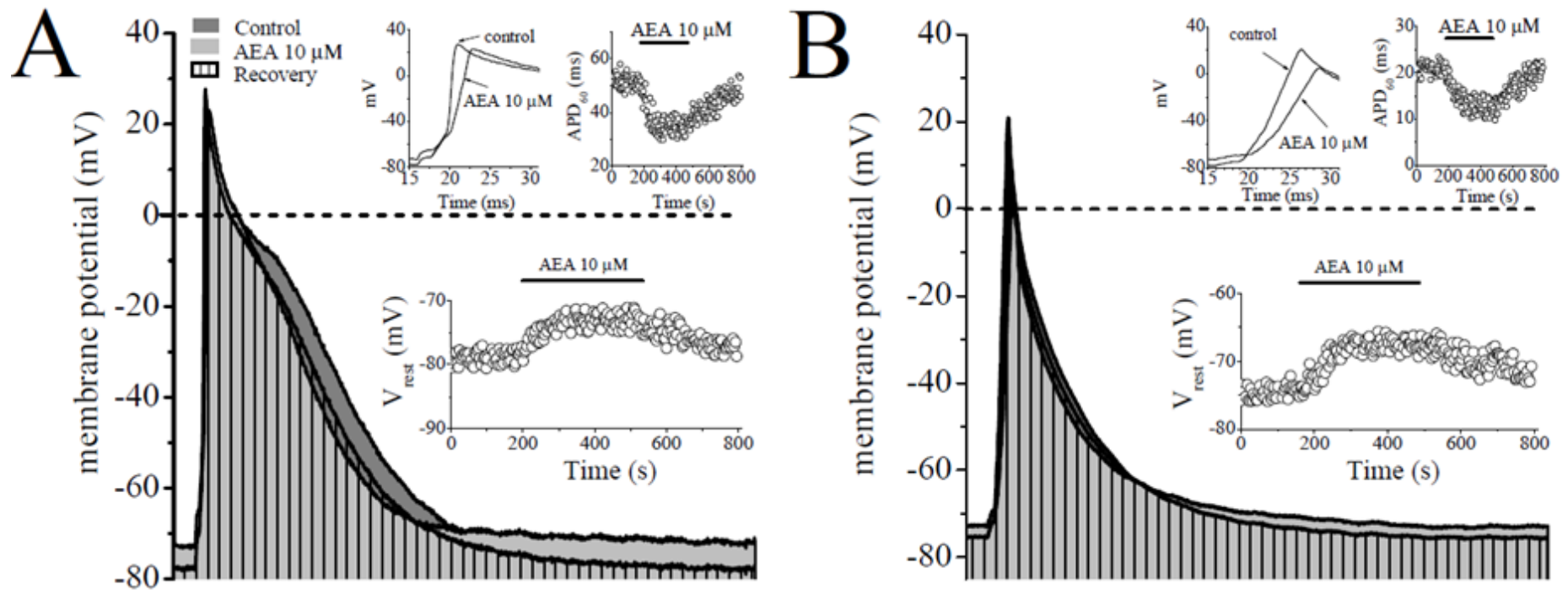


**Figure 3.12 Effects of high concentration of AEA on the excitability of ventricular myocytes:** Representative recordings of APs in controls (dark grey area), in the presence of 10  $\mu$ M AEA (light grey area) and after washout (striped area) in ventricular endocardial (**A**) and epicardial (**B**) myocytes; the *insets* on panels A and B show the time course of the action potential duration (APD<sub>60</sub>) and resting potential (V<sub>rest</sub>) changes in response to AEA application (indicated by horizontal bars).

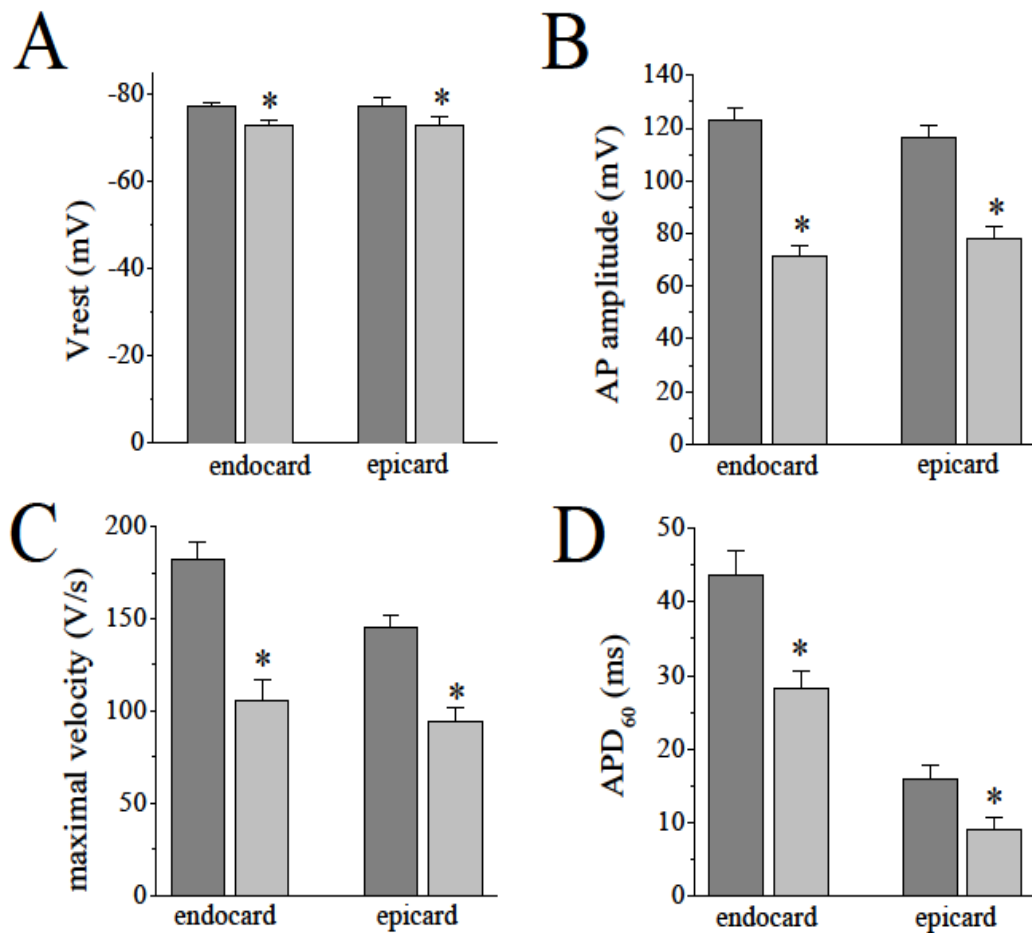


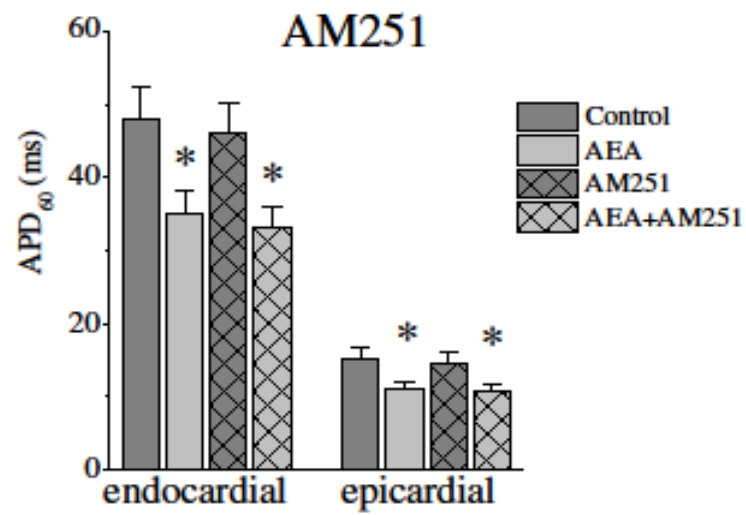
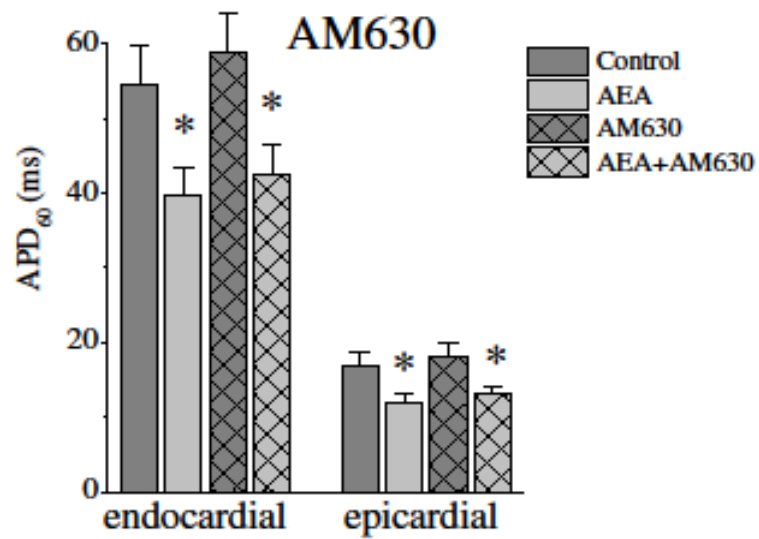
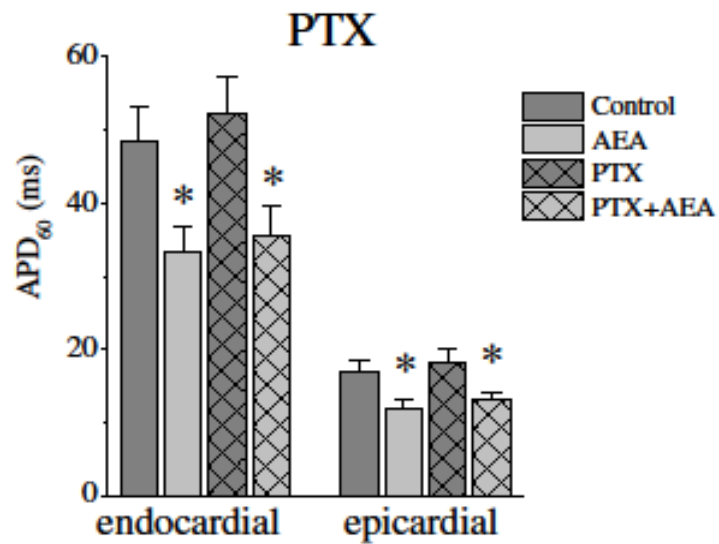
**Figure 3.13 Summary of the effect of high concentration of AEA on the amplitude and the shape of APs in cardiomyocytes:** Quantification of the changes in  $V_{rest}$  (A), AP amplitude (B) AP maximal rate of rise (C) and AP duration (D), characterized by  $APD_{60}$  in controls (dark grey bars) and in response to  $10 \mu\text{M}$  AEA (light grey bars). Data are analyzed using paired  $t$ -test and are expressed as means  $\pm$  S.E.M. from 18 to 24 myocytes (for A-C) and from 13 to 20 (for D). \* indicates statistically significant difference at the level of  $P < 0.05$ .

### **3.8 Cannabinoid receptors are not involved in the effect of anandamide on the action potentials in ventricular myocytes**

In these experiments, the effects of CB<sub>1</sub> receptor antagonist AM251 (0.3 μM) and CB<sub>2</sub> receptor antagonist AM630 (0.3 μM) on AEA-induced changes in the AP duration of endocardial and epicardial myocytes were investigated. The effect of AEA on APD<sub>60</sub> remained unaltered in the presence of AM251 (n=5-7 cells;  $P>0.05$ ; Figure 3.14A). Similarly, pretreatment with AM630 did not cause a significant effect on AEA-induced changes in APD<sub>60</sub> in both endocardial and epicardial myocytes (n=5-7 cells;  $P>0.05$ ; Figure 13.4B). Since the actions of cannabinoid receptors (CB<sub>1</sub> and CB<sub>2</sub>) are mediated by the activation of G<sub>i/o</sub> proteins sensitive to PTX treatment, we tested whether PTX pretreatment (2 μg/ml, 3 hours at 37 °C) alters AEA-induced changes in AP duration in endocardial and epicardial myocytes. PTX did not cause a significant alteration in the effects of AEA on both endocardial and epicardial myocytes (n=5-7 cells;  $P>0.05$ ; Figure 3.14C).

### **3.9 Anandamide inhibits voltage-dependent Na<sup>+</sup> channels in ventricular myocytes**

Previous studies have indicated that AEA has significant antiarrhythmic effects (Ugdyzhekova, et al., 2001; Li, et al., 2009). Since voltage-activated inward Na<sup>+</sup> ( $I_{Na}$ ) and Ca<sup>2+</sup> ( $I_{L,Ca}$ ) currents are the major ion currents shaping the action potential in ventricular myocytes, we have conducted a series of experiments under conditions that enable reliable isolation of either  $I_{Na}$  or  $I_{L,Ca}$  in voltage-clamp mode. In the first set of experiments,  $I_{Na}$  was typically elicited by pulses from -80 mV to +60 mV for 50 ms. Figure 3.15A shows recordings of  $I_{Na}$  in ventricular myocytes before and after application of 10 μM AEA.

**A****B****C**

**3.14 Effect of cannabinoid receptor antagonists and PTX pretreatment on AEA-induced changes in myocyte excitability:** (A) Effect of CB<sub>1</sub> receptor antagonist AM251 (0.3 μM) on AEA-induced changes in APD<sub>60</sub> in endocardial and epicardial myocytes. APD<sub>60</sub> was presented in control and in the presence of 1 μM AEA, 0.3μM AM251, and 1 μM AEA + 0.3μM AM251. (B) Effect of CB<sub>2</sub> receptor antagonist AM630 (0.3 μM) on AEA-induced changes in APD<sub>60</sub> in endocardial and epicardial myocytes. APD<sub>60</sub> was presented in control and in the presence of 1 μM AEA, 0.3 μM AM630, and 1 μM AEA + 0.3 μM AM630. (C) Effect of PTX treatment on AEA-induced changes in APD<sub>60</sub> in endocardial and epicardial myocytes. Changes are presented in control, in presence of 1 μM AEA, in control + PTX, and in presence of 1μM AEA + PTX. Data are analyzed using ANOVA and are expressed as means ± S.E.M., from 5 to 7 myocytes of each type; \* indicate statistically significant difference at the level of  $P < 0.05$ .



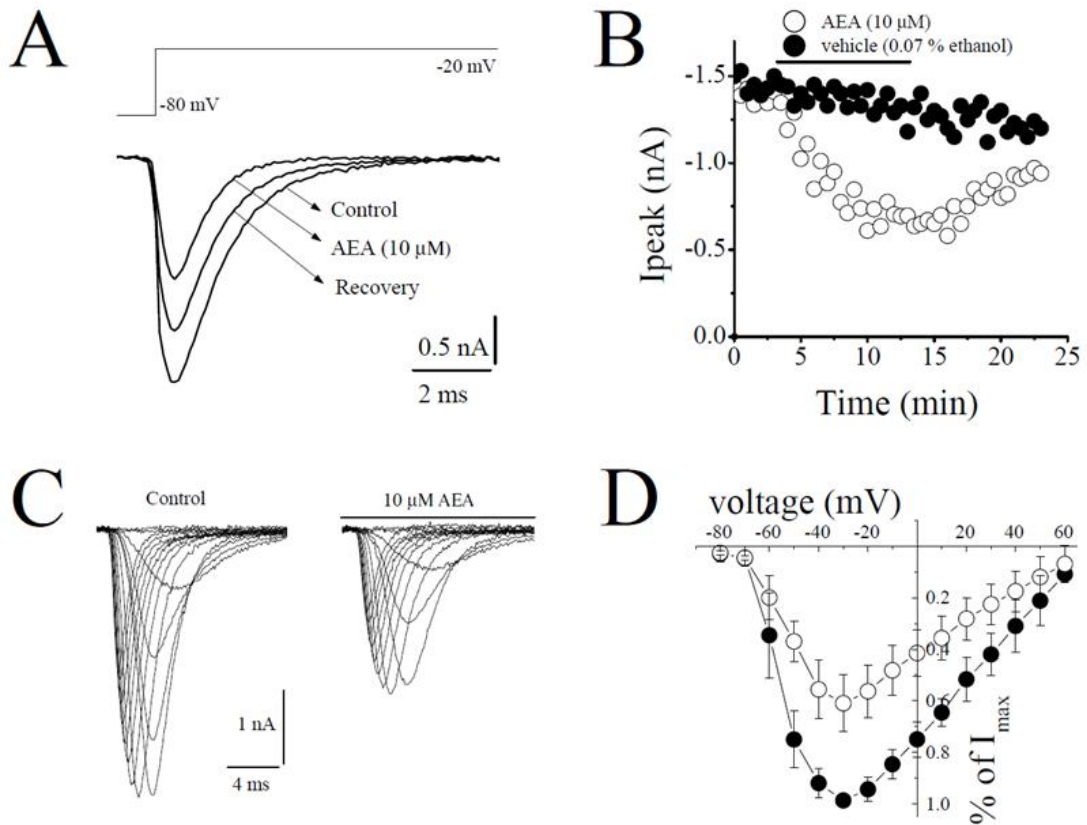


**Figure 3.15 Effect of AEA on  $I_{Na}$  in rat ventricular myocytes:** (A) AEA inhibits  $I_{Na}$  recorded using whole cell voltage clamp mode of patch clamp technique.  $I_{Na}$  was recorded during 50 ms voltage pulses to -20 mV from a holding potential of -80 mV. Current traces were recorded before (control) and after 10 minutes application of 10  $\mu$ M AEA. (B) Maximal currents of VGSCs presented as a function of time in the presence of vehicle (0.07 % ethanol) and 10  $\mu$ M AEA (n=5-6 cells). (C) Representative recordings of  $I_{Na}$  in response to the depicted pulse protocol under control conditions and after application of 10  $\mu$ M AEA. (D) Normalized and averaged  $I-V$  relationships of control  $I_{Na}$  (filled circles) and  $I_{Na}$  in the presence of 10  $\mu$ M AEA (open circles) determined by applying a series of step depolarizing pulses from -80 mV to +60 mV in 10 mV increments for a duration of 50 ms. Data are analyzed using paired  $t$ -test and are expressed as means  $\pm$  S.E.M. from 5 to 7 cells.

The effect of AEA was detectable within 2-3 minutes and reached a steady-state level within 10-15 minutes. The recovery was partial during the experiments lasting up to 25 to 30 minutes (Figure 3.15B).

With 40 mM Na<sup>+</sup> outside and Cs<sup>+</sup> as the major intracellular cation, inward  $I_{Na}$  in response to incremental step depolarizations ( $V_m$ , 10 mV increment) applied from a holding potential  $V_h = -80$  mV,  $I_{Na}$  started to activate at  $V_m = -60$  mV, and reached maximal amplitude at about  $V_m = -30$  mV. At more positive potentials the inward current decreased, reversing its direction at an apparent reversal potential ( $V_{rev}$ ) of around +60 mV. Traces of  $I_{Na}$  in the absence and presence of 10  $\mu$ M AEA were presented in Figure 3.15C. AEA inhibited  $I_{Na}$  without causing significant changes in the  $I$ - $V$  relationship. The  $I$ - $V$  relationship for  $I_{Na}$  is illustrated in Figure 3.15D. AEA inhibited  $I_{Na}$  without changing the threshold, peak and reversal potentials.

In this study, AEA was dissolved in ethanol, and therefore, we have tested the effect of ethanol as a vehicle. In agreement with earlier studies (Danziger, et al., 1991; Bebarova, et al., 2010), our results indicate that maximal amplitudes of  $I_{Na}$  were altered after 10 minutes vehicle application in experiments lasting up to 20 to 25 minutes (Figure 3.16A). Due to the effect of vehicle, we have tested each concentration of AEA and vehicle separately and plotted the concentration response curve after subtraction of vehicle effect. The effect of increasing AEA and corresponding ethanol concentrations and corrected concentration-response curve were presented in Figure 3.16B.

In order to exclude the possibility of the involvement of degradation products of AEA in the inhibition of  $I_{Na}$ , the effect of 10  $\mu$ M metAEA was tested.

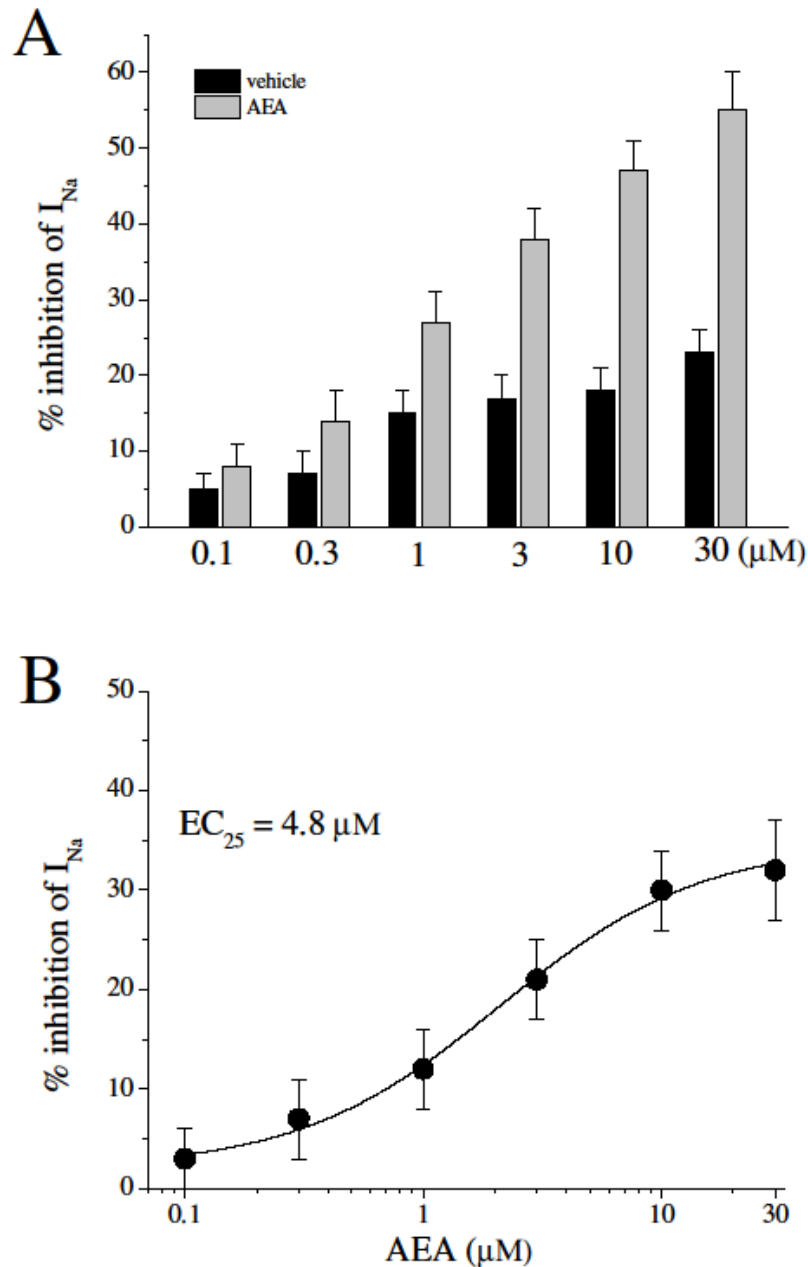


**Figure 3.16** Effect of increasing AEA and vehicle concentrations on  $I_{Na}$  recorded in rat ventricular myocytes: **(A)** Effects of AEA (0.1 to 30 μM) and corresponding vehicle concentrations on the maximal amplitudes of  $I_{Na}$  currents. Data are analyzed using paired  $t$ -test and are expressed as means  $\pm$  S.E.M. from 5 to 7 cells. **(B)** Corrected concentration response curve for the inhibitory effect of AEA on  $I_{Na}$ . The amount of inhibition induced by the vehicle was subtracted from the AEA-induced inhibition at corresponding AEA concentrations. Data was fit with logistic equation using Origin data analysis software.

10 minute application of metAEA caused a significant inhibition of  $I_{Na}$  ( $36 \pm 4$  % of controls;  $n=5$  cells;  $P>0.05$ ).

Steady-state activation (SSA) curves of  $I_{Na}$ , before and after AEA application, were derived by fitting the respective  $I$ - $V$  relationships with the product of Boltzmann equation (Figure 3.17A). This allowed us to determine if AEA influences the parameters of  $I_{Na}$  SSA: the voltage of half-maximal activation ( $V_{1/2}$ ) and slope factor ( $k$ ). In controls,  $V_{1/2}$  and  $k$  values were  $-45.2$  mV and  $7.1$  mV, respectively. In the presence of  $10 \mu\text{M}$  AEA,  $V_{1/2}$  and  $k$  values were  $-42.3$  mV, and  $7.5$  mV. There were no statistically significant differences between controls and AEA-treated cells ( $n=8-10$  cells;  $P>0.05$ ).

In order to determine if AEA influences the properties of inactivation of VGSCs, SSI dependencies of  $I_{Na}$  in the absence and presence of AEA were compared. Steady state inactivation curves were acquired using a standard voltage protocol consisting of prolonged (400 ms) conditioning pre-pulse to various  $V_m$ , in the range of  $-100$  mV to  $+70$  mV, which was immediately followed by a constant  $I_{Na}$  activating test pulse to  $V_m = -20$  mV. Steady state inactivation-dependency was plotted as normalized amplitude of  $I_{Na}$  at  $V_m = -20$  mV against the value of conditioning  $V_m$ . The fit of the obtained data points using the Boltzmann equation (Figure 3.17B) has indicated that under control conditions,  $V_{1/2}$  and  $k$  values were  $-70.2$  mV and  $-5.8$  mV, respectively. In the presence of  $10 \mu\text{M}$  AEA,  $V_{1/2}$  and  $K$  values were  $-81.4$  mV and  $-5.1$  mV, respectively. Thus, AEA induced a significant hyperpolarizing shift in the voltage-dependence of SSI of cardiac VGSCs ( $-11.4$  mV;  $P<0.05$ ). Comparison of  $I_{Na}$  currents, in the absence and

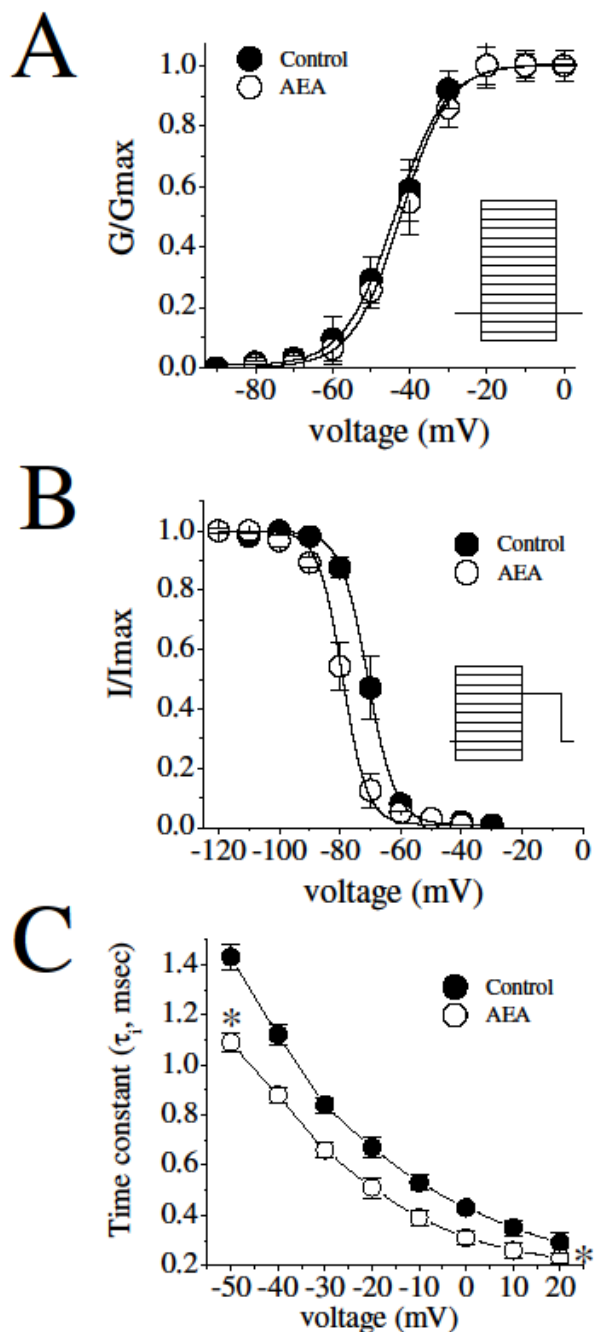


**Figure 3.17 Effect of AEA on steady state activation and inactivation of  $I_{Na}$  in rat ventricular myocytes: (A) Steady-state activation (SSA) and (B) steady-state inactivation (SSI) curves of  $I_{Na}$  in the absence (filled circles) and presence of 1  $\mu$ M AEA (open circles). (C) Voltage-dependence of  $I_{Na}$  inactivation time constant ( $\tau_i$ ) under control conditions (filled circles) and in the presence of 1  $\mu$ M AEA (open circles). Data are analyzed using paired  $t$ -test and are expressed as means  $\pm$  S.E.M., are from 7 cells. \* indicates statistically significant difference at the level of  $P < 0.05$ .**

presence of AEA, revealed noticeable acceleration of the current's inactivation kinetics by AEA. Quantification of the time constant of  $I_{Na}$  inactivation ( $\tau_i$ ), by fitting the currents' decay phase with exponential functions, showed that AEA (10  $\mu$ M) significantly reduced  $\tau_i$  in the range of  $V_m$  between -50 mV and +20 mV (Figure 3.17C). Furthermore, the results of this study show that the inhibitory effect of AEA on the maximal amplitudes of  $I_{Na}$  was not significantly affected by PTX pretreatment (Figure 3.18).

### **3.10 Anandamide inhibits voltage-dependent $Ca^{2+}$ channels in ventricular myocytes**

The effect of AEA on the L-type  $Ca^{2+}$  currents ( $I_{L,Ca}$ ) was also tested. Figure 3.19A shows a typical record of  $I_{L,Ca}$  elicited by applying a single 300 ms voltage pulse to +10 mV from a holding potential of -50 mV in rat ventricular myocyte before and after 10 minutes superfusion with 1  $\mu$ M AEA. Time course of the effect of AEA on the density of  $I_{L,Ca}$  was presented in Figure 3.19B. The effects of AEA were also investigated on the biophysical properties of  $I_{L,Ca}$  in rat ventricular myocytes. L-type  $Ca^{2+}$  current was recorded in the presence of intracellular  $Cs^+$  and extracellular  $TEA^+$  to suppress  $K^+$  currents, while retaining 95 mM  $Na^+$  in the extracellular solution. Elimination of contaminating  $Na^+$  current during recording of  $I_{L,Ca}$  was achieved by applying voltage step-pulses from relatively depolarized  $V_h$  of -50 mV, which produced steady-state  $I_{Na}$  inactivation (Voitychuk, et al., 2012). As evident from original recordings and  $I$ - $V$  relationships (Figures 3.19C and D),  $I_{L,Ca}$  had a much slower kinetics in response to step depolarization, and activated at more positive potentials than  $I_{Na}$ : it started to appear at  $V_m = -30$  mV, reached maximum at around  $V_m = +10$  mV, and

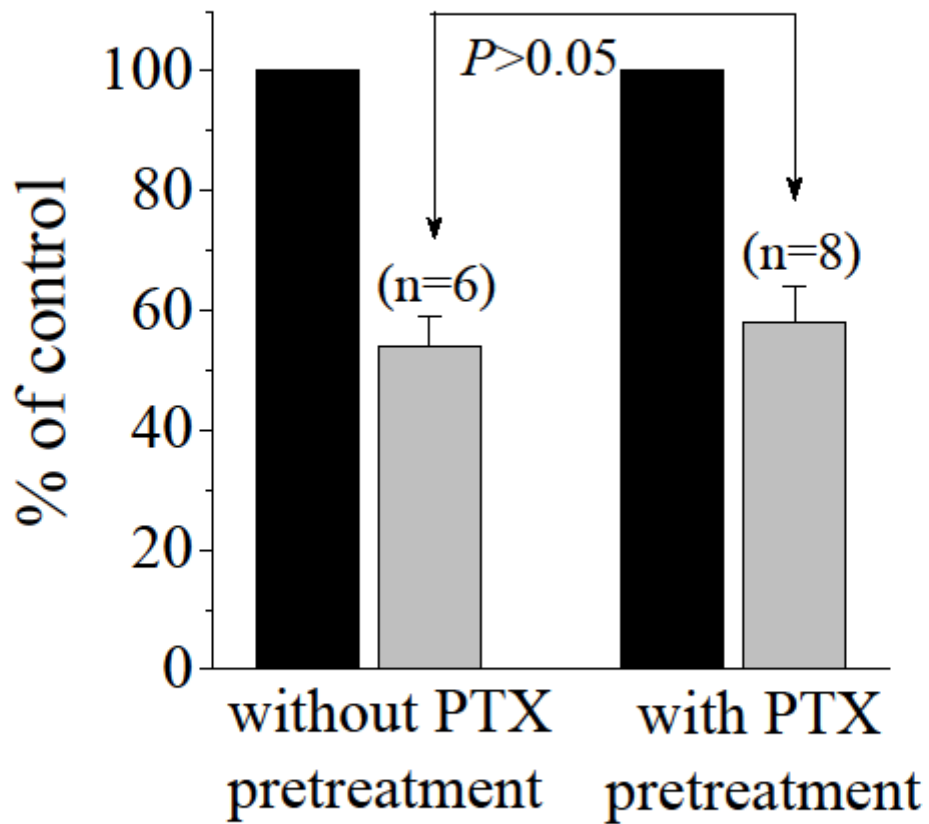


**Figure 3.18** Effect of PTX pretreatment on AEA inhibition of the maximal  $I_{Na}$  amplitudes. Black bars indicate controls. Data are analyzed using independent sample  $t$ -test and are expressed as means  $\pm$  S.E.M., from 6 to 8 cells.

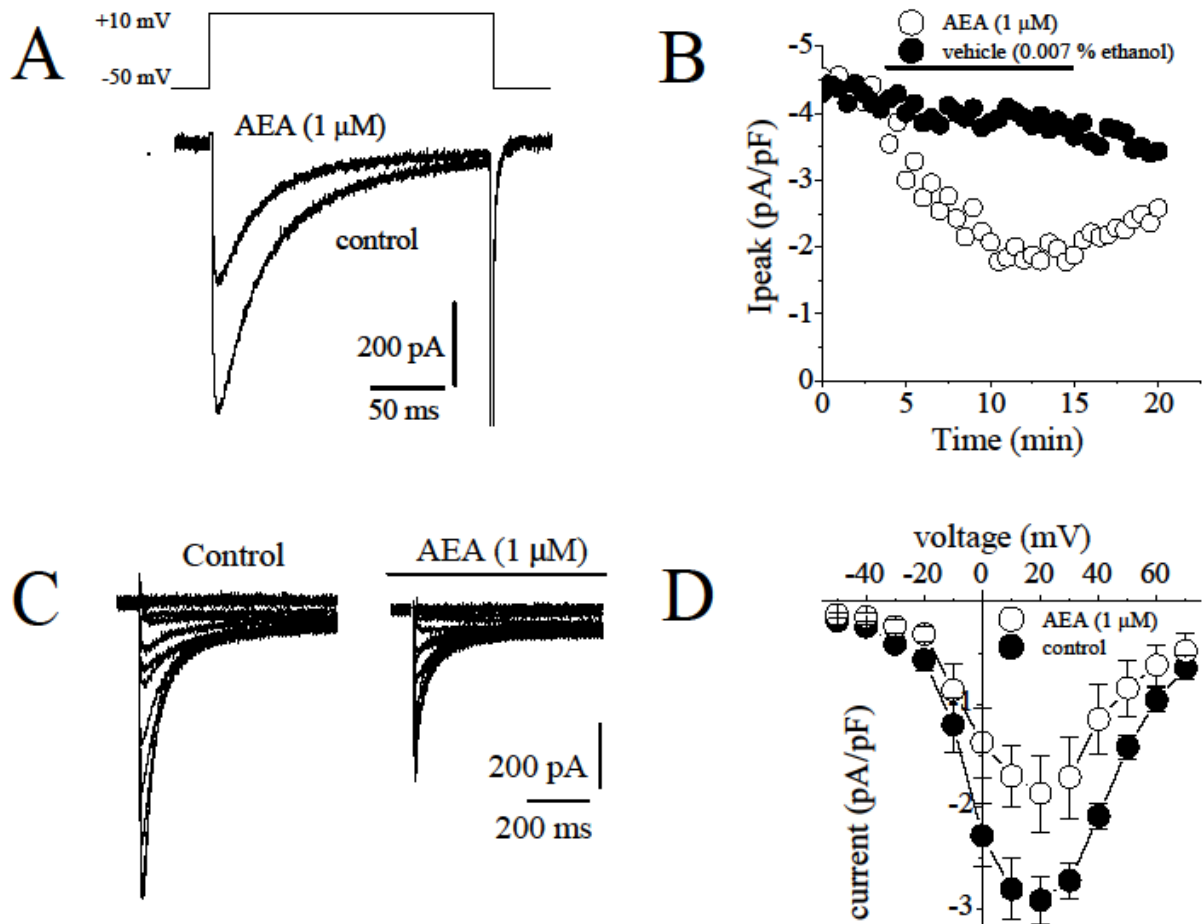


**Figure 3.19 Effect of AEA on  $I_{L,Ca}$  in rat ventricular myocytes:** (A) AEA inhibits  $I_{L,Ca}$  recorded using whole-cell voltage-clamp mode of patch clamp technique.  $I_{L,Ca}$  was recorded during 300 ms voltage pulses to +10 mV from a holding potential of -50 mV. Current traces recorded before (control) and after 10 minutes application of 1  $\mu\text{M}$  AEA. (B) Maximal currents presented as a function of time in the presence of vehicle (0.007 % ethanol) and 1  $\mu\text{M}$  AEA (n=5 cells). (C) Representative recordings of  $I_{L,Ca}$  in response to the depicted pulse protocol under control conditions and after application of 1  $\mu\text{M}$  AEA. (D) Normalized and averaged  $I$ - $V$  relationships of control  $I_{L,Ca}$  (open circles) and  $I_{L,Ca}$  in the presence of 1  $\mu\text{M}$  AEA (filled circles) determined by applying a series of step depolarizing pulses from -70mV to +70 mV in 10 mV increments for a duration of 300 ms. Data are analyzed using paired  $t$ -test and are expressed as means  $\pm$  S.E.M. from 5 to 7 cells.



decreased at higher voltages approaching zero at about  $V_m = +60$  mV (Figure 3.19D).

Current density of  $I_{L,Ca}$  was also altered after 10 minutes application of ethanol in experiments lasting up to 20 to 25 minutes. Effects of increasing AEA and corresponding ethanol concentrations on  $I_{L,Ca}$  and corrected concentration-response curve were presented in Figure 3.20.

In order to exclude the possibility of involvement of degradation products of AEA in the inhibition of  $I_{L,Ca}$ , the effect of 1  $\mu$ M metAEA was tested. MetAEA caused a significant inhibition of  $Ca^{2+}$  currents ( $46 \pm 4\%$  inhibition of controls;  $n=5$  cells;  $P<0.05$ ). In addition, the effect of FAAH inhibition on AEA-induced inhibitory effect was tested. Pretreatment with 1  $\mu$ M URB597 for 45 minutes at 37 °C (controls incubated with 0.007 % ethanol alone) did not alter the extent of AEA inhibition of L-type  $Ca^{2+}$  currents. In the absence and presence of URB597, AEA (1  $\mu$ M) inhibited L-type  $Ca^{2+}$  currents to  $32.7 \pm 3.6$  % of and  $35.3 \pm 4.2$  % of controls, respectively ( $n=5-7$ ;  $P>0.05$ ).

AEA produced a depolarizing shift of  $I_{L,Ca}$  SSA by 12.6 mV (i.e.,  $V_{1/2} = -9.4 \pm 0.3$  mV, in control, to  $V_{1/2} = +3.2 \pm 0.2$  mV, in the presence of AEA) and hyperpolarizing shift of  $I_{L,Ca}$  SSI by 4.3 mV (i.e., from  $V_{1/2} = -18.9 \pm 0.1$  mV, in control, to  $V_{1/2} = -23.2 \pm 0.1$  mV, in the presence of AEA) with little influence on the slopes of respective dependencies ( $k = 7.2 \pm 0.4$  mV and  $k = -5.3 \pm 0.3$  mV for the control activation and inactivation, respectively, vs.  $k = 6.9 \pm 0.3$  mV and  $k = -5.1 \pm 0.2$  mV for the AEA-modified activation and inactivation, respectively), which altogether resulted in the notable reduction of  $I_{L,Ca}$  “window current” responsible for the stationary  $Ca^{2+}$  entry in the range of membrane

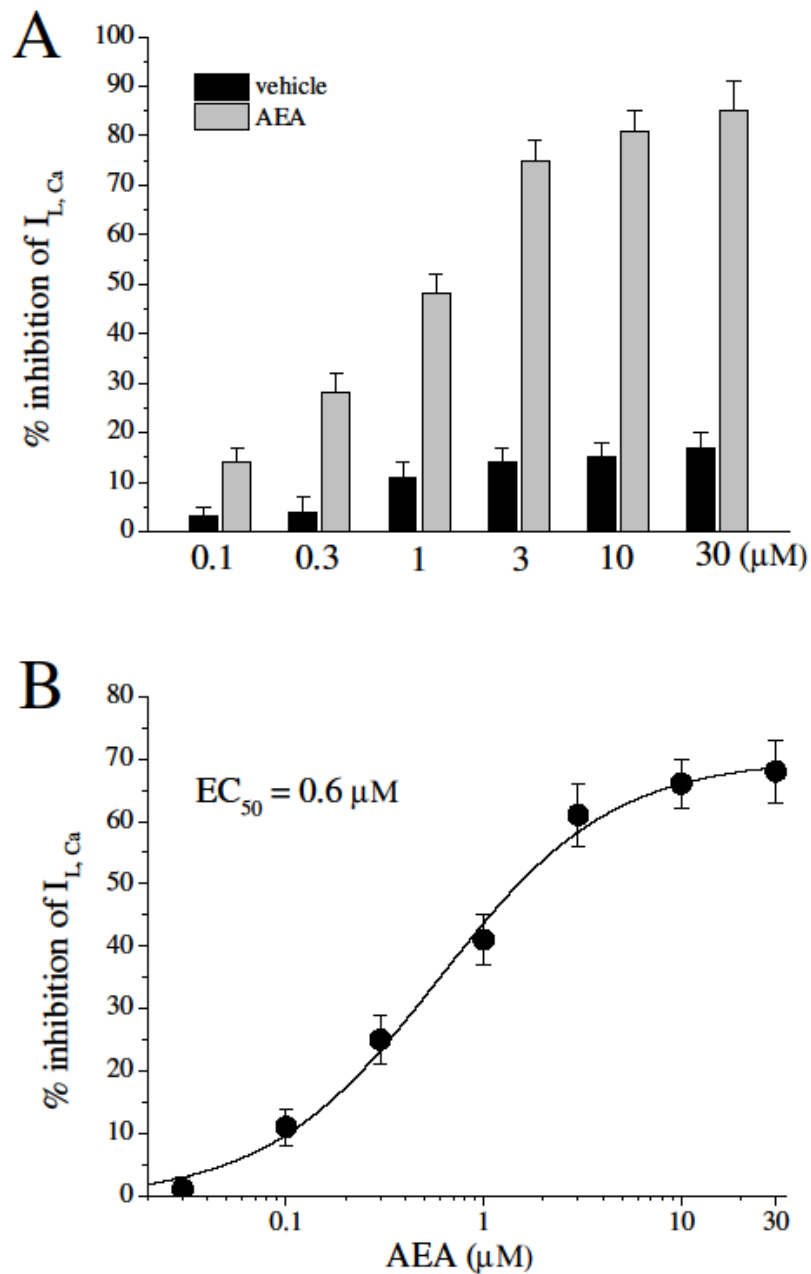


**Figure 3.20** Effects of increasing AEA and vehicle concentrations on  $I_{L,Ca}$  recorded in rat ventricular myocytes: **(A)** Effects of AEA (0.1 to 30 μM) and corresponding vehicle concentrations on the maximal amplitudes of  $I_{L,Ca}$ . Data are analyzed using paired *t*-test and are expressed as means ± S.E.M., from 5 to 7 cells. **(B)** Corrected concentration response curve for the inhibitory effect of AEA on  $I_{L,Ca}$ . The amount of inhibition induced by the vehicle was subtracted from AEA-induced inhibition at corresponding AEA concentrations. Data was fit with logistic equation using Origin data analysis software.

potentials from -40 mV to +10 mV (Figure 3.21A and 3.21B). Thus, the mechanism of AEA action on cardiac L-type VGCC most likely involves influence on channel gating that reduces “window current” as well as partial blockade of the ion-conducting pathway that decreases current amplitude.

In line with earlier reports (Soldatov, et al., 1998), kinetic analysis of  $I_{L,Ca}$  currents were fit to double-exponential function with fast ( $\tau_f$ ) and slow ( $\tau_s$ ) inactivation time constants. Comparison of  $I_{L,Ca}$  currents in the absence and presence of AEA revealed noticeable acceleration of the current's inactivation kinetics by AEA. Quantification of the time constants of  $I_{L,Ca}$  inactivation showed that AEA (1 $\mu$ M) significantly reduced  $\tau_i$  in the range of  $V_m$  -20 mV and +10 mV (Figure 3.21C).

In earlier electrophysiological studies, sidedness of AEA actions on various ion channels has been reported (Oz, 2006). For this reason, the effect of intracellular application of AEA by including AEA (1 $\mu$ M) inside the patch electrode was tested (Figure 3.22). The extent of AEA inhibition (compared after 15 minutes of AEA exposure) was not significantly different between intracellular and extracellular AEA applications (n=11-14 cells;  $P>0.05$ ).

In order to test if the modulation of  $Ca^{2+}$  binding site can mediate the effect of AEA on the inactivation kinetics of L-type VGCCs, extracellular  $Ca^{2+}$  was replaced with  $Ba^{2+}$  and the effect of AEA on  $Ba^{2+}$  currents ( $I_{Ba}$ ) through L-type VGCCs was tested. In line with earlier studies (Soldatov, et al., 1998), inactivation of  $I_{Ba}$  fit to mono-exponential decay function (Figure 3.23A) with significant voltage-dependency. In the presence of AEA, inactivation time

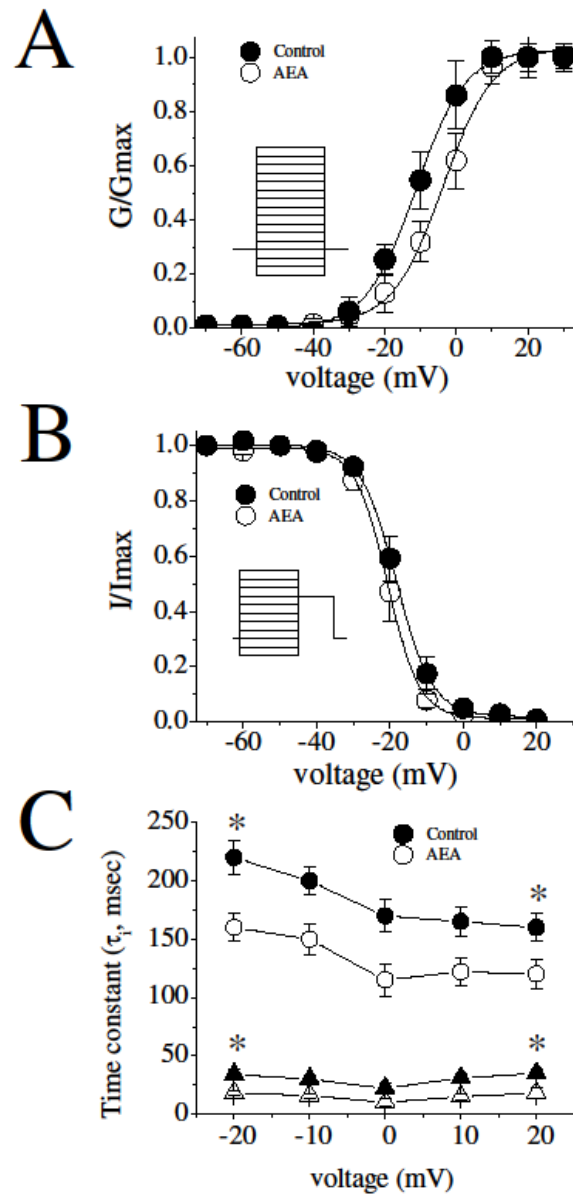


**Figure 3.21** Effect of AEA on steady state activation and inactivation of  $I_{L,Ca}$  in rat ventricular myocytes: (A) Steady-state activation (SSA) and (B) steady-state inactivation (SSI) curves of  $I_{L,Ca}$  in the absence (filled circles) and presence of 1  $\mu$ M AEA (open circles). (C) Voltage-dependent fast (triangles) and slow (circles) inactivation time constants ( $\tau_i$ ) of  $I_{L,Ca}$  under control conditions (filled circles and triangles) and in the presence of 1 $\mu$ M AEA (open circles and triangles). Data are analyzed using paired  $t$ -test and are expressed as means  $\pm$  SEM. from 5-6 cells. \* indicates statistically significant difference at the level of  $P < 0.05$ .

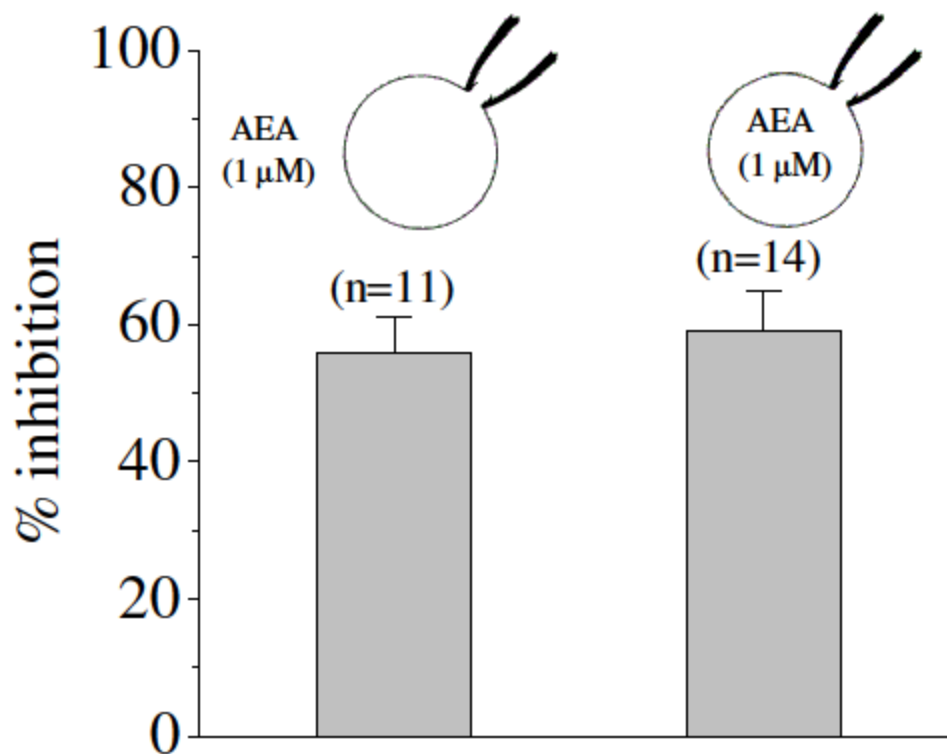


**Figure 3.22 Effect of sidedness of AEA application on  $I_{L,Ca}$  in rat ventricular myocytes:** Comparison of the intracellular and extracellular application of AEA on the maximal inhibition of  $I_{L,Ca}$ . Data are analyzed using independent sample  $t$ -test and are expressed as means  $\pm$  S.E.M. from 11-14 cells.

constant (Figure 3.23A and 3.23B), and the maximal amplitudes of  $I_{Ba}$  were significantly inhibited compared to control values ( $n=7-8$  cells;  $P<0.05$ ).

Since the known cannabinoid receptors  $CB_1$  and  $CB_2$  [for a review, (Pertwee, et al., 2010)] are coupled to PTX sensitive  $G_{i/o}$  type G-proteins, we have tested whether the inhibitory effects of AEA on L-type VGCCs are mediated by the activation of cannabinoid receptors. In the presence of 0.3  $\mu$ M AM251 and 0.3  $\mu$ M AM630, AEA (1 $\mu$ M) inhibition of  $I_{L,Ca}$  remained unaltered. Application of AM251 or AM630 alone did not have a significant effect on the amplitudes of  $I_{L,Ca}$  (Figure 3.24) ( $n=6-9$  cells;  $P>0.05$ ). Furthermore, the results of this study show that the inhibitory effect of AEA on the maximal amplitudes of  $I_{L,Ca}$  was not affected by PTX pretreatment (Figure 3.25).

In positive control experiments, PTX, as it has been reported earlier (Zhang, et al., 2005), effectively attenuated the inhibitory actions of BRL-37344, a  $\beta_3$  adrenergic receptor agonist, on  $I_{L,Ca}$  recorded in ventricular myocytes (Figures 3.26A and 3.26B) indicating that G-proteins are functionally coupled to their target receptors.

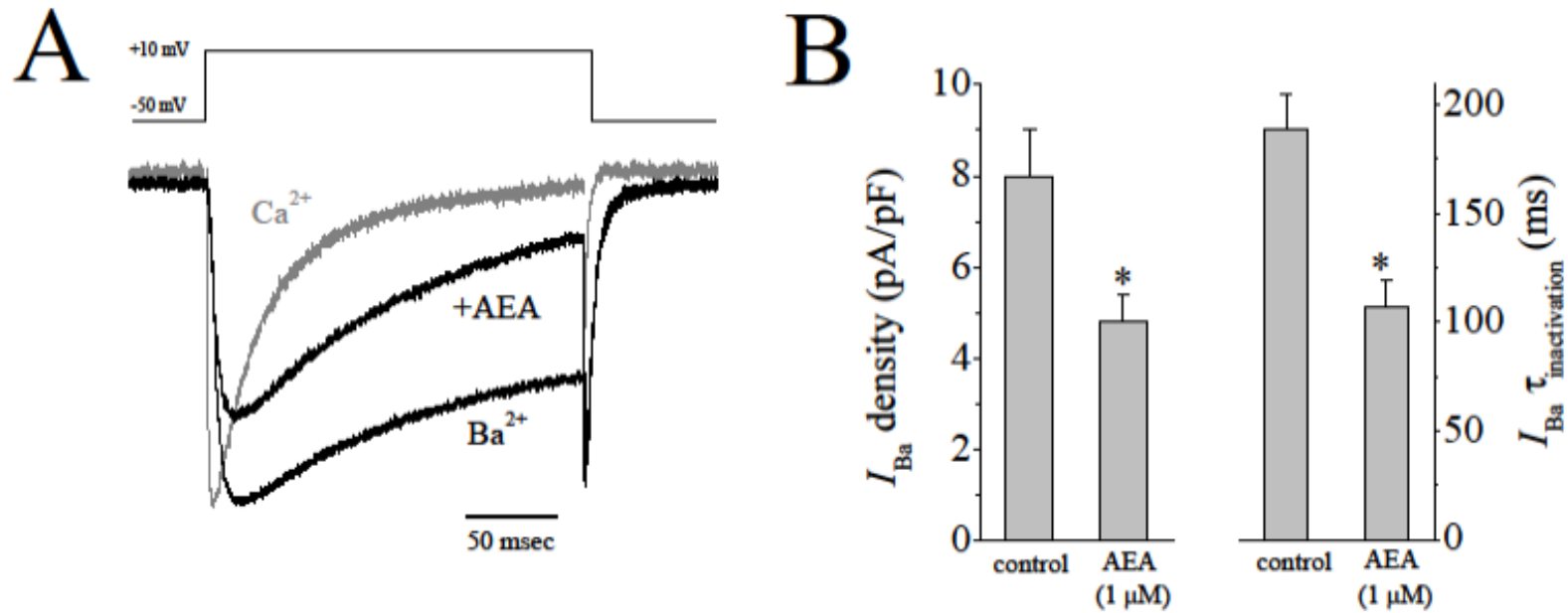


**Figure 3.23 Effect of AEA on  $Ba^{2+}$  currents mediated by L-type VGCCs:** (A) Traces of normalized  $Ca^{2+}$  and  $Ba^{2+}$  currents through L-type VGCCs. Normalized  $Ba^{2+}$  current in the presence 1  $\mu M$  AEA is also presented in the figure. (B) Effect of 1  $\mu M$  AEA on the maximal amplitudes and the inactivation kinetics of  $Ba^{2+}$  currents. Data are analyzed using paired *t*-test and are expressed as means  $\pm$  S.E.M. from 7-8 cells.\* indicates statistically significant difference at the level of  $P < 0.05$ .

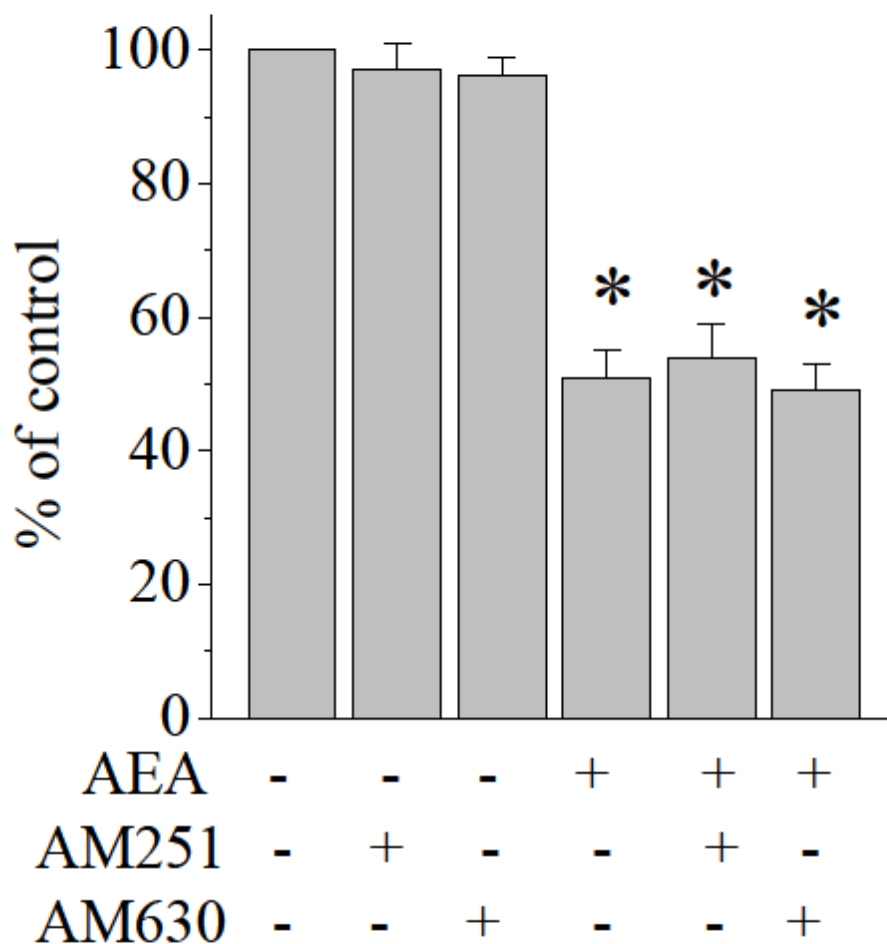


**Figure 3.24 Effects of cannabinoid receptor antagonists on AEA inhibition of L-type VGCCs:** Effects of CB<sub>1</sub> antagonist AM251 (0.3 μM) and CB<sub>2</sub> antagonist AM630 (0.3 μM) on AEA (1 μM) inhibition of *I<sub>L,Ca</sub>*. Data are analyzed using ANOVA and are expressed as means ± S.E.M. from 6-9 cells.\* indicates statistically significant difference at the level of P <0.05.



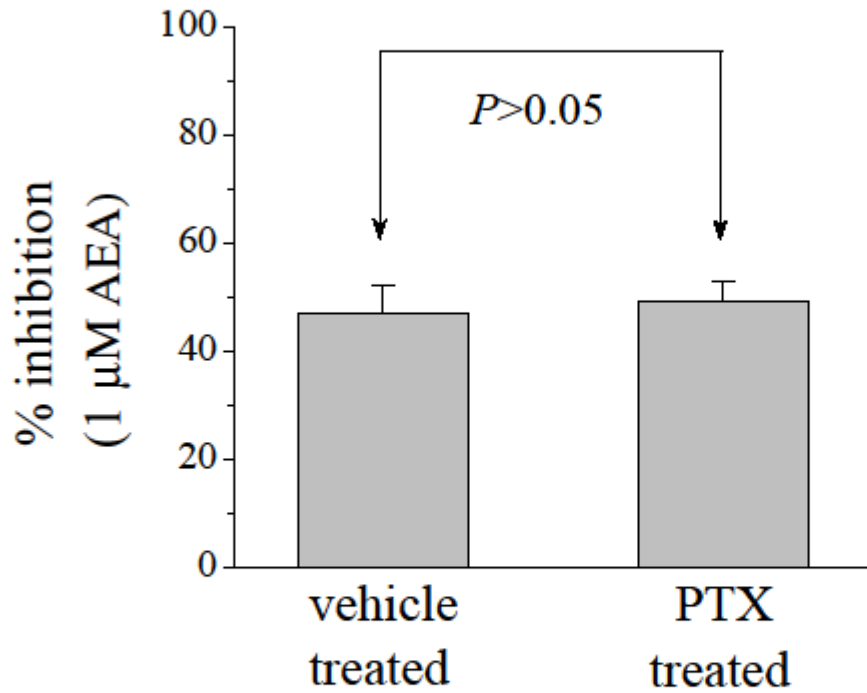


**Figure 3.25 Effects of PTX pretreatment on AEA inhibition of L-type VGCCs:** Percent inhibition of  $I_{L, Ca}$  after vehicle (distilled water) and PTX (2  $\mu$ g/ $\mu$ l, 3hours). Data are analyzed using independent sample  $t$ -test and are expressed as means  $\pm$  S.E.M. from 6-8 cells.

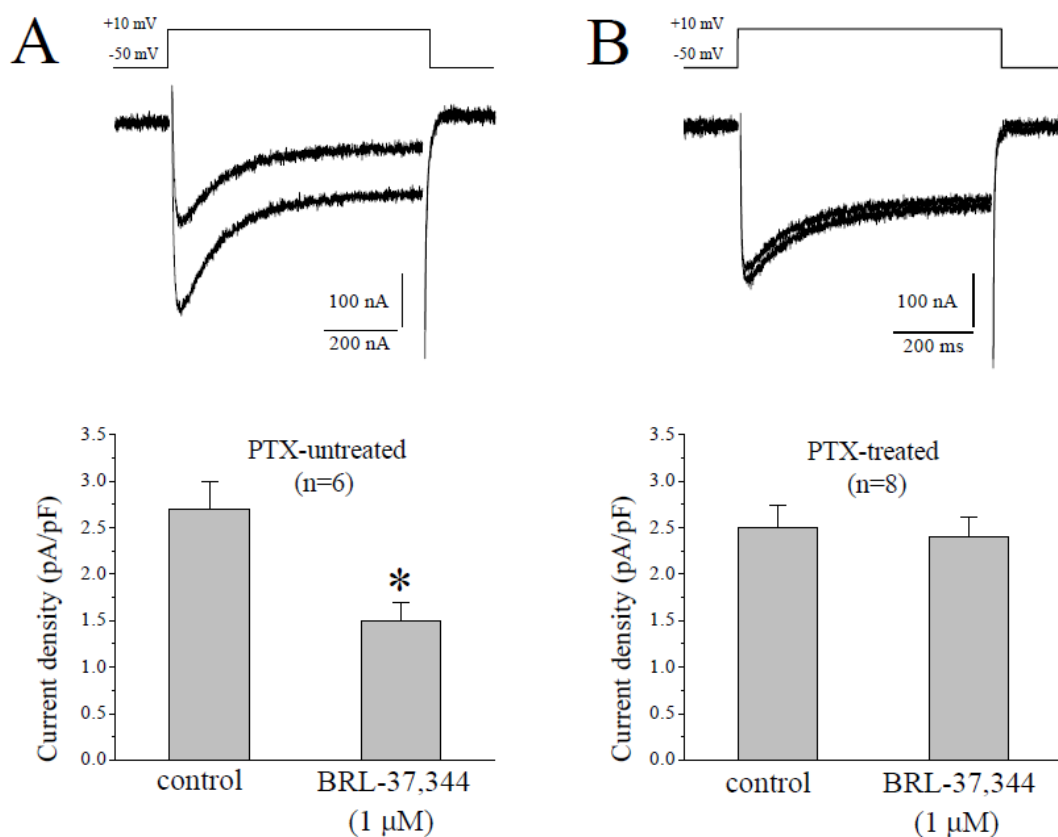


**Figure 3.26 Effect of PTX pretreatment on BRL-37344 inhibition of  $I_{L,Ca}$  recorded in rat ventricular myocytes:** (A) Records of currents presenting the effect of BRL-37344, on  $I_{L,Ca}$  in the absence and presence of PTX (2  $\mu$ g/ml for 3 hours in 37 °C) pretreatment. Records were obtained by applying a step depolarizing pulse from -50 mV to +10 mV for duration of 300 ms (B) Presentation of results on the effect of PTX pretreatment on BRL-37344 inhibition of  $I_{L,Ca}$ . Data are analyzed using independent sample *t*-test and are expressed as means  $\pm$  S.E.M. from 5-7 cells.\* indicates statistically significant difference at the level of  $P < 0.05$ .

### 3.11 Anandamide inhibits $\text{Na}^+/\text{Ca}^{2+}$ exchanger in ventricular myocytes

Currents mediated by NCX1 were elicited by a descending voltage ramp pulses applied between +100 mV and -100 mV ( $dV/dt = 0.1$  V/s) from a holding potential of -40 mV for 2 seconds. In order to verify that the currents recorded in our experimental conditions are mediated by the NCX1,  $\text{Ni}^{2+}$  (10 mM) was used routinely at the end of each experiment to determine the  $\text{Ni}^{2+}$ -sensitive NCX1 current (Figure 3.27A and 3.27B). Bath application of  $\text{Ni}^{2+}$  for 5 minutes reversibly suppressed  $I_{\text{NCX1}}$ , indicating that these currents are mediated by NCX1 in cardiomyocytes (Figures 3.27A and 3.27B). Command pulses were applied every 15 seconds, and amplitudes of currents at +100 mV and -100 mV were plotted as a function of time (Figure 3.27A). Anandamide largely attenuated both the outward and inward components of  $\text{Ni}^{2+}$ -sensitive current. The effect of AEA was detectable at 2-3 minutes and reached a steady-state level within 5 minutes. Within the time period of our experiment, the recovery was partial. Figure 3.27B shows representative current traces in control solution, in the presence of AEA (10  $\mu\text{M}$ ) and in the presence of  $\text{Ni}^{2+}$  (10 mM). In this experiment, AEA was dissolved in ethanol. The maximal amplitudes of  $I_{\text{NCX1}}$  were not altered by 10 to 15 minutes application of ethanol up to the concentration of 0.07% (V/V;  $n=6$ ).

Figure 3.27C shows the mean  $I$ - $V$  relationships for  $\text{Ni}^{2+}$ -sensitive  $I_{\text{NCX1}}$  in control and in the presence of 10  $\mu\text{M}$  AEA.  $I_{\text{NCX1}}$  was calculated by subtracting the currents recorded in  $\text{Ni}^{2+}$  from the current recorded without  $\text{Ni}^{2+}$ . Evaluation of the AEA inhibition of  $I_{\text{NCX1}}$  at different membrane potentials (Figure 3.27D) indicated that AEA inhibits both outward and inward components of  $I_{\text{NCX1}}$  equally.

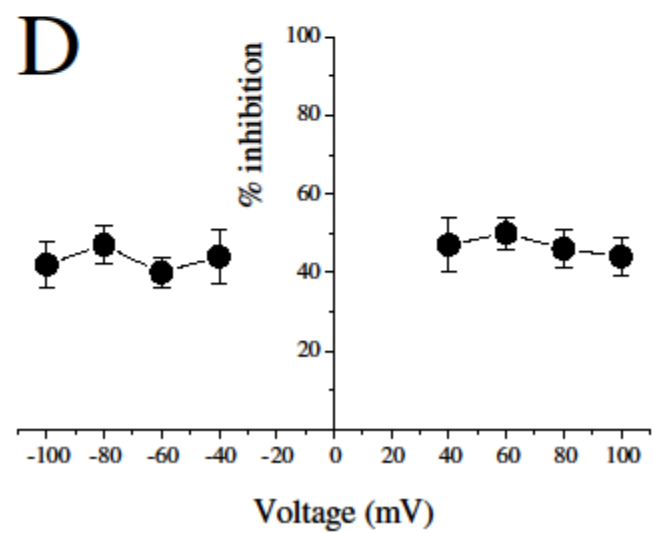
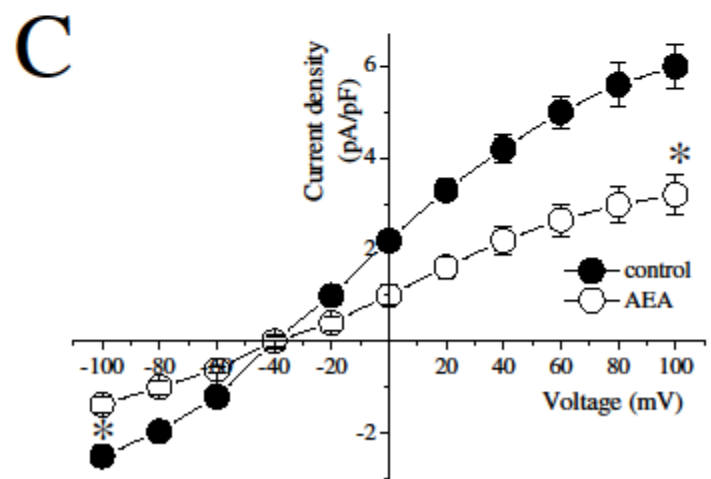
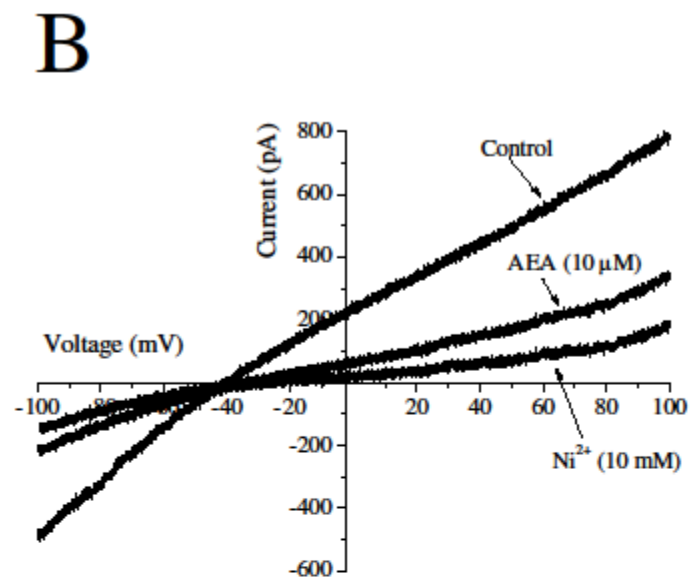
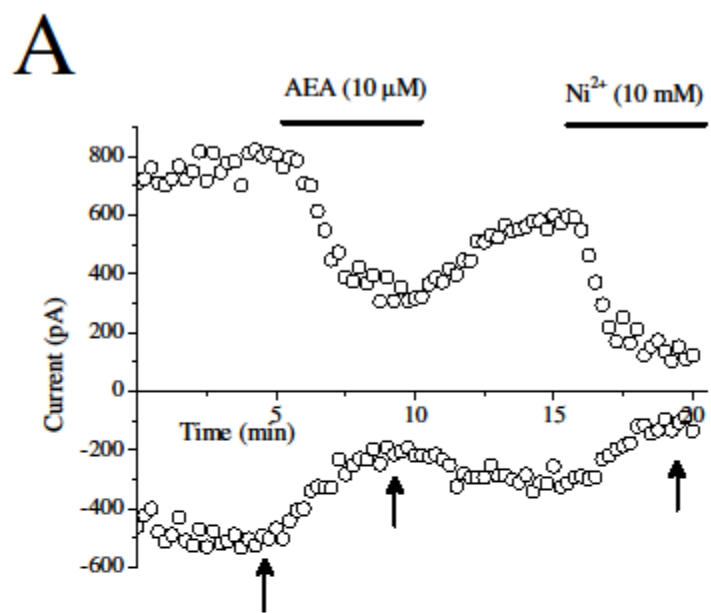


**Figure 3.27 Effect of AEA on  $I_{\text{NCX1}}$  in rat ventricular myocytes:** AEA inhibits  $I_{\text{NCX1}}$  recorded using whole cell voltage clamp mode of patch clamp technique.

**(A)** Time course of the effects of AEA on the inward and outward  $I_{\text{NCX1}}$  recorded in a cardiomyocyte.  $I_{\text{NCX1}}$  was elicited by 2 seconds voltage ramps from +100 mV to -100 mV every 15 seconds. Amplitudes of currents recorded at +100 mV and -100 mV were presented as a function of time. Horizontal bars indicate drug application times. Arrows correspond to the time points for the currents shown in Figure 3.27B

**(B)** Current traces were recorded in control, after 5 minutes application of 10  $\mu\text{M}$  AEA, and following 10 mM  $\text{Ni}^{2+}$  for 5 minutes.

**(C)** Mean  $I$ - $V$  relationship of NCX1 in the absence and presence of 10  $\mu\text{M}$  AEA. Data points (mean  $\pm$  S.E.M.) are from 7 cells.

**(D)** Quantification of the extent of AEA inhibition of  $I_{\text{NCX1}}$  at different membrane potentials. Data points (mean  $\pm$  S.E.M.) are from 6 cells. Paired  $t$ -test was used to compare the amplitude of current currents recorded at +100 mV and -100 mV.\* indicates statistically significant difference at the level of  $P < 0.05$ .

Collectively, these observations indicate that, AEA (10  $\mu\text{M}$ ) exerts an inhibitory effect on NCX1 in ventricular myocytes.

The effect of increasing AEA concentrations on the outward (measured at +100 mV) components of  $I_{\text{NCX1}}$  was demonstrated in Figure 3.28. AEA inhibited  $I_{\text{NCX1}}$  in a concentration-dependent manner with  $\text{IC}_{50}$  values of 4.7  $\mu\text{M}$ . The effect of metAEA was also tested to avoid the likely confounding effects of degradation products and oxygenated metabolites on NCX1. At a concentration of 10  $\mu\text{M}$ , metAEA also caused a significant inhibition of exchanger current (Figure 3.29A). Furthermore, the effect of AEA on NCX1 in the presence of the specific FAAH inhibitor URB597 was also tested. After incubation of cardiomyocytes with 1  $\mu\text{M}$  URB597 for 1 hour, AEA continued to inhibit the function of NCX1 (Figure 3.29B) further suggesting that the intact AEA molecule, but not the degradation products, mediates its effect on the exchanger.

In the presence of 1  $\mu\text{M}$  AM251 and 1  $\mu\text{M}$  AM630, AEA (10  $\mu\text{M}$ ) inhibition of  $I_{\text{NCX1}}$  remained unaltered ( $n=6-8$ , Figure 3.30). In addition, the results of this study show that the inhibitory effect of AEA on the maximal amplitudes of  $I_{\text{NCX1}}$  was not affected by PTX pretreatment (Figure 3.31A). In positive control experiments (section 3.10), PTX, as it has been reported earlier (Zhang, et al., 2005), effectively attenuated the inhibitory actions of BRL-37344, a  $\beta_3$  adrenergic receptor agonist, on L-type VGCCs recorded in ventricular myocytes (Figure 3.26). GDP- $\beta$ -S is also commonly used to inhibit the responses mediated by the activation of G-protein receptors (Bondarenko, et al., 2013). For this reason, the effect of AEA in the presence of GDP- $\beta$ -S in intracellular solution was tested. After the inclusion of GDP- $\beta$ -S (1mM) in pipette solution, AEA continued to inhibit NCX1 (Figure 3.31B).

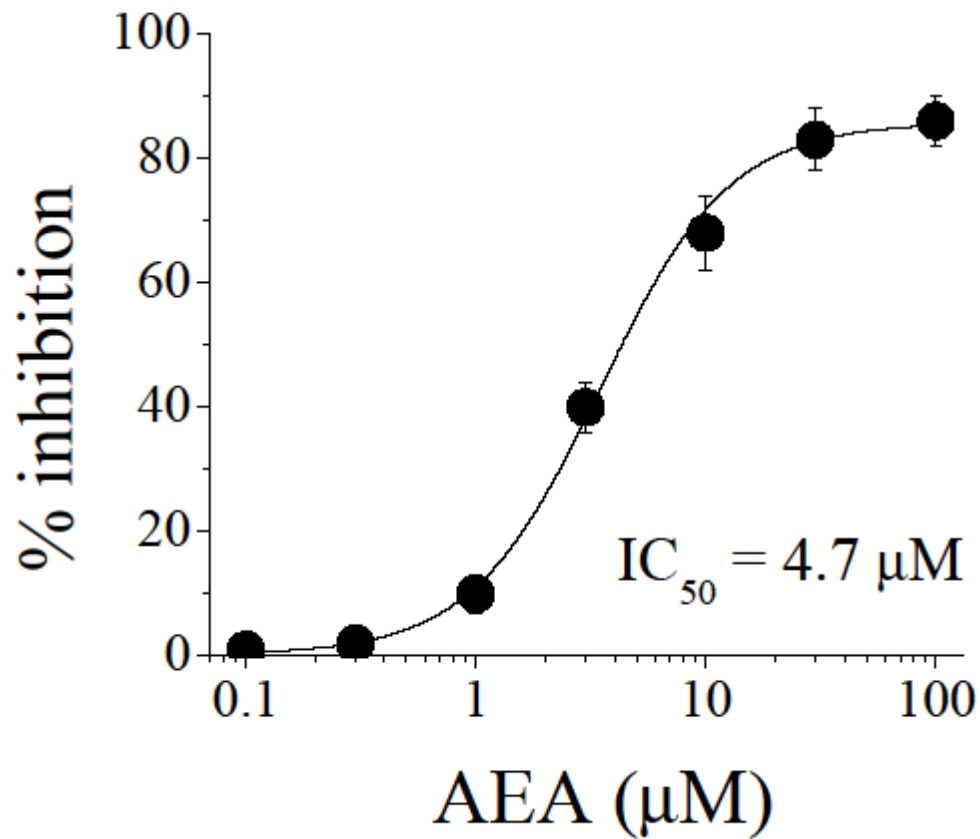


**Figure 3.28** Effect of increasing AEA concentration on  $I_{NCX1}$  in rat ventricular myocytes: AEA inhibits  $I_{NCX1}$  in a concentration-dependent manner.  $\text{Ni}^{2+}$ -sensitive current was measured at +100 mV. Data points (mean  $\pm$  S.E.M.) are from 6 to 8 cells.

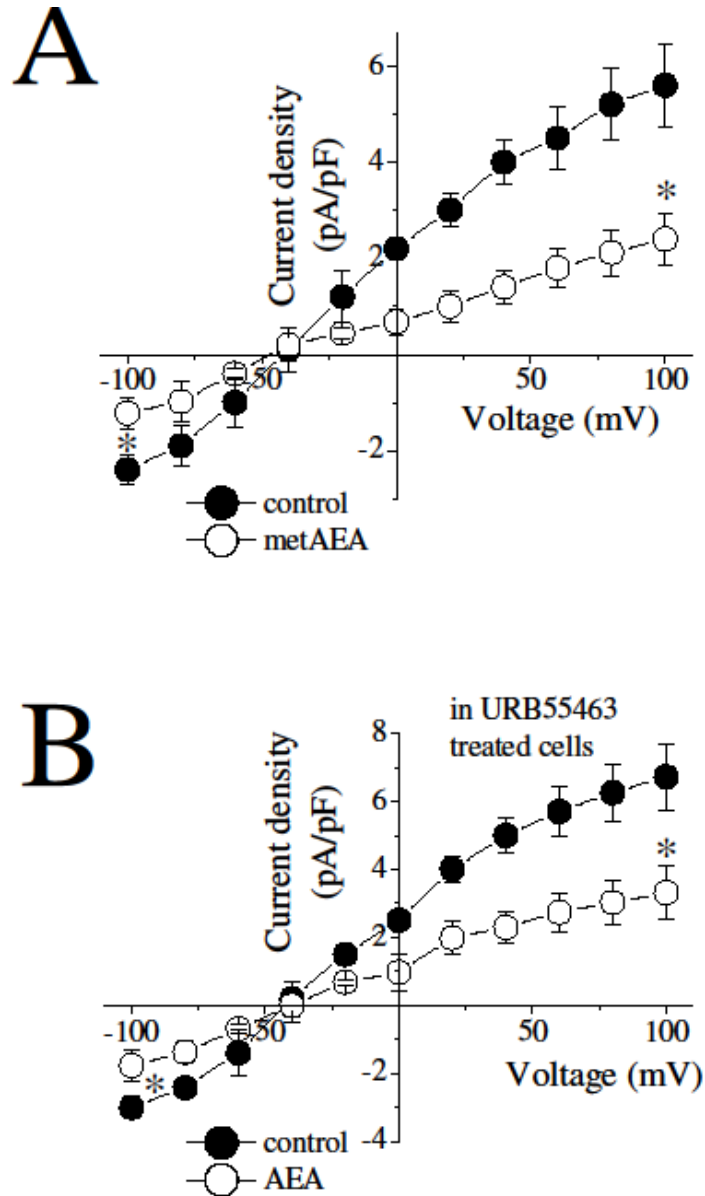


**Figure 3.29 Effects of metAEA and URB597 on  $I_{NCX1}$  in rat ventricular myocytes:** (A) Effect of 10  $\mu\text{M}$  metAEA on net  $I_{NCX1}$  (after subtraction of current in 10 mM  $\text{Ni}^{2+}$ ). Data points (mean  $\pm$  S.E.M.) are from 5 cells. (B) Effect of 10  $\mu\text{M}$  AEA on  $I_{NCX1}$  in cardiomyocytes incubated with 1  $\mu\text{M}$  URB597 for 1 hour. Data points (mean  $\pm$  S.E.M.) are from 6 cells. Paired  $t$ -test was used to compare the amplitude of current currents recorded at +100 mV and -100 mV.\* indicates statistically significant difference at the level of  $P < 0.05$ .



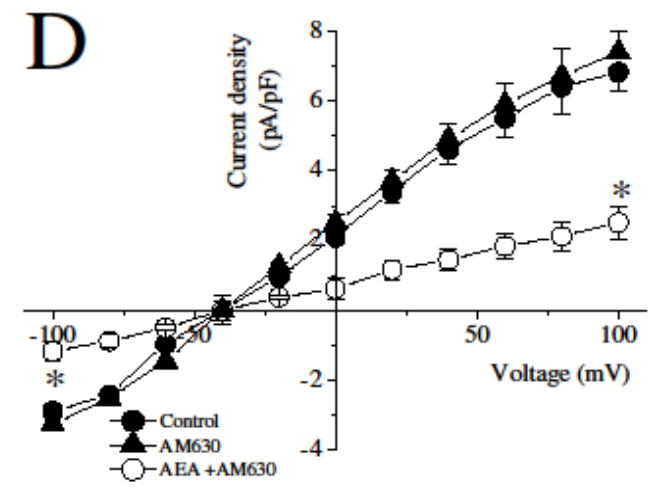
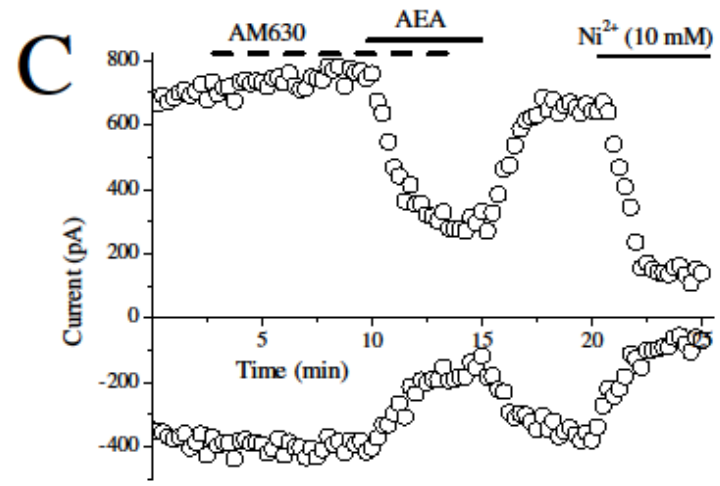
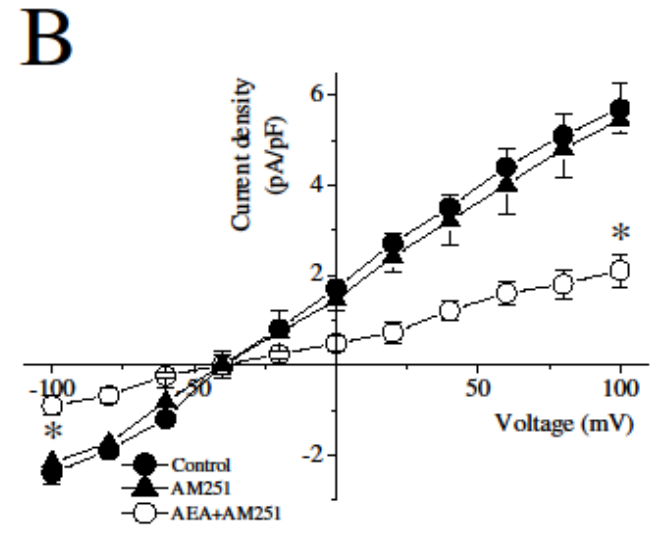
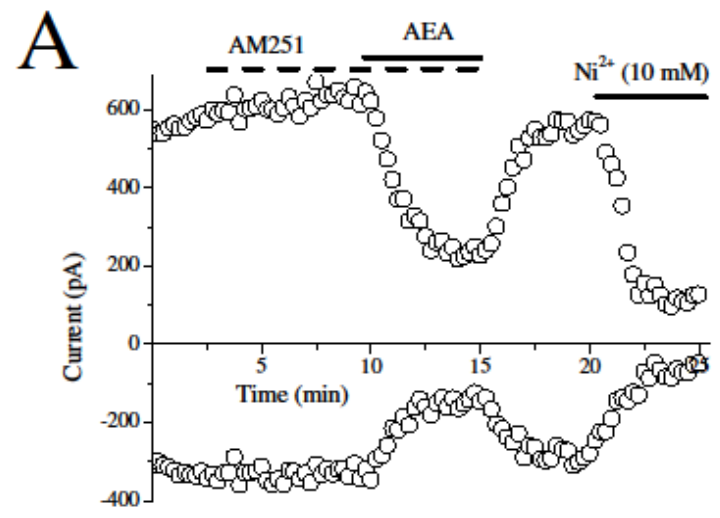


**Figure 3.30 Effects of cannabinoid receptor antagonists on AEA inhibition of  $I_{\text{NCX1}}$  recorded in ventricular cardiomyocytes:** (A) Time course of the effects of  $\text{CB}_1$  antagonist AM251 (1  $\mu\text{M}$ ) on AEA inhibition of  $I_{\text{NCX1}}$ . (B) Effect of 1  $\mu\text{M}$  AM251 on AEA inhibition of net NCX1 current at different membrane potentials (after subtraction of current in 10 mM  $\text{Ni}^{2+}$ ). (C) Time course of the effects of  $\text{CB}_2$  antagonist AM630 (1  $\mu\text{M}$ ) on AEA inhibition of  $I_{\text{NCX1}}$  (D) Time course of the effect of 1  $\mu\text{M}$  AM630 on AEA inhibition of  $I_{\text{NCX1}}$  at different membrane potentials (after subtraction of current in 10 mM  $\text{Ni}^{2+}$ ). Data points (mean  $\pm$  S.E.M.) are from 6-8 cells. Paired  $t$ -test was used to compare the amplitude of current currents recorded at +100 mV and -100 mV.\* indicates statistically significant difference at the level of  $P < 0.05$ .

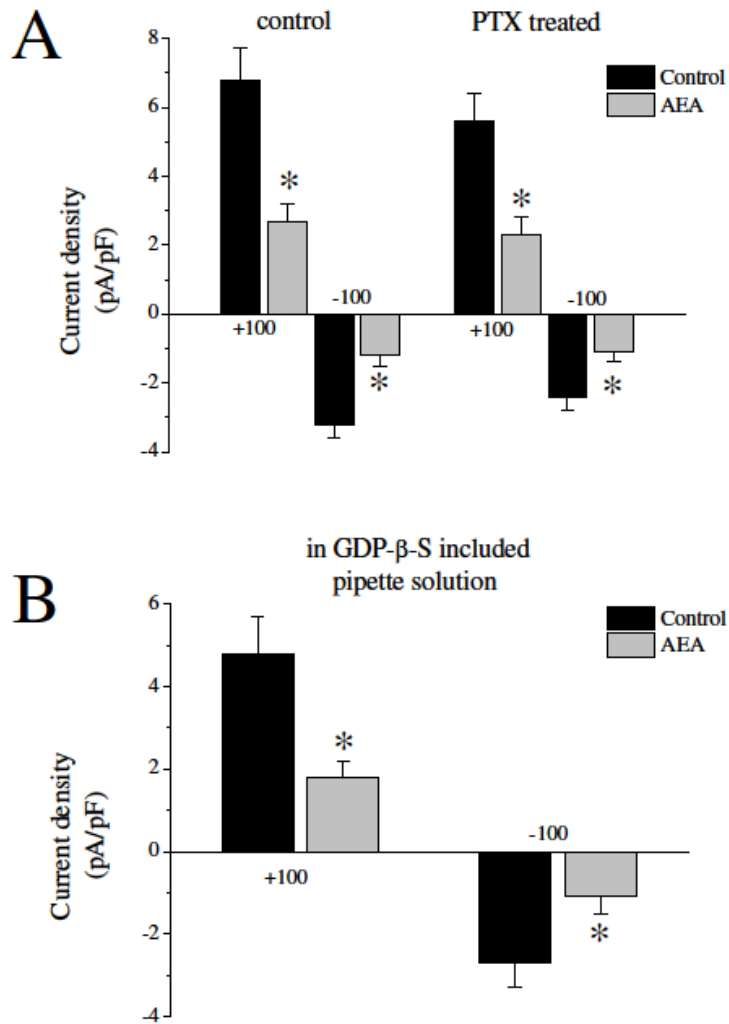


**Figure 3.31 Effects of PTX pretreatment and intracellular application of GDP-β-S on AEA inhibition of  $I_{NCX1}$  in ventricular cardiomyocytes:** (A) Effect of PTX pretreatment on AEA inhibition of  $I_{NCX1}$ . Amplitudes of inward and outward components of  $I_{NCX1}$  were measured at +100 mV and -100 mV, respectively. Data points (mean ± S.E.M.) are from 6 cells. (B) Effect of GDP-β-S inclusion in the patching pipette on AEA inhibition of  $I_{NCX1}$ . Amplitudes of inward and outward components of  $I_{NCX1}$  were measured at +100 mV and -100 mV, respectively. Data points (mean ± S.E.M.) are from 7 cells. Data are analyzed using paired  $t$ -test. \* indicates statistically different from the control values at the level of  $P < 0.05$ .

### **3.12 Anandamide has no effect on cell viability in ventricular myocytes**

Cell viability was assessed using the MTT assay. Cell death was induced by 1 % Triton X-100 (Abood, et al., 2001). The effect of AEA (10  $\mu$ M) on cell viability of ventricular cardiomyocytes was examined after 40 minutes treatment. As shown in figure 3.32A, no change in cell morphology was seen. On assaying the effect of AEA on cell viability, no significant change in cell viability was observed (Figure 3.32B).

### **3.13 Anandamide has no effect on membrane integrity in ventricular myocytes**

Membrane integrity was assessed using the lactate dehydrogenase (LDH) assay. LDH is a soluble enzyme located in the cytosol which is released into the surrounding culture medium upon cell damage or lysis, a process that commonly correlates with both apoptosis and necrosis (Bonfoco, et al., 1995). The levels of LDH released into the surrounding media can, therefore, serve as a reliable measurement for cytotoxicity. Cell death was induced by 1 % Triton X-100 (Abood, et al., 2001) and was set to be total LDH activity (100 %). Data from control and treated cells were normalized to total LDH release and calculated as percentage cytotoxicity. Results of the LDH assay are summarized in Figure 3.33. As depicted in the figure, no significance difference in LDH activity was observed between vehicle and AEA-treated cells.

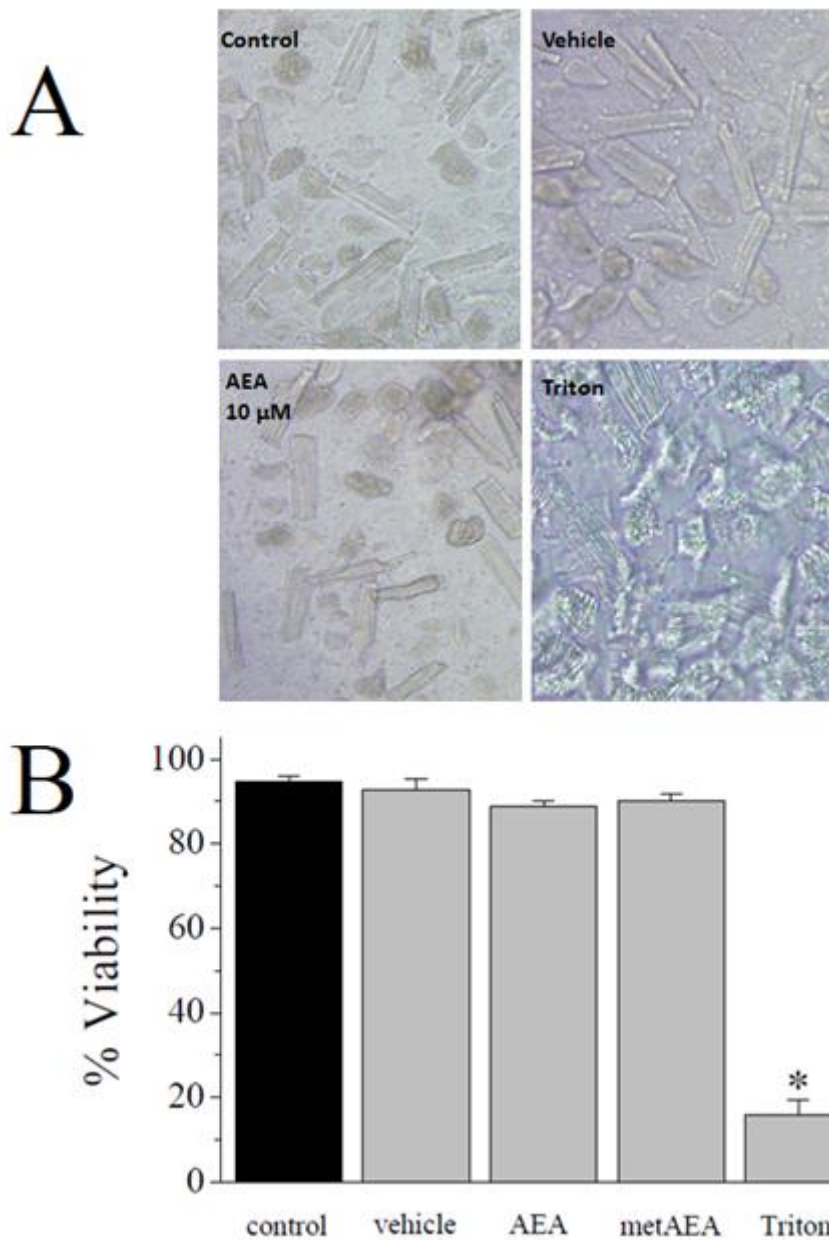


**Figure 3.32 Effect of AEA on morphological characteristics and cell viability of ventricular cardiomyocytes:** (A) Ventricular cardiomyocytes were treated with either vehicle or 10  $\mu$ M AEA for 40 minutes. (B) Effect of vehicle, AEA, or metAEA on cell viability as determined by MTT assay. Data are analyzed using ANOVA and are expressed as means  $\pm$  S.E.M. of five independent experiments. \* indicates statistically different from the control values at the level of  $P < 0.05$ .

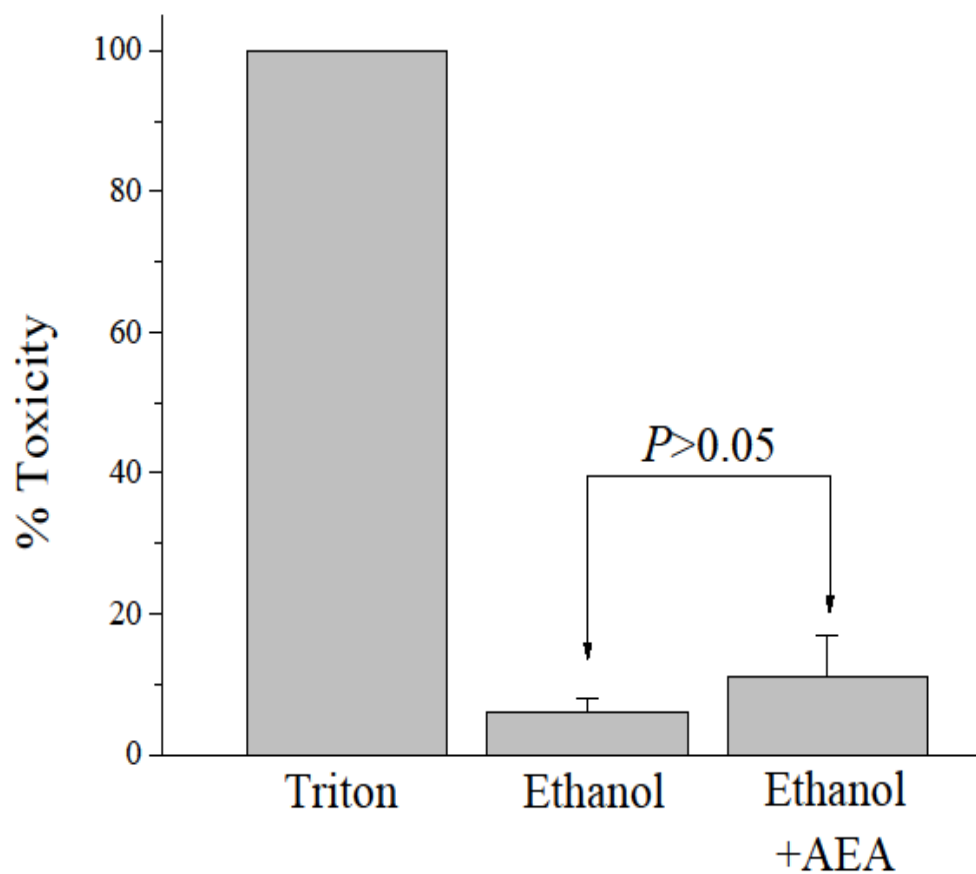


**Figure 3.33 Cytotoxicity of AEA as assessed by LDH assay:** Cells are treated with vehicle or vehicle + AEA (10  $\mu$ M) for 40 minutes. Values represent means  $\pm$  S.E.M., expressed as a percentage of the total LDH activity induced by 1 % Triton X-100. Data are analyzed using independent sample *t*-test and are expressed as means  $\pm$  S.E.M.

#### 4. DISCUSSION

The results of this study indicate for the first time that impaired  $\text{Ca}^{2+}$  signaling underlies the negative inotropic actions of AEA in rat ventricular myocytes, and that direct interaction of AEA with ion channel(s) shaping APs, rather than the activation of known cannabinoid receptors, mediate, at least in part, the effects of AEA on myocyte contractility. These findings also show that AEA-induced alterations in APs of myocytes are due to direct inhibition of voltage-dependent  $\text{Na}^+$  and  $\text{Ca}^{2+}$  channels. In addition, the results of this study indicate for the first time that under normal conditions, AEA can directly inhibit the activity of NCX1 in ventricular myocytes.

Systemic administration of AEA causes complex hemodynamic changes involving phases of both increased and decreased blood pressure as well as changes in heart rate and contractility (for reviews, Randall, et al., 2004; Batkai and Pacher, 2009). It has been suggested that these cardiovascular actions of endocannabinoids involve multiple sets of cellular and molecular mechanisms (Randall, et al., 2004; Malinowska, et al., 2012). In addition to receptor-mediated and direct actions of endocannabinoids on muscular structures, neuronal and endothelial cells have also been shown to be influenced by AEA and its metabolic products (Oz, 2006).

The use of video edge detection in individual myocytes has several advantages over *in vivo* experiments and traditional *in vitro* systems such as Langendorff-perfused heart preparation, since it allows measurement of contractility at single-cell level in a relatively isolated environment and excludes the influence of autonomic nerve endings, gap-junctions, neurotransmitter uptake system, and coronary perfusion status (Oz et al., 2006; Malinowska, et al., 2012).

For example, AEA has been reported to inhibit noradrenaline release from atrium subjected to electrical field stimulation (Goodfellow and Glass, 2009) and to enhance vagal activity (for a review, Malinowska, et al., 2012) in *in vivo* and in *in vitro* muscle preparations. Similarly, the modulation of the functional properties of dopamine (DA), serotonin, and glycine transporters and gap junctions (Venance, et al., 1995) by AEA and AA has been reported in neurons, cultured neurons, glia, and synaptosomal preparations (Chen, et al., 2003; Pearlman, et al., 2003; Steffens and Feuerstein, 2004; Oz, et al., 2010). However, it is unlikely that these reuptake mechanisms are involved in our studies on ventricular myocytes. Therefore, using acutely isolated ventricular myocytes, we have been able to bypass various potential target sites for AEA, and focus on characterizing its action on cardiomyocytes.

#### **4.1 Myocyte shortening and intracellular Ca<sup>2+</sup> measurements experiments**

In myocyte shortening experiments, bath application of AEA caused a significant reduction in the maximal shortening amplitudes without causing significant alteration in the time course of myocyte contraction. Negative-inotropic actions of AEA might be attributed to the impaired release of Ca<sup>2+</sup> from the SR. In fact, AEA and other various cannabinoid receptor agonists have been reported to modulate the ryanodine sensitive intracellular Ca<sup>2+</sup> stores and Ca<sup>2+</sup>-ATPase activity in various cell types (Epps, et al., 1982; Mombouli, et al., 1999; Zhuang, et al., 2005; Rao and Kaminski, 2006); for recent reviews, (Goodfellow and Glass, 2009; De and Di, V, 2009b). However, in our recent study (Al Kury, et al., 2014a), we have shown that binding of ryanodine to SR membranes was not altered by AEA. Similarly, in the presence of AEA (0.1 and 1 μM), passive Ca<sup>2+</sup>



release from SR membrane vesicles remained unchanged. In line with these findings, in the current study, the amplitude and kinetics of caffeine-induced  $\text{Ca}^{2+}$  release from intracellular  $\text{Ca}^{2+}$  stores were not altered by AEA. Collectively, these results indicate that ryanodine-sensitive intracellular  $\text{Ca}^{2+}$  stores are not involved in the negative inotropic effects of AEA.

On the other hand, the decrease in  $T_{\text{HALF}}$  decay and AMP of the  $\text{Ca}^{2+}$  transient by AEA during twitch responses may be due to increased uptake of cytosolic  $\text{Ca}^{2+}$  to SR. In fact, our recent study (Al Kury, et al., 2014a), indicates that AEA, (0.1 and 1  $\mu\text{M}$ ) caused a significant increase in  $\text{Ca}^{2+}$ -ATPase activity in cardiac SR membranes suggesting that increased  $\text{Ca}^{2+}$  uptake by SR might contribute to the observed changes in  $\text{Ca}^{2+}$  transients. Interestingly, NAEs with varying carbon chain lengths (Epps, et al., 1982) and fatty acid-based compounds, such as AA, have also been shown to modulate the activity of  $\text{Ca}^{2+}$ -ATPase in cardiac and skeletal SR membranes. Potentiation of the  $\text{Ca}^{2+}$ -ATPase activity without altering  $\text{Ca}^{2+}$  release and ryanodine-binding to the  $\text{Ca}^{2+}$  release channel may account for the decrease in  $T_{\text{HALF}}$  decay and amplitude of the  $\text{Ca}^{2+}$  transient caused by AEA (1  $\mu\text{M}$ ). Decreases in  $T_{\text{HALF}}$  decay and amplitudes of the  $\text{Ca}^{2+}$  transients by low concentration of AEA (1  $\mu\text{M}$ ) during twitches, but not caffeine-induced  $\text{Ca}^{2+}$  transients, may suggest that compared to caffeine-induced responses which involve the release of large amounts of  $\text{Ca}^{2+}$  from SR, fast  $\text{Ca}^{2+}$  transients during electrical stimulations are relatively more sensitive to alterations in  $\text{Ca}^{2+}$ -ATPase activity.

Activation of cannabinoid receptors alters the levels of second messengers such as cAMP, cGMP and protein kinase C (Demuth and Molleman, 2006; Goodfellow and Glass, 2009) which are known to be involved in tuning the  $\text{Ca}^{2+}$

sensitivity of the contractile proteins. However, sensitivity of contractile proteins to intracellular  $\text{Ca}^{2+}$  remains unchanged in the presence of AEA, suggesting that phosphorylation and de-phosphorylation of the contractile proteins do not play a significant role in the negative inotropic actions of AEA. An earlier study in isolated rat atria demonstrated that AEA caused negative inotropic effects by decreasing cAMP and increasing nitric oxide (NO) levels (Sterin-Borda, et al., 2005). However, AEA still decreased contractile performance in the presence of L-NAME, a NOS inhibitor, excluding a NO-mediated negative inotropic effect on human atrial muscle (Bonz, et al., 2003). Similarly, in another study in rat isolated heart, the negative inotropic actions of synthetic cannabinoid HU-210 were not correlated with the intracellular concentrations of cAMP and cGMP (Maslov, et al., 2004). Collectively, these findings, in agreement with the results of the current work, suggest that the effects of AEA on myocyte contractility are not related to changes in intracellular  $\text{Ca}^{2+}$  release machinery or sensitivity of myofilaments to  $\text{Ca}^{2+}$ . Furthermore, in the presence of AEA (1  $\mu\text{M}$ ), intracellular  $\text{Ca}^{2+}$  levels and resting cell length of ventricular myocytes remain unaltered suggesting that AEA does not significantly affect  $\text{Ca}^{2+}$  homeostasis under resting conditions.

In several earlier investigations, it has been reported that in the concentration range used in our study, AEA activates TRP channels such as TRPV1 receptors and causes increased levels of intracellular  $\text{Ca}^{2+}$  in various cell types (De and Di, V, 2010; Bradshaw, et al., 2013). However, TRP channels are not likely to be involved in the observed actions of AEA in cardiomyocytes for the following reasons. First, TRP channels are highly permeable to  $\text{Ca}^{2+}$  and their activation causes increased intracellular  $\text{Ca}^{2+}$  concentrations. However, application of AEA (0.1 to 1  $\mu\text{M}$ ) does not cause any alteration in intracellular

Ca<sup>2+</sup> levels. Secondly, any opening of TRP channels would be associated with decreased input resistance of the cell, and we have not observed a detectable change in the input resistance of myocytes during voltage clamp experiments. Thirdly, in earlier studies, TRPV1 channels, the main TRP channel subtype that is activated by AEA, are not expressed in adult cardiomyocytes (Dvorakova and Kummer, 2001).

AEA is metabolized by FAAH and degradation products such as AA, and AA derivatives have been shown to cause negative inotropic actions in cardiomyocytes (Hoffmann, et al., 1995; Mamas and Terrar, 2001; Liu, 2007). However, metAEA, the non-hydrolyzed analogue of AEA (Abadji, et al., 1994), also decreases the shortening of myocytes. In addition, AEA continues to inhibit myocyte shortening after pretreatment of these cells with URB597, a specific inhibitor of FAAH (Piomelli, et al., 2006). Furthermore, the negative inotropic effects of AEA are also insensitive to indomethacin application, indicating that the effect was unlikely to involve the stimulation of the release and metabolism of endogenous AA. These findings provide evidence that degradation products of AEA are not involved in the observed effects of this compound. Collectively, myocyte shortening experiments indicate that the negative inotropic effect of AEA results from a direct interaction of AEA with ventricular myocytes, rather than its action on nerve endings and neurotransmitter uptake systems that have been reported in various neuronal structures (Ishac, et al., 1996; Oz, et al., 2010).

#### **4.2 Involvement of cannabinoid receptors in the negative inotropic effect**

Involvement of cannabinoid receptors in the negative inotropic actions of cannabinoids has been reported in several earlier studies (Ford, et al., 2002; Bonz, et al., 2003; Sterin-Borda, et al., 2005; Su, et al., 2011). However, the results of

these investigations have not been conclusive (for reviews, Malinowska, et al., 2012; Randall, et al., 2004; Mendizabal and Adler-Graschinsky, 2007). Both cannabinoid receptor-dependent and -independent mechanisms have been suggested (Malinowska, et al., 2012). While Ford *et al.*, showed that in rat cardiac muscle, the inhibitory effect of AEA on contractility was not reversed in the presence of CB<sub>1</sub> (SR141716A) and CB<sub>2</sub> (SR144528) receptor antagonists (Ford, et al., 2002), Bonz *et al.* reported that AEA, metAEA, and HU-210 decreased contractile performance in human atrial muscle via activation of CB<sub>1</sub> receptors (Bonz, et al., 2003). In another study in rat atria, AEA was suggested to have negative and positive inotropic effects mediated by the activation of CB<sub>1</sub> and CB<sub>2</sub> receptors, respectively (Sterin-Borda, et al., 2005). Under our experimental conditions, two structurally different CB<sub>1</sub> antagonists AM251 (0.3 μM) and SR141716 (0.3 μM) are not able to reverse the inhibitory effect of AEA on cardiomyocyte shortening. Similarly, two different CB<sub>2</sub> antagonists AM630 (0.3 μM) and SR144528 (0.3 μM) fail to antagonize AEA-induced decrease of cardiomyocyte shortening. However, at higher concentrations such as 1 μM, these antagonists themselves show inhibitory actions on cardiomyocyte shortening (n=9-12). To our knowledge, the negative inotropic actions of relatively high concentrations of AM251 and AM630 have not been reported previously. However, negative inotropic actions of SR141716 and SR144528 on the contractile functions of isolated rat heart have also been attributed to their direct effects on the contractility of cardiomyocytes (Krylatov, et al., 2005). Earlier studies on cardiac muscle and other preparations also indicate that cannabinoid receptor antagonists with different chemical structures can have off-target binding

sites on various ion channels and enzymes (Ford, et al., 2002; Batkai, et al., 2004a; Patil, et al., 2011; Baur, et al., 2012).

### **4.3 Action potential measurements**

During excitation-contraction coupling, alterations in the amplitudes and kinetics of cardiac APs are closely associated with corresponding changes in the contractility of myocytes. In agreement with several earlier electrophysiological studies on rat ventricular myocytes, we have identified two distinctly different groups of cells displaying either epicardial (short duration) or endocardial (long duration) APs (for a review, Antzelevitch, et al., 1991). In the current study, low AEA concentration (0.1  $\mu\text{M}$ ) does not cause significant alterations in amplitudes and kinetics of APs in either epicardial or endocardial myocytes (Figure 3.11). However, there is a slight hyperpolarization in  $V_{\text{rest}}$  values, which reaches a statistically significant level at 1  $\mu\text{M}$  AEA. At this concentration, AEA decreases the durations of APs without significantly affecting the amplitudes and  $dV/dt_{\text{max}}$  of APs. At higher concentration (10  $\mu\text{M}$ ), AEA induces changes in AP duration accompanied with depolarization of the  $V_{\text{rest}}$  and decreases of  $dV/dt_{\text{max}}$  in the endocardial and epicardial ventricular myocytes, suggesting that AEA acts on multiple ion channels with different potencies. Importantly, no change in  $\text{APD}_{60}$  was observed in a subpopulation of cells, suggesting that some of the actions of AEA on these channels are cell specific.

Although, this is the first patch clamp study investigating the effect of AEA on the cardiac APs, an earlier report using intracellular recording methods in rat papillary muscle fibers reported that AEA, in the concentration range of 1-100 nM, potently inhibited AP durations in an AM251 sensitive manner (Li, et al., 2009), suggesting that activation of  $\text{CB}_1$  receptors mediated the negative inotropic

actions of AEA. However, under the experimental conditions of this study, changes on neither amplitudes nor kinetics of epicardial and endocardial APs are detectable until 1  $\mu$ M concentration of AEA. Importantly, the effects of AEA on the duration of both types of APs are not reversed in the presence of CB receptor antagonists tested; AM251 and AM630 (Figure 3.13A and B). In addition, AEA continues to affect AP duration after PTX pretreatment (Figure 3.14C). It is likely that differences in methods (patch clamp versus intracellular sharp electrode recording) and preparations (ventricular myocytes versus intact muscle fibers with nerve endings and gap junction connections) used in these studies may account for some of the discrepancies.

In summary, based on the insensitivity of the effect of AEA on myocyte shortening and action potential shortening to CB<sub>1</sub> and CB<sub>2</sub> antagonists, as well as to the pretreatments with PTX and NEM, it is likely that AEA decreases myocyte shortening and shortens AP duration in a manner that is independent of CB<sub>1</sub> and CB<sub>2</sub> cannabinoid receptors.

#### **4.4 Experiments with voltage-dependent Na<sup>+</sup> channels**

In cardiac muscle, extracellular Ca<sup>2+</sup> required to trigger Ca<sup>2+</sup> release from SR enters through L-type VGCCs which are opened during the AP. The results using voltage-clamp mode of whole-cell patch clamp technique indicate that in agreement with the changes in the amplitudes, duration and  $dV/dt_{\max}$  of APs, AEA caused significant inhibition of voltage-dependent Na<sup>+</sup> and L-type Ca<sup>2+</sup> channels in cardiomyocytes. Furthermore, the results indicate that the inhibition of these channels by AEA is not sensitive to CB<sub>1</sub> or CB<sub>2</sub> receptor antagonists. These findings are in agreement with the direct inhibition of Na<sup>+</sup> and L-type Ca<sup>2+</sup>

channels observed in earlier studies. For example, AEA, at similar or higher concentrations, has been shown to inhibit directly the functions of voltage-gated Na<sup>+</sup> channels in neuronal structures (Nicholson, et al., 2003; Kim, et al., 2005; Duan, et al., 2008), L-type Ca<sup>2+</sup> channels (Oz, et al., 2000; Oz, et al., 2004b) and various types of K<sup>+</sup> channels (Oz, et al., 2007a; for a review, Oz, 2006).

In cardiac muscles, VGSCs are almost exclusively represented by their TTX-resistant Nav1.5 isoform (Catterall, et al., 2005a). Therefore, the changes in the biophysical properties of  $I_{Na}$  by AEA, namely induction of the hyperpolarizing shift in the voltage-dependence of its SSI can be attributed to their effects on the gating of Nav1.5 channel. A hyperpolarizing shift of the SSI indicates that a higher proportion of VGSCs would be inactivated at resting membrane potential and therefore, substantially fewer channels would be available for activation, resulting in a decreased amplitude and rate of rise during the upstroke of the AP.

Our previous radioligand studies indicated that the specific binding of [<sup>3</sup>H]BTX-B to ventricular muscle membranes was inhibited by metAEA. In addition, the results with CB<sub>1</sub> and CB<sub>2</sub> antagonists suggested that the effect of metAEA on VGSCs was not mediated by the activation of CB<sub>1</sub> or CB<sub>2</sub> cannabinoid receptors (Al Kury, et al, 2014b, article *In Press*). Earlier investigations have shown that local anesthetics and class I antiarrhythmics also interact with the binding site for [<sup>3</sup>H]BTX-B on the cardiac sodium channel (Sheldon, et al., 1994). It is likely that AEA synthesized during cell stress can bind to Nav1.5 channel and modulate the actions of local anesthetics and class I antiarrhythmics. Although, this to our knowledge, is the first demonstration of the direct inhibitory action of AEA on a muscle type voltage-dependent Na<sup>+</sup> channel, in several earlier investigations, AEA, at similar or higher concentrations, has

been shown to inhibit directly the function of VGSCs in neuronal structures (Nicholson, et al., 2003; Kim, et al., 2005; Duan, et al., 2008). In agreement with our findings, both AEA (Theile and Cummins, 2011) and its metabolite AA (Bendahhou, et al., 1997) have been shown to increase the inactivation of Na<sup>+</sup> channels. Inhibition of VGSCs by AEA would slow the conduction of depolarization and modulate the automaticity in the ventricles.

In conclusion, the inhibitory effect of AEA, on VGSC, which is the major inward current during the upstroke (phase 0) of the AP is in agreement with the results of the current-clamp experiments (Al Kury, et al., 2014a) indicating that AEA decreases the amplitude and initial rate of rise of the AP in ventricular myocytes.

#### **4.5 Experiments with voltage-dependent Ca<sup>2+</sup> channels**

In addition to  $I_{Na}$ , AEA causes a significant inhibition of  $I_{L,Ca}$  in cardiomyocytes. This current contributes to the plateau of the cardiac AP (phase 2), therefore, its suppression causes both the decrease of plateau amplitude and the shortening of the AP duration. The results of this work, in agreement with an earlier study (Li, et al., 2009), show that AEA decreases the amplitude of the plateau and causes shortening of AP duration. Results also show that AEA affects the activation and inactivation gating of cardiac L-type VGCCs producing a significant reduction in  $I_{L,Ca}$  “window current” in the range of  $V_m$  between -40 mV and +10 mV, and inducing partial blockade of the ion-conducting pathway leading to decreased amplitude of  $I_{L,Ca}$ .

Diminished stationary Ca<sup>2+</sup> entry as a consequence of smaller “window current” may prevent Ca<sup>2+</sup> overload and cause reduction of necrosis, whereas, inhibition of  $I_{L,Ca}$  may largely determine the decrease in the amplitude of AP



plateau and AP shortening observed in the presence of AEA. Collectively, the results of the electrophysiological experiments suggest that during excitation-contraction coupling, shortening of AP due to the inhibition of L-type  $\text{Ca}^{2+}$  channels decreases  $\text{Ca}^{2+}$ -induced  $\text{Ca}^{2+}$  release from SR and causes negative inotropic effect of AEA reported in earlier studies. In line with this hypothesis, although caffeine-induced  $\text{Ca}^{2+}$  transients and myofilament sensitivity to  $\text{Ca}^{2+}$  remain unchanged, electrically-induced  $\text{Ca}^{2+}$  transients are significantly depressed by AEA, further suggesting that  $\text{Ca}^{2+}$ -induced  $\text{Ca}^{2+}$  release is impaired in the presence of AEA. Overall, AEA-mediated suppression of voltage-activated  $I_{L,\text{Ca}}$  would provide a mechanism for the negative inotropic effects observed in earlier studies.

The mechanism of the inhibitory effect of AEA does not seem to involve the  $\text{Ca}^{2+}$ -induced inactivation process, since the amplitudes of  $\text{Ba}^{2+}$  currents through L-type VGCCs were effectively inhibited by AEA. In addition, AEA was equally effective upon intracellular or extracellular application suggesting that there is no sidedness for AEA actions on L-type VGCCs. Considering the highly lipophilic nature of AEA; it is not surprising that AEA can access its binding site from both extra and intracellular sites effectively.

The results of our radioligand binding studies also indicated that AEA directly interacts with and inhibits the function of L-type  $\text{Ca}^{2+}$  channels in ventricular muscle membranes (Al Kury, et al., 2014b, article *In Press*). Although, to our knowledge, this is the first demonstration of the direct effects of AEA on the L-type VGCC in cardiac muscle, similar results demonstrating the effects AEA on skeletal muscle L-type VGCCs have also been described in biochemical studies (Oz, et al., 2000; Oz, et al., 2004a). In rabbit skeletal muscle, it has been

demonstrated that AEA inhibits the specific binding of [<sup>3</sup>H]Isradipine to skeletal T-tubule membranes, and directly inhibits the function of skeletal muscle L-type Ca<sup>2+</sup> channels (Oz, et al., 2000; Oz, et al., 2004a) in a manner that is independent of known cannabinoid receptors. In fact, earlier studies searching for endogenous modulators of L-type Ca<sup>2+</sup> channels have also identified AEA as a ligand for L-type Ca<sup>2+</sup> (Johnson, et al., 1993). Subsequently, investigations indicated that the effects of AEA are not limited to L-type VGCCs in muscles. Different types of Ca<sup>2+</sup> currents in neurons and other excitable cells are also inhibited directly by endocannabinoids such as AEA [for a recent review, (Lozovaya, et al., 2009)].

In a recent study, it was found that the synthetic cannabinoid A-955840 inhibits the function of L-type Ca<sup>2+</sup> channels in rabbit heart in a manner insensitive to CB<sub>1</sub> and CB<sub>2</sub> antagonists (Su, et al., 2011). In another recent study, AEA was reported to inhibit L-type Ca<sup>2+</sup> channels by the activation of CB<sub>1</sub> receptors (Li, et al., 2009). In this study, AEA in the concentration range of 10 nM to 1 μM potently inhibited the function of Ca<sup>2+</sup> channels and the effect of AEA was reversed by CB<sub>1</sub> receptor antagonists. In our experiments, AEA is not effective at concentrations lower than 0.1 μM. In addition, in our study, the inhibitory effect of AEA is not reversed by the antagonists of CB<sub>1</sub> and CB<sub>2</sub> receptors. The differences between these two studies could be due to different strains of rats used (Sprague-Dawley in their study versus Wistar rats in the present study). Our findings suggest that neither CB<sub>1</sub> nor CB<sub>2</sub> receptors are involved in AEA inhibition of L-type Ca<sup>2+</sup> channels in rat cardiomyocytes. Although PTX-sensitive signal transduction is well documented for cannabinoid agonists, cannabinoid coupling to PTX-insensitive G<sub>q</sub> has been reported in several studies (McIntosh, et al., 2007; Straiker, et al., 2002; Ishii and Chun, 2002).

Therefore, the effect of AEA through a PTX-insensitive pathway cannot be excluded. However, the results of our experiments with NEM, which inactivate G-proteins indicate that activation of G-proteins is not required for AEA actions in cardiomyocytes.

Degradation products of AEA, such as AA and fatty acids-based compounds, have been shown to inhibit the function of cardiac L-type  $\text{Ca}^{2+}$  channels [(Li, et al., 2009), for a review; (Oz, 2006)]. However, metAEA also inhibited L-type  $\text{Ca}^{2+}$  currents to the same extent with AEA. In addition, AEA continued to inhibit L-type  $\text{Ca}^{2+}$  currents after pretreatment of these cells with the specific inhibitor of FAAH, URB597 (Piomelli, et al., 2006).

#### **4.6 Experiments with cardiac $\text{Na}^+/\text{Ca}^{2+}$ exchanger**

The results of this study indicate for the first time that under normal conditions, AEA has a direct inhibitory effect on both the forward and reverse mode of NCX1 in ventricular myocytes. Under physiological conditions, inhibition of NCX1 operating in reverse mode is expected to decrease  $\text{Ca}^{2+}$  entrance during cardiac action potential, and induce negative inotropic actions. Therefore, it is likely that the inhibition of NCX function in the reverse mode can cause the suppression of AP plateau and the decrease of the AP duration.

The findings of this study suggest that neither  $\text{CB}_1$  nor  $\text{CB}_2$  receptors are involved in AEA inhibition of NCX in rat cardiomyocytes. Firstly, AEA inhibition is altered by neither  $\text{CB}_1$  nor  $\text{CB}_2$  receptor antagonists. Secondly, treatment with PTX or inclusion of GDP- $\beta$ -S in pipette solution does not affect the activity of NCX1 further suggesting that G-proteins are not involved in AEA actions. Thirdly, in our recent study (Al Kury et al., 2014c) we have shown that AEA significantly inhibited NCX1-mediated currents in HEK-293 cells which do

not contain CB<sub>1</sub> or CB<sub>2</sub> receptors (Oz, et al., 2010). Collectively these results suggest that AEA interacts directly with NCX1 in ventricular myocytes in a manner that is independent of CB<sub>1</sub> and CB<sub>2</sub> receptors.

In rat odontoblasts, cannabinoid-induced Ca<sup>2+</sup> influx through TRPV1 was recently shown to be functionally coupled to NCX-mediated Ca<sup>2+</sup> extrusion (Tsumura, et al., 2012). However, it is unlikely that TRPV1 activation is involved in the effects of AEA observed in this study since adult cardiomyocytes do not express TRPV1 channels (Dvorakova and Kummer, 2001). In another recent study, it was reported that under ischemic conditions, AEA inhibits NCX1 by activating CB<sub>2</sub> receptors via PTX-sensitive G<sub>i/o</sub> proteins (Li, et al., 2013). However, a recent study in endothelial cells demonstrated that AEA, in the concentration range used in our study, significantly inhibits the activity of NCX1 in a manner that is independent of G-protein receptors (Bondarenko, et al., 2013).

Metabolic degradation products of AEA, such as AA and related fatty acids have also been shown to regulate NCX1 function (Xiao, et al., 2004). In the current study, the metabolically stable analogue of AEA, metAEA (Abadji et al., 1994), also inhibits *I*<sub>NCX1</sub>. Furthermore, in the presence of URB597, *I*<sub>NCX1</sub> is suppressed to the same extent by AEA, suggesting that the degradation products of AEA are not involved in the inhibition of NCX1 in cardiac myocytes. In our recent study in HEK-293 cells (Al Kury et al., 2014c), cell surface expression of NCX1, as determined from the intensity of YFP-NCX1 expression levels, was not altered after AEA application suggesting that AEA is not likely to alter NCX1 trafficking to the cell surface.

In addition to the NCX, SR Ca<sup>2+</sup>-ATPase (SERCA2a) also plays an important role in cardiac contraction and rhythmicity (Inesi, et al., 2008; Eisner, et

al., 2013). Under the experimental conditions of this work, we cannot rule out the contribution of SERCA2a to the observed actions of AEA on the function of NCX in cardiomyocytes. In fact, our recent study (Al Kury, et al., 2014a) indicates that AEA causes a significant increase in SERCA2a activity in cardiac SR membranes. AEA continued to inhibit the NCX1 currents in HEK-293 cells which, although express SERCA2 endogenously (Vafiadaki, et al., 2009), is devoid of excitability. Furthermore, bath application of AEA does not alter intracellular  $Ca^{2+}$  levels in these cell lines (Oz, et al., 2010).

#### **4.7 Mechanism of action of AEA**

Anandamide belongs to long-chain NAEs which are produced abundantly in response to tissue necrosis and cellular stress (Hansen, et al., 2000; Berger, et al., 2004). In fact, accumulation of NAEs was first observed in experimental myocardial infarction induced by ligation of coronary arteries in canine heart [(Epps, et al., 1979; Epps, et al., 1982), for a review, (Schmid and Berdyshev, 2002)]. Although the content of NAEs in various mammalian tissues ranges from about 0.1 to 20 nmol/g (Hansen, et al., 2000), it was demonstrated that NAEs content increases up to 500 nmol/g (approximately 500  $\mu$ M) in infarcted areas of canine heart during ischemia (Epps, et al., 1979). AEA constitutes minor (1-3 %) portion of total NAE levels (Schmid and Berdyshev, 2002), however, the partition coefficient of AEA is in the same order with that of AA to biological membranes ( $2-9 \times 10^4$ ) (Meves, 1994). Thus, the membrane concentration of AEA would reach much higher levels than those estimated for intracellular concentrations.

It was previously reported that other NAE species, such as N-stearoylethanolamine (SEA) and N-oleoylethanolamine (OEA), are also produced during ischemia and that they have significant effects on the amplitudes and

kinetics of APs and accompanying ionic currents. The effects of SEA and OEA could account for the negative inotropic actions of these compounds on ventricular myocytes (Voitychuk, et al., 2012). Similar to AEA, other NAEs, metabolic degradation products of NAEs, and structurally related compounds have been shown to modulate the function of voltage-gated  $\text{Ca}^{2+}$  (Voitychuk, et al., 2012; Oz, et al., 2000; Oz, et al., 2005; Alptekin, et al., 2010) and  $\text{Na}^+$  (Nicholson, et al., 2003; Kim, et al., 2005; Duan, et al., 2008) channels. Furthermore, AEA has been shown to block T-type  $\text{Ca}^{2+}$  channels (Cav3.1 and Cav 3.2) (Chemin, et al., 2007) and cardiac Kv1.5 (Barana, et al., 2010) and Kv4.3 (Amoros, et al., 2010) channels in a receptor-independent manner. These effects may contribute to the overall actions of AEA on action potential and cardiac myocyte function.

Therefore, in the concentrations used in this study, AEA is likely to have important implications regarding the contractile and electrical responses of ventricular myocytes to ischemia and cellular stress (Hansen, et al., 2000; Berger, et al., 2004; Schmid and Berdyshev, 2002). In fact, shortening of AP duration by AEA can be beneficial or harmful, depending on the underlying pathology. Thus, during acute ischemia, in which the duration of the cardiac AP is already shortened, a further decrease should be proarrhythmic (Den Ruijter, et al., 2007). However, shortening of AP duration should be beneficial in preventing those arrhythmias caused by triggered activities observed in conditions such as heart failure (Den Ruijter, et al., 2007; Den Ruijter and Coronel, 2009).

Binding site(s) of AEA and other endocannabinoids on their target proteins is currently unknown. Apart from specific binding sites on the ion channels and receptors (Figure 4.1), AEA can accumulate and reach substantially high concentrations in biological membranes, thereby causing significant alterations in

physico-chemical properties of these membranes. As mentioned earlier, the membrane concentration of AEA can reach much higher levels than those estimated for intracellular or extracellular concentrations. It is likely that due to its high lipophilicity, AEA can alter the physico-chemical characteristics of the lipid environment, or indeed, bind to hydrophobic sites on the ion channels and regulate the functional properties of these proteins [(Mavromoustakos, et al., 2001); for a review, (Oz, 2006)]. Concentrations of AEA modulating the activities of ion channels and exchangers studied in our investigation appear to be within the range of 0.1 to 10  $\mu$ M. It is not known whether these concentrations can be achieved under physiological conditions. The concentrations of AEA in the rat brain have been reported to range from 2.5 to 29 pmol/g (Schmid, et al., 2002). The concentration of AEA in rat and human plasma is in the nM range of 0.7–8 nM and 4-20 nM, respectively (Giuffrida, et al., 2000; Bojesen and Bojesen, 1994). However, as mentioned earlier, due to high partition coefficients, AEA can effectively accumulate in cell membranes and reach significantly higher concentrations. Furthermore, during ischemia and cell stress, tissue concentrations of AEA can increase further (Epps, et al., 1979; Schmid and Berdyshev, 2002)

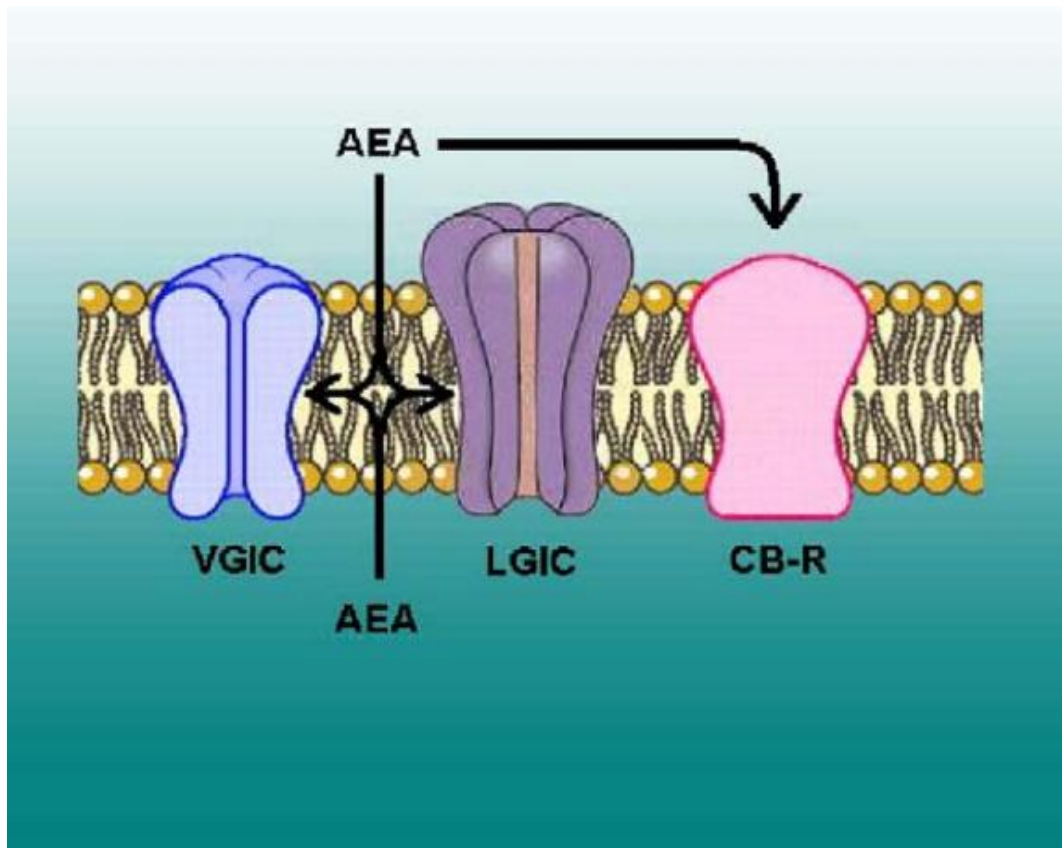


**Figure 4.1 Proposed model for the actions of AEA on cellular excitability:** According to the model, the effects of AEA are mediated by G-protein coupled cannabinoid receptors, ligand-gated ion channels and voltage-gated ion channels. CB-R, cannabinoid receptor; LGIC, ligand-gated ion channel; VGIC, voltage-gated ion channel. Adapted from Oz, 2006.



It has been more than a century since the Overton-Meyer rule stated that membrane permeability of any molecule depends on its hydrophobicity. Although the Overton-Meyer rule predicts the accessibility of hydrophobic molecules such as various lipids, fatty acids and endocannabinoids to their membrane-delimited actions and hence somewhat the potency of these molecules on their target proteins, it does not elucidate the mechanism(s) of action of these molecules. One school of thought focuses on the influence of lateral pressure profiles on integral membrane proteins to describe how proteins sense the effects of hydrophobic molecules in membrane bilayers (van den Brink-van der Laan, et al., 2004), and hydrophobic mismatch between the lengths of the hydrophobic membrane-spanning domains and the bilayer thickness (Lundbaek, 2006). Changes in the lateral pressure profile with altered lipid composition (Cantor, 2001; Van den Brink-van der Laan, et al., 2004) or by partitioning of hydrophobic molecules (Cantor, 2001) have been shown to modulate the functions of ion channels and other integral membrane proteins. It has been hypothesized that if the hydrophobic length of the transmembrane domains of the ion channels does not match the hydrophobic thickness of the membrane phospholipid bilayer, such a mismatch would create stress between the channel and the membrane (Andersen, et al., 1999). As a result, this tension requires that the thickness of the cell membrane be decreased at its contact with the interface of the transmembrane regions of the ion channel so that their hydrophobic regions match, and thus, affect the conformational state and conductance of the ion channel (Jensen and Mouritsen, 2004).

In an earlier study, it was suggested that alterations in the lipid order of synaptic membranes caused by various cannabinoids might be a necessary

property for their pharmacological activities (Bloom, et al., 1997). However, the influences of lateral membrane pressure and membrane thickness are not observed universally, and other membrane properties can also play roles in lipid-protein interactions (Lee, et al., 2005). Another school of thought on the question of how lipophilic molecules such as cannabinoids affect the function of ion channels focuses on the protein-lipid interface. Recent investigations suggest that lipids such as fatty acids displace or interact with lipids and/or hydrophobic amino acids located at the specific lipid-protein interfaces of the ion channels, rather than altering bulk physico-chemical properties of cell membranes (McIntosh and Simon, 2006). Thus, although hydrophobicity is an important factor determining the bioavailability of the drug at its action site, highly hydrophobic molecules such as cannabinoids may not need to change bulk membrane characteristics to alter the function of ion channels (Barrantes, 2004; Garcia, 2004).

An extensive volume of work in the literature indicates that the bilayer is not simply an inert thin layer of lipid whose primary purpose is to provide a barrier to ions (McIntosh and Simon, 2006). Following their insertion into the fluid membrane bilayer, ion channels assume an energetically minimal conformational state leading to a stable structure. Importantly, the binding of ligands, such as AEA, leads to conformational changes associated with the alterations in the hydrophobic domains of the ion channels (Lee and MacKinnon, 2004; Lee, et al., 2005; Garcia, 2004). The energetic requirements of these conformational changes depend on the lipid environment in which they are immersed (Spivak, et al., 2007). Although the exact mechanisms of action of AEA on ion channels and receptors are currently unknown, such interaction with

proteins is likely to mediate some of the pharmacological actions of AEA in the cardiovascular and nervous systems.

## 5. CONCLUSION

In conclusion, the results generated from the present study, indicate for the first time that AEA inhibits myocyte contractility by acting on multiple target proteins. We have shown that AEA decreases the duration of APs and modulates the activity of Na<sup>+</sup> and L-type Ca<sup>2+</sup> channels and inhibits the function of NCX1 in a CB<sub>1</sub> and CB<sub>2</sub> receptor-independent manner. Considering massive release of various NAEs, including AEA, during ischemia and hypoxic conditions, further understanding of their action mechanisms and target proteins is essential in the development of better treatment modalities for these pathological conditions.

## 6. LIMITATIONS AND FUTURE WORK

- The main work limitations in this study are:

1. Physiological temperature: All patch clamp experiments were conducted at room temperature (22-23 °C) in order to ensure longer survival time of patched cells and a better time resolution of the membrane currents. Giga-ohm seals in patch-clamp experiments are known to be unstable at raised temperatures. For this reason, we chose to work at room temperature. A similar approach was taken in earlier studies in various cell types (Voitychuk et al., 2012; Li et al., 2013; Bondarenko et al., 2013).

2. The influence of solvent: AEA was dissolved in ethanol. As with earlier studies, ethanol alone caused a decrease in the contractility of ventricular myocytes and the amplitudes of  $I_{Na}$  and  $I_{L,Ca}$ . Therefore, for each set of experiments, it was necessary to test the effect of the solvent separately.

- In order to extend our findings in this thesis, the following experiments can be done in the future:

1. Our study showed that AEA can decrease the AP amplitude and shorten AP duration in rat ventricular myocytes which might be one of the mechanisms for anti-arrhythmic effect of AEA. However, the mechanism of action of AEA is not completely understood and the effect of AEA on the cardiac conduction system remains unknown. Therefore, investigating the effect of AEA on sinoatrial and atrioventricular nodes would be very informative.

2. In addition to the endocannabinoid AEA, levels of 2-AG have been shown to be increased in a range of cardiovascular disorders. Therefore, understanding the

electrophysiological and pharmacological effects of this endogenous cannabinoid in the heart may aid in further understanding of any potential role of 2-AG in cardiovascular pathologies.

3. Cardiac  $K^+$  channels play an important role in determining the resting membrane potential and the shape and duration of the cardiac AP. Although the effect of AEA on outward  $K^+$  currents ( $I_{to}$ ) and ATP-sensitive  $K^+$  currents ( $I_{ATP}$ ) has been shown previously, the contribution of other  $K^+$  conductances such as the rapid ( $I_{Kr}$ ) and slow ( $I_{Ks}$ ) components of the delayed rectifier and the inward rectifier ( $I_{K1}$ ) remains unknown. Therefore, studying the effect AEA on these conductances would help in better understanding the mechanism of action of AEA on cardiac cells.

4. Since the kinetics and voltage dependence of channel gating are modified by auxiliary subunits of voltage gated  $Na^+$  and  $Ca^{2+}$  channels, studying the direct effect of AEA on different subunits of voltage-gated ion channels, using expression systems such as Chinese Hamster Ovary (CHO) or Human Embryonic Kidney (HEK) 293 cells, would give a more detailed picture on the mechanism of the direct effect of AEA on these channels.

## 7. BIBLIOGRAPHY

Abadji V, Lin S, Taha G, Griffin G, Stevenson LA, Pertwee RG and Makriyannis A (1994) (R)-methanandamide: a chiral novel anandamide possessing higher potency and metabolic stability. *J Med Chem* 37:1889-1893.

Abood ME, Rizvi G, Sallapudi N and McAllister SD (2001) Activation of the CB1 cannabinoid receptor protects cultured mouse spinal neurons against excitotoxicity. *Neurosci Lett* 309:197-201.

Ahn K, McKinney MK and Cravatt BF (2008) Enzymatic pathways that regulate endocannabinoid signaling in the nervous system. *Chem Rev* 108:1687-1707.

Al Kury LT, Voitychuk OI, Ali RM, Galadari S, Yang KH, Howarth FC, Shuba YM and Oz M (2014a) Effects of endogenous cannabinoid anandamide on excitation-contraction coupling in rat ventricular myocytes. *Cell Calcium* 55: 104-118.

Al Kury LT, Voitychuk OI, Yang KH, Thayyullathil F, Doroshenko, P, Ali RM, Shubha YM, Galadari S, Howarth FC and Oz M (2014b) Effects of endogenous cannabinoid anandamide on voltage-dependent sodium and calcium channels in rat ventricular myocytes. *Br J Pharmacol*, article *In Press*.

Al Kury LT, Yang KH, Thayyullathil F, Mohanraj R, Ali RM, Shuba YM, Howarth FC, Galadari S and Oz M (2014c) Effects of endogenous cannabinoid anandamide on cardiac Na<sup>+</sup>/Ca<sup>2+</sup> exchanger. *Cell Calcium*, 55:231-237.

Alexander SP and Kendall DA (2007) The complications of promiscuity: endocannabinoid action and metabolism. *Br J Pharmacol* 152:602-623.

Alger BE and Kim J (2011) Supply and demand for endocannabinoids. *Trends Neurosci* 34:304-315.

Alptekin A, Galadari S, Shuba Y, Petroianu G and Oz M (2010) The effects of anandamide transport inhibitor AM404 on voltage-dependent calcium channels. *Eur J Pharmacol* 634:10-15.

Amin AS, Asghari-Roodsari A and Tan HL (2010) Cardiac sodium channelopathies. *Pflugers Arch* 460:223-237.

Amoros I, Barana A, Caballero R, Gomez R, Osuna L, Lillo MP, Tamargo J and Delpon E (2010) Endocannabinoids and cannabinoid analogues block human cardiac Kv4.3 channels in a receptor-independent manner. *J Mol Cell Cardiol* 48:201-210.

Andersen OS, Nielsen C, Maer AM, Lundbaek JA, Goulian M and Koeppe RE (1999) Ion channels as tools to monitor lipid bilayer-membrane protein interactions: gramicidin channels as molecular force transducers. *Methods Enzymol* 294:208-24.:208-224.

Antzelevitch C, Sicouri S, Litovsky SH, Lukas A, Krishnan SC, Di Diego JM, Gintant GA and Liu DW (1991) Heterogeneity within the ventricular wall. Electrophysiology and pharmacology of epicardial, endocardial, and M cells. *Circ Res* 69:1427-1449.

Bahring R and Covarrubias M (2011) Mechanisms of closed-state inactivation in voltage-gated ion channels. *J Physiol* 589:461-479.

Barana A, Amoros I, Caballero R, Gomez R, Osuna L, Lillo MP, Blazquez C, Guzman M, Delpon E and Tamargo J (2010) Endocannabinoids and cannabinoid analogues block cardiac hKv1.5 channels in a cannabinoid receptor-independent manner. *Cardiovasc Res* 85:56-67.

Bari M, Battista N, Fezza F, Gasperi V and Maccarrone M (2006) New insights into endocannabinoid degradation and its therapeutic potential. *Mini Rev Med Chem* 6:257-268.

Barrantes FJ (2004) Structural basis for lipid modulation of nicotinic acetylcholine receptor function. *Brain Res Brain Res Rev* 47:71-95.

Bassani JW, Yuan W and Bers DM (1995) Fractional SR Ca release is regulated by trigger Ca and SR Ca content in cardiac myocytes. *Am J Physiol* 268:C1313-C1319.

Batkai S and Pacher P (2009) Endocannabinoids and cardiac contractile function: pathophysiological implications. *Pharmacol Res* 60:99-106.

Batkai S, Pacher P, Jarai Z, Wagner JA and Kunos G (2004a) Cannabinoid antagonist SR-141716 inhibits endotoxic hypotension by a cardiac mechanism not involving CB1 or CB2 receptors. *Am J Physiol Heart Circ Physiol* 287:H595-H600.

Batkai S, Pacher P, Osei-Hyiaman D, Radaeva S, Liu J, Harvey-White J, Offertaler L, Mackie K, Rudd MA, Bukoski RD and Kunos G (2004b) Endocannabinoids acting at cannabinoid-1 receptors regulate cardiovascular function in hypertension. *Circulation* 110:1996-2002.

Batkai S, Rajesh M, Mukhopadhyay P, Hasko G, Liaudet L, Cravatt BF, Csiszar A, Ungvari Z and Pacher P (2007) Decreased age-related cardiac dysfunction, myocardial nitrative stress, inflammatory gene expression, and apoptosis in mice lacking fatty acid amide hydrolase. *Am J Physiol Heart Circ Physiol* 293:H909-H918.

Baur R, Gertsch J and Sigel E (2012) The cannabinoid CB1 receptor antagonists rimonabant (SR141716) and AM251 directly potentiate GABA(A) receptors. *Br J Pharmacol* 165:2479-2484.

Bebarova M, Matejovic P, Pasek M, Ohlidalova D, Jansova D, Simurdova M and Simurda J (2010) Effect of ethanol on action potential and ionic membrane currents in rat ventricular myocytes. *Acta Physiol (Oxf)* 200:301-314.



- Bendahhou S, Cummins TR and Agnew WS (1997) Mechanism of modulation of the voltage-gated skeletal and cardiac muscle sodium channels by fatty acids. *Am J Physiol* 272:C592-C600.
- Benowitz NL and Jones RT (1975) Cardiovascular effects of prolonged delta-9-tetrahydrocannabinol ingestion. *Clin Pharmacol Ther* 18:287-297.
- Berger C, Schmid PC, Schabitz WR, Wolf M, Schwab S and Schmid HH (2004) Massive accumulation of N-acyl ethanolamines after stroke. Cell signalling in acute cerebral ischemia? *J Neurochem* 88:1159-1167.
- Bers DM (2002) Cardiac excitation-contraction coupling. *Nature* 415:198-205.
- Bers DM, Bridge JH and Spitzer KW (1989) Intracellular Ca<sup>2+</sup> transients during rapid cooling contractures in guinea-pig ventricular myocytes. *J Physiol* 417:537-553.
- Bers DM and Weber CR (2002) Na/Ca exchange function in intact ventricular myocytes. *Ann N Y Acad Sci* 976:500-512.
- Bezanilla F (2005) Voltage-gated ion channels. *IEEE Trans Nanobioscience* 4:34-48.
- Bilfinger TV, Salzet M, Fimiani C, Deutsch DG, Tramu G and Stefano GB (1998) Pharmacological evidence for anandamide amidase in human cardiac and vascular tissues. *Int J Cardiol* 64 Suppl 1:S15-22.
- Bisogno T (2008) Endogenous cannabinoids: structure and metabolism. *J Neuroendocrinol* 20 Suppl 1:1-9. doi: 10.1111/j.1365-2826.2008.01676.x:1-9.
- Bisogno T, Melck D, Bobrov MY, Gretskaya NM, Bezuglov VV, De PL and Di M, V (2000) N-acyl-dopamines: novel synthetic CB(1) cannabinoid-receptor ligands and inhibitors of anandamide inactivation with cannabimimetic activity in vitro and in vivo. *Biochem J* 351 Pt 3:817-824.
- Blaustein MP and Lederer WJ (1999) Sodium/calcium exchange: its physiological implications. *Physiol Rev* 79:763-854.
- Bloom AS, Edgemond WS and Moldvan JC (1997) Nonclassical and endogenous cannabinoids: effects on the ordering of brain membranes. *Neurochem Res* 22:563-568.
- Bodi I, Mikala G, Koch SE, Akhter SA and Schwartz A (2005) The L-type calcium channel in the heart: the beat goes on. *J Clin Invest* 115:3306-3317.
- Bojesen IN and Bojesen E (1994) Binding of arachidonate and oleate to bovine serum albumin. *J Lipid Res* 35:770-778.
- Bondarenko AI, Drachuk K, Panasiuk O, Sagach V, Deak AT, Malli R and Graier WF (2013) N-arachidonoyl glycine suppresses Na<sup>+</sup>/Ca<sup>2+</sup> exchanger-mediated Ca<sup>2+</sup> entry into endothelial cells and activates BK<sub>Ca</sub> channels independently of GPCRs. *Br J Pharmacol* 169:933-948.

Bonfoco E, Krainc D, Ankarcrona M, Nicotera P and Lipton SA (1995) Apoptosis and necrosis: two distinct events induced, respectively, by mild and intense insults with N-methyl-D-aspartate or nitric oxide/superoxide in cortical cell cultures. *Proc Natl Acad Sci U S A* 92:7162-7166.

Bonz A, Laser M, Kullmer S, Kniesch S, Babin-Ebell J, Popp V, Ertl G and Wagner JA (2003) Cannabinoids acting on CB1 receptors decrease contractile performance in human atrial muscle. *J Cardiovasc Pharmacol* 41:657-664.

Borrelli F and Izzo AA (2009) Role of acylethanolamides in the gastrointestinal tract with special reference to food intake and energy balance. *Best Pract Res Clin Endocrinol Metab* 23:33-49.

Bouchard JF, Lepicier P and Lamontagne D (2003) Contribution of endocannabinoids in the endothelial protection afforded by ischemic preconditioning in the isolated rat heart. *Life Sci* 72:1859-1870.

Bracey MH, Hanson MA, Masuda KR, Stevens RC and Cravatt BF (2002) Structural adaptations in a membrane enzyme that terminates endocannabinoid signaling. *Science* 298:1793-1796.

Bradshaw HB, Raboune S and Hollis JL (2013) Opportunistic activation of TRP receptors by endogenous lipids: exploiting lipidomics to understand TRP receptor cellular communication. *Life Sci* 92:404-409.

Bridge JH, Smolley JR and Spitzer KW (1990) The relationship between charge movements associated with  $I_{Ca}$  and  $I_{Na-Ca}$  in cardiac myocytes. *Science* 248:376-378.

Butt C, Alptekin A, Shippenberg T and Oz M (2008) Endogenous cannabinoid anandamide inhibits nicotinic acetylcholine receptor function in mouse thalamic synaptosomes. *J Neurochem* 105:1235-1243.

Calandra B, Portier M, Kerneis A, Delpech M, Carillon C, Le FG, Ferrara P and Shire D (1999) Dual intracellular signaling pathways mediated by the human cannabinoid CB1 receptor. *Eur J Pharmacol* 374:445-455.

Canitano A, Papa M, Boscia F, Castaldo P, Sellitti S, Tagliatalata M and Annunziato L (2002) Brain distribution of the  $Na^+/Ca^{2+}$  exchanger-encoding genes NCX1, NCX2, and NCX3 and their related proteins in the central nervous system. *Ann N Y Acad Sci* 976:394-404.:394-404.

Cantor RS (2001) Breaking the Meyer-Overton rule: predicted effects of varying stiffness and interfacial activity on the intrinsic potency of anesthetics. *Biophys J* 80:2284-2297.

Cantrell AR and Catterall WA (2001) Neuromodulation of  $Na^+$  channels: an unexpected form of cellular plasticity. *Nat Rev Neurosci* 2:397-407.

Carruba MO, Bondiolotti G, Picotti GB, Catteruccia N and Da PM (1987) Effects of diethyl ether, halothane, ketamine and urethane on sympathetic activity in the rat. *Eur J Pharmacol* 134:15-24.

Catterall WA (2011) Voltage-gated calcium channels. *Cold Spring Harb Perspect Biol* 3:a003947.

Catterall WA (2012) Voltage-gated sodium channels at 60: structure, function and pathophysiology. *J Physiol* 590:2577-2589.

Catterall WA, Goldin AL and Waxman SG (2005a) International Union of Pharmacology. XLVII. Nomenclature and structure-function relationships of voltage-gated sodium channels. *Pharmacol Rev* 57:397-409.

Catterall WA, Perez-Reyes E, Snutch TP and Striessnig J (2005b) International Union of Pharmacology. XLVIII. Nomenclature and structure-function relationships of voltage-gated calcium channels. *Pharmacol Rev* 57:411-425.

Cens T, Rousset M, Leyris JP, Fesquet P and Charner P (2006) Voltage- and calcium-dependent inactivation in high voltage-gated Ca<sup>2+</sup> channels. *Prog Biophys Mol Biol* 90:104-117.

Chaytor AT, Martin PE, Evans WH, Randall MD and Griffith TM (1999) The endothelial component of cannabinoid-induced relaxation in rabbit mesenteric artery depends on gap junctional communication. *J Physiol* 520 Pt 2:539-550.

Chemin J, Monteil A, Perez-Reyes E, Nargeot J and Lory P (2001) Direct inhibition of T-type calcium channels by the endogenous cannabinoid anandamide. *EMBO J* 20:7033-7040.

Chemin J, Nargeot J and Lory P (2007) Chemical determinants involved in anandamide-induced inhibition of T-type calcium channels. *J Biol Chem* 282:2314-2323.

Chen N, Appell M, Berfield JL and Reith ME (2003) Inhibition by arachidonic acid and other fatty acids of dopamine uptake at the human dopamine transporter. *Eur J Pharmacol* 478:89-95.

Christopoulos A and Wilson K (2001) Interaction of anandamide with the M(1) and M(4) muscarinic acetylcholine receptors. *Brain Res* 915:70-78.

Chung SH and Kuyucak S (2002) Recent advances in ion channel research. *Biochim Biophys Acta* 1565:267-286.

Clapper JR, Duranti A, Tontini A, Mor M, Tarzia G and Piomelli D (2006) The fatty-acid amide hydrolase inhibitor URB597 does not affect triacylglycerol hydrolysis in rat tissues. *Pharmacol Res* 54:341-344.

Cravatt BF, Demarest K, Patricelli MP, Bracey MH, Giang DK, Martin BR and Lichtman AH (2001) Supersensitivity to anandamide and enhanced endogenous cannabinoid signaling in mice lacking fatty acid amide hydrolase. *Proc Natl Acad Sci U S A* 98:9371-9376.

Cravatt BF, Giang DK, Mayfield SP, Boger DL, Lerner RA and Gilula NB (1996) Molecular characterization of an enzyme that degrades neuromodulatory fatty-acid amides. *Nature* 384:83-87.

Cravatt BF, Saghatelian A, Hawkins EG, Clement AB, Bracey MH and Lichtman AH (2004) Functional disassociation of the central and peripheral fatty acid amide signaling systems. *Proc Natl Acad Sci U S A* 101:10821-10826.

Danziger RS, Sakai M, Capogrossi MC, Spurgeon HA, Hansford RG and Lakatta EG (1991) Ethanol acutely and reversibly suppresses excitation-contraction coupling in cardiac myocytes. *Circ Res* 68:1660-1668.

De Petrocellis L, Cascio MG and Di Marzo, V (2004) The endocannabinoid system: a general view and latest additions. *Br J Pharmacol* 141:765-774.

De Petrocellis L and Di Marzo, V (2009a) An introduction to the endocannabinoid system: from the early to the latest concepts. *Best Pract Res Clin Endocrinol Metab* 23:1-15.

De Petrocellis L and Di Marzo, V (2009b) Role of endocannabinoids and endovanilloids in Ca<sup>2+</sup> signalling. *Cell Calcium* 45:611-624.

De Petrocellis L and Di Marzo, V (2010) Non-CB1, non-CB2 receptors for endocannabinoids, plant cannabinoids, and synthetic cannabimimetics: focus on G-protein-coupled receptors and transient receptor potential channels. *J Neuroimmune Pharmacol* 5:103-121.

Dedkova EN and Blatter LA (2013) Calcium signaling in cardiac mitochondria. *J Mol Cell Cardiol* 58:125-133.

Defer N, Wan J, Souktani R, Escoubet B, Perier M, Caramelle P, Manin S, Deveaux V, Bourin MC, Zimmer A, Lotersztajn S, Pecker F and Pavoine C (2009) The cannabinoid receptor type 2 promotes cardiac myocyte and fibroblast survival and protects against ischemia/reperfusion-induced cardiomyopathy. *FASEB J* 23:2120-2130.

Delbridge LM, Connell PJ, Harris PJ and Morgan TO (2000) Ethanol effects on cardiomyocyte contractility. *Clin Sci (Lond)* 98:401-407.

Demuth DG and Molleman A (2006) Cannabinoid signalling. *Life Sci* 78:549-563.

Den Ruijter HM, Berecki G, Opthof T, Verkerk AO, Zock PL and Coronel R (2007) Pro- and antiarrhythmic properties of a diet rich in fish oil. *Cardiovasc Res* 73:316-325.

Den Ruijter HM and Coronel R (2009) The response to fish oil in patients with heart disease depends on the predominant arrhythmia mechanism. *Cardiovasc Drugs Ther* 23:333-334.

Derkinderen P, Ledent C, Parmentier M and Girault JA (2001) Cannabinoids activate p38 mitogen-activated protein kinases through CB1 receptors in hippocampus. *J Neurochem* 77:957-960.

Deutsch DG and Chin SA (1993) Enzymatic synthesis and degradation of anandamide, a cannabinoid receptor agonist. *Biochem Pharmacol* 46:791-796.

Deutsch DG, Goligorsky MS, Schmid PC, Krebsbach RJ, Schmid HH, Das SK, Dey SK, Arreaza G, Thorup C, Stefano G and Moore LC (1997) Production and physiological actions of anandamide in the vasculature of the rat kidney. *J Clin Invest* 100:1538-1546.

Devane WA, Dysarz FA, III, Johnson MR, Melvin LS and Howlett AC (1988) Determination and characterization of a cannabinoid receptor in rat brain. *Mol Pharmacol* 34:605-613.

Devane WA, Hanus L, Breuer A, Pertwee RG, Stevenson LA, Griffin G, Gibson D, Mandelbaum A, Etinger A and Mechoulam R (1992) Isolation and structure of a brain constituent that binds to the cannabinoid receptor. *Science* 258:1946-1949.

Di Marzo, V (2006) A brief history of cannabinoid and endocannabinoid pharmacology as inspired by the work of British scientists. *Trends Pharmacol Sci* 27:134-140.

Di Marzo, V, Bisogno T and De Petrocellis L (2007) Endocannabinoids and related compounds: walking back and forth between plant natural products and animal physiology. *Chem Biol* 14:741-756.

Di Marzo, V, Bisogno T, Melck D, Ross R, Brockie H, Stevenson L, Pertwee R and De Petrocellis L (1998) Interactions between synthetic vanilloids and the endogenous cannabinoid system. *FEBS Lett* 436:449-454.

Di Marzo, V, Blumberg PM and Szallasi A (2002) Endovanilloid signaling in pain. *Curr Opin Neurobiol* 12:372-379.

Di Marzo, V and Cristino L (2008) Why endocannabinoids are not all alike. *Nat Neurosci* 11:124-126.

Dib-Hajj SD, Black JA and Waxman SG (2009) Voltage-gated sodium channels: therapeutic targets for pain. *Pain Med* 10:1260-1269.

Dong M, Sun X, Prinz AA and Wang HS (2006) Effect of simulated  $I_{to}$  on guinea pig and canine ventricular action potential morphology. *Am J Physiol Heart Circ Physiol* 291:H631-H637.

Duan Y, Zheng J and Nicholson RA (2008) Inhibition of [3H]batrachotoxinin A-20alpha-benzoate binding to sodium channels and sodium channel function by endocannabinoids. *Neurochem Int* 52:438-446.

Dvorakova M and Kummer W (2001) Transient expression of vanilloid receptor subtype 1 in rat cardiomyocytes during development. *Histochem Cell Biol* 116:223-225.

Eisner D, Bode E, Venetucci L and Trafford A (2013) Calcium flux balance in the heart. *J Mol Cell Cardiol* 58:110-117.

Ellis EF, Moore SF and Willoughby KA (1995) Anandamide and delta 9-THC dilation of cerebral arterioles is blocked by indomethacin. *Am J Physiol* 269:H1859-H1864.

Epps DE, Mandel F and Schwartz A (1982) The alteration of rabbit skeletal sarcoplasmic reticulum function by N-acylethanolamine, a lipid associated with myocardial infarction. *Cell Calcium* 3:531-543.

Epps DE, Schmid PC, Natarajan V and Schmid HH (1979) N-Acylethanolamine accumulation in infarcted myocardium. *Biochem Biophys Res Commun* 90:628-633.

Fabiato A (1983) Calcium-induced release of calcium from the cardiac sarcoplasmic reticulum. *Am J Physiol* 245:C1-14.

Felder CC, Joyce KE, Briley EM, Mansouri J, Mackie K, Blond O, Lai Y, Ma AL and Mitchell RL (1995) Comparison of the pharmacology and signal transduction of the human cannabinoid CB1 and CB2 receptors. *Mol Pharmacol* 48:443-450.

Ferreira G, Yi J, Rios E and Shirokov R (1997) Ion-dependent inactivation of barium current through L-type calcium channels. *J Gen Physiol* 109:449-461.

Fimiani C, Mattocks D, Cavani F, Salzet M, Deutsch DG, Pryor S, Bilfinger TV and Stefano GB (1999) Morphine and anandamide stimulate intracellular calcium transients in human arterial endothelial cells: coupling to nitric oxide release. *Cell Signal* 11:189-193.

Foldy C, Neu A, Jones MV and Soltesz I (2006) Presynaptic, activity-dependent modulation of cannabinoid type 1 receptor-mediated inhibition of GABA release. *J Neurosci* 26:1465-1469.

Ford WR, Honan SA, White R and Hiley CR (2002) Evidence of a novel site mediating anandamide-induced negative inotropic and coronary vasodilator responses in rat isolated hearts. *Br J Pharmacol* 135:1191-1198.

Fowler CJ (2007) The contribution of cyclooxygenase-2 to endocannabinoid metabolism and action. *Br J Pharmacol* 152:594-601.

Fowler CJ, Jonsson KO and Tiger G (2001) Fatty acid amide hydrolase: biochemistry, pharmacology, and therapeutic possibilities for an enzyme hydrolyzing anandamide, 2-arachidonoylglycerol, palmitoylethanolamide, and oleamide. *Biochem Pharmacol* 62:517-526.

Frank KF, Bolck B, Erdmann E and Schwinger RH (2003) Sarcoplasmic reticulum Ca<sup>2+</sup>-ATPase modulates cardiac contraction and relaxation. *Cardiovasc Res* 57:20-27.

Frohnwieser B, Chen LQ, Schreibmayer W and Kallen RG (1997) Modulation of the human cardiac sodium channel alpha-subunit by cAMP-dependent protein kinase and the responsible sequence domain. *J Physiol* 498:309-318.

- Fu J, Oveisi F, Gaetani S, Lin E and Piomelli D (2005) Oleoylethanolamide, an endogenous PPAR- $\alpha$  agonist, lowers body weight and hyperlipidemia in obese rats. *Neuropharmacology* 48:1147-1153.
- Fulton D and Quilley J (1998) Evidence against anandamide as the hyperpolarizing factor mediating the nitric oxide-independent coronary vasodilator effect of bradykinin in the rat. *J Pharmacol Exp Ther* 286:1146-1151.
- Garcia ML (2004) Ion channels: gate expectations. *Nature* 430:153-155.
- Gebremedhin D, Lange AR, Campbell WB, Hillard CJ and Harder DR (1999) Cannabinoid CB1 receptor of cat cerebral arterial muscle functions to inhibit L-type Ca<sup>2+</sup> channel current. *Am J Physiol* 276:H2085-H2093.
- Giuffrida A, Rodriguez de FF, Nava F, Loubet-Lescoulie P and Piomelli D (2000) Elevated circulating levels of anandamide after administration of the transport inhibitor, AM404. *Eur J Pharmacol* 408:161-168.
- Glass CK and Ogawa S (2006) Combinatorial roles of nuclear receptors in inflammation and immunity. *Nat Rev Immunol* 6:44-55.
- Glass M and Felder CC (1997) Concurrent stimulation of cannabinoid CB1 and dopamine D2 receptors augments cAMP accumulation in striatal neurons: evidence for a Gs linkage to the CB1 receptor. *J Neurosci* 17:5327-5333.
- Godlewski G, Alapafuja SO, Batkai S, Nikas SP, Cinar R, Offertaler L, Osei-Hyiaman D, Liu J, Mukhopadhyay B, Harvey-White J, Tam J, Pacak K, Blankman JL, Cravatt BF, Makriyannis A and Kunos G (2010) Inhibitor of fatty acid amide hydrolase normalizes cardiovascular function in hypertension without adverse metabolic effects. *Chem Biol* 17:1256-1266.
- Goldhaber JJ, Lamp ST, Walter DO, Garfinkel A, Fukumoto GH and Weiss JN (1999) Local regulation of the threshold for calcium sparks in rat ventricular myocytes: role of sodium-calcium exchange. *J Physiol* 520 Pt 2:431-438.
- Gomes AV, Potter JD and Szczesna-Cordary D (2002) The role of troponins in muscle contraction. *IUBMB Life* 54:323-333.
- Goodfellow CE and Glass M (2009) Anandamide receptor signal transduction. *Vitam Horm* 81:79-110.
- Grant AO (2009) Cardiac ion channels. *Circ Arrhythm Electrophysiol* 2:185-194.
- Guo J and Ikeda SR (2004) Endocannabinoids modulate N-type calcium channels and G-protein-coupled inwardly rectifying potassium channels via CB1 cannabinoid receptors heterologously expressed in mammalian neurons. *Mol Pharmacol* 65:665-674.
- Hajrasouliha AR, Tavakoli S, Ghasemi M, Jabehdar-Maralani P, Sadeghipour H, Ebrahimi F and Dehpour AR (2008) Endogenous cannabinoids contribute to remote ischemic preconditioning via cannabinoid CB2 receptors in the rat heart. *Eur J Pharmacol* 579:246-252.

- Hallaq H, Wang DW, Kunic JD, George AL, Jr., Wells KS and Murray KT (2012) Activation of protein kinase C alters the intracellular distribution and mobility of cardiac Na<sup>+</sup> channels. *Am J Physiol Heart Circ Physiol* 302:H782-H789.
- Hansen HS (2010) Palmitoylethanolamide and other anandamide congeners. Proposed role in the diseased brain. *Exp Neurol* 224:48-55.
- Hansen HS, Moesgaard B, Hansen HH and Petersen G (2000) N-Acylethanolamines and precursor phospholipids - relation to cell injury. *Chem Phys Lipids* 108:135-150.
- Hanus L, bu-Lafi S, Fride E, Breuer A, Vogel Z, Shalev DE, Kustanovich I and Mechoulam R (2001) 2-arachidonyl glyceryl ether, an endogenous agonist of the cannabinoid CB1 receptor. *Proc Natl Acad Sci U S A* 98:3662-3665.
- Hejazi N, Zhou C, Oz M, Sun H, Ye JH and Zhang L (2006) Delta9-tetrahydrocannabinol and endogenous cannabinoid anandamide directly potentiate the function of glycine receptors. *Mol Pharmacol* 69:991-997.
- Hermann H, De PL, Bisogno T, Schiano MA, Lutz B and Di M, V (2003) Dual effect of cannabinoid CB1 receptor stimulation on a vanilloid VR1 receptor-mediated response. *Cell Mol Life Sci* 60:607-616.
- Herradon E, Martin MI and Lopez-Miranda V (2007) Characterization of the vasorelaxant mechanisms of the endocannabinoid anandamide in rat aorta. *Br J Pharmacol* 152:699-708.
- Hiley CR (2009) Endocannabinoids and the heart. *J Cardiovasc Pharmacol* 53:267-276.
- Hilgemann DW and Ball R (1996) Regulation of cardiac Na<sup>+</sup>,Ca<sup>2+</sup> exchange and KATP potassium channels by PIP<sub>2</sub>. *Science* 273:956-959.
- Hilgemann DW, Lin MJ, Fine M, Frazier G and Wang HR (2013) Toward an understanding of the complete NCX1 lifetime in the cardiac sarcolemma. *Adv Exp Med Biol* 961:345-352.
- Hillard CJ (2000) Biochemistry and pharmacology of the endocannabinoids arachidonylethanolamide and 2-arachidonylglycerol. *Prostaglandins Other Lipid Mediat* 61:3-18.
- Hinde AK, Perchenet L, Hobai IA, Levi AJ and Hancox JC (1999) Inhibition of Na/Ca exchange by external Ni in guinea-pig ventricular myocytes at 37 degrees C, dialysed internally with cAMP-free and cAMP-containing solutions. *Cell Calcium* 25:321-331.
- Ho BY, Uezono Y, Takada S, Takase I and Izumi F (1999) Coupling of the expressed cannabinoid CB1 and CB2 receptors to phospholipase C and G protein-coupled inwardly rectifying K<sup>+</sup> channels. *Receptors Channels* 6:363-374.



- Ho WS, Barrett DA and Randall MD (2008) 'Entourage' effects of N-palmitoylethanolamide and N-oleoylethanolamide on vasorelaxation to anandamide occur through TRPV1 receptors. *Br J Pharmacol* 155:837-846.
- Hoffmann P, Richards D, Heinroth-Hoffmann I, Mathias P, Wey H and Toraason M (1995) Arachidonic acid disrupts calcium dynamics in neonatal rat cardiac myocytes. *Cardiovasc Res* 30:889-898.
- Holland M, John Challiss RA, Standen NB and Boyle JP (1999) Cannabinoid CB1 receptors fail to cause relaxation, but couple via G<sub>i</sub>/G<sub>o</sub> to the inhibition of adenylyl cyclase in carotid artery smooth muscle. *Br J Pharmacol* 128:597-604.
- Howarth FC, Qureshi MA and White E (2002) Effects of hyperosmotic shrinking on ventricular myocyte shortening and intracellular Ca<sup>2+</sup> in streptozotocin-induced diabetic rats. *Pflugers Arch* 444:446-451.
- Howlett AC (2002) The cannabinoid receptors. *Prostaglandins Other Lipid Mediat* 68-69:619-31.:619-631.
- Howlett AC, Bidaut-Russell M, Devane WA, Melvin LS, Johnson MR and Herkenham M (1990) The cannabinoid receptor: biochemical, anatomical and behavioral characterization. *Trends Neurosci* 13:420-423.
- Howlett AC and Fleming RM (1984) Cannabinoid inhibition of adenylate cyclase. Pharmacology of the response in neuroblastoma cell membranes. *Mol Pharmacol* 26:532-538.
- Howlett AC, Qualy JM and Khachatrian LL (1986) Involvement of G<sub>i</sub> in the inhibition of adenylate cyclase by cannabimimetic drugs. *Mol Pharmacol* 29:307-313.
- Huang CC, Lo SW and Hsu KS (2001) Presynaptic mechanisms underlying cannabinoid inhibition of excitatory synaptic transmission in rat striatal neurons. *J Physiol* 532:731-748.
- Huke S and Knollmann BC (2010) Increased myofilament Ca<sup>2+</sup>-sensitivity and arrhythmia susceptibility. *J Mol Cell Cardiol* 48:824-833.
- Inesi G, Prasad AM and Pilankatta R (2008) The Ca<sup>2+</sup> ATPase of cardiac sarcoplasmic reticulum: Physiological role and relevance to diseases. *Biochem Biophys Res Commun* 369:182-187.
- Ishac EJ, Jiang L, Lake KD, Varga K, Abood ME and Kunos G (1996) Inhibition of exocytotic noradrenaline release by presynaptic cannabinoid CB1 receptors on peripheral sympathetic nerves. *Br J Pharmacol* 118:2023-2028.
- Ishii I and Chun J (2002) Anandamide-induced neuroblastoma cell rounding via the CB1 cannabinoid receptors. *Neuroreport* 13:593-596.
- Ishioka N and Bukoski RD (1999) A role for N-arachidonylethanolamine (anandamide) as the mediator of sensory nerve-dependent Ca<sup>2+</sup>-induced relaxation. *J Pharmacol Exp Ther* 289:245-250.

Iwamoto T, Pan Y, Wakabayashi S, Imagawa T, Yamanaka HI and Shigekawa M (1996) Phosphorylation-dependent regulation of cardiac Na<sup>+</sup>/Ca<sup>2+</sup> exchanger via protein kinase C. *J Biol Chem* 271:13609-13615.

Jackson SN, Singhal SK, Woods AS, Morales M, Shippenberg T, Zhang L and Oz M (2008) Volatile anesthetics and endogenous cannabinoid anandamide have additive and independent inhibitory effects on alpha(7)-nicotinic acetylcholine receptor-mediated responses in *Xenopus* oocytes. *Eur J Pharmacol* 582:42-51.

Janis RA, Shrikhande AV, Johnson DE, McCarthy RT, Howard AD, Greguski R and Scriabine A (1988) Isolation and characterization of a fraction from brain that inhibits 1,4-[3H]dihydropyridine binding and L-type calcium channel current. *FEBS Lett* 239:233-236.

Jarai Z, Wagner JA, Varga K, Lake KD, Compton DR, Martin BR, Zimmer AM, Bonner TI, Buckley NE, Mezey E, Razdan RK, Zimmer A and Kunos G (1999) Cannabinoid-induced mesenteric vasodilation through an endothelial site distinct from CB1 or CB2 receptors. *Proc Natl Acad Sci U S A* 96:14136-14141.

Jensen MO and Mouritsen OG (2004) Lipids do influence protein function-the hydrophobic matching hypothesis revisited. *Biochim Biophys Acta* 1666:205-226.

Johnson DE, Heald SL, Dally RD and Janis RA (1993) Isolation, identification and synthesis of an endogenous arachidonic amide that inhibits calcium channel antagonist 1,4-dihydropyridine binding. *Prostaglandins Leukot Essent Fatty Acids* 48:429-437.

Kanakis C, Jr., Pouget JM and Rosen KM (1976) The effects of delta-9-tetrahydrocannabinol (cannabis) on cardiac performance with and without beta blockade. *Circulation* 53:703-707.

Karmazinova M and Lacinova L (2010) Measurement of cellular excitability by whole cell patch clamp technique. *Physiol Res* 59 Suppl 1:S1-S7.

Kathuria S, Gaetani S, Fegley D, Valino F, Duranti A, Tontini A, Mor M, Tarzia G, La RG, Calignano A, Giustino A, Tattoli M, Palmery M, Cuomo V and Piomelli D (2003) Modulation of anxiety through blockade of anandamide hydrolysis. *Nat Med* 9:76-81.

Keating MT and Sanguinetti MC (2001) Molecular and cellular mechanisms of cardiac arrhythmias. *Cell* 104:569-580.

Kettenmann H, Sonnhof U and Schachner M (1983) Exclusive potassium dependence of the membrane potential in cultured mouse oligodendrocytes. *J Neurosci* 3:500-505.

Kim HI, Kim TH, Shin YK, Lee CS, Park M and Song JH (2005) Anandamide suppression of Na<sup>+</sup> currents in rat dorsal root ganglion neurons. *Brain Res* 1062:39-47.

Kirstein M, Eickhorn R, Kochsiek K and Langenfeld H (1996) Dose-dependent alteration of rat cardiac sodium current by isoproterenol: results from direct measurements on multicellular preparations. *Pflugers Arch* 431:395-401.

Kozak KR, Gupta RA, Moody JS, Ji C, Boeglin WE, DuBois RN, Brash AR and Marnett LJ (2002) 15-Lipoxygenase metabolism of 2-arachidonylglycerol. Generation of a peroxisome proliferator-activated receptor alpha agonist. *J Biol Chem* 277:23278-23286.

Krylatov AV, Maslov LN, Lasukova OV and Pertwee RG (2005) Cannabinoid receptor antagonists SR141716 and SR144528 exhibit properties of partial agonists in experiments on isolated perfused rat heart. *Bull Exp Biol Med* 139:558-561.

Krylatov AV, Uzhachenko RV, Maslov LN, Ugdyzhekova DS, Bernatskaia NA, Pertwee R, Stefano GB and Makriyannis A (2002) [Anandamide and R-(+)-methanandamide prevent development of ischemic and reperfusion arrhythmia in rats by stimulation of CB2-receptors]. *Eksp Klin Farmakol* 65:6-9.

Kunos G, Jarai Z, Batkai S, Goparaju SK, Ishac EJ, Liu J, Wang L and Wagner JA (2000) Endocannabinoids as cardiovascular modulators. *Chem Phys Lipids* 108:159-168.

Lacerda AE, Kim HS, Ruth P, Perez-Reyes E, Flockerzi V, Hofmann F, Birnbaumer L and Brown AM (1991) Normalization of current kinetics by interaction between the alpha 1 and beta subunits of the skeletal muscle dihydropyridine-sensitive Ca<sup>2+</sup> channel. *Nature* 352:527-530.

Lake KD, Compton DR, Varga K, Martin BR and Kunos G (1997a) Cannabinoid-induced hypotension and bradycardia in rats mediated by CB1-like cannabinoid receptors. *J Pharmacol Exp Ther* 281:1030-1037.

Lake KD, Martin BR, Kunos G and Varga K (1997b) Cardiovascular effects of anandamide in anesthetized and conscious normotensive and hypertensive rats. *Hypertension* 29:1204-1210.

Lambert DM and Muccioli GG (2007) Endocannabinoids and related N-acyl ethanolamines in the control of appetite and energy metabolism: emergence of new molecular players. *Curr Opin Clin Nutr Metab Care* 10:735-744.

Lauckner JE, Hille B and Mackie K (2005) The cannabinoid agonist WIN55,212-2 increases intracellular calcium via CB1 receptor coupling to G<sub>q/11</sub> G proteins. *Proc Natl Acad Sci U S A* 102:19144-19149.

Ledent C, Valverde O, Cossu G, Petitet F, Aubert JF, Beslot F, Bohme GA, Imperato A, Pedrazzini T, Roques BP, Vassart G, Fratta W and Parmentier M (1999) Unresponsiveness to cannabinoids and reduced addictive effects of opiates in CB1 receptor knockout mice. *Science* 283:401-404.

Lee SY, Lee A, Chen J and MacKinnon R (2005) Structure of the K<sub>v</sub>AP voltage-dependent K<sup>+</sup> channel and its dependence on the lipid membrane. *Proc Natl Acad Sci U S A* 102:15441-15446.

Lee SY and MacKinnon R (2004) A membrane-access mechanism of ion channel inhibition by voltage sensor toxins from spider venom. *Nature* 430:232-235.

Lee TI, Kao YH, Chen YC, Pan NH, Lin YK and Chen YJ (2011) Cardiac peroxisome-proliferator-activated receptor expression in hypertension co-existing with diabetes. *Clin Sci (Lond)* 121:305-312.

Lenman A and Fowler CJ (2007) Interaction of ligands for the peroxisome proliferator-activated receptor gamma with the endocannabinoid system. *Br J Pharmacol* 151:1343-1351.

Lepicier P, Bouchard JF, Lagneux C and Lamontagne D (2003) Endocannabinoids protect the rat isolated heart against ischaemia. *Br J Pharmacol* 139:805-815.

Lepicier P, Lagneux C, Sirois MG and Lamontagne D (2007) Endothelial CB1-receptors limit infarct size through NO formation in rat isolated hearts. *Life Sci* 81:1373-1380.

Li Q, Cui N, Du Y, Ma H and Zhang Y (2013) Anandamide reduces intracellular Ca<sup>2+</sup> concentration through suppression of Na<sup>+</sup>/Ca<sup>2+</sup> exchanger current in rat cardiac myocytes. *PLoS One* 8:e63386.

Li Q, Ma HJ, Zhang H, Qi Z, Guan Y and Zhang Y (2009) Electrophysiological effects of anandamide on rat myocardium. *Br J Pharmacol* 158:2022-2029.

Lichtman AH, Hawkins EG, Griffin G and Cravatt BF (2002) Pharmacological activity of fatty acid amides is regulated, but not mediated, by fatty acid amide hydrolase in vivo. *J Pharmacol Exp Ther* 302:73-79.

Litwin SE, Li J and Bridge JH (1998) Na-Ca exchange and the trigger for sarcoplasmic reticulum Ca release: studies in adult rabbit ventricular myocytes. *Biophys J* 75:359-371.

Liu J, Gao B, Mirshahi F, Sanyal AJ, Khanolkar AD, Makriyannis A and Kunos G (2000) Functional CB1 cannabinoid receptors in human vascular endothelial cells. *Biochem J* 346 Pt 3:835-40.:835-840.

Liu SJ (2007) Inhibition of L-type Ca<sup>2+</sup> channel current and negative inotropy induced by arachidonic acid in adult rat ventricular myocytes. *Am J Physiol Cell Physiol* 293:C1594-C1604.

London B, Michalec M, Mehdi H, Zhu X, Kerchner L, Sanyal S, Viswanathan PC, Pfahnl AE, Shang LL, Madhusudanan M, Baty CJ, Lagana S, Aleong R, Gutmann R, Ackerman MJ, McNamara DM, Weiss R and Dudley SC, Jr. (2007) Mutation in glycerol-3-phosphate dehydrogenase 1 like gene (GPD1-L) decreases cardiac Na<sup>+</sup> current and causes inherited arrhythmias. *Circulation* 116:2260-2268.

Lovinger DM (2008) Presynaptic modulation by endocannabinoids. *Handb Exp Pharmacol* 435-477.

Lozovaya N, Min R, Tsintsadze V and Burnashev N (2009) Dual modulation of CNS voltage-gated calcium channels by cannabinoids: Focus on CB1 receptor-independent effects. *Cell Calcium* 46:154-162.

Lundbaek JA (2006) Regulation of membrane protein function by lipid bilayer elasticity-a single molecule technology to measure the bilayer properties experienced by an embedded protein. *J Phys Condens Matter* 18:S1305-S1344.

Lytton J (2007) Na<sup>+</sup>/Ca<sup>2+</sup> exchangers: three mammalian gene families control Ca<sup>2+</sup> transport. *Biochem J* 406:365-382.

Mach F, Montecucco F and Steffens S (2008) Cannabinoid receptors in acute and chronic complications of atherosclerosis. *Br J Pharmacol* 153:290-298.

Mackie K (2008) Cannabinoid receptors: where they are and what they do. *J Neuroendocrinol* 20 Suppl 1:10-14.

Mackie K, Devane WA and Hille B (1993) Anandamide, an endogenous cannabinoid, inhibits calcium currents as a partial agonist in N18 neuroblastoma cells. *Mol Pharmacol* 44:498-503.

Mackie K and Hille B (1992) Cannabinoids inhibit N-type calcium channels in neuroblastoma-glioma cells. *Proc Natl Acad Sci U S A* 89:3825-3829.

Malinowska B, Baranowska-Kuczko M and Schlicker E (2012) Triphasic blood pressure responses to cannabinoids: do we understand the mechanism? *Br J Pharmacol* 165:2073-2088.

Malinowska B, Godlewski G, Bucher B and Schlicker E (1997) Cannabinoid CB1 receptor-mediated inhibition of the neurogenic vasopressor response in the pithed rat. *Naunyn Schmiedebergs Arch Pharmacol* 356:197-202.

Mallat A and Lotersztajn S (2008) Endocannabinoids and liver disease. I. Endocannabinoids and their receptors in the liver. *Am J Physiol Gastrointest Liver Physiol* 294:G9-G12.

Mamas MA and Terrar DA (2001) Actions of arachidonic acid on contractions and associated electrical activity in guinea-pig isolated ventricular myocytes. *Exp Physiol* 86:437-449.

Manitiu ML (2013) The endocannabinoid system and its role in the pathogenesis and treatment of cardiovascular disturbances in cirrhosis. *Acta Gastroenterol Belg* 76:195-199.

Martin BR, Mechoulam R and Razdan RK (1999) Discovery and characterization of endogenous cannabinoids. *Life Sci* 65:573-595.

Maslov LN, Lasukova OV, Krylatov AV, Uzhachenko RV and Pertwee R (2004) Selective cannabinoid receptor agonist HU-210 decreases pump function of

isolated perfused heart: role of cAMP and cGMP. *Bull Exp Biol Med* 138:550-553.

Matsuda LA, Lolait SJ, Brownstein MJ, Young AC and Bonner TI (1990) Structure of a cannabinoid receptor and functional expression of the cloned cDNA. *Nature* 346:561-564.

Mavromoustakos T, Papahatjis D and Laggner P (2001) Differential membrane fluidization by active and inactive cannabinoid analogues. *Biochim Biophys Acta* 1512:183-190.

McAllister SD, Griffin G, Satin LS and Abood ME (1999) Cannabinoid receptors can activate and inhibit G protein-coupled inwardly rectifying potassium channels in a xenopus oocyte expression system. *J Pharmacol Exp Ther* 291:618-626.

McIntosh BT, Hudson B, Yegorova S, Jollimore CA and Kelly ME (2007) Agonist-dependent cannabinoid receptor signalling in human trabecular meshwork cells. *Br J Pharmacol* 152:1111-1120.

McIntosh TJ and Simon SA (2006) Roles of bilayer material properties in function and distribution of membrane proteins. *Annu Rev Biophys Biomol Struct* 35:177-98.:177-198.

McKinney MK and Cravatt BF (2005) Structure and function of fatty acid amide hydrolase. *Annu Rev Biochem* 74:411-32.:411-432.

Mechoulam R, Ben-Shabat S, Hanus L, Ligumsky M, Kaminski NE, Schatz AR, Gopher A, Almog S, Martin BR, Compton DR and . (1995) Identification of an endogenous 2-monoglyceride, present in canine gut, that binds to cannabinoid receptors. *Biochem Pharmacol* 50:83-90.

Mechoulam R and Gaoni Y (1965) Hashish. IV. The isolation and structure of cannabinolic cannabidiolic and cannabigerolic acids. *Tetrahedron* 21:1223-1229.

Mendizabal VE and Adler-Graschinsky E (2007) Cannabinoids as therapeutic agents in cardiovascular disease: a tale of passions and illusions. *Br J Pharmacol* 151:427-440.

Meves H (1994) Modulation of ion channels by arachidonic acid. *Prog Neurobiol* 43:175-186.

Michaux C, Muccioli GG, Lambert DM and Wouters J (2006) Binding mode of new (thio)hydantoin inhibitors of fatty acid amide hydrolase: comparison with two original compounds, OL-92 and JP104. *Bioorg Med Chem Lett* 16:4772-4776.

Min X, Thibault ST, Porter AC, Gustin DJ, Carlson TJ, Xu H, Lindstrom M, Xu G, Uyeda C, Ma Z, Li Y, Kayser F, Walker NP and Wang Z (2011) Discovery and molecular basis of potent noncovalent inhibitors of fatty acid amide hydrolase (FAAH). *Proc Natl Acad Sci U S A* 108:7379-7384.

- Minor DL, Jr. and Findeisen F (2010) Progress in the structural understanding of voltage-gated calcium channel (Ca<sub>v</sub>) function and modulation. *Channels (Austin)* 4:459-474.
- Moesgaard B, Petersen G, Mortensen SA and Hansen HS (2002) Substantial species differences in relation to formation and degradation of N-acyl-ethanolamine phospholipids in heart tissue: an enzyme activity study. *Comp Biochem Physiol B Biochem Mol Biol* 131:475-482.
- Mombouli JV, Schaeffer G, Holzmann S, Kostner GM and Graier WF (1999) Anandamide-induced mobilization of cytosolic Ca<sup>2+</sup> in endothelial cells. *Br J Pharmacol* 126:1593-1600.
- Montecucco F and Di M, V (2012) At the heart of the matter: the endocannabinoid system in cardiovascular function and dysfunction. *Trends Pharmacol Sci* 33:331-340.
- Montecucco F, Lenglet S, Braunersreuther V, Burger F, Pelli G, Bertolotto M, Mach F and Steffens S (2009) CB2 cannabinoid receptor activation is cardioprotective in a mouse model of ischemia/reperfusion. *J Mol Cell Cardiol* 46:612-620.
- Morad M, Cleemann L and Menick DR (2011) NCX1 phosphorylation dilemma: a little closer to resolution. Focus on "Full-length cardiac Na<sup>+</sup>/Ca<sup>2+</sup> exchanger 1 protein is not phosphorylated by protein kinase A". *Am J Physiol Cell Physiol* 300:C970-C973.
- Moreno C, Macias A, Prieto A, de la Cruz A, Gonzalez T and Valenzuela C (2012) Effects of n-3 Polyunsaturated Fatty Acids on Cardiac Ion Channels. *Front Physiol* 3:245. doi: 10.3389/fphys.2012.00245.:245.
- Moreno-Galindo EG, Barrio-Echavarria GF, Vasquez JC, Decher N, Sachse FB, Tristani-Firouzi M, Sanchez-Chapula JA and Navarro-Polanco RA (2010) Molecular basis for a high-potency open-channel block of Kv1.5 channel by the endocannabinoid anandamide. *Mol Pharmacol* 77:751-758.
- Mukhopadhyay P, Batkai S, Rajesh M, Czifra N, Harvey-White J, Hasko G, Zsengeller Z, Gerard NP, Liaudet L, Kunos G and Pacher P (2007) Pharmacological inhibition of CB1 cannabinoid receptor protects against doxorubicin-induced cardiotoxicity. *J Am Coll Cardiol* 50:528-536.
- Mukhopadhyay P, Horvath B, Rajesh M, Matsumoto S, Saito K, Batkai S, Patel V, Tanchian G, Gao RY, Cravatt BF, Hasko G and Pacher P (2011) Fatty acid amide hydrolase is a key regulator of endocannabinoid-induced myocardial tissue injury. *Free Radic Biol Med* 50:179-195.
- Mukhopadhyay P, Mohanraj R, Batkai S and Pacher P (2008) CB1 cannabinoid receptor inhibition: promising approach for heart failure? *Congest Heart Fail* 14:330-334.

- Mukhopadhyay P, Rajesh M, Batkai S, Patel V, Kashiwaya Y, Liaudet L, Evgenov OV, Mackie K, Hasko G and Pacher P (2010) CB1 cannabinoid receptors promote oxidative stress and cell death in murine models of doxorubicin-induced cardiomyopathy and in human cardiomyocytes. *Cardiovasc Res* 85:773-784.
- Munro S, Thomas KL and Bu-Shaar M (1993) Molecular characterization of a peripheral receptor for cannabinoids. *Nature* 365:61-65.
- Murray KT, Hu NN, Daw JR, Shin HG, Watson MT, Mashburn AB and George AL, Jr. (1997) Functional effects of protein kinase C activation on the human cardiac Na<sup>+</sup> channel. *Circ Res* 80:370-376.
- Netzeband JG, Conroy SM, Parsons KL and Gruol DL (1999) Cannabinoids enhance NMDA-elicited Ca<sup>2+</sup> signals in cerebellar granule neurons in culture. *J Neurosci* 19:8765-8777.
- Nicholson RA, Liao C, Zheng J, David LS, Coyne L, Errington AC, Singh G and Lees G (2003) Sodium channel inhibition by anandamide and synthetic cannabimimetics in brain. *Brain Res* 978:194-204.
- Nicholson RA, Zheng J, Ganellin CR, Verdon B and Lees G (2001) Anesthetic-like interaction of the sleep-inducing lipid oleamide with voltage-gated sodium channels in mammalian brain. *Anesthesiology* 94:120-128.
- Niederhoffer N and Szabo B (1999) Effect of the cannabinoid receptor agonist WIN55212-2 on sympathetic cardiovascular regulation. *Br J Pharmacol* 126:457-466.
- O'Sullivan SE, Kendall DA and Randall MD (2009a) Time-dependent vascular effects of Endocannabinoids mediated by peroxisome proliferator-activated receptor gamma (PPARgamma). *PPAR Res* 2009:425289. doi: 10.1155/2009/425289. Epub; 2009 Apr 29.:425289.
- O'Sullivan SE, Sun Y, Bennett AJ, Randall MD and Kendall DA (2009b) Time-dependent vascular actions of cannabidiol in the rat aorta. *Eur J Pharmacol* 612:61-68.
- O'Sullivan SE, Tarling EJ, Bennett AJ, Kendall DA and Randall MD (2005) Novel time-dependent vascular actions of Delta9-tetrahydrocannabinol mediated by peroxisome proliferator-activated receptor gamma. *Biochem Biophys Res Commun* 337:824-831.
- Ono K, Kiyosue T and Arita M (1989) Isoproterenol, DBcAMP, and forskolin inhibit cardiac sodium current. *Am J Physiol* 256:C1131-C1137.
- Ottolia M, Torres N, Bridge JH, Philipson KD and Goldhaber JI (2013) Na/Ca exchange and contraction of the heart. *J Mol Cell Cardiol* 61:28-33. doi: 10.1016/j.yjmcc.2013.06.001. Epub; 2013 Jun 12.:28-33.
- Oz M (2006) Receptor-independent actions of cannabinoids on cell membranes: focus on endocannabinoids. *Pharmacol Ther* 111:114-144.



- Oz M, Alptekin A, Tchugunova Y and Dinc M (2005) Effects of saturated long-chain N-acylethanolamines on voltage-dependent  $\text{Ca}^{2+}$  fluxes in rabbit T-tubule membranes. *Arch Biochem Biophys* 434:344-351.
- Oz M, Jaligam V, Galadari S, Petroianu G, Shuba YM and Shippenberg TS (2010) The endogenous cannabinoid, anandamide, inhibits dopamine transporter function by a receptor-independent mechanism. *J Neurochem* 112:1454-1464.
- Oz M, Tchugunova Y and Dinc M (2004a) Differential effects of endogenous and synthetic cannabinoids on voltage-dependent calcium fluxes in rabbit T-tubule membranes: comparison with fatty acids. *Eur J Pharmacol* 502:47-58.
- Oz M, Tchugunova YB and Dunn SM (2000) Endogenous cannabinoid anandamide directly inhibits voltage-dependent  $\text{Ca}^{2+}$  fluxes in rabbit T-tubule membranes. *Eur J Pharmacol* 404:13-20.
- Oz M, Yang KH, Dinc M and Shippenberg TS (2007a) The endogenous cannabinoid anandamide inhibits cromakalim-activated  $\text{K}^+$  currents in follicle-enclosed *Xenopus* oocytes. *J Pharmacol Exp Ther* 323:547-554.
- Oz M, Yang KH, Shippenberg TS, Renaud LP and O'Donovan MJ (2007b) Cholecystokinin B-type receptors mediate a G-protein-dependent depolarizing action of sulphated cholecystokinin octapeptide (CCK-8s) on rodent neonatal spinal ventral horn neurons. *J Neurophysiol* 98:1108-1114.
- Oz M, Zhang L and Morales M (2002) Endogenous cannabinoid, anandamide, acts as a noncompetitive inhibitor on 5-HT<sub>3</sub> receptor-mediated responses in *Xenopus* oocytes. *Synapse* 46:150-156.
- Oz M, Zhang L, Ravindran A, Morales M and Lupica CR (2004b) Differential effects of endogenous and synthetic cannabinoids on  $\alpha 7$ -nicotinic acetylcholine receptor-mediated responses in *Xenopus* Oocytes. *J Pharmacol Exp Ther* 310:1152-1160.
- Pacher P, Batkai S and Kunos G (2004) Haemodynamic profile and responsiveness to anandamide of TRPV1 receptor knock-out mice. *J Physiol* 558:647-657.
- Pacher P, Batkai S and Kunos G (2005a) Cardiovascular pharmacology of cannabinoids. *Handb Exp Pharmacol* 599-625.
- Pacher P, Batkai S and Kunos G (2006) The endocannabinoid system as an emerging target of pharmacotherapy. *Pharmacol Rev* 58:389-462.
- Pacher P, Batkai S, Osei-Hyiaman D, Offertaler L, Liu J, Harvey-White J, Brassai A, Jarai Z, Cravatt BF and Kunos G (2005b) Hemodynamic profile, responsiveness to anandamide, and baroreflex sensitivity of mice lacking fatty acid amide hydrolase. *Am J Physiol Heart Circ Physiol* 289:H533-H541.
- Pacher P and Hasko G (2008) Endocannabinoids and cannabinoid receptors in ischaemia-reperfusion injury and preconditioning. *Br J Pharmacol* 153:252-262.

- Pacher P and Kunos G (2013) Modulating the endocannabinoid system in human health and disease--successes and failures. *FEBS J* 280:1918-1943.
- Pacher P, Mukhopadhyay P, Mohanraj R, Godlewski G, Batkai S and Kunos G (2008) Modulation of the endocannabinoid system in cardiovascular disease: therapeutic potential and limitations. *Hypertension* 52:601-607.
- Pan X, Ikeda SR and Lewis DL (1996) Rat brain cannabinoid receptor modulates N-type  $Ca^{2+}$  channels in a neuronal expression system. *Mol Pharmacol* 49:707-714.
- Patil M, Patwardhan A, Salas MM, Hargreaves KM and Akopian AN (2011) Cannabinoid receptor antagonists AM251 and AM630 activate TRPA1 in sensory neurons. *Neuropharmacology* 61:778-788.
- Pearlman RJ, Aubrey KR and Vandenberg RJ (2003) Arachidonic acid and anandamide have opposite modulatory actions at the glycine transporter, GLYT1a. *J Neurochem* 84:592-601.
- Perez-Reyes E, Kim HS, Lacerda AE, Horne W, Wei XY, Rampe D, Campbell KP, Brown AM and Birnbaumer L (1989) Induction of calcium currents by the expression of the alpha 1-subunit of the dihydropyridine receptor from skeletal muscle. *Nature* 340:233-236.
- Pert CB and Snyder SH (1973) Opiate receptor: demonstration in nervous tissue. *Science* 179:1011-1014.
- Pertwee RG (2001) Cannabinoid receptors and pain. *Prog Neurobiol* 63:569-611.
- Pertwee RG (2006) The pharmacology of cannabinoid receptors and their ligands: an overview. *Int J Obes (Lond)* 30 Suppl 1:S13-8.:S13-S18.
- Pertwee RG, Howlett AC, Abood ME, Alexander SP, Di M, V, Elphick MR, Greasley PJ, Hansen HS, Kunos G, Mackie K, Mechoulam R and Ross RA (2010) International Union of Basic and Clinical Pharmacology. LXXIX. Cannabinoid receptors and their ligands: beyond CB and CB. *Pharmacol Rev* 62:588-631.
- Pertwee RG and Ross RA (2002) Cannabinoid receptors and their ligands. *Prostaglandins Leukot Essent Fatty Acids* 66:101-121.
- Piomelli D (2003) The molecular logic of endocannabinoid signalling. *Nat Rev Neurosci* 4:873-884.
- Piomelli D, Tarzia G, Duranti A, Tontini A, Mor M, Compton TR, Dasse O, Monaghan EP, Parrott JA and Putman D (2006) Pharmacological profile of the selective FAAH inhibitor KDS-4103 (URB597). *CNS Drug Rev* 12:21-38.
- Plane F, Holland M, Waldron GJ, Garland CJ and Boyle JP (1997) Evidence that anandamide and EDHF act via different mechanisms in rat isolated mesenteric arteries. *Br J Pharmacol* 121:1509-1511.

Porter AC, Sauer JM, Knierman MD, Becker GW, Berna MJ, Bao J, Nomikos GG, Carter P, Bymaster FP, Leese AB and Felder CC (2002) Characterization of a novel endocannabinoid, virodhamine, with antagonist activity at the CB1 receptor. *J Pharmacol Exp Ther* 301:1020-1024.

Pratt PF, Hillard CJ, Edgmond WS and Campbell WB (1998) N-arachidonylethanolamide relaxation of bovine coronary artery is not mediated by CB1 cannabinoid receptor. *Am J Physiol* 274:H375-H381.

Premkumar LS and Ahern GP (2000) Induction of vanilloid receptor channel activity by protein kinase C. *Nature* 408:985-990.

Qu Z and Chung D (2012) Mechanisms and determinants of ultralong action potential duration and slow rate-dependence in cardiac myocytes. *PLoS One* 7:e43587.

Rajesh M, Mukhopadhyay P, Batkai S, Hasko G, Liaudet L, Huffman JW, Csiszar A, Ungvari Z, Mackie K, Chatterjee S and Pacher P (2007) CB2-receptor stimulation attenuates TNF-alpha-induced human endothelial cell activation, transendothelial migration of monocytes, and monocyte-endothelial adhesion. *Am J Physiol Heart Circ Physiol* 293:H2210-H2218.

Rajesh M, Mukhopadhyay P, Hasko G, Liaudet L, Mackie K and Pacher P (2010) Cannabinoid-1 receptor activation induces reactive oxygen species-dependent and -independent mitogen-activated protein kinase activation and cell death in human coronary artery endothelial cells. *Br J Pharmacol* 160:688-700.

Ralevic V, Kendall DA, Randall MD, Zygmunt PM, Movahed P and Hogestatt ED (2000) Vanilloid receptors on capsaicin-sensitive sensory nerves mediate relaxation to methanandamide in the rat isolated mesenteric arterial bed and small mesenteric arteries. *Br J Pharmacol* 130:1483-1488.

Randall MD, Alexander SP, Bennett T, Boyd EA, Fry JR, Gardiner SM, Kemp PA, McCulloch AI and Kendall DA (1996) An endogenous cannabinoid as an endothelium-derived vasorelaxant. *Biochem Biophys Res Commun* 229:114-120.

Randall MD, Harris D, Kendall DA and Ralevic V (2002) Cardiovascular effects of cannabinoids. *Pharmacol Ther* 95:191-202.

Randall MD and Kendall DA (1997) Involvement of a cannabinoid in endothelium-derived hyperpolarizing factor-mediated coronary vasorelaxation. *Eur J Pharmacol* 335:205-209.

Randall MD, Kendall DA and O'Sullivan S (2004) The complexities of the cardiovascular actions of cannabinoids. *Br J Pharmacol* 142:20-26.

Randall MD, McCulloch AI and Kendall DA (1997) Comparative pharmacology of endothelium-derived hyperpolarizing factor and anandamide in rat isolated mesentery. *Eur J Pharmacol* 333:191-197.

Rao GK and Kaminski NE (2006) Cannabinoid-mediated elevation of intracellular calcium: a structure-activity relationship. *J Pharmacol Exp Ther* 317:820-829.

Ren X and Philipson KD (2013) The topology of the cardiac Na<sup>+</sup>/Ca<sup>2+</sup> exchanger, NCX1. *J Mol Cell Cardiol* 57:68-71. doi: 10.1016/j.yjmcc.2013.01.010. Epub; %2013 Jan 31.:68-71.

Reuter H, Pott C, Goldhaber JJ, Henderson SA, Philipson KD and Schwinger RH (2005) Na<sup>+</sup>-Ca<sup>2+</sup> exchange in the regulation of cardiac excitation-contraction coupling. *Cardiovasc Res* 67:198-207.

Rhee MH, Bayewitch M, Avidor-Reiss T, Levy R and Vogel Z (1998) Cannabinoid receptor activation differentially regulates the various adenylyl cyclase isozymes. *J Neurochem* 71:1525-1534.

Rockwell CE and Kaminski NE (2004) A cyclooxygenase metabolite of anandamide causes inhibition of interleukin-2 secretion in murine splenocytes. *J Pharmacol Exp Ther* 311:683-690.

Rockwell CE, Snider NT, Thompson JT, Vanden Heuvel JP and Kaminski NE (2006) Interleukin-2 suppression by 2-arachidonyl glycerol is mediated through peroxisome proliferator-activated receptor gamma independently of cannabinoid receptors 1 and 2. *Mol Pharmacol* 70:101-111.

Rodriguez de FF, Del A, I, Bermudez-Silva FJ, Bilbao A, Cippitelli A and Navarro M (2005) The endocannabinoid system: physiology and pharmacology. *Alcohol Alcohol* 40:2-14.

Rogart RB, Cribbs LL, Muglia LK, Kephart DD and Kaiser MW (1989) Molecular cloning of a putative tetrodotoxin-resistant rat heart Na<sup>+</sup> channel isoform. *Proc Natl Acad Sci U S A* 86:8170-8174.

Ross HR, Gilmore AJ and Connor M (2009) Inhibition of human recombinant T-type calcium channels by the endocannabinoid N-arachidonoyl dopamine. *Br J Pharmacol* 156:740-750.

Ross RA, Gibson TM, Brockie HC, Leslie M, Pashmi G, Craib SJ, Di M, V and Pertwee RG (2001) Structure-activity relationship for the endogenous cannabinoid, anandamide, and certain of its analogues at vanilloid receptors in transfected cells and vas deferens. *Br J Pharmacol* 132:631-640.

Sather WA and McCleskey EW (2003) Permeation and selectivity in calcium channels. *Annu Rev Physiol* 65:133-59. Epub; %2002 Nov 21.:133-159.

Schmid HH and Berdyshev EV (2002) Cannabinoid receptor-inactive N-acyl ethanolamines and other fatty acid amides: metabolism and function. *Prostaglandins Leukot Essent Fatty Acids* 66:363-376.

Schmid HH, Schmid PC and Berdyshev EV (2002) Cell signaling by endocannabinoids and their congeners: questions of selectivity and other challenges. *Chem Phys Lipids* 121:111-134.

Schmid HH, Schmid PC and Natarajan V (1996) The N-acylation-phosphodiesterase pathway and cell signalling. *Chem Phys Lipids* 80:133-142.

Schmid PC, Schwartz KD, Smith CN, Krebsbach RJ, Berdyshev EV and Schmid HH (2000) A sensitive endocannabinoid assay. The simultaneous analysis of N-acylethanolamines and 2-monoacylglycerols. *Chem Phys Lipids* 104:185-191.

Schmid PC, Zuzarte-Augustin ML and Schmid HH (1985) Properties of rat liver N-acylethanolamine amidohydrolase. *J Biol Chem* 260:14145-14149.

Schulze DH, Muqhal M, Lederer WJ and Ruknudin AM (2003) Sodium/calcium exchanger (NCX1) macromolecular complex. *J Biol Chem* 278:28849-28855.

Shannon TR, Ginsburg KS and Bers DM (2000) Potentiation of fractional sarcoplasmic reticulum calcium release by total and free intra-sarcoplasmic reticulum calcium concentration. *Biophys J* 78:334-343.

Sheldon RS, Duff HJ, Thakore E and Hill RJ (1994) Class I antiarrhythmic drugs: allosteric inhibitors of [3H] batrachotoxinin binding to rat cardiac sodium channels. *J Pharmacol Exp Ther* 268:187-194.

Shen M and Thayer SA (1998) The cannabinoid agonist Win55,212-2 inhibits calcium channels by receptor-mediated and direct pathways in cultured rat hippocampal neurons. *Brain Res* 783:77-84.

Shigekawa M and Iwamoto T (2001) Cardiac Na<sup>+</sup>-Ca<sup>2+</sup> exchange: molecular and pharmacological aspects. *Circ Res* 88:864-876.

Shimasue K, Urushidani T, Hagiwara M and Nagao T (1996) Effects of anandamide and arachidonic acid on specific binding of (+) -PN200-110, diltiazem and (-) -desmethoxyverapamil to L-type Ca<sup>2+</sup> channel. *Eur J Pharmacol* 296:347-350.

Shire D, Calandra B, Bouaboula M, Barth F, Rinaldi-Carmona M, Casellas P and Ferrara P (1999) Cannabinoid receptor interactions with the antagonists SR 141716A and SR 144528. *Life Sci* 65:627-635.

Siedlecka U, Arora M, Kolettis T, Soppa GK, Lee J, Stagg MA, Harding SE, Yacoub MH and Terracciano CM (2008) Effects of clenbuterol on contractility and Ca<sup>2+</sup> homeostasis of isolated rat ventricular myocytes. *Am J Physiol Heart Circ Physiol* 295:H1917-H1926.

Singer D, Biel M, Lotan I, Flockerzi V, Hofmann F and Dascal N (1991) The roles of the subunits in the function of the calcium channel. *Science* 253:1553-1557.

Siqueira SW, Lapa AJ and Ribeiro d, V (1979) The triple effect induced by delta 9-tetrahydrocannabinol on the rat blood pressure. *Eur J Pharmacol* 58:351-357.

Smart D, Gunthorpe MJ, Jerman JC, Nasir S, Gray J, Muir AI, Chambers JK, Randall AD and Davis JB (2000) The endogenous lipid anandamide is a full agonist at the human vanilloid receptor (hVR1). *Br J Pharmacol* 129:227-230.

Smith PF (2004) Medicinal cannabis extracts for the treatment of multiple sclerosis. *Curr Opin Investig Drugs* 5:727-730.

Soldatov NM, Oz M, O'Brien KA, Abernethy DR and Morad M (1998) Molecular determinants of L-type  $\text{Ca}^{2+}$  channel inactivation. Segment exchange analysis of the carboxyl-terminal cytoplasmic motif encoded by exons 40-42 of the human  $\alpha 1\text{C}$  subunit gene. *J Biol Chem* 273:957-963.

Spivak CE, Lupica CR and Oz M (2007) The endocannabinoid anandamide inhibits the function of  $\alpha 4\beta 2$  nicotinic acetylcholine receptors. *Mol Pharmacol* 72:1024-1032.

Spurgeon HA, duBell WH, Stern MD, Sollott SJ, Ziman BD, Silverman HS, Capogrossi MC, Talo A and Lakatta EG (1992) Cytosolic calcium and myofilaments in single rat cardiac myocytes achieve a dynamic equilibrium during twitch relaxation. *J Physiol* 447:83-102.:83-102.

Steffens M and Feuerstein TJ (2004) Receptor-independent depression of DA and 5-HT uptake by cannabinoids in rat neocortex-involvement of  $\text{Na}^+/\text{K}^+$ -ATPase. *Neurochem Int* 44:529-538.

Stein EA, Fuller SA, Edgmond WS and Campbell WB (1996) Physiological and behavioural effects of the endogenous cannabinoid, arachidonylethanolamide (anandamide), in the rat. *Br J Pharmacol* 119:107-114.

Sterin-Borda L, Del Zar CF and Borda E (2005) Differential CB1 and CB2 cannabinoid receptor-inotropic response of rat isolated atria: endogenous signal transduction pathways. *Biochem Pharmacol* 69:1705-1713.

Stienstra R, Duval C, Muller M and Kersten S (2007) PPARs, Obesity, and Inflammation. *PPAR Res* 2007:95974.:95974.

Straiker A, Stella N, Piomelli D, Mackie K, Karten HJ and Maguire G (1999) Cannabinoid CB1 receptors and ligands in vertebrate retina: localization and function of an endogenous signaling system. *Proc Natl Acad Sci U S A* 96:14565-14570.

Straiker AJ, Borden CR and Sullivan JM (2002) G-protein alpha subunit isoforms couple differentially to receptors that mediate presynaptic inhibition at rat hippocampal synapses. *J Neurosci* 22:2460-2468.

Su Z, Preusser L, Diaz G, Green J, Liu X, Polakowski J, Dart M, Yao B, Meyer M, Limberis JT, Martin RL, Cox BF and Gintant GA (2011) Negative inotropic effect of a CB2 agonist A-955840 in isolated rabbit ventricular myocytes is independent of CB1 and CB2 receptors. *Curr Drug Saf* 6:277-284.

Sugiura T, Kodaka T, Kondo S, Tonegawa T, Nakane S, Kishimoto S, Yamashita A and Waku K (1996) 2-Arachidonoylglycerol, a putative endogenous cannabinoid receptor ligand, induces rapid, transient elevation of intracellular free  $\text{Ca}^{2+}$  in neuroblastoma x glioma hybrid NG108-15 cells. *Biochem Biophys Res Commun* 229:58-64.

Sugiura T, Kondo S, Sukagawa A, Nakane S, Shinoda A, Itoh K, Yamashita A and Waku K (1995) 2-Arachidonoylglycerol: a possible endogenous cannabinoid receptor ligand in brain. *Biochem Biophys Res Commun* 215:89-97.

Theile JW and Cummins TR (2011) Inhibition of Navbeta4 peptide-mediated resurgent sodium currents in Nav1.7 channels by carbamazepine, riluzole, and anandamide. *Mol Pharmacol* 80:724-734.

Tourino C, Oveisi F, Lockney J, Piomelli D and Maldonado R (2010) FAAH deficiency promotes energy storage and enhances the motivation for food. *Int J Obes (Lond)* 34:557-568.

Trafford AW, Diaz ME and Eisner DA (2001) Coordinated control of cell Ca<sup>2+</sup> loading and triggered release from the sarcoplasmic reticulum underlies the rapid inotropic response to increased L-type Ca<sup>2+</sup> current. *Circ Res* 88:195-201.

Tsumura M, Sobhan U, Muramatsu T, Sato M, Ichikawa H, Sahara Y, Tazaki M and Shibukawa Y (2012) TRPV1-mediated calcium signal couples with cannabinoid receptors and sodium-calcium exchangers in rat odontoblasts. *Cell Calcium* 52:124-136.

Twitchell W, Brown S and Mackie K (1997) Cannabinoids inhibit N- and P/Q-type calcium channels in cultured rat hippocampal neurons. *J Neurophysiol* 78:43-50.

Ugdyzhekova DS, Bernatskaya NA, Stefano JB, Graier VF, Tam SW and Mekhoulam R (2001) Endogenous cannabinoid anandamide increases heart resistance to arrhythmogenic effects of epinephrine: role of CB(1) and CB(2) receptors. *Bull Exp Biol Med* 131:251-253.

Underdown NJ, Hiley CR and Ford WR (2005) Anandamide reduces infarct size in rat isolated hearts subjected to ischaemia-reperfusion by a novel cannabinoid mechanism. *Br J Pharmacol* 146:809-816.

Vafiadaki E, Arvanitis DA, Pagakis SN, Papalouka V, Sanoudou D, Kontrogianni-Konstantopoulos A and Kranias EG (2009) The anti-apoptotic protein HAX-1 interacts with SERCA2 and regulates its protein levels to promote cell survival. *Mol Biol Cell* 20:306-318.

Valk PJ and Delwel R (1998) The peripheral cannabinoid receptor, Cb2, in retrovirally-induced leukemic transformation and normal hematopoiesis. *Leuk Lymphoma* 32:29-43.

Van den Brink-van der Laan, Killian JA and de KB (2004) Nonbilayer lipids affect peripheral and integral membrane proteins via changes in the lateral pressure profile. *Biochim Biophys Acta* 1666:275-288.

Van dB, I and Vanheel B (2000) Influence of cannabinoids on the delayed rectifier in freshly dissociated smooth muscle cells of the rat aorta. *Br J Pharmacol* 131:85-93.

Van S, Duncan M, Kingsley PJ, Mouihate A, Urbani P, Mackie K, Stella N, Makriyannis A, Piomelli D, Davison JS, Marnett LJ, Di M, V, Pittman QJ, Patel KD and Sharkey KA (2005) Identification and functional characterization of brainstem cannabinoid CB2 receptors. *Science* 310:329-332.

Vandevorde S and Lambert DM (2005) Focus on the three key enzymes hydrolysing endocannabinoids as new drug targets. *Curr Pharm Des* 11:2647-2668.

Varga K, Lake K, Martin BR and Kunos G (1995) Novel antagonist implicates the CB1 cannabinoid receptor in the hypotensive action of anandamide. *Eur J Pharmacol* 278:279-283.

Varga K, Lake KD, Huangfu D, Guyenet PG and Kunos G (1996) Mechanism of the hypotensive action of anandamide in anesthetized rats. *Hypertension* 28:682-686.

Vaughan CW and Christie MJ (2005) Retrograde signalling by endocannabinoids. *Handb Exp Pharmacol* 367-383.

Venance L, Piomelli D, Glowinski J and Giaume C (1995) Inhibition by anandamide of gap junctions and intercellular calcium signalling in striatal astrocytes. *Nature* 376:590-594.

Vizi ES, Katona I and Freund TF (2001) Evidence for presynaptic cannabinoid CB(1) receptor-mediated inhibition of noradrenaline release in the guinea pig lung. *Eur J Pharmacol* 431:237-244.

Voitychuk OI, Asmolikova VS, Gula NM, Sotkis GV, Galadari S, Howarth FC, Oz M and Shuba YM (2012) Modulation of excitability, membrane currents and survival of cardiac myocytes by N-acyl ethanolamines. *Biochim Biophys Acta* 1821:1167-1176.

Vollmer RR, Cavero I, Ertel RJ, Solomon TA and Buckley JP (1974) Role of the central autonomic nervous system in the hypotension and bradycardia induced by (-)-delta 9-trans-tetrahydrocannabinol. *J Pharm Pharmacol* 26:186-192.

Wagner JA, Hu K, Bauersachs J, Karcher J, Wiesler M, Goparaju SK, Kunos G and Ertl G (2001a) Endogenous cannabinoids mediate hypotension after experimental myocardial infarction. *J Am Coll Cardiol* 38:2048-2054.

Wagner JA, Hu K, Karcher J, Bauersachs J, Schafer A, Laser M, Han H and Ertl G (2003) CB(1) cannabinoid receptor antagonism promotes remodeling and cannabinoid treatment prevents endothelial dysfunction and hypotension in rats with myocardial infarction. *Br J Pharmacol* 138:1251-1258.

Wagner JA, Jarai Z, Batkai S and Kunos G (2001b) Hemodynamic effects of cannabinoids: coronary and cerebral vasodilation mediated by cannabinoid CB(1) receptors. *Eur J Pharmacol* 423:203-210.



- Wei BQ, Mikkelsen TS, McKinney MK, Lander ES and Cravatt BF (2006a) A second fatty acid amide hydrolase with variable distribution among placental mammals. *J Biol Chem* 281:36569-36578.
- Wei BQ, Mikkelsen TS, McKinney MK, Lander ES and Cravatt BF (2006b) A second fatty acid amide hydrolase with variable distribution among placental mammals. *J Biol Chem* 281:36569-36578.
- Wei SK, Ruknudin A, Hanlon SU, McCurley JM, Schulze DH and Haigney MC (2003) Protein kinase A hyperphosphorylation increases basal current but decreases beta-adrenergic responsiveness of the sarcolemmal Na<sup>+</sup>-Ca<sup>2+</sup> exchanger in failing pig myocytes. *Circ Res* 92:897-903.
- White R and Hiley CR (1997) A comparison of EDHF-mediated and anandamide-induced relaxations in the rat isolated mesenteric artery. *Br J Pharmacol* 122:1573-1584.
- White R and Hiley CR (1998) The actions of the cannabinoid receptor antagonist, SR 141716A, in the rat isolated mesenteric artery. *Br J Pharmacol* 125:689-696.
- White R, Ho WS, Bottrill FE, Ford WR and Hiley CR (2001) Mechanisms of anandamide-induced vasorelaxation in rat isolated coronary arteries. *Br J Pharmacol* 134:921-929.
- Wilson RI, Kunos G and Nicoll RA (2001) Presynaptic specificity of endocannabinoid signaling in the hippocampus. *Neuron* 31:453-462.
- Wu BW, Liu QH and Zhang L (2012) [Cardiac inwardly rectifying potassium channel and arrhythmias]. *Sheng Li Xue Bao* 64:751-757.
- Xiao YF, Ke Q, Chen Y, Morgan JP and Leaf A (2004) Inhibitory effect of n-3 fish oil fatty acids on cardiac Na<sup>+</sup>/Ca<sup>2+</sup> exchange currents in HEK293t cells. *Biochem Biophys Res Commun* 321:116-123.
- Xiong W, Wu X, Li F, Cheng K, Rice KC, Lovinger DM and Zhang L (2012) A common molecular basis for exogenous and endogenous cannabinoid potentiation of glycine receptors. *J Neurosci* 32:5200-5208.
- Yu FH and Catterall WA (2003) Overview of the voltage-gated sodium channel family. *Genome Biol* 4:207.
- Zhang Y, Jiang X, Snutch TP and Tao J (2013) Modulation of low-voltage-activated T-type Ca<sup>2+</sup> channels. *Biochim Biophys Acta* 1828:1550-1559.
- Zhang ZS, Cheng HJ, Onishi K, Ohte N, Wannenburg T and Cheng CP (2005) Enhanced inhibition of L-type Ca<sup>2+</sup> current by beta3-adrenergic stimulation in failing rat heart. *J Pharmacol Exp Ther* 315:1203-1211.
- Zhuang SY, Bridges D, Grigorenko E, McCloud S, Boon A, Hampson RE and Deadwyler SA (2005) Cannabinoids produce neuroprotection by reducing intracellular calcium release from ryanodine-sensitive stores. *Neuropharmacology* 48:1086-1096.

Zimmer T (2010) Effects of tetrodotoxin on the mammalian cardiovascular system. *Mar Drugs* 8:741-762.

Zoratti C, Kipmen-Korgun D, Osibow K, Malli R and Graier WF (2003) Anandamide initiates  $Ca^{2+}$  signaling via CB2 receptor linked to phospholipase C in calf pulmonary endothelial cells. *Br J Pharmacol* 140:1351-1362.

Zygmunt PM, Hogestatt ED, Waldeck K, Edwards G, Kirkup AJ and Weston AH (1997) Studies on the effects of anandamide in rat hepatic artery. *Br J Pharmacol* 122:1679-1686.

Zygmunt PM, Petersson J, Andersson DA, Chuang H, Sorgard M, Di Marzo V, Julius D and Hogestatt ED (1999) Vanilloid receptors on sensory nerves mediate the vasodilator action of anandamide. *Nature* 400:452-457.

## APPENDIX

**At the time of printing this thesis, the majority of its contents has been published or accepted for publication:**

**Al Kury LT**, Voitychuk OI, Ali RM, Galadari S, Yang KH, Howarth FC, Shuba YM and Oz M (2014a) Effects of endogenous cannabinoid anandamide on excitation-contraction coupling in rat ventricular myocytes. *Cell Calcium* **55**: 104-118.

**Al Kury LT**, Voitychuk OI, Yang KH, Thayyullathil F, Doroshenko P, Ali RM, Shubha, YM, Galadari S, Howarth FC and Oz M (2014b) Effects of endogenous cannabinoid anandamide on voltage-dependent sodium and calcium channels in rat ventricular myocytes. *Br J Pharmacol*, article *In Press*.

**Al Kury LT**, Yang KH, Thayyullathil F, Mohanraj R, Ali RM, Shuba YM, Howarth FC, Galadari S and Oz M (2014c) Effects of endogenous cannabinoid anandamide on cardiac Na<sup>+</sup>/Ca<sup>2+</sup> exchanger. *Cell Calcium* **55**:231-237.